Influence of CerS on T cell function and colitis

Dissertation
zur Erlangung des Doktorgrades
der Naturwissenschaften

vorgelegt beim Fachbereich 15 Biowissenschaften
der Johann Wolfgang Goethe-Universität
in Frankfurt am Main

von
Jennifer Christina Hartel
aus Gelnhausen

Frankfurt am Main, 2023

(D30)

vom Fachbereich 15 Biowissenschaften der Johann Wolfgang Goethe-Universität als Dissertation angenommen.

That's a real lastin' legacy to leave

- Taylor Swift

Table of contents

Table of contents

List of Figures

List of Figures

List of Supplementary Figures

List of Tables

1. Introduction

1.1. Ulcerative Colitis

1.1.1 Characterization and epidemiology

Ulcerative colitis (UC) is a chronic, inflammatory disease of the colon. According to the Deutsche Morbus Crohn/Colitis ulcerosa Vereinigung (DCCV e.V.) more than 170 000 people suffer from UC and approximately 3200 patients fall ill with UC per year in Germany. Men and women are equally affected. Like Morbus Crohn, UC is classified as an inflammatory bowel disease (IBD). IBDs are relapsing or continuously chronic systemic inflammatory diseases of the intestine [1]. UC starts mostly as a mucosal inflammation that can spread from distal to proximal until the whole colon is affected. Prevalence of UC stabilized in Europe and North America, but the incidence is rising globally, especially in newly industrialized countries like Africa, Asia and South America [2]. Nowadays, UC incidences worldwide surpassed ~3 %, which means that the disease is globally-relevant, according to the International Statistical Classification of Diseases and Related Health Problems (ICD) guidelines. Patients suffer from symptoms like diarrhoea, rectal bleeding, bloody stool, abdominal pain and cramping, fatigue, fever and often feel the urgency to defecate, but are still not able to do so [3]. UC can also manifest extra-intestinal, leaving patients with anaemia, arthropathies, uveitis or episcleritis [4]. According to the Montreal classification, extension (E) of UC is divided into three main stages: E1-3. When the inflammation only affects the rectal area (proctitis), the patient is classified in E1. When inflammation is more distal and reaches to the splenic flexure it is classified as E2 [4]. E3 classification is often called extensive colitis, meaning the inflammation reached the proximal flexture, and now affects nearly the whole colon [4]. Patients in E2 or E3 stadium face a higher risk of dysplasia and colorectal cancer (CRC) development [5, 6]. Montreal's Classification of patients into the different severity classes (S) of UC is based on biochemical and clinical parameter assessment by Truelove and Witt's modified criteria (Table 1). Even though the disease has an early set-on at the age of 25 to 40, old age is a risk factor for UC. Not only age, but also genetic pre-disposition is a very important risk factor. People with IBDs in family history have a higher risk for UC. People of any race or ethnicity can get UC, but Ashkenazi Jewish people have a higher risk for developing UC. Environmental factors like bacteria and substances that cause intestinal inflammation can also contribute to UC development. Some scientists state that diet

and poor lifestyle choices can also contribute, as the consumption of polyunsaturated Fatty acids (FAs), often found in junk food, is linked with digestive problems. So far UC is treatable, but not curable.

Table 1: Parameters for assessment of UC severity after Trulove and Witt's modified criteria

Parameter	S1 mild UC	S2 moderate UC	S3 severe UC
Bloody stool per day [n]	<4	4-6	>6
Body temperature [°C]	<37.5	37.5-37.8	>37.8
Pulse [beats per minute (bpm)]	<90	≤90	>90
Haemoglobin [g/dL]	>11.5	11.5-10.5	<10.5
C-reactive protein (CPR) [mg/L]	normal	<30	>30
Erythrocyte sedimentation rate (ESR) [mm/h]	<20	20-30	>30

1.1.2 Pathophysiology of UC

In its healthy state, the epithelial barrier is covered in mucin, which does not only provide a physical, but also an antimicrobial barrier to the colon [7, 8]. Mucin synthesis is impaired in patients with UC, which leads to an elevated permeability causing increased entry of pathogens and subsequent stimulation of the immune system [9].

Molecular characterization of the pathways leading to UC development is essential for targeting the disease. Peroxisome proliferator-activated receptor (PPARγ), for example, is a negative regulator of many inflammatory signalling pathways including Nuclear Factor Kappa B (NFκB) and Activating Protein (AP1) pathway [10]. PPARγ is significantly downregulated in epithelial colon cells from UC patients (Figure 1) [11]. PPARγ-dependent inhibition of transcription factors for pro-inflammatory genes is a crucial anti-inflammatory effect that cannot be carried out properly in UC patients [10]. Pathogens that crossed the first barrier in the colon are recognized by Toll like receptor (TLR) 4 expressed on immature Dendritic Cells (DCs), which are immune cells that are responsible for foreign antigen presentation to other immune cells (Figure 1) [11]. TLRs are not only expressed in DCs, but also on other immune cells like T cells and macrophages [12, 13]. TLR signalling activates NFκB and Janus kinase (JAK) signalling which then promote TNFα, Interleukin (IL) 12 and IL23 release in T cells and macrophages [14]. Normally, TLR3 and 5 are highly expressed in healthy colon cells, whereas TLR2 and 4 expression is nearly absent [15]. In UC patients, TLR4 expression

2

is significantly increased in the Lamina propria (LP) cells [16]. The cytokine profile in UC is crucial to the pathophysiology: IL1β, IL4, IL5, IL8, Il12p40, IFNγ and TNFα are significantly increased in UC patients compared to healthy control patients [17]. All cytokines have different functions, but in general they are necessary for immune cell recruitment and regulation [18, 19]. TNFα has an important role in UC [20]. With its many functions, TNFα is able to increase pro-inflammatory cytokine release, cell infiltration, tissue remodelling and permeability (Figure 1). TNFα-dependent NFκB stimulation leads to a degradation of the mucosa through increased metalloproteinases (MMPs) in cells located in the LP [21]. IL1β and IL6 release is also stimulated via TNF signalling [22]. It could also be demonstrated that Lipopolysaccharide Induced TNF Factor (LITAF), which promotes TNF production, is increased in UC patients [23]. The immune cell recruitment mediated by TNFα triggers a chain reaction, where different cell types are activated by TNFα thereby producing more TNFα or other cytokines that recruit different immune cells, which also release new cytokines for immune cell recruitment [24]. This vicious cycle ends in a chronic inflammatory process.

One of the major sources for these cytokines are T cells (Figure 1). T cells are part of the adaptive immune system and mediate inflammatory responses to pathogens. Dysregulation of these processes can lead to a pathologically raised immune response. How T cells are linked to pathophysiology of UC, is described in Chapter 1.2.3.

1. Introduction
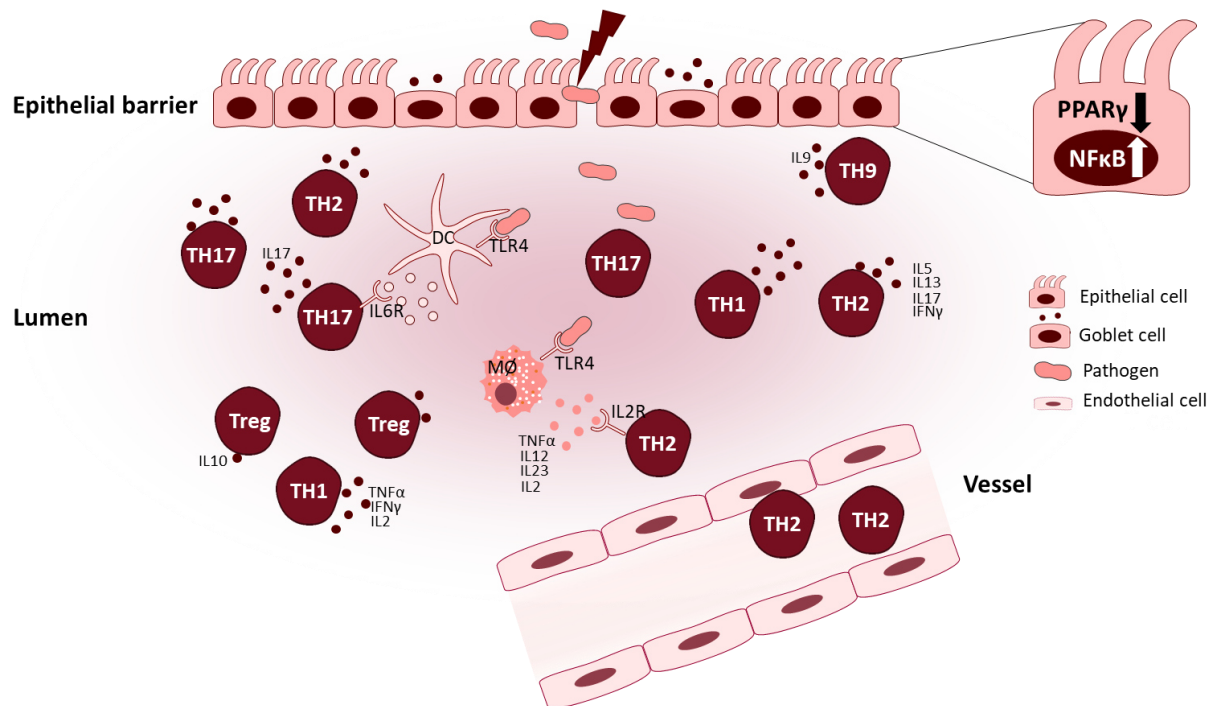
Figure 1: Depiction of inflammatory processes in UC. PPARγ expression is reduced leading to enhanced NFκB pathway in epithelial cells. Epithelial barrier function is disturbed and pathogens pass this barrier and trigger APCs via TLR4 signalling. Pro-inflammatory cytokines activate T Helper cells type (TH) 2, TH1, TH9 and TH17 cells that then produce more pro-inflammatory cytokines and promote T cell recruitment from the blood vessel to the tissue. Imbalance of TH17 and Tregs leads to failure of immunomodulatory Treg function.

1.1.3 Current Therapies

UC is treatable, but not curable. There are many approaches to treat Ulcerative colitis. The usage of anti-inflammatory drugs such as 5-amino salicylates, like Sulfasalazine or Mesalamine, is the state of the art treatment for UC patients [25, 26]. Inhibition of the pro-inflammatory prostaglandin formation is one of the major anti-inflammatory effects of those drugs [27]. They are used for patients with S1/2 for induction of remission [28]. For patients that do not respond to Sulfasalazine or 5-aminosalicylates, corticosteroids are used, but they are rarely prescribed and also not used long-term due to the severe side effects including Cushing-syndrome or formation of gastric ulcers [29, 30]. There is also the possibility of usage of immunosuppressants for treatment of UC. Azathioprine and 6-mercaptopurine, both mild cytostatics, can be used to inhibit immune cell proliferation and infiltration [31, 32]. Cyclosporine is only prescribed to patients that do not respond to other medications due to serious side effects and is not intended for long-term use [33–35]. So-called small molecules are also used for UC treatment. Tofactinib, for example, targets JAK and leads to inhibition

4

of immune cell functions [36]. A big group of medications for UC consists of biologicals (Table 2) [37]. With Vedolizumab, α4β7 integrin is targeted, impairing adhesion of immune cells to endothelial cells and thereby prohibiting immune cell infiltration to the inflammatory site [38, 39]. Since cytokines have an important impact on immune cell function and their migration and proliferation is one of the main factors in the development of UC, targeting these proteins lends itself to the development of a treatment [19, 40, 41]. TNFα is successfully targeted with Infliximab, a mononuclear antibody against soluble and transmembrane TNFα, with a pro-apoptotic effect on T cells in the LP [42, 43]. In a DSS induced colitis model in mice, neutralization of IL9 via an antibody was very efficient and attenuated disease progression [44]. Several other antibodies targeted against cytokines are currently in clinical trials (Table 2) [45–48].

But not every cytokine turned out to be a good target for UC treatment. Up to date there is no clinical trial for targeting IL17 due to contradictory data in mouse models, on the one hand suggesting a protective role for IL17 [49–51], on the other hand suggesting a harmful role for IL17 [52–56]. IL13 seemed to be a good target for UC treatment, considering its dominant role in UC's pathophysiology [57, 58]. Tralokinumab, a specific antibody against IL13, is already in use for treatment of atopic dermatitis [59], but failed in a study for UC treatment [60]. In many cases a combination of different drugs and medications proved to be efficient for some patients [61, 62]. However, the search for new targets for new therapeutics is essential to help more patients suffering from UC.

Table 2: A selection of biologics targeting cytokines in clinical trials

Medication	Target	Phase	Reference
Basiliximab	IL2R	II	NCT01061996
Bradizikumab	IL23p19	II	NCT03616821, NCT04277546
Golimumab	TNFα	IV	NCT02425865
Mirikizumab	IL23p19	II-III	NCT03518086, NCT03524092, NCT03519945, NCT04469062, NCT04004611

Ustekinumab	IL12/23p40	IV	NCT03885713, NCT03809728, NCT04259138

1.2 T cells

The human immune system is a complex network that consists of an innate and an adaptive part, that work closely together in order to defend the body from pathogens or foreign substances [63]. The first trespassing of germs happens at the skin, which is part of the innate immune system and forms the first barrier [64]. If pathogens break through this barrier, the innate immune system triggers a cascade of signalling pathways and immune cell recruitment by the innate immune system [65]. Cells of the innate immune system, like macrophages and Natural Killer (NK) cells, can either neutralize or directly kill pathogens [66, 67]. Antigen-presenting cells (APC) can process components and parts of the pathogens and present them as antigens via Major Histocompatibility Complex (MHC) class I or II proteins to cells from the adaptive immune system [68].

T cells, B cells and the antibodies they produce are part of the adaptive immune system [69, 70]. B cells mature in the bone marrow and are activated by T helper (TH) cells. Antigens of TH cells bind at the surface immunoglobulin (Ig) of the B cells and stimulate them [71]. B cell stimulation leads to the release of soluble antibodies that enable humoral immune response. It neutralizes pathogens and activates the complement system for facilitation of lysis and phagocytosis of pathogens [72, 73].

T cell precursors derive from the bone-marrow and mature in the thymus, where they are selected and afterwards migrate through the blood to the tissues. T cells patrol the body and if they get in contact with a foreign antigen, they are activated and proliferate to respond to this stimulus with either killing of the pathogen or release of cytokines to recruit other immune cells.

1.2.1 T cell Receptor structure

T cells are characterized by their prominent T cell Receptor (TCR), which is a surface receptor complex that is responsible for the recognition of antigens presented by MHC class I or II proteins on APCs [74]. It is a heterodimeric complex that consists of two

different protein chains [75]. There are two types of TCR, one that consists of an α- and β-chain, and they make up 95 % of all T cells [76]. The other 5 % have a γ- and δ-chain TCR [76]. Variability of the ligand-binding pocket is reached through variable (V), joining (J) and diversity (D) recombination, a genetic recombination of the DNA segments in every single T cell catalysed by Recombination Activating Gene (RAG) 1 and 2 recombinases [77, 78]. The α- (γ) chain is generated by VJ recombination, while the β- (δ) chain needs VDJ recombination [78]. The re-arranged segments are then added with palindromic and non-template coding nucleotides to reach a higher diversity in TCR complexes [79]. In total, $5.8*10^6$ different possibilities for VDJ recombination exist, while the addition of palindromic and non-template coding nucleotides adds $2*10^{11}$ more possibilities to it, making it $2*10^{18}$ various recombination possibilities for TCR complex formation. The highly variable α- and β-chains (γ/δ) have two extracellular domains, the constant (C) region is proximal to the cell membrane and is connected with a transmembrane region and a short cytoplasmic tail, the variable (V) part of the chain is exclusively extracellular and binds to the peptide presented through MHC I or II. The TCR complex is formed by association of the α- and β-chain (γ/δ) with the adaptor signalling molecules Cluster of Differentiation (CD) 3δ, CD3ε, CD3ξ and CD3γ, while CD3δ and CD3ε build a heterodimer, as well as CD3ε and CD3γ, CD3ξ builds a homodimer [80]. The signalling motifs for TCR signalling are tyrosine residues in the short cytoplasmic tails of the CD3 adaptor proteins that will be phosphorylated upon TCR stimulation [81]. These tyrosine residues are located in a specific amino acid sequence which is called immunoreceptor tyrosine-based activation motif (ITAM) [82]. Each CD3 adaptor protein has one ITAM, except for CD3ξ which contains three ITAMs, so a TCR complex has a total of ten ITAMs [81].

1.2.2 T cell Receptor Activation and Signalling

The adaptive inflammatory response is highly dependent on the T cell activation. TCR signalling is activated by the binding of antigens presented by MHC class I or II molecules on APCs to their respective TCR [83]. But the TCR signalling pathway is not only dependent on MHC binding, but also on co-receptors expressed on the T cell like CD4 or CD8 [84]. CD4 is a glycoprotein containing an extracellular and transmembrane domain, as well as an intracellular tail [84]. CD8 is a hetero- or homo-dimeric protein consisting of CD8α/β, CD8α/α or CD8β/β [85]. The intracellular tail of CD4 or 8 binds

lymphocyte-specific protein tyrosine kinase (LCK) to bring it closer to the ITAMs of the TCR [86]. In an inactive state, LCK is phosphorylated at Y505 by the C-terminal sarcoma-cellular (src) Kinase (CSK) [87]. After T cell activation this phosphorylation is removed by CD45 to activate LCK properly [88]. LCK can then phosphorylate tyrosine residues on the ITAMs of the TCR, which is required for subsequent Zeta-chain-associated protein kinase 70 (Zap70) phosphorylation [89, 90]. Zap70 phosphorylation triggers translocation of different transcription factors into the nucleus promoting cell proliferation, survival, differentiation and effector function [91–94].

There are three major pathways following Zap70 activation.

Nuclear factor of activated T cells (NFAT). Phosphorylated Zap70 activates Phospholipase C γ (PLCγ) 1 which breaks down Phosphatidylinositol 4,5-Biphosphate (PIP$_2$) into diacylglycerol (DAG) and inositol triphosphate (IP$_3$) [95, 96]. IP$_3$ then activates Ca^{2+}-dependent calcineurin NFAT pathway [97, 98]. IP$_3$ binds to permeable ion-channel receptors located in the Endoplasmic reticulum (ER) membrane and releases stored Ca^{2+} into the cytoplasm [99]. Calcineurin is then activated and de-phosphorylates NFAT which then translocates into the nucleus. It can form a complex with AP1 and induce IL-2 and other cytokine expression, but it can also act alone and activate genes responsible for anergy (state of unresponsiveness) regulation [100, 101]. NFAT can therefore regulate function and responsiveness of T cells.

Nuclear factor kappa B (NFκB). Protein Kinase C θ (PKCθ) is induced by Zap70 and can then activate the non-canonical and canonical NFκB pathway [102, 103]. Non-canonical NFκB pathway is mediated through NFκB-inducing kinase (NIK) activation. The canonical pathway is started by assembly of the caspase recruitment domain family member (CARD) 11- B-cell chronic lymphocytic leukemia/lymphoma (BCL) 10-mucosa-associated lymphoid tissue lymphoma translocation gene (MALT) 1 complex (CBM) [104, 105]. This complex induces degradation of the inhibitor of nuclear factor kappa-B kinase subunit gamma (IKKγ), which then leads to an activation of IKβ kinases that are no longer inhibited by IKKγ [106, 107]. IKβ kinase phosphorylates IKβ and leads to its ubiquitination thereby releasing NFκB [106]. NFκB is a heterodimeric transcription factor that translocates into the nucleus upon phosphorylation [108]. NFκB signalling is considered to be pro-inflammatory, promoting survival and homeostasis of T cells and leads to the activation of their effector function [109–111].

Activating Protein (AP1). AP1 is a heterodimeric complex consisting of c-Jun and c-Fos. AP1 pathway is activated via the relocation of Rapidly accelerated sarcoma guanyl nucleotide-releasing protein (RASGPR) 1 to the plasma membrane which is induced by DAG [112, 113]. As a Guanine nucleotide (GTP) exchange factor (GEF), RASGPR1 activates RAS in T cells [114]. Ras binds to GTP, thereby inducing mitogen-activated protein kinase (MAPK) Kinase Kinase (MAPKKK) rapidly accelerated fibro sarcoma (Raf) 1 [115]. MAPKKK phosphorylates and activates MAPK Kinase (MAPKK) which subsequently activates MAPK extracellular-signal regulated kinases (ERK) 1/2 [116]. C-Fos assembles with phosphorylated c-Jun to translocate to the nucleus and activate genes involved in T cell development, differentiation and TCR induced signal strength [117, 118].

In order to avoid anergy in T cells and to amplify TCR signalling, other co-stimulatory receptors on the T cell surface, like CD28, can be activated [119]. Upon stimulation of CD28 by CD80 and CD86, phosphoinositid-3-Kinases (PIP$_3$K) are activated, which catalyse the phosphorylation of PIP$_2$ to PIP$_3$. PIP$_3$ is able to bind Protein Kinase B (Akt) which can enhance NFAT and NFκB pathway, but is also an inactivator of glycogen synthase kinase (GSK) 3 which normally inhibits IL-2 transcription [120–122].

1.2.3 T cell subsets and their role in UC

As major part of the adaptive immune system T cells have a broad spectrum of functions. They can be divided into two main subtypes: CD4$^+$ and CD8$^+$ cells. They are mainly distinguishable by their transcription factor expression, surface marker composition and cytokine release profile. Immune cell recruitment is one of the major issues in UC. T cells have a special role in the disease progression. CD4$^+$ cells especially display a pathologically raised immune response that can also affect other cell types and contribute to a pro-inflammatory nature [123, 124].

CD8. Although not very prominent for UC development, CD8$^+$ gained a lot of attention in this context. T cells expressing CD8, so-called cytotoxic T cells, are able to kill pathogens and cancer cells. They are activated through MHC class I antigens from APCs to mature and to be activated to fight off infections [125, 126]. A CD8 response can also be obtained via CD4-dependent activation to non-inflammatory antigens without APC involvement [127, 128]. Differentiation of CD8$^+$ cells is promoted by IL12

signalling (Figure 2) [129, 130]. IL12 signalling activates T-box transcription factor (Tbet) via mammalian target of rapamycin (mTOR) signalling pathway (Figure 2) [131–133]. When CD8$^+$ cells recognize their antigen on DCs, activated T cells upregulate C-X-C motif chemokine receptor (CXCR) 3 to enter the peripheral tissues [134]. Cytotoxic T cells can directly or indirectly kill hostile cells. Direct killing of hostile cells is performed by perforins and granzymes [135]. Granzymes are a group of serine proteases and perforins form pores into the target cell's cell membrane so that granzymes can enter and cleave viral and cellular proteins of the infected cell [136]. Indirect killing is mediated by induction of apoptosis by Fas Cell Surface Death Receptor (Fas)-FasL interaction where caspase proteases are activated [137, 138]. Apoptotic target cells are then phagocytized by macrophages [139]. Direct killing is also essential in anti-tumor immunity, where CD8$^+$ cells play a major role in tumor-cell killing [140]. The most prominent cytokines released by CD8$^+$ cells, next to perforins and granzymes, are Interferon (IFN) γ and Tumor necrosis Factor (TNF) α which can promote cytotoxic ability (Figure 2) [141, 142]. CD8$^+$ cells are known to contribute to different diseases like IBD, Parkinson and also to cancerous processes [143–146]. It could be shown that CD8$^+$ cells in IBD patients can be divided into groups with different expression patterns that are connected to either a mild or a severe disease progression [147]. Activated IFNγ$^+$ CD8$^+$ cells were elevated in the peripheral blood of UC patients and linked with increase of inflammation markers in the plasma [148]. Another large subtype of CD8$^+$ cells relevant for UC are Tissue-resident memory T cells (Trm). They contribute to a potent barrier immunity in the mucosa and can transform rapidly to effector cells and release cytokines to recruit other immune cells [149]. Roosenboom et al. found a decrease of CD103$^+$ CD8$^+$ (Trms) cells in UC patients [150] and Noble et al. observed a reduction of mucosal Trms in IBD patients, which normally responded to bacterial antigens [151].

CD4-expressing T cells are called T helper (TH) cells. They got their name through their first detected function that was described as supporting role for CD8$^+$ and other immune cell's functions. There are many TH subtypes and they are all involved in UC disease progression.

TH1. TH1 cells are more often linked to Crohn's disease than UC, nevertheless they contribute to UC. Mainly activated through infection by intracellular pathogens, TH1 cells promote the function of a variety of other immune cells via the release of cytokines

[152]. TH1 cells are typically activated via IL12 signalling, which is produced by DCs (Figure 2) [153, 154]. IL12 signalling leads to Tbet and Signal transducer and activator of transcription (STAT) 4 expression (Figure 2). Both of these transcription factors induce IFNγ expression. IFNγ release can promote IL12-dependent TH1 differentiation through STAT1 enhancement which in turn promotes Tbet expression [155, 156]. IL12 signalling can also be promoted by IL18 engagement [157] or via APC's CD40 and TH1's CD40 ligand interaction [158]. Secretion of IL12, IFNγ and TNFα are crucial functions of TH1 cells. TNFα can act on many immune cells, but has a special role at the endothelium, where it facilitates immune cell adhesion and thereby migration from the blood vessels to the tissues [159, 160]. Macrophages are also activated via TNFα and IFNγ and produce MMPs to facilitate leukocyte migration into the inflamed tissues, but also Nitrogen Oxide (NO), that is also released by macrophages for pathogen killing, and other cytokines recruit more immune cells [161–163]. NK cells and innate lymphoid cells (ILCs) are also activated by IL2, IFNγ and TNFα [164, 165]. The broad function and effects of TH1 cells on so many cell types hints at their possible involvement in the pathophysiology of many inflammatory diseases like IBD, especially Morbus Crohn, where it is one of the main drivers, systemic lupus erythematosus (SLE), autoimmune diseases and also cancer [166–170]. It could be shown that in a Dextran Sodium Sulfate (DSS) induced colitis model in IFNγ$^{-/-}$ mouse model, disease was less severe [171]. In a severe combined immunodeficency (SCID) adoptive transfer mouse model, cells that lack Tbet, failed to induce colitis [172]. Contradictory studies showed a beneficial role for TH1 in UC. In a DSS induced colitis model, Tbet-deficient mice showed more severe colitis symptoms compared to WT, and in another SCID adoptive transfer mouse model, Tbet deficient cell transfer led to the same disease onset as in the WT control [173, 174]. A study could also demonstrate IFNγ-independent colitis onset, in which mice were more sensitive to the induced colitis [175]. The role of TH1 cells in UC remains controversial.

TH2. One of the most abundant TH subtypes in the body and in the pathophysiology of UC are TH2 cells (Figure 1 and Figure 2). TH2 activation predominantly exerts immunity against extracellular parasites, bacteria, allergens, toxins and gastrointestinal nematodes [152, 176, 177]. IL2 and IL4 signalling triggers TH2 differentiation (Figure 2). IL4 signalling acts in a positive feedback loop, where STAT6 phosphorylation enhances GATA binding protein (GATA) 3 expression [178]. IL2 induces STAT5 enhancement and STAT5 and GATA3 act in concert to produce IL4 [179]. TH2 cells

display a great plasticity. ILCs, macrophages and DCs secrete different pro-inflammatory cytokines to induce TH2 differentiation. The specific microenvironment will shape the TH2 phenotype and cytokine profile. TH2 cells release IL13 and thereby activate B cells and their IgE release and have a protective role in airway immunity [180, 181]. Whereas, IL5, IFNγ, IL4 and IL17 production by TH2 cells is associated with chronic allergic inflammation that can facilitate macrophage polarization and B cell proliferation as well as their Ig class-switch [182–184]. It's no surprise that TH2 cells, too, are involved in multiple inflammatory conditions, like allergic airway diseases, IBD, especially UC and also cancer [166, 167, 169, 185–188]. Release of IL5, together with Granulocyte-macrophage colony-stimulating factor (GM-CSF), promotes eosinophil activation and tissue damage in IL23 dependent colitis [189–191]. IL13 driven effects include impairment of tight junction formation, induction of apoptosis in epithelial cells and increase of membrane permeability [57, 58]. In a DSS induced colitis model, mice with GATA3 overexpression, showed more severe colitis compared to the control with an upregulation of IL13 in the mucosa [192]. STAT6, also a transcription factor for the GATA3 promotor, is highly phosphorylated in UC patients and phosphorylation status is linked with disease severity [193]. GATA3 expression levels are also linked with disease severity [193] and Shih et al. observed a higher NFAT expression in UC patients [194]. NFATc2$^{-/-}$ mice showed reduced colitis in a chemical induced mouse model [195]. Later NFAT gene could be established as a marker for susceptibility to IBD [196]. There is also evidence that there is a TH2 subtype that expresses CD161, a NK T cell marker, and can also produce IL13 [197, 198].

TH17. Their discovery in 2005 defined TH17 cells as IL17 producing T cells that are important for host defence against pathogens in the mucosal and epithelial barrier of the gut [199]. It is now known that TH17 mainly provide tissue immunity throughout the whole body. TH17 differentiation is initiated by Tumor Growth Factor (TGF) β and IL6/21 signalling that increases IL23R in activated TH17 cells (Figure 2) [200]. IL23 signalling maintains TH17 lineage and proliferation [201]. Two of the most important transcription factors, that are often referred to as Th17 markers, are the Retinoic-acid-receptor-related orphan nuclear receptor gamma and alpha (RORγt and RORα) [202]. They work synergistically to induce IL17A + F expression, and IL17A deficiency is linked to a reduced Th17 development and function [203]. Their function, mediated by IL17, exerts a response of epithelial and endothelial cells, as well as fibroblasts, which all express IL17R on their surface [204–208]. Besides IL17, TH17 cells can also

produce IL22 that targets predominantly non-hematopoietic cells and supports host defence and formation of anti-microbial peptides like β defensins [209]. TH17 cells display a protective role against pathogens, but imbalance of TH17 cells can shift very quickly to pathophysiological processes like IBD, autoimmune diseases, Multiple Sclerosis (MS) or cancer [210–215]. Disrupted barrier function in UC leads to pathogen infiltration into the colon mucosa. These bacteria are able to induce IL1β and IL6 release in dendritic cells which then help TH17 cells to differentiate into a pathogenic subtype [201, 216]. Frank et al. showed, that the microbiome of UC patients differ from those of healthy controls supporting the hypothesis of bacteria driving TH17 cells into a pathogenic phenotype [217]. Several studies observed an accumulation of TH17 cells in inflammatory areas of the colon in UC patients (Figure 1) [218–220]. In UC patients, also an increase of TH17 associated cytokines was observed (Figure 1) [221, 222], but they seem to affect more non-hematopoietic cells, hence, epithelial cells [223]. Nevertheless, IL17 is able to activate the NFκB and MAPK pathways [224] leading to induction of pro-inflammatory cytokines in other cell types and neutrophil activation [225]. However, TH17 are not only linked to pathophysiology of UC. TH17 also display an important role in protection of the intestinal barrier function by promoting tight junction formation and antimicrobial peptides [226–229].

TH9. The knowledge of involvement of TH9 cells in UC is rather new, but only because TH9 cells were considered to be a subtype of TH2 cells. This TH type produces IL9 and is mainly induced by TGFβ and IL4 signalling (Figure 2) [230–232]. Firstly, TGFβ signalling can upregulate PU.1 which directly binds to the IL9 promotor [233, 234]. Secondly, IL4 signalling increases STAT6 expression, which induces Interferon Regulatory Factor (IRF) 4, a transcription factor that also binds to the IL9 promotor [235]. Thirdly, IL-25 can also stimulate IL9 production *in vivo* via NFκB binding [236–238]. In a TH9 T cell transfer experiment, TH9 cells were able to induce colitis in mice [230]. In an encephalomyelitis model TH9 transfer also aggravated disease progression and could be ameliorated with IL9 antibody treatment (Figure 1) [230, 239–241]. Contribution of IL9 and TH9 cells is reported for many inflammatory diseases like allergies, IBD, but also in diabetic heart disease and cancer [215, 242–244]. Nevertheless, TH9 cell can also promote Treg function and IL9 blocking showed an impaired Treg cell-mediated suppression in encephalomyelitis [245]. IL9 is upregulated in UC patients and promotes immune cell proliferation, as well as prevention of apoptosis [246]. IL9$^{-/-}$ mice are even protected from UC [246], whereas

elevated IL9 levels in UC patients are linked with poor prognosis [247]. Activated peripheral blood lymphocytes isolated from UC patients showed significant increase in IL9 production [248].

Treg. There is also a pivotal role for Tregs in UC. Regulatory T cells are the police officers in between all TH lineages. They control self-tolerance and immune cell homeostasis by controlling other T cells. Typical markers for Tregs are CD25 and Forkhead-Box-Protein P3 (FoxP3) (Figure 2) [249], but their phenotype can also differ from this "classical" type. These cells are highly dynamic and their surrounding microenvironment can shape their function and cytokine release [250]. In the gut, for example, Tregs are associated with C-C-Chemokine Receptor (CCR) 6, CD25, FoxP3 and RORγt expression, whereas in visceral adipose tissue FoxP3 and PPARγ are more dominant [251, 252]. IL6, IL1, TNFα and IL23 are mainly responsible for the high plasticity of those cells. Their main function to restrict other T cells is mediated by cytokines like TGFβ and IL10 that regulate T cell tolerance and IL35 that controls proliferation (Figure 2) [253, 254]. Many studies showed a reduced Treg population and/or Treg dysfunction in several colitis models [255–258]. Since the discovery of TH17 cells in 2005, more and more studies implicated an important role of TH17 and Treg balance in many diseases including IBD in general, UC and CRC (Figure 1) [259–262]. Some studies could show a TGFβ-dependent downregulation of TH17 cells in IBD [263, 264]. Surprisingly, FoxP3 expression is elevated in the mucosa of IBD patients, hinting at an attempt to restore TH17/Treg balance in the colon [265]. Researchers are now looking for ways to promote TH17/Treg balance. Tregs can be transferred adoptively to the colon to control IBD [266], but for that they need to be primed to home to the gut [267]. Other groups look for substances that can restore TH17/Treg balance like phytochemicals, e. g. parthenolide, stigmasterol or baicalein [268–271]. The balance of effector and regulatory T cells is immensely important for effective immunity and gained a lot of attention in recent studies. More and more Treg therapy and Treg transfer studies are conducted in order to reach new therapies.
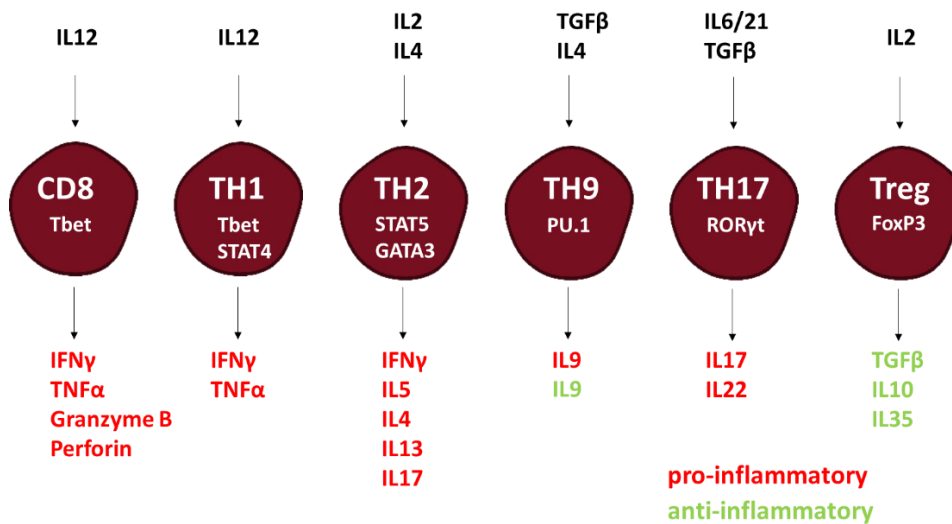
Figure 2: Different subtypes of T cells associated with UC. Different T cell subtypes that are linked to UC are depicted here including their activating cytokines, their major transcription factors and pro- or anti-inflammatory cytokine production profile. For more details, see text.

1.3 Sphingolipids

Sphingolipids (Sphs) are not only important structural elements of the eukaryotic cell membrane, but they are also involved in signalling pathways and in the formation of so-called lipid rafts that serve as signalling platforms for receptor and protein interactions at the plasma membrane. Since it is already known, that TCR signalling takes place in lipid rafts, it is necessary to elucidate and understand the role of Sphs and Sph metabolism in T cells and their function.

1.3.1 Structure and nomenclature

Sphs are one of the three most important classes of membrane lipids [272]. They consist of a sphingoid base that characterizes and defines the structural unit of the sphingolipid. The most common sphingoid base is sphingosine, which consists of 18 C-atoms (C18), two hydroxyl groups (d) and one double bond (:1) (d18:1). Phosphorylation of this molecule will build Sphingosine-1-phosphate (S1P), one of the best researched signalling lipid molecules of our times [273–278]. Ceramides (Cer) are formed through attachment of fatty acyl chain (FA) to the sphingoid bases. Cer are the simplest sphingolipids and can serve as precursors of the more complex sphingolipids, but they can also act in signalling and structural processes in the cell [279–281]. They can be build *de novo* or retrieved from already existing sphingolipids by various

enzymes. Their structure can differ in the amount of unsaturated or saturated bonds and also in the length of the FA chains that are bound to the sphingoid base. Both, the saturation status and the FA chain length determine the function and later fate of the respective Cer [280]. So-called long chain ceramides consist of 14 to 20 C-atoms. Very long-chain ceramides of 22 to 26 C-atoms and Cer with above 26 C-atoms are called ultra long-chain ceramides. The amount of C atoms in the FA chain of Cer is also described in the nomenclature, where the sphingoid base is placed first and the attached FA chain is described second (e.g. saturated C14 Ceramide with sphingosine as backbone is d18:1/14:0). Because Cer function as the backbones for more complex sphingolipids, they are the centre molecules of the sphingolipid metabolism. By attachment of different rest (R) groups to the primary hydroxyl group of the sphingosine, a variety of complex sphingolipids is obtained. For example, for sphingomyelin (SM) a phosphocholine R group is attached, whereas for glucosylceramides (GlcCer), lactosylceramides (LacCer) or galactosylceramides (GalCer) the respective sugar R group is added.

1.3.2 Sphingolipid Metabolism

De novo synthesis of Sphs occurs in the ER, where at first the serine palmitoyltransferase complex (SPT) condensates L-serine and palmitoyl-CoA to 3-ketosphinganine (Figure 3) [282–284]. This is followed by a reduction catalysed by 3-ketosphinganine reductase (3-KR) in order to get sphinganine, also called dihydrosphingosine. In the next step, Ceramidesynthases (CerS) covalently add a FA of a specific chain length (C_{4-32}) to the sphinganine forming dihydroceramide (dHCer) by N-acylation (Figure 3) [285, 286]. There are six different isoforms of CerS (CerS1-6), which are all responsible for different chain lengths, e.g. CerS3 use mainly C_{18-32} - FA [287]. After reduction of dhCer to Cer by dihydroceramide desaturase and their transport to the Golgi apparatus (Golgi), Cer can be further synthesized to more complex sphingolipids or act as a signalling molecule itself [288]. The transport to the Golgi is mediated by ceramide transfer protein (CERT) or vesicular trafficking [289, 290]. When Cer serve as a precursor for more complex Sphs, different enzymes can use Cer as a substrate to attach different R groups to the 1-hydroxyl residue. These more complex Sphs are produced in different compartments of the Golgi by SM

synthases, Uridine diphosphate (UDP)-glucose ceramide glucosyltransferases (UGCG) or glucosylceramide synthases (Figure 3) [291].

Cer can also be formed via the salvage pathway, where ceramides are obtained by constitutive degradation of SM or GlcCers at the plasma membrane or in endosomes and lysosomes (Figure 3) [292]. SMs and glycosphingolipids are hydrolytically released from the membranes and then subsequently degraded by acid sphingomyelinase (aSMase) [293]. Afterwards, ceramides are then degraded to sphingosine by acid ceramidase (aCDase) [294].
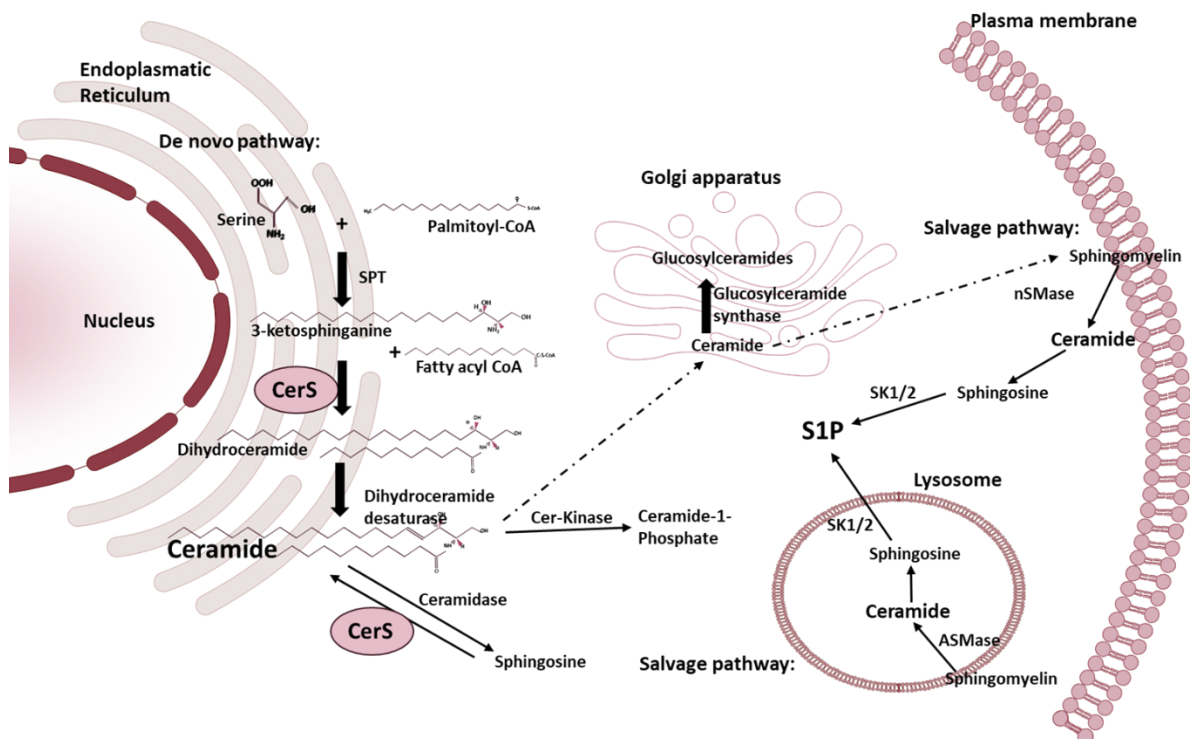
Figure 3: Sphingolipid *de novo* and salvage pathway depicted in their cellular compartment. Enzymatic reactions are displayed with black arrows, transportation is depicted with a punctured arrow. Abbreviations and references are mentioned in the text. Adapted from Hartel et al. [295].

1.3.3 Role of Ceramidesynthases

The production of Cer is the key step of Sph metabolism (Figure 3) [296]. Because CerS are involved in the production of Cer, their regulation and activity is crucial to the Sph pathways [297]. CerS are responsible for the N-acylation of FA to sphinganine to produce dhCer, but CerS can also produce Cer directly, if they use sphingosine as a substrate. CerS reside in the ER membrane. Human CerS proteins are encoded in the Longevity assurance genes (Lass) [285]. The six isoforms of CerS display a unique

specificity towards FA of varying chain lengths (Figure 4). CerS1 has a specificity towards C_{18}, CerS2 to C_{20-26}, CerS3 to C_{18-32}, whereas CerS4 generates C_{18-20} ceramides, CerS5 add C_{16} FA to dHCer and CerS6 favours C_{14-16} (Figure 4). CerS are expressed in every tissue, but not homogenously [287]. In leukocytes, for example, CerS2 and CerS4 expression is very high, and CerS3 can pre-dominantly be found in testis, prostate and skin tissue. CerS1 expression is very high in brain tissue, whereas CerS5 levels are high in prostate and skeletal muscle tissue. CerS6 show high mRNA levels in the intestine, lymph nodes, thymus and spleen. The different tissue expression pattern of CerS hints at their own and their products differing functions, but also at the importance of the right balance of CerS expression throughout the tissue.

The importance of a balanced CerS expression can be shown with a few examples for CerS1 and 3.

C_{18}-Cer is mainly produced *de novo* by CerS1 and is highly distributed throughout the central nervous system. Overexpression of CerS1 in glioma cells leads to an accumulation of C_{18}-Cer and subsequent cell death by induction of apoptosis [298]. Mutation in the CerS1-gene is also linked with progressive myoclonic epilepsy (PME), a group of conditions defined by uncontrolled muscle contraction (myoclonus) and seizures [299].

CerS3 knockout (KO) in mice is lethal and mutation in the CerS3 gene in humans cause autosomal recessive congenital ichthyosis, a rare genetic disorder of the skin characterized by abnormal skin scaling over the patient's whole body [300–302]. CerS expression is affected by transcriptional, posttranscriptional and –translational mechanisms, but there is no profound knowledge about those regulatory processes. It is assumed that Phospho Kinase C (PKC) activation can increase *de novo* synthesis of Cer and some CerS could be phosphorylated [303].
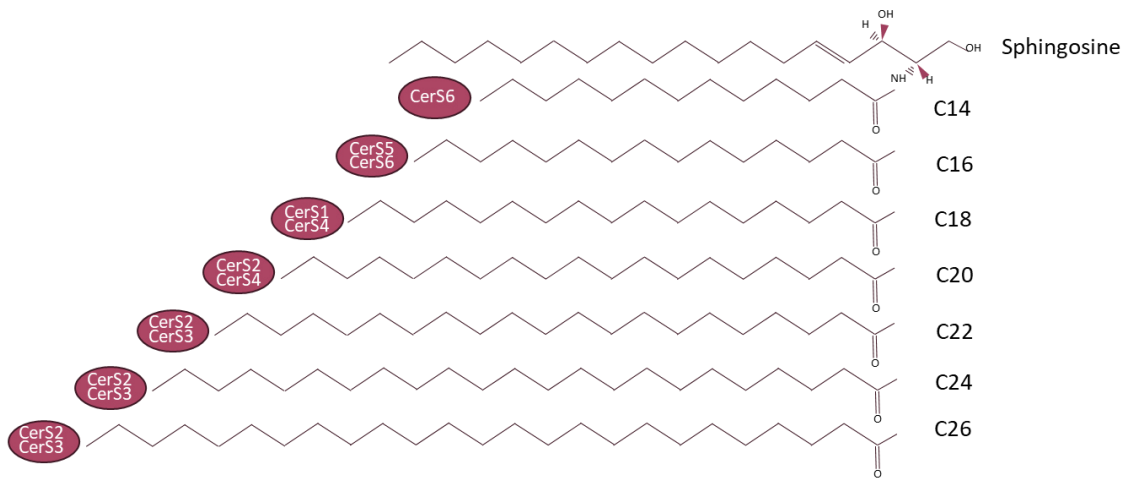
Figure 4: Structure of ceramides with different chain lengths and their responsible CerS. Sphingosine serves as sphingoid base and CerS attach a FA of specific chain length to sphingosine to obtain Cer.

1.3.4 Functions of Sphingolipids

Plasma membranes contain many different lipid species and depending on the cell type and cell organelle, the composition of these lipids can differ greatly. There are at least 300 different Sph species that are important structural elements of plasma membranes, but also other organelle's membranes [304]. They can directly influence physico-chemical properties of membranes. Order and composition of different sphingolipids in membranes is strictly balanced. The membrane system is highly dynamic and in this dynamic nature every little change can disturb certain functions. When Cer are incorporated into the membrane, the fluidity can be influenced depending on their chain length. Membrane fluidity increases when C_{16}-Cer is increased and/or $C_{24:0}$-Cer, $C_{24:1}$-Cerand C_{22}-Cer is decreased [280]. Ceramides can also have an impact on acyl chain orders within the membrane, thereby affecting membrane stability. Membrane stability is also indirectly affected by permeability changes. Increased SMase activity reduces SM and increases Cer in the plasma membrane, leading to impairment of integrin adhesion and reduction of protein mobility [305]. When Cer is upregulated in the plasma membrane, the membrane gets more permeable to water-soluble solutes [306, 307]. The specific composition of membranes can have an effect on bilayer thickness. Transition of different lipid molecules from the inside to the outside, and vice versa (flip-flop), alters outer and inner membrane leaflets and can be induced by Cer [308].

1. Introduction

In the skin, for example, ultra long-chain ceramides ($C_{30\text{-}32}$-Cer) contribute to a good barrier function. In the intercellular matrix of the stratum corneum, ceramides make up 40 to 50 % of all intercellular lipid molecules. Ceramides in this matrix do not form a typical bilayer. Instead they form multilamellar membranes. Lateral packing of this lipids into an orthorhombic shape makes these multilamellar membranes very tight and provide good barrier function [309]. Decrease of Cer in this matrix is linked to dry skin in atopic dermatitis [310]. It is proposed that the orthorhombic order of lipids changes into a more hexagonal style, which leads to more space between the molecules, ergo providing more permeability into the matrix structure [311]. Not only order, but also composition of Cer is important for their function, e.g. it is also known that in atopic dermatitis patients there is a reduction of lipids with ultra long-chain lengths which also contributes to reduced skin barrier function [312, 313].

As they are crucial elements of the plasma membrane, sphingolipids also play a part in vesicle formation [314–316]. Extracellular vesicle formation is an important mechanism for the release of different proteins, cytokines and chemokines, respectively [317]. Extracellular vesicle release can be linked to a variety of diseases including neurodegenerative, renal, cardiovascular and respiratory diseases [315, 318–320]. It is supposed that the breakdown of SM to Cer is a key step in extracellular vesicle formation [321, 322]. This process is highly regulated and there is also evidence that extracellular vesicle lipid composition differs from the origin's cell lipid composition [323].

Sphingolipids can also assemble in a specific order and composition and form micro-domains at the plasma membrane: lipid rafts [324, 325]. Lipid rafts were first officially defined at the Keystone Symposium on Lipid Rafts and Cell Function in 2006 as "small (10-200nm) heterogeneous, highly dynamic, sterol- and sphingolipid-enriched domains". Since then, the understanding of lipid raft has grown profoundly. They consist of 30 to 40 % cholesterol and 10 to 30 % sphingolipids [326]. Lipid rafts are organized in order to get receptors and proteins closer together for signalling pathways and protein-protein interactions. Proteins that are localized in lipid rafts are often post-translationally modified, for example via glycosylphosphatidylinositol (GPI) anchors or via palmitoylation (covalent attachment of C_{16} to the protein) [327–329]. The post-translational modifications are not obligatory for proteins to reside in lipid rafts, but rather facilitate intracellular translocation and subsequent translocation to the plasma

membrane [330–333]. Clustering of lipids and proteins in the membrane enables different signalling pathways to function. For TCR signalling, co-localization of lymphocyte-specific protein tyrosine kinase (LCK) and linker for activation of T cells (LAT) in lipid rafts is very important [334]. T cell activation is only possible if respective proteins are organized in lipid rafts [335]. S1P signalling is also dependent on lipid rafts [336]. S1P Receptor (S1PR) localization in lipid rafts is also important for S1PR function and for its further downstream signalling [337, 338].

As already mentioned, sphingolipids can also act as bioactive molecules [339]. Cer and S1P as bioactive molecules are very well understood. Cer can directly interact with other proteins, C_{18}-Cer, for example, has an impact on the SET protein (also known as inhibitor 2 of protein phosphatase 2 A), reducing the interaction of SET with protein phosphatase 2 A (PP2A) [340]. PP2A interferes with Wingless/Integrated (Wnt)-, mammalian target of Rapamycin (mTOR)- and MAPK pathway, but also in cell cycle processes [341–344]. When S1P binds to S1P1, phosphorylation of the receptor and subsequent internalisation is triggered [345]. Downstream effects of S1PR activation are cell migration, proliferation and differentiation, especially in T cells [346–348].

1.3.4 Sphingolipids in UC

Considering the functions of Sphs in so many signalling pathways, the importance of the role of sphingolipids in diseases becomes obvious. Sphingolipid levels are altered throughout every kind of disease, especially in the case of IBD.

In these diseases, lipopolysaccharide (LPS) from gram-negative bacteria can stimulate aSMase activity in macrophages, thereby increasing Cer levels [349]. Increased Cer levels can lead to a disrupted epithelial barrier function because of an accumulation of Cer in junctional complexes, thereby reducing cholesterols and their stability [350]. *De novo* synthesis of Sphs is essential for barrier integrity. Loss of SPT leads to a decrease in goblet cells and mucin and increases LPS in the gut [351]. ASMase activity seems to have an unclear role in colitis. While inhibition of aSMase in macrophages reduces severe colitis and shows less TNFα release [352], aSMase KO in mice increases TH1 and TH17 differentiation and showed more bacteria in the gut [353]. These findings support the hypothesis that a balance of Sph species in different tissues and cells is important.

It has become evident, that chain length of Cer contribute to their function. C_{16}-Cer accumulation, either by *de novo* synthesis via CerS or the salvage pathway, has a great impact on apoptosis induction [354, 355]. Not only C_{16}–Cer accumulation is beneficial for apoptosis induction, but also C_{18}-Cer accumulation [298, 356]. Long-chain ceramides ($C_{16/18}$-Cer) contribute to apoptosis, while very long-chain $C_{24:0}$- and $C_{24:1}$-Cer show a pro-proliferative effect, which cancer cells often benefit from [357]. Short-chain Cer, like C_6- or C_8-Cer are responsible for destabilization of membranes and increase of membrane permeability [358]. In a DSS-induced colitis model of CerS2 KO mice there was a reduction of very long- ($C_{24:0/1}$-Cer) and long-chain Cer in plasma and colon of the mice, that were more susceptible to DSS treatment [359]. CerS6 deficient mice showed less C_{16}-Cer and S1P in colon tissue and showed more severe colitis compared to the control [360] and CerS5 KO in mice exacerbated DSS-induced colitis symptoms [361].

Human *in vitro* data showed that dietary gangliosides, like GD3, are important for epithelial barrier function in the gut [362]. A colon-epithelial cell line (Caco-2) was treated with GD3 and Miklavcic et al. showed inhibited NFκB activation in those cells as well as improved barrier function with enhanced tight junction integrity [362]. In a big lipid screen of UC patients, it could be shown that C_{16}- and C_{24}-LacCer are enhanced in colon samples, while C_{16}-, $C_{24:0}$- and $C_{24:1}$–dhCer are decreased [363]. S1P levels in the blood of these patients are decreased and dhCer are increased [363]. A recent study also managed to find increased C_{16}-LacCer levels in the blood of children with IBD compared to healthy controls, indicating a possible role for C_{16}-LacCer as a new plasma marker for IBD [364].

In conclusion, it is very clear that Sphs display an important role in the pathophysiology of UC and therefore are potential targets for new therapeutic approaches.

1.3.5 Sphingolipids in T cells

T cells have been established as major drivers of UC for a long time. Uncontrolled T cell activity and imbalance between regulatory end effector subtypes are characteristic for disease progression. As Sphs are enriched in lipid rafts and indispensable for their formation, it is quite obvious that there is an involvement of Sph in T cell activation. The TCR itself and LCK are both located in lipid rafts and their recruitment into those

micro-domains is essential for TCR signalling [365].The CD28 assembly in lipid rafts was also shown to be necessary for optimal TCR signalling [366] and PKC θ activity depends on its translocation to the lipid rafts effecting the following NFκB pathway [367].

Interfering with the lipid order by aSMase 2 deletion in mice leads to a reduced T cell activation [368]. In another aSMase$^{-/-}$ model impaired T cell function and enhanced tumor burden could be observed [369]. Overexpression of aSMase promoted TH1 differentiation and showed reduced Tregs in *Plasmodium yoelii* infection, as well as enhanced TCR signalling [370]. Pharmacological inhibition of aSMase with anti-depressants in patients suffering from depression leads to more Tregs in the blood [371, 372]. These findings indicate an important role for aSMase activity in T cells and display an opportunity for therapeutic approaches [373].

Sphs are also able to interfere with T cell development and differentiation. In FoxP3$^+$ T cells, SM Synthase (SMS) 1 synthase is reduced and leads to increased Cer levels [374]. C_{18}-Cer interacts with the SET protein and leads to a reduced SET and PP2A interaction enhancing PP2A activity [374]. PP2A inhibits mTOR-dependent Akt pathway, which is very important for Treg development [374]. Downregulation of UGCG in a DSS induced colitis model in mice leads to GlcCer reduction in T cells and a reduction of Tregs proposing a vital role of GlcCer in Tregs [375]. This is supported by the findings that treatment of UGCG$^{-/-}$ mice with GlcCer in nanoparticles leads to a prevention of DSS-induced colitis [375]. Gangliosides and LacCer are enhanced during TH17 development and Ganglioside synthase 3 (GM3S) deletion inhibited differentiation of TH17 cells, demonstrating the importance of gangliosides in TH17 development [376, 377]. As TH17 differentiation highly depends on TGFβ and IL6 signalling, the association of Sph in lipid rafts is of great interest, because both TGFβR and IL6R signalling depend on lipid raft localization [378–380].

In 2017, Sofi et al. showed that CerS6 was required for T cell activation, especially for Zap70 phosphorylation [381]. They also demonstrated that CerS6 regulates ERK signalling in T cells and pharmacological inhibition of CerS6 blocked T cell migration into the organs thereby preventing Graft vs. Host disease (GvHD), a systemic inflammation caused by uncontrolled T cell activation that occurs after allogenic cell transplantations [382, 383]. Moreover, we could show that CerS5 downregulation in a CD4$^+$ Jurkat cell line leads to impaired T cell signalling [361]. Depletion of CerS4 in T

cells prolonged cytokine release and enhanced tumor-burden in an azoxymethane (AOM)/DSS CRC model in mice [384]. Downregulation of CerS4 in Jurkat cells resembled the activated status of control cells and lead to a steady-state activity of T cells without any further stimulus [384].

T cell migration is heavily dependent on S1P signalling [347]. S1P can bind to the G-coupled receptors S1P1-5 and activate signalling cascades that promote survival, proliferation and, for S1P1, lymphocyte trafficking [385]. A specific S1P gradient exists between lymph organs, blood and tissues. T cells mainly express S1P1 and 4 [386]. High concentrations of S1P in the thymus together with low concentrations in the blood will inhibit T cells to migrate from the thymus to the blood. If concentration gradient switches, so there is a high concentration of S1P in the blood and low concentration in the thymus, T cells will exit the thymus and migrate towards the S1P gradient. S1P plasma concentrations range from 0.1 µM to 0.8 µM [387]. Sph Kinases (SphK) maintain high S1P levels in blood, whereas low S1P concentration in lymphoid organs is regulated by S1P lyase activity [388]. Upon S1P binding to the S1PR, S1PR is internalized and only expressed again on the surface, when S1P levels in the environment drop [385]. T cells with internalized S1PR are unresponsive to S1P signals. S1P-dependent lymphocyte egress is promoted by CCR7 expression on the surface, which will be downregulated once the TCR is activated which leads to more T cell migration [389]. Desensitization of S1PR is very important for S1P1 signalling and incomplete S1PR internalization promotes TH17 dependent autoimmune neuro inflammation [386]. Deletion of S1PR in Tregs led to autoimmunity in a MS model [390].

In summary, Sphs are involved in T cell development, differentiation and function in many different ways and therefore are also included in UC disease progression. Sphs and their metabolism should be considered possible new therapeutic targets in UC treatments.

1.4 Objectives

The aim of this dissertation was to study the role of CerS and their products in T cell function as well as their contribution to disease progression in order to find new therapeutic targets for UC treatment. Preliminary work showed a significant impairment of TCR signalling in CerS5 Knockdown Jurkat cells and an activated state of CerS4 knockdown Jurkat cells without any stimulus [361, 384]. CerS3 and CerS1 expression were significantly increased in the white blood cells from human colitis patients [363].

To investigate the role of CerS1 and CerS3 in T cell function, the following questions were considered in my dissertation:

1) Does CerS1 and CerS3 influence TCR activation and signalling, migration and cytokine release in T cells?

For this question stable knockdown and overexpression of CerS1 and CerS3 were established in a CD4$^+$ cell line (Jurkats) *in vitro*. Knockdown and overexpression cells were stimulated and the CerS mRNA expression pattern, as well as sphingolipid contents after activation were measured. TCR signalling and downstream pathways were analysed and the proliferation, migration and cytokine release profile of cells were assessed. To confirm *in vitro* cell line findings, primary human T cells were isolated from healthy donors. For knockdown of CerS3, primary T cells were treated with siRNA. Afterwards CerS mRNA expression after stimulation was checked, as well as cytokine release and migration capacity.

2) Does CerS3 have an impact on DSS-induced colitis in mice?

To elucidate the role of CerS3 in colitis, a DSS-induced acute colitis model in mice with a T cell specific knockout of CerS3 was conducted. Disease progression, weight changes, colon length and tissue immune cell distribution in mice *in vivo* as well as murine T cell differentiation and effector function *ex vivo* were assessed.

3) Does CerS3 affect T cell adhesion and migration in a human IBD model?

For confirmation of murine *in vivo* data, an organ-on-a-chip model for the intestine was established. A chip, containing a top and a bottom channel that are connected in the middle via a porous (7 µm) membrane, was prepared with colon epithelial cells (Caco-2) in the top, and with endothelial cells (Human umbilical vein endothelial cells (HUVEC)) in the bottom channel to mimick colon tissue. The bottom chamber was

perfused with either CerS3 knockdown or control Jurkat T cells to observe migration of T cells into the epithelial barrier, as well as adhesion to the endothelium.

2. Materials

2.1 Chemicals and Reagents

Table 3 in the following section lists all chemicals and reagents used (for this dissertation).

Table 3: Chemicals and Reagents with their respective manufacturers

Chemical/ Reagent	Manufacturer
100 bp DNA ladder	Invitrogen, Waltham, USA
2-Propanol (Isopropanol)	Carl Roth GmbH & Co. KG, Karlsruhe, Germany
4-(2-hydroxyethyl)-1-piperazineethanesulfonic acid (HEPES)	Gibco® by Life Technologies, Carlsbad, USA
5X siRNA Buffer	Horizon Discovery, Waterbeach, UK
7-amino-actinomycin D solution (7AAD)	Miltenyi Biotec GmbH, Bergisch Gladbach
Accell Green non-targeting siRNA	Horizon Discovery, Waterbeach, UK
Accell SMARTpool CerS3 siRNA	Horizon Discovery, Waterbeach, UK
Acrylamide solution	BioRad, Feldkirchen, Germany
Agarose	VWR, Radnor, USA
Ammonium chloride (NH_4Cl)	Carl Roth GmbH & Co. KG, Karlsruhe, Germany
Ammonium persulfate (APS)	Carl Roth GmbH & Co. KG, Karlsruhe, Germany
Ampicillin-salt	Sigma-Aldrich, Deisenhofen
Basal media for large human endothelial cells	Gibco® by Life Technologies, Carlsbad, USA
Basic Fibroblast growth factor (bFGF)	PELOBiotech, Planegg, Germany
Bi-sodiumhydrogenphosphate (Na_2HPO)	Carl Roth GmbH & Co. KG, Karlsruhe, Germany
Bovine Serumalbumine (BSA)	Sigma-Aldrich, Deisenhofen, Germany
Bradford Reagent	Sigma-Aldrich, Deisenhofen, Germany
Bromphenol blue	Sigma-Aldrich, Deisenhofen, Germany
Calcium-Chloride ($CaCl_2$)	Sigma-Aldrich, Deisenhofen, Germany
CBA Flex Set IFNγ, human	BD Biosciences, San José, USA
CBA Flex Set IFNγ, mouse	BD Biosciences, San José, USA
CBA Flex Set IL-10, mouse	BD Biosciences, San José, USA
CBA Flex Set IL-17, human	BD Biosciences, San José, USA
CBA Flex Set IL-17, mouse	BD Biosciences, San José, USA
CBA Flex Set IL-4, mouse	BD Biosciences, San José, USA
CBA Flex Set IL-6, human	BD Biosciences, San José, USA
CBA Flex Set IL-6, mouse	BD Biosciences, San José, USA
CBA Flex Set TNFα, human	BD Biosciences, San José, USA
CBA Flex Set TNFα, mouse	BD Biosciences, San José, USA
CellTrace™ Violet Proliferation Kit	Invitrogen, Waltham, USA

2. Materials

Chloroform	Honeywell, Offenbach, Germany
Chloroquine	Sigma-Aldrich, Deisenhofen, Germany
Collagene Type I	Sigma-Aldrich, Deisenhofen, Germany
Dextran Sodium Sulfate (DSS), colitis grade	MP Biomedicals, Canada
Digitonin	SERVA Electrophoresis GmbH, Heidelberg, Germany
Dimethyl sulfoxide (DMSO)	Carl Roth GmbH & CO. KG, Karlsruhe, Germany
Dithiothreitol (DTT)	AppliChem GmbH, Darmstadt, Germany
D-Sucrose	Sigma-Aldrich, Deisenhofen, Germany
Dulbecco's Phosphate-Buffered Saline, 1X (DPBS)	Gibco® by Life Technologies, Carlsbad, USA
Dulbecco's Modified Eagle Medium (DMEM) + GlutaMax I + 4.5 g/l D-glucose	Gibco® by Life Technologies, Carlsbad, USA
Dulbecco's Modified Eagle Medium (DMEM) Advanced	Gibco® by Life Technologies, Carlsbad, USA
Dynabeads Mouse T Activator CD3/CD28 for T cell expansion and activation	Gibco® by Life Technologies, Carlsbad, USA
Endothelial cell basal medium (ECBM)	PELOBiotech, Planegg, Germany
Endothelial Growth Factor (EGF)	PELOBiotech, Planegg, Germany
ER-1	Emulatebio, Boston, USA
ER-2	Emulatebio, Boston, USA
Essential Amino Acids (EAA)	Gibco® by Life Technologies, Carlsbad, USA
Ethanol, 70%	Carl Roth GmbH & Co. KG, Karlsruhe, Germany
Ethanol, absolute	Sigma-Aldrich, Deisenhofen, Germany
Ethylene glycol-bis(β-aminoethyl ether)-N,N,N′,N′-tetraacetic acid (EGTA)	Carl Roth GmBH & Co. KG, Karlsruhe, Germany
Ethylenediaminetetraacetic acid (EDTA)	Sigma-Aldrich, Deisenhofen, Germany
Fatty Acid Free BSA	Carl Roth GmbH & Co. KG, Karlsruhe, Germany
Fetal Bovine Serum (FBS)	Gibco® by Life Technologies, Carlsbad, USA
Fluorescence Activated Cell Sorting (FACS) flow buffer	BD Biosciences, San José, USA
Fura-2 AM Ester	Biotium, San Francisco, USA
GelzanTM CM (low acyl gellan gum)	Sigma-Aldrich, Dreisenhofen, Germany
GeneJuice® Transfection Reagent	Sigma-Aldrich, Deisenhofen, Germany
Glacial acetic acid	Merck KGaA, Darmstadt, Germany
Glutamax	Gibco® by Life Technologies, Carlsbad, USA
Glutamin	PELOBiotech, Planegg, Germany
Glycerine	Janssen Pharmaceutical, Beerse, Belgium
Glycine	Carl Roth GmbH & Co. KG, Karlsruhe, Germany
GT KAPA Mix	Roche Sequencing, Madison, USA

Hank's balanced salt solution (HBSS)	Gibco® by Life Technologies, Carlsbad, USA
HBSS without Ca^{2+} or Mg^{2+}	Gibco® by Life Technologies, Carlsbad, USA
Hemacolor Kit	Sigma, Deisenhofen, Germany
Heparin	PELOBiotech, Planegg, Germany
Human TNF OPTI-enzyme-linked immunoassay (ELISA) Set	BD Biosciences, San José, USA
Hydrocortisone	PELOBiotech, Planegg, Germany
Hydrogen Peroxide (H_2O_2)	BD Biosciences, San José, USA
Kanamycin-salt	Carl Roth GmbH & Co. KG, Karlsruhe, Germany
Lamina Propria (LP) Dissociation Kit, mouse	Miltenyi Biotec GmbH, Bergisch Gladbach, Germany
Large Vessel Endothelial Supplement (LVES)	Gibco® by Life Technologies, Carlsbad, USA
Lennox broth (LB)- Medium	Carl Roth GmbH & Co. KG, Karlsruhe
Long R3 Insulin Like Growth Factor 1 (R3-IGF-1)	PELOBiotech, Planegg, Germany
Magnesium chloride ($MgCl_2$)	Carl Roth GmbH & Co. KG, Karlsruhe, Germany
Matrigel	Corning, New York, USA
Methanol	Sigma-Aldrich, Deisenhofen, Germany
Milk powder	Sigma-Aldrich, Deisenhofen, Germany
Neomycin (G418/Geneticin)	Invivogen, San Diego, USA
Non-Essential Amino Acids (NEAA)	Gibco® by Life Technologies, Carlsbad, USA
Octoxinol 9 (NP40)	Roche Diagnostics Deutschland GmbH, Mannheim, Germany
ORA™ SEE qPCR Green ROX L Mix 2X	HighQu GmbH, Kraichtal, Germany
Penicillin and Streptomycin-solution (P/S)	Gibco® by Life Technologies, Carlsbad, USA
Percoll	Sigma-Aldrich, Deisenhofen, Germany
Phentylmethylsulfonylfluorid (PMSF)	Carl Roth GmbH & Co. KG, Karlsruhe, Germany
Phosphoric acid (H_3PO_4)	Sigma-Aldrich, Deisenhofen, Germany
PhosphoSafe™	Extraction Reagent EMD Biosciences Inc., Darmstadt, Germany
PKH26 red fluorescent dye	Sigma-Aldrich, Deisenhofen, Germany
PKH67 green fluorescent dye	Sigma-Aldrich, Deisenhofen, Germany
Polyethylene glycol (PEG)-it	SBI System Biosciences, Palo Alto, USA
Ponceau S	Carl Roth GmbH & Co. KG, Karlsruhe, Germany
Potassium chloride (KCl)	Honeywell, Offenbach, Germany
Potassiumdihydrogenphosphate (KH_2PO_4)	Carl Roth GmbH & Co. KG, Karlsruhe, Germany
Potassiumhydrogencarbonate ($KHCO_3$)	Carl Roth GmbH & Co. KG, Karlsruhe, Germany
Precision Plus Protein™ Standards, Dual Color	Bio-Rad, Munich, Germany
Puromycin	InvivoGen, Toulouse, France
QIAGEN Plasmid Maxi Kit	Qiagen GmbH, Hilden, Germany

2. Materials

Recombinant, human G protein-coupled receptor 15 ligand (GPR15L)	Prepotech, Hamburg, Germany
Recombinant, human IL-15	Prepotech, Hamburg, Germany
Recombinant, human IL-2	Prepotech, Hamburg, Germany
Recombinant, human IL-7	Prepotech, Hamburg, Germany
Recombinant, human Interferon gamma induced protein (IP10)	Prepotech, Hamburg, Germany
Recombinant, human macrophage inflammatory protein 3 alpha (MIP-3α)	Prepotech, Hamburg, Germany
Recombinant, human monocyte chemoattractant protein 1 (MCP-1)	Prepotech, Hamburg, Germany
Recombinant, human mucosae associated epithelia chemokine (MEC)	Prepotech, Hamburg, Germany
Recombinant, human stromal cell-derived factor 1 (SDF-1α)	Prepotech, Hamburg, Germany
Recombinant, human TGFβ	Prepotech, Hamburg, Germany
Recombinant, human thymus-expressed chemokine (TECK)	Prepotech, Hamburg, Germany
Recombinant, human TNFα	Prepotech, Hamburg, Germany
Recombinant, mouse IFNγ	Prepotech, Hamburg, Germany
Recombinant, mouse IL-12	Prepotech, Hamburg, Germany
Revert700 Total Protein Stain	BioRad, Feldkirchen, Germany
RNeasy Mini Kit	Qiagen GmbH, Hilden, Germany
Roche cOmplete™, Mini, Protease Inhibitor Cocktail tablets	Roche Diagnostics Deutschland GmbH, Mannheim, Germany
Roswell Park Memorial Institute + Glutamax Media (RPMI)	Gibco® by Life Technologies, Carlsbad, USA
Roti®-Safe GelStain DNA binding fluorescence dye	Carl Roth GmbH & Co. KG, Karlsruhe, Germany
RPMI powder, HEPES	Gibco® by Life Technologies, Carlsbad, USA
Serum-free Delivery Media siRNA	Horizon Discovery, Waterbeach, UK
SEW2871	Tocris, Bristol, UK
Sodium azide	Carl Roth GmbH & Co. KG, Karlsruhe
Sodium chloride (NaCl)	Sigma-Aldrich, Deisenhofen, Germany
Sodium dodecyl sulfate (SDS)	Carl Roth GmbH & Co. KG, Karlsruhe
Sodium pyruvate	Gibco® by Life Technologies, Carlsbad, USA
Sodiumcarbonate (Na$_2$CO$_3$)	Sigma-Aldrich, Deisenhofen, Germany
Sodiumhydrogencarbonate (NaHCO$_3$)	Sigma-Aldrich, Deisenhofen, Germany

Sphingosine-1-phosphate (S1P) for $[Ca2+]_i$ measurement	Sigma Aldrich, Dreisenhofen, Germany
Sphingosine-1-phosphate (S1P) for migration assay	Cayman Chemicals, Ann Arbor, USA
StraightFrom® Buffycoat REAlease® CD4 MicroBeads, human	Miltenyi Biotec GmbH, Bergisch Gladbach, Germany
StraightFrom® Buffycoat REAlease® CD8 MicroBeads, human	Miltenyi Biotec GmbH, Bergisch Gladbach, Germany
SybrSelect	ABgene Limited, Epsom, UK
T cell Activation/Expansion Kit, human	Miltenyi Biotec GmbH, Bergisch Gladbach, Germany
Tetramethylbenzidine (TMB)	BD Biosciences, San José, USA
TexMACS Medium	Miltenyi Biotec GmbH, Bergisch Gladbach, Germany
TissueTek O.C.T.	Sakura Fintek, Umkirch, Germany
Trichloroacetic acid (TCA)	Carl Roth GmbH & Co. KG, Karlsruhe, Germany
TRI-Reagent Set	Sigma- Aldrich, St. Louis, USA
Tris	Carl Roth GmbH & Co. KG, Karlsruhe, Germany
Tris Base	AppliChem GmbH, Darmstadt, Germany
Trypanblue solution 0.4%	Sigma-Aldrich, Deisenhofen, Germany
Trypsin-EDTA, 0.05% (1X)	Gibco® by Life Technologies, Carlsbad, USA
Tween® 20	AppliChem GmbH, Darmstadt, Germany
Vascular Endothelial Growth Factor (VEGF)	PELOBiotech, Planegg, Germany
Verso cDNA Synthesis Kit	Thermo Scientific, Waltham, USA
β-Mercaptoethanol	Sigma-Aldrich, Deisenhofen, Germany

2.2 Buffers and Media

Table 4 lists all buffers that are described in the Methods section

Table 4: Buffers/Media and their respective recipes

Buffer/Media	Recipe
10X Erythrocyte's lysis Buffer	89,9 g NH_4Cl 10g $KHCO_3$ 370 g EDTA 7,3 pH Ad 1 l H_2O
10X SDS	30 g TrisBase 150 g Glycine 10 g SDS

2. Materials

	Ad 1 l H_2O
1X PBS	14 mM NaCl, 1 mM KCl, 0.64 mM Na_2HPO, 0.2 mM KH_2PO_4
2X RPMI Medium	390 ml water to a packet of RPMI powder media for 1 l 1 g Sodium bicarbonate 100 ml FBS pH to 6.8 to 7.1 (after filtration, media has a pH of 7 to 7.4) Filter through 0.2 µm filter
Antibody Buffer	PBS 3 % BSA
Assay Diluent	PBS + 10 % FBS
Bandshift Lysis Buffer	10 mM Tris-HCl pH7.4 10 mM NaCl 3 mM $MgCl_2$ 1 mM PMSF
Blocking Buffer	PBS 5 % Milk powder
Buoyancy medium	1.6 % v/v Gelzan solution in Percoll (1.6 ml Gelzan in 98.4 ml Percoll) Heat for 30 min at 37 °C De-Gas with Steriflip without turning the filter around
CBA Buffer	PBS 0.05 % FBS 0.09 % sodium azide
Coating Buffer	7.13 g $NaHCO_3$ 1.59 g Na_2CO_3 1 l H_2O pH 9.5
Digestion Buffer	HBSS 5 % FBS
Endothelial Cell Basal Medium (ECBM) + supplements	500 ml ECBM Medium w/o Glutamine + 1 vial Hydrocortisone +1 vial Heparin +1 vial EGF +1 vial VEGF +1 vial bFGF +1 vial R3-IGF-1
FACS Flow	PBS

	0.5 % FBS
Gelzan solution	1 % w/v GelzanTM
HBSS + Ca^{2+}	118 mM NaCl
	5 mM KCl
	1 mM CaCl$_2$
	1 mM MgCl$_2$
	5 mM D-glucose
	15 mM HEPES
	pH 7.4
Laemmli Buffer (Laemmli 1970)	50 mM Tris
	384 mM Glycine
	0. 1 % [w/v] SDS
	0.01 % Bromphenol blue
	20 % (v/v) β-Mercaptoethanol
LB Medium	20 g LB-Medium
	1 l H$_2$O
MACS Separation Buffer	PBS
	0,5 % FBS
	2 mM EDTA pH 7.5
Nucleus Lysis Buffer I	20 mM HEPES pH 7.4
	600 mM KCl
	0,2 mM EDTA
	2 mM DTT
	1 mM PMSF
Nucleus Lysis Buffer II	20 mM HEPES pH 7.4
	0,2 mM EDTA
	2 mM DTT
	1 mM PMSF
PB Buffer	PBS
	0.5 % FBS
PBST	1X PBS
	1 % Tween20
PhosphoSafe Mix	PhospoSafe™Extraction Reagent,
	Roche Complete™ Protease Inhibitor Cocktail, 7X in H$_2$O,
	DTT 2mM
Pre-Digestion Buffer	HBSS (without Ca^{2+} or Mg^{2+})
	5 mM EDTA
	5 % FBS
	1 mM DTT
Revert Wash Buffer	6.7 % (v/v) glacial acetic acid

2. Materials

	30 % (v/v) Methanol in H_2O
TNF ELISA Wash Buffer	PBS + 0.05% Tween20
TRI reagent (bought from Sigma-Aldrich, St. Louis, USA)	0.4 M Ammoniumthiocyanate 0.8 Guanidiumthiocyanate 0.1 M Sodium acetate 5 % Glycerin 1 kg Phenol Acetic acid 2.6 l H_2O
Wet Blot Buffer	15.5 g Tris base 72 g Glycine 1 l Methanol 4 l H_2O

2.3 Primers

Table 5 lists all primers that were used in qRT-PCRs and genotyping experiments.

Table 5: Primers and their nucleotide sequence.

Primer	Sequence
CerS1_for	5'-CCTCCAGCCCAGAGAT-3'
CerS1_rev	5'-AGAAGGGGTAGTCGGTG-3'
CerS2_for	5'-CCAGGTAGAGCGTTGGTT-3'
CerS2_rev	5'-CCAGGGTTTATCCACAATGAC-3'
CerS3_for	5'-CCTGGCTGCTATTAGTCTGAT-3'
CerS3_rev	5'-GCAAGGATTTCAAGGAGAG-3'
CerS4_for	5'-GCAAGGATTTCAAGGAGAG-3'
CerS4_rev	5'-AACAGCAGCACCAGAGAG-3'
CerS5_for	5'-CAAGTATCAGCGGCTCTGT-3'
CerS5_rev	5'-ATTATCTCCCAACTCTCAAAGA-3'
CerS6_for	5'-ATTATCTCCCAACTCTCAAAGA-3'-3'
CerS6_rev	5'-AATCTGACTCCGTAGGTAAATACA-3'
L3_for	5'-ACATATCTCCCTTTGCCCTGATG– 3'
L3_rev	5'-ATAATTGCAAGAGACGGCAATGA– 3'
LCK A_for	5'-CACGTGGGCTCCAGCATT-3'
LCK B_rev	5'-TCACCAGTCATTTCTGCCTTTG-3'
LCK_for	5'-CAGTCAGGAGCTTGAATCCC-3'
LCK_rev	5'-CACTAAAGGGAACAAAAGCTGG-3'
Murine CerS3_for	5'-CCTGGCTGCTATTAGTCTGATG-3'

Murine CerS3_rev	5'-CTGCTTCCATCCAGCATAGG-3'
Murine PPIA_fwd	5'-GCTGGACCAAACACAAACGG
Murine PPIA_rev	5'-GCCATTCCTGGACCCAAAAC
RPL13A_for	5'-CTCCTCACTGTTGTTCTACGC -3'
RPL13A_rev	5'-AACGGAGAACCAATAAGCACC-3'

2.4 Plasmids

The following Table 6 states all used plasmids in this dissertation.

Table 6: Plasmids used for transfection and transduction.

Plasmid	Resistance in bacteria	Resistance in cells	Manufacturer	Application
CerS3myc (LASS3 Human Tagged ORF clone)	Kanamycin	Neomycin	OriGene	Overexpression plasmid for CerS3 (Supplementary Figure 12)
Gag/pol pCMV-dR8.91	Ampicillin	-	promega	Virus production (Supplementary Figure 9)
GIPZ CerS1 V3LMM_432975	Ampicillin	Puromycin	dharmacon	Plasmid for shCerS1-RNA expression (Supplementary Figure 8)
GIPZ CerS3 V3LHS_373185	Ampicillin	Puromycin	dharmacon	Plasmid for shCerS3-RNA expression (Supplementary Figure 8)
GIPZ CerS3 V3LHS_373159	Ampicillin	Puromycin	dharmacon	Plasmid for shCerS3-RNA expression (Supplementary Figure 8)
GIPZ CerS3 V3LHS_373183	Ampicillin	Puromycin	dharmacon	Plasmid for shCerS3-RNA expression (Supplementary Figure 8)
GIPZ NC	Ampicillin	Puromycin	dharmacon	Plasmid for control shRNA expression (Supplementary Figure 8)
NCmyc pCMV6-Entry	Kanamycin	Puromycin	OriGene	Control plasmid for overexpression (Supplementary Figure 11)
VSV-G pMD2.G	Ampicillin	-	promega	Virus production (Supplementary Figure 10)

3. Methods

3.1. Animal related Methods

3.1.1 Animal Model

All animal experiments were approved by the local Ethics Committee for Animal Research (Regierungspräsidium Darmstadt, Germany) under the approval identification FK 2008. The experiments were conducted in compliance with the guidelines of the *Gesellschaft für Versuchstierkunde*/Society for Laboratory Animal Science (GV-SOLAS) for animal welfare in science and the European and German regulations for animal research. All possible efforts were taken to reduce the suffering of the animals to a minimum.

Mice were bought from a commercial vendor and further bred and kept in the *Zentrale Forschungseinrichtung* of the University Clinic Frankfurt am Main, Germany. The mice were kept under a constant room temperature of 21 ± 1 °C and in a 12 h light-dark cycle. Mice were fed and had access to water *ad libitum.* Mice aged 6 to 20 weeks were used for the experiments.

For a T-cell specific knockout of CerS3 in mice, exon 7 of the CerS3 gene was deleted and replaced by an exon that is flanked by LoxP sites (CerS3$^{fl/fl}$, later referred to as WT). CerS3$^{fl/fl}$ mice were crossed with LCK-Cre (B6-Cg-Tg(Lck-cre)548Jxm) (Charles River, Sulzfeld, Germany) mice to obtain the T-cell specific knockout generating CerS3$^{fl/fl}$LCK-Cre^{+} mice (later referred to as CerS3 LCK Cre). CerS3$^{fl/fl}$ mice were kindly gifted to us by Dr. Roger Sandhoff (*Deutsches Krebs Forschungszentrum*, Heidelberg, Germany).

Acute Colitis in mice was induced by supplementing the drinking water with 2 % of DSS for 5 days, following three days of normal water supply. After 8 days, mice were sacrificed and different organs were collected. During the experiment the mice were observed daily. The observation protocol was based on the Canadian Council on Animal Care 1998. Disease progression was controlled by a score system. Body weight, stool consistency and body posture changes, as well as bleeding, were included in the score assessment. The humane endpoint for this experiment was reached when mice had a Score > 3. No mice had to be sacrificed before the endpoint of the experiment.

3.1.2 Tissue collection and preparation

For the analysis of immune cell distribution various tissues (colon, thymus, spleen, lymph nodes and blood) were dissected and further processed. The colon was obtained and washed with PBS before it was cut longitudinally. The colon length was captured by cell phone camera pictures with a metric ruler next to the colon. Thymus, spleen and lymph nodes were removed from the body and put in PBS on ice for further proceeding. Blood samples were retrieved by cardiac puncture and collected in an EDTA-K tube on ice. For mRNA isolation, a piece of liver was cut out and then further processed.

3.1.3 Immune Cell isolation

Immune Cells were isolated from various tissues for flow cytometry. White blood cells were isolated by mixing 100 µl of ice-cold EDTA blood with 100 µl of 1 M HEPES. After centrifugation of the mixture at 600 x g for 10 min at 4 °C the plasma was collected and stored at -80 °C for further sphingolipid (LC-MS/MS) and cytokine (CBA) analysis. The red blood cells were lysed with an erythrocyte's lysis buffer for 10 min at RT and then centrifuged again at aforementioned conditions. After that, the pellet was resuspended in 100 ml FACS flow and kept on ice until further processing. Immune cells from spleen, lymph node and thymus were isolated by passing the organs with a stamp through a 40 µm or 70 µm cell strainer (Greiner BioOne, Frickenhausen, Germany), respectively. Cells were rinsed with 3 ml of PBS and afterwards lysed with an erythrocyte's lysis buffer for 10 min at RT. Following a centrifugation step at 600 x g for 10 min at 4 °C the cell pellet was resuspended in 100 µl FACS flow and stored on ice for flow cytometry staining with the Immune Cell panel (Table 13) and following flow cytometry analysis (Supplementary Figure 3, Supplementary Figure 4 and Supplementary Figure 5). When thymocytes were used for further cell culture experiments, the isolation was performed under a half-sterile biosafety cabinet.

3.1.4 IEL and LP isolation

The longitudinally cut colon was sliced into little pieces for Intraepithelial lymphocyte (IEL) and LP fraction isolation. The pieces were digested with pre-digestion solution by rotation at 37 °C for 20 min, vortexed for at least 30 s and then pushed through a 70

µm strainer. This step was repeated once again, before the pieces were then digested for 20 min at 37 °C by rotation with HBSS without Ca^{2+} or Mg^{2+} and 10 mM HEPES. After centrifugation at 300 x g for 10 min, the IEL fraction of the colon is obtained. The colon pieces were collected in a gentle MACS c-tube (Miltenyi Biotec, Mönchen-Gladbach, Germany) and mixed with an enzyme mix containing 100 µl Enzyme D, 50 µl Enzyme R and 12.5 µl Enzyme A and 2.35 ml of the digestion solution that was pre-warmed at 37 °C. The tubes were put on the gentle MACS dissociator (Miltenyi Biotec, Mönchen-Gladbach, Germany) to enzymatically dissociate the LP with the pre-installed 37C_m_LPDK_1 program. The solution was then filtered through a 100 µm strainer and washed three times with PB Buffer. Cells were centrifuged at 300 x g for 10 minutes. IEL and LP fraction cells were resuspended in 100 µl FACS flow and stored on ice for flow cytometry staining with the Immune Cell panel (Table 13) for the following flow cytometry analysis (Supplementary Figure 2).

3.1.5 Histology analysis

For histological analysis of the colon, the colon was washed with PBS and cut longitudinally before rolled from the proximal to the distal part and embedded in TissueTek solution in a medium biopsy mold (15x15x5mm, Sakura Finetek, Umkirch, Germany). The tissue was frozen on dry ice and stored at -80 °C. The colon swiss rolls were cut into 10 µm slices at a cryotome (CM 3050S microtome, LEICA, Wetzlar, Germany) and put on slides (Superfrost Plus, Thermo Fisher Scientific, Waltham, USA) at -80 °C. For staining of cell nuclei, cytoplasm and organelles, slices were stained with the Hemacolor kit. Slices were fixed with Hemacolor solution 1 for 5 s. Afterwards Hemacolor solution 2 was added for 3 s for pink staining of cytoplasm, organelles and extracellular matrices. Hemacolor solution 3 was put on the slices for 6 s to stain nuclei blue. Slices were washed twice in Hemacolor solution 4 (pH 7.2) for 10 s and air-dried. Pictures of colon swiss rolls were obtained with the BioRevo BZ9000 microscope (Keyence, Neu-Isenburg, Germany). Cutting and staining of slices were performed by Karin Schilling (Institute of Clinical Pharmacology, Frankfurt am Main, Germany).

3.2 Cell Culture Methods

3.2.1 Cell Culture

The human CD4$^+$ T cell Jurkat cell-line (#ACC 282, *German Collection of Microorganisms and Cell Cultures GmbH* (DMSZ), Braunschweig, Germany) was incubated at 37 °C and 5 % CO_2 in RPMI 1640 medium containing 10 % FBS, 2 mM GlutaMax and 1 % P/S. The cells were split every five days. Since these are suspension cells, the cells were centrifuged at 1200 rpm for 3 min and taken up in fresh medium. The pH indicator in the medium showed a shift from red to yellow at low pH levels, while at higher pH levels the medium turns purple. When medium shifted from red to yellow, fresh medium was added until medium was again red (pH 7.4).

HEK cells (#ACC 305, DMSZ, Braunschweig, Germany) for virus production were maintained in culture in DMEM (GlutaMax I + 4.5 g/l D-glucose) + 10 % FBS medium at 37 °C and 5 % CO_2. These adhesion cells were split every three days. For this, the flask containing the cells was slightly hit and the medium with the cells was centrifuged at 1200 rpm for 3 min. The desired cells were then resuspended in fresh medium.

Caco-2 (#ACC 169, DSMZ, Braunschweig, Germany) cells for colon chips were cultured in Complete Caco-2 Medium (DMEM Advanced + 1 % P/S + 20 % FBS) in an incubator at 37 °C and 5 % CO_2. For cell passaging, cells in a T175 flask were washed with 5 ml PBS and then trypsinized for 3 min with 5 ml Trypsin-EDTA at 37 °C. Afterwards, cells were resuspended thoroughly before cell counting.

HUVECs (#C0035C, Invitrogen, Toulouse, France) were kept in basal media for large human endothelial cells supplemented with 10 % LVES and 1 % P/S at 37 °C and 5 % CO_2. For cell passaging, cells in a T175 flask were washed with 5 ml PBS and then trypsinized for 3 min with 5 ml Trypsin-EDTA at 37 °C. Afterwards, cells were resuspended thoroughly before cell counting.

Primary human CD4$^+$ or CD8$^+$ cells, isolated from Buffycoats, were cultured in TexMACS medium at 37 °C and 5 % CO_2. Cells were activated with CD2/3/28 activation beads in a cell-to-bead ratio of 1:1 and 200 U/ml IL-2. Every three to four days, the cells were re-stimulated with IL-2 and every 14 days after isolation, they were reactivated with CD2/3/28 activation beads. Depending on the colour of the medium, like already described for the Jurkat cells, fresh medium was added.

Primary murine thymocytes were cultured in RPMI 1640 medium supplemented with 1 % P/S, 1 % NEAA, 1 % EAA, 1 % NaPyruvate, 1 % HEPES and 10 % FBS in an incubator at 37 °C and 5 % CO_2. Cells were activated prior to culture with Mouse T-Activator CD3/28 Activation beads, 50 mM β-mercaptoethanol, 200 U/ml human IL-2 and 20 ng/ml human IL-7. Every two days β-mercaptoethanol, IL-2 and IL-7 were freshly added to the cells.

3.2.2 Cell harvesting

Before harvesting the cells, a little fraction was stained with trypan blue to mark dead cells and afterwards cells were counted in a *Neubauer* chamber. Counted cells were then transferred into a tube and centrifuged for 3 min at 1200 rpm. The pellets were stored at -20 °C or -80 °C depending on further processing.

3.2.3 Isolation of CD4$^+$/8$^+$ cells from Buffycoats

The isolation of CD4$^+$/8$^+$ cells was performed via positive magnetic selection. Wanted cells were magnetically labelled and then separated from the unwanted cells with the StraightFrom® Buffycoat REAlease® MicroBeads. Later the cells were also freed from all attached beads.

Buffycoats were obtained from the Deutsche Blutspendedienst (University Clinic Frankfurt am Main, Germany) on the day of isolation. 2 ml CD4/8-Biotin Beads were added per 80 ml Buffycoat and incubated for 10 min at RT. After that, 15 ml Anti-Biotin Microbeads were added to the solution and the tube inverted. After a 5 min incubation time period at RT, the Buffycoat-Bead Mixture was divided on twelve Whole Blood Columns that were pre-labelled with 2 ml of SB Buffer and put into the Midi-MACS Separator (Miltenyi Biotec, Mönchen-Gladbach, Germany). After the cell suspension successfully surpassed the magnet, the columns were washed twice with 2 ml SB Buffer. The Columns were then placed into a 15 ml conical tube, and 4 ml of REAlease Bead Release Reagent (1:50 REAlease Bead Release Reagent + SB Buffer) were used to push the cells through with a plunger. After incubating 10 min at RT the cells were free of the Anti-Biotin beads. The cells were centrifuged at 300 x g for 10 min at RT for removal of the CD4/8 Biotin beads. Cells were resuspended in 25 ml SB Buffer and then 500 μl of REAlease Realease Reagent was added. The tube was inverted

and incubated for 5 min at RT. After that the cells were counted in a *Neubauer* chamber and the cell density was adjusted to $1*10^6$ cells/ml with TexMACS medium before the cells were activated via CD2/3/28 activation beads and IL-2 treatment.

3.2.4 Activation of T cells

For the activation of human T cells a combination of CD2/3/28 activation beads and IL-2 was used. For $1*10^8$ beads 100 µl of each Anti-CD2-Biotin-, Anti-CD3-Biotin- and Anti-CD28-Biotin-antibodies were mixed with 500 µl Anti-Biotin MACSiBeads particles and 200 µl SB Buffer. After 2 h of incubation at 4 °C under rotation, beads were ready to use. Cells were always activated in a cell-to-bead ratio of 1:1 and with an addition of 200 U/ml IL-2. The beads and IL-2 were directly pipetted to the cells.

Murine T cells were activated by Mouse T- Activator CD3/28 activation beads. For $1.5 * 10^6$ cells 30 µl of beads were used. The same volume of PBS + 0.5 % FBS was added and the mixture was vortexed for 30 s. After centrifugation at 13000 rpm for 1 min, the cells were resuspended in their respective medium.

3.2.5 Staining of T cells with tracer dyes

T cells for Immune cell recruitment experiments were dyed with the fluorescence dye PKH26 or 67, respectively. $4 * 10^6$ cells were washed in PBS and then centrifuged at 1200 rpm for 3 minutes and resuspended in 4 ml serum-free RPMI medium. Cells were centrifuged for 5 min at 400 x g to obtain a loose pellet. Cells were resuspended in 40 µl Diluent C (2X cell suspension). Prior to staining 0.5 µl of PKH26 (or 67) was added to 125 µl of Diluent C (2X dye) and mixed. Equal volumes of cells and dyes were mixed and incubated for 5 min with periodic mixing, then the reaction was stopped by adding 4 ml of normal medium (containing FBS). Cells were then centrifuged for 5 min at 500 x g and resuspended with PBS. Cells were again centrifuged at 500 x g for 5 min and then kept in normal growth medium until use.

3.2.6 Proliferation assay

To track the proliferation of different cells, cells were labelled with CellTrace Violet. This dye gets more diluted with every cell division and can be therefore used to track

the proliferation status of cells. A 5 mM stock solution of CellTrace Violet was obtained by adding 20 µl DMSO to the CellTrace Violet vial. For a 10 µM working solution, 2 µl of the 5 mM stock solution of CellTrace Violet was added to 998 ml of pre-warmed PBS. The working solution was mixed with $1.5*10^6$ cells and incubated for 20 min at 37 °C. Cells were then washed twice with 4 ml of respective medium at 1200 rpm for 3 min. For the first measurement at 0 h, 300 µl of cells were transferred into a FACS tube and centrifuged at 500 x g for 5 min. Cells were then resuspended in 300 µl FACS flow for flow cytometry analysis. The rest of the cells were seeded into a 24 well plate ($1.2 * 10^6$ cells per well) and activated with CD2/3/28 activation beads and 200 U/ml IL-2. Every 24 h 300 µl cells were obtained and prepared for flow cytometry analysis. In total 25000 events were measured for every time point and analysed by FlowJo Software (Supplementary Figure 6).

3.2.7 Migration assay

This assay is based on the migration of cells through an 8 µM pore-sized membrane to a S1P gradient. The Transwell-inserts (Greiner BioOne, Frickenhausen) were put into a 12 well plate well. In each insert a total of $1*10^5$ T cells were seeded in RPMI 1640 + Glutamax medium supplemented with 4 % fatty-acid free BSA. The cells were incubated for 2 h at 37 °C on the inserts prior to the assay. Afterwards the inserts were placed into the wells containing 600 µl medium w/o FBS with 100 nM S1P or medium with 10 % FBS as positive control and medium without FBS as negative control. The cells were then incubated for another 2 h to allow the cells to migrate towards the S1P gradient. After incubation, the medium in the bottom was collected and centrifuged at 500 x g for 5 min and resuspended in 300 µl FACS flow. Cells were then analysed at a flow cytometer by measuring the cells for 1 min. The analysis was done with FlowJo Software (Supplementary Figure 6).

3.2.8 T cell Differentiation assay

To study the differentiation capacity of T cells into different T cell subpopulations, murine thymocytes were treated with different cytokines to induce differentiation. After isolation of the cells from the thymus, $1.5 *10^6$ cells were activated with 30 µl Mouse T- Activator CD3/28 activation beads, 50 mM β-mercaptoethanol, 200 U/ml human IL-

2 and 20 ng/ml human IL-7. To differentiate the naïve T cells into Tregs, the cells were treated with 60 ng/ml of human IL-15. For the TH1 subpopulation cells were treated with 10 ng/ml mouse IFNγ and 6 ng/ml mouse IL-12. Cytotoxic T cells were induced by treatment with 60 ng/ml human TGFβ. Before treatment of the cells, 250 μl cells were obtained for the 0 h time point. Every two days fresh β-mercaptoethanol, IL-2 and IL-7 was added to the cells and every 24 h 250 μl cells were transferred to a FACS tube for flow cytometry analysis. Cells were stained according to the T cell panel (Table 14) and 250000 events were measured for each time point by flow cytometry. The analysis was done with FlowJo Software (Supplementary Figure 3).

3.2.9 Intracellular Calcium measurement

For measurement of intracellular calcium concentration ($[Ca^{2+}]_i$), Jurkat cells were labelled with fura-2-AM Ester. Cells were first washed with 5 ml HBSS + Ca^{2+} and centrifuged for 3 min at 1200 rpm. Afterwards $1*10^7$ cells were resuspended in 10 ml HBSS + Ca^{2+} buffer and 10 μl of fura-2-AM (stock solution: 1mM, endconcentration: 1 μM) were added. Cells were incubated for 1 h protected from light. Then cells were washed twice with 10 ml HBSS with Ca^{2+}. 2 ml cells were put in cuvettes in a density of $1*10^6$ cells/ml for fluorescence spectrophotometrical measurement at the F2500 fluorescence spectrophotometer (HITACHI, Asemo, Japan) provided by Prof. Dr. Joseph Pfeilschifter (Institute of general pharmacology and toxicology, Faculty of Medicine, Goethe University Frankfurt, Germany). Excitation was altered between 340 nm and 380 nm and emission was recorded at 510 nm. Cells were either stimulated with 1 μM S1P or 1 μM SEW 2871. To determine maximal $[Ca^{2+}]_i$ values, 60 μl 1.5 % digitonin was added to the cells, and for minimum $[Ca^{2+}]_i$ values 15 mM EGTA was added to the cells.

3.3 DNA Methods

3.3.1 Plasmid isolation

For plasmid isolation respective glycerol cultures of *Escherichia coli* were cultivated in 200 ml LB-media containing antibiotics (100 μg/ml for Ampicillin and 25 μg/ml for Kanamycin) under shaking at 37 °C overnight. Plasmid isolation and purification was performed with the Qiagen Plasmid Purification Maxi Kit as described in the kit

instructions. Afterwards DNA concentration was measured spectral-photometric at an absorption of 260 nm with a Tecan Reader (Tecan, Männedorf, Switzerland).

3.3.2 Virus production

For constitutive downregulation of certain genes, cells can be transduced with lentiviruses for a specific short hairpin (sh) RNA. The production of lentiviruses requires several steps. Three important main genes are necessary for virus production: gag (retroviral core), pol (reverse transcriptase, RNase H and integrase) and env (viral envelope). For safety reasons, the lentiviral genes are divided into two different plasmids, which are then transfected together into a HEK cell line so that the virus can be produced in those cells. In addition to both plasmids for virus production, the vector for the shRNA is also transfected into the cells. For virus production $3.8*10^6$ HEK cells were seeded in a 60.1 cm^2 dish in 10 ml DMEM + GlutaMax I + 4.5 g/l D-glucose + 10 % FBS medium. The cells were used at a confluency of 70 to 90 %. In an Eppendorf tube, 7.5 µg shRNA vector, 12.5 µg gag/pol and 1 µg envelope plasmids were mixed and filled up to 450 µl with H_2O. To this, 50 µl $CaCl_2$ was added. In a 50 ml tube, 500 µl HBSS was placed and the DNA-$CaCl_2$ mixture was added dropwise. Simultaneously the mixture was supplied with air by using a 10 ml pipette. The HEK cells were treated with 25 µM chloroquine solution to inhibit lysosomal DNases. After incubation at RT for 15 min, the DNA-$CaCl_2$ mixture with HBSS was added dropwise to the cells in the dish in a circular fashion. After six to eight hours, the medium was changed and 5 ml DMEM + GlutaMax I + 4.5 g/l D-glucose + 5 % FBS medium was added. The next day, cells were checked under the light microscope for successful transfection (plaques, holes in cell membrane and no doubling of cells). The medium was then removed from the cells using a syringe and filtered through a 0.45 µm sterile filter (Corning, New York, USA). The cells were incubated for another 24 h with the 5 % FBS medium. Virus supernatant was mixed with cold PEG-it in a 4:1 ratio for virus precipitation and incubated for at least 12 h at 4 °C. The virus PEG-it solution was then centrifuged at 1500 x g at 4 °C for 30 min. The supernatant was tipped off and the pellet resuspended in 20 to 30 µl cold 1X PBS and stored at -80 °C until further usage.

All steps were performed under a S2 Biosafety cabinet.

3.3.3 Virus transduction

For stable knockdown of CerS3 in Jurkat cells, $1.5 * 10^4$ cells/well were seeded in a 12 well plate in 1 ml RPMI 1640 + 2 mM Glutamax I + 1 % P/S + 10 % FBS medium. Four different shCerS3 viruses, or one shNC or shCerS1 virus (Table 6) were added to the cells, by pipetting each 1 µl of virus solution to the cells. Afterwards the cells were centrifuged for 45 min at 1800 rpm and 37 °C. Again 1 ml medium was added to the cells and they were incubated for 48 to 72 h. Every day the expression of Green fluorescent protein (GFP) was checked under a fluorescence microscope (Zeiss, Roßdorf, Germany). On the last day of incubation, the cells were centrifuged at 1200 rpm for 3 min and resuspended in fresh medium containing 10 mg/ml Puromycin for selection.

3.3.4 Transfection

For stable overexpression of CerS3 in Jurkat cells, the cells were transfected with a CerS3myc or NCmyc overexpression plasmid (Supplementary Figure 12 and Supplementary Figure 11). On the first day, Jurkat cells were seeded in a density of 0.5 to $2 * 10^5$ cells/ml to reset all cells to the same cell cycle. The next day, $1.5 * 10^5$ cells were seeded in 250 µl Medium. In an Eppendorf tube, 12.5 µl OptiMEM medium was placed and 0.75 µl GeneJuice Reagent was added dropwise for each well. The mixture was vortexed and incubated for 5 min at RT. Then 250 ng of overexpression plasmid was added and gently mixed by pipetting. After 15 min of incubation at RT the mixture was added dropwise to the cells and they were incubated for 24 to 48 h. Upon 48 h of incubation 200 ng/ml Neomycin was added to the medium for selection.

3.3.5 Genotyping

To varify the genotypes of the mice used in the experiments, mice were punched in the ear to get tissue for DNA isolation. DNA was isolated with the GT KAPA genotyping kit. Ear punch tissue was mixed with 10 % v/v tail lysis buffer supplemented with 2 % v/v protease K. The samples were then incubated for 10 min at 70 °C under gentle shaking and then for 5 min at 95 °C under gentle shaking. For the conditional KO of CerS3, amplification was performed by Taq DNA Polymerase with primer sequences for CerS3 and LCK-Cre in two different PCR programs (Table 7). The PCR for CerS3

resulted in amplicons of 315 bp for WT, 419 bp for flox/cond and 315 + 419 bp for WT/cond. PCR for LCK Cre resulted in an amplicon of 250 bp. For amplicon size conformation PCR products were loaded onto a 2 % agarose gel containing 5 % v/v Roti-Safe GelStain DNA binding fluorescence dye and a GeneRuler^{TM} DNA Ladder mix as a standard. Electrophoresis was performed to separate PCR products at 100 V (PowerPac Basic, BioRad, Hercules, USA) for 1 h and visualized on a Gel Doc XR+ System with the Imagelab^{TM} software (BioRad, Hercules, USA).

Table 7: Composition of different PCR mixtures for genotyping of CerS3 LCK Cre mice and respective PCR programs

Component	Volume [µl]		PCR program		
	CerS3 PCR	LCK Cre PCR	CerS3 PCR	LCK Cre PCR	
H$_2$O	4	1.5	95 °C 2 min	95 °C 5 min	
Taq Polymerase Mix	12.5	12.5	95 °C 45 s	95 °C 30 s	
Primer 1	1.25 (L3_for)	1.25 (LCK_for)	58 °C 30 s	60 °C 30 s	35x
Primer 2	1.25 (L3_rev)	1.25 (LCK_rev)	72 °C 40 s	72 °C 60 s	
Primer 3	-	1.25 (LCK A_for)	72 °C 5 min	72 °C 10 min	
Primer 4	-	1.25 (LCK B_rev)			
Template	1	1			
Total Volume	20	20			

3.4 RNA Methods

3.4.1 RNA isolation of human cells

RNA was isolated with the QIAGEN RNA Purification Kit as described in the manufacturer's instructions. After isolation, the concentration of RNA was determined spectral-photometric at the Infinite Pro Tecan Reader (Tecan, Männedorf, Switzerland) at 260 nm. RNA was stored at – 80 °C.

3.4.2 RNA isolation of murine cells and tissue

Isolation of RNA of murine liver tissue and T cells was performed with TRI reagent. A piece of liver was lysed with 200 µl TRI reagent and potted with an electric potter to

disrupt the tissue and then 800 ml TRI reagent was added. T cells were resuspended in 400 µl TRI reagent. Samples were vortexed and incubated for 10 min at RT and then 200 µl (to liver) / 80 µl (to T cells) chloroform was added and vortexed and incubated again for 10 min at RT. Samples were then centrifuged at 12200 x g for 15 min at 4 °C. The watery phase above was then placed into a new Eppendorf tube and filled with 500 µl (200 µl) isopropanol, respectively. Samples were vortexed and then incubated for 10 min at RT. Afterwards, RNA was centrifuged at 12200 x g for 8 min at 4 °C. Supernatant was discarded and then 500 (250) µl 75 % ethanol was added and centrifuged for 5 min at 7500 x g at 4 °C. Supernatant was discarded and pellets were left do dry for 20 minutes, before pellets were resuspended in 15 to 400 µl RNAse-free water (depending on pellet size). RNA concentrations were measured at the Nanodrop-photometer (Thermofisher, Waltham, USA) at 260 nm. RNA was stored at − 80 °C.

3.4.3 cDNA synthesis

For synthesis of cDNA, 400 to 800 ng RNA were used for the verso kit. The components and their respective volumes for one cDNA approach are listed in Table 8. The mixture was treated for 30 min at 42 °C and afterwards for 2 min at 92°C. After cDNA synthesis, every sample was filled with 50 µl RNase-free water.

Table 8: Required Volumes and components for a 20 µl sample of cDNA

Component	Volume [µl]
5X synthesis buffer	4
dNTP Mix	2
Hexamers	0.7
Oligo Mix	0.3
RT Enhancer	1
Verso Enzyme	1
400 to 800 ng RNA	
RNase free water	Ad 20

3.4.4 Quantative RealTime-PCR (qRT-PCR)

To determine transcript quantity of different genes, qRT-PCR was performed (Table 9). The expression of each target gene was determined in triplicates. Fluorescence of

3. Methods

SYBR Select or ORA SEE qPCR Green ROX was measured after each elongation step, respectively. Therefore the formation of the PCR product could be observed in real time. The formation of the product correlates with the C (t) value. This value indicates the threshold at which the fluorescence, and thus the formation of the product, exponentially exceeds the background fluorescence.

Table 9: qRT-PCR preparation for qRT-PCR of genes of interest

Preparation for 1 qPCR		qPCR program		
SybrSelect qPCR Master Mix or ORA SEE qPCR Green ROX Master Mix	5 µl	50 °C	2 min	45 cycles
Forward Primer	1 µl	95 °C	15 min	
Reverse Primer	1 µl	95 °C	15 sec	
RNase-free H_2O	2 µl	60 °C	1 min	
cDNA	1 µl			

For the qRT-PCR of S1P1, 4 and 5, Taqman's probe was used as described in Table 10.

Table 10: Preparation for S1PR qRT-PCR

Preparation for 1 qPCR		qPCR program		
Taqman Buffer	5 µl	95 °C	30 s	
Taqman's probe	0.5 µl	95 °C	1 s	50 cycles
RNase-free H_2O	3.5 µl	60 °C	25 s	
cDNA	1 µl			

The relative expression of the target genes was calculated using the Δ C (t) values. The C (t) values of the target genes were related to the expression of the constitutively expressed gene RPL13A. The C (t) ratio was calculated as follows:

$$\Delta C(t) = C(t)(\text{target gen}) - C(t)(\text{RPL13A}) \qquad (1.1)$$

$$Ratio = 2\text{-}\triangle cT \qquad\qquad (1.2)$$

3.4.5 siRNA treatment of primary T cells

For transient knockdown of CerS3 in primary T cells isolated from the blood of healthy donors, Accell small interfering (si) RNA was used. Stock solution of siRNA in a concentration of 100 µM were conducted by resuspending 20 nmol siRNA with 200 µl of 1X siRNA Buffer. SiRNA was incubated for 70 to 90 min at 37 °C under constant shaking. After incubation, siRNA was centrifuged at a table centrifuge for some seconds. Primary cells were washed trice with DPBS. $1*10^5$ cells per approach were resuspended in 99 µl Delivery Media and added to 1 µl siRNA in a 96-well plate well. The sample was mixed briefly and the cells were stimulated with 200 U/ml IL-2 but without activation beads to keep cells alive, but not fully activated. Cells were incubated for 48 h at 37 °C and 5 % CO_2. After 48 h incubation, cells were activated with 200 U/ml IL-2 and CD2/3/28 activation beads in a 1:1 cell-to-bead ratio. Every 24 h cells were harvested for RNA isolation following qRT-PCR of CerS1-6.

3.5 Protein Methods

3.5.1 Whole Protein isolation

The cells were mixed with 200 µl of Phosphosafe Buffer, 30 µl of 7X Complete Phosphatase Inhibitor Cocktail and 0.4 µl of DTT and vortexed. Using the sonicator, the cells were lysed on ice three times with three shocks at level three with 30 % output with ultrasonic waves. This was followed by centrifugation at 15000 rpm for 30 min at 37 °C. The proteins in the supernatant were transferred into a new Eppendorf tube and stored at -80 °C. The Bradford method [391] was used to determine the protein concentration. For this, a BSA standard series of 1 to 8 µg BSA was prepared. In each case, 200 µl Bradford reagent was added to 1 µl protein solution with 9 µl water and the OD was documented at 595 nm on the Tecan Reader and with the X-Fluor® software.

3.5.2 Nuclear Protein isolation

For fractional lysis of proteins, $1.5 * 10^7$ cells were resuspended in 250 µl Bandshift lysis buffer and then incubated for 10 min on ice. After this incubation, 13.25 µl of 10 % NP40 was added and again incubated for 2 min on ice before centrifugation at 2500 rpm for 5 min at 4 °C. The supernatant contains the cytoplasmic proteins and was stored at -80 °C. The nucleus pellet was then quickly resuspended in 30 µl nucleus lysis buffer I and incubated for 30 min on ice. After incubation the cells were centrifuged for 10 min at 14000 rpm at 4 °C. Supernatant was added to Eppendorf tubes prepared with 30 µl nucleus lysis buffer II and mixed very well. The samples were portioned in small aliquots and snap-frozen in liquid nitrogen before storage at -80 °C.

3.5.3 SDS PAGE

For analysis and quantification of proteins the Western Blot (WB) method can be used. First proteins are separated by size via a sodium dodecyl sulfate polyacrylamide gel electrophoresis (SDS PAGE).

To denature the proteins prior to loading, Laemmli buffer was added 4:1 to the protein samples and boiled at 95 °C for 5 min. The 7.5 % (for NFAT1 protein detection only) or 12 % SDS gel was clamped in a running chamber and then the chamber was filled with 1X SDS running buffer. Separation gel and stacking gel of the 12 % SDS gel are composed as in Table 11. For subsequent protein sizing, 2.5 µl of Precision Plus Protein™ Standards, Dual Colour Marker was applied (10-250 kDa). The separation of the proteins was performed at 80 V. As soon as the running front reached the separation gel, the voltage was increased to 110 V and the protein extracts were separated electrophoretically for approximately 1 to 1.5 h.

Table 11: Composition of the SDS Separation and stacking gels

Gel	Composition
Separation gel (12 %)	1.97 ml Acrylamide 1.23 ml 1,5 M Tris, pH=8.8 49.2 µl 10 % SDS 24.6 µl 10 % APS

	2.46 µl TEMED
	1.72 ml H_2O
Separation gel (7.5 %)	1.23 ml Acrylamide
	1,23 ml 1,5 M Tris, pH=8.8
	49.2 µl 10 % SDS
	24.6 µl 10 % APS
	2.46 µl TEMED
	2.46 ml H_2O
Stacking gel	0,65 ml Acrylamide
	1.25 ml 0,5 M Tris, pH=6.8
	50 µl 10 % SDS
	50 µl 10 % APS
	5 µl TEMED
	3.05 ml H_2O

3.5.4 Wet blotting

For transfer of the separated proteins in a SDS gel to a nitrocellulose membrane, the wet blotting technique was used. The nitrocellulose membrane and two membrane-sized pieces of Whatman paper were soaked in wet blot buffer. For the blotting sandwich the different layers were stacked as follows:

Cathode

Filter

Blotting Paper

Gel

Membrane

Blotting Paper

Filter

Anode

The closed clamp was transferred into the blotting chamber as well as a cooling pack that was placed right next to it. The chamber was filled with wet blot buffer and a voltage of 100 V was applied for 1 h to transfer the proteins to the membrane.

3.5.5 Western Blot analysis

After blotting, the membrane was stained with ponceau S in 0.1 % TCA for 1 min to stain the protein lanes and then washed with water. The membrane was then scanned or photographed and then blocked in blocking buffer for 1.5 to 2 h. If the membrane was stained with Revert700 Total Protein stain, the blot was stained prior to blocking of the membrane (s. 3.5.6). After blocking, the membrane was incubated with primary antibodies diluted with antibody buffer (Table 12) overnight at 4 °C under rotation. Following, the membrane was incubated for 1 h at RT under rotation before it was washed three times with PBST. The membrane was then incubated with the secondary antibody for 1.5 h at RT under rotation. Afterwards the membrane was washed again three times with PBST. When β-Actin or p84 were used as a loading control, those antibodies were incubated for 30 to 60 min at RT. The detection of the fluorescent-marked proteins was performed at the Odyssey Infrared Scanner (LI-COR Biosciences, Lincoln, USA).

Table 12: Antibodies used in WB analysis

Target	Host	Molecular weight	Dilution	Manufacturer
CerS3 (HPA006092)	rabbit	55 kDa	1:100	Sigma/Atlas Antibodies
c-Fos (9F6)	rabbit	62 kDa	1:200	Cell Signalling
c-Jun (L70B11)	rabbit	48 kDa	1:200	Cell Signalling
Mouse IRDye® 800CW or 680RD	goat	-	1:10000	LI-COR Biosciences
NFAT1 (4389)	rabbit	140 kDa	1:200	Cell Signalling
p84 (5E10)	mouse	84 kDa	1:1000	Abcam
Phospho-c-jun (D47G9)	mouse	48 kDa	1:200	Cell Signalling
Phospho-Zap70 (65E4)	rabbit	70,72 kDa	1:200	Cell Signalling
Rabbit IRDye® 800CW or 680RD	goat	-	1:10000	LI-COR Biosciences

S1P1 (sc-48356)	mouse	43 kDa	1:100	Santa Cruz
ß-Actin (8H10D10, 13E5)	Mouse, rabbit	42 kDa	1:1000	Cell Signalling
Zap70 (L1E5)	mouse	70,72 kDa	1:200	Cell Signalling

3.5.6 Revert700 Staining of nitrocellulose membrane

For a whole protein staining prior to incubation of the first primary antibody, the membrane was dried for 10 min at 37 °C on a filter paper. The membrane was then re-hydrated for 5 min in PBS at RT under shaking. After rehydration, the membrane was washed with ultrapure water and then incubated for 5 min with 5 ml of Revert700 Total Protein Stain solution at RT under shaking. Following staining, the membrane was washed three times with Revert wash buffer for 30 s and incubated in ultrapure water. The membrane was then scanned at the Infrared Scanner (LI-COR Biosciences, Lincoln, USA) to obtain images of the stained protein lanes.

3.5.7 Flow Cytometry

To determine immune cell populations, surface proteins of cells were stained and analysed by flow cytometry. Cells were blocked with 2 µl F_cR blocking reagent for 15 min at RT protected from light. The respective antibody cocktail (depending on the cells of interest) was added to the cell suspension and incubated for 15 min at RT protected from light (Table 13 and Table 14). After staining, cells were washed with 500 µl FACS flow for 5 min at 500 x g at 4 °C and resuspended in 300 µl FACS flow. Flow cytometric analysis of fluorescence emission was performed using the FACS symphony B 5 and the BD FACSDiva^{TM} software (BD Biosciences, San José, USA), both provided by Prof. Dr. Bernhard Brüne (Institute of Biochemistry I, Faculty of Medicine, Goethe-University Frankfurt, Germany). Analysis of immune cell populations was performed with FlowJo software v10 (Treestar, Ashland, USA). The gating strategy of respective experiments is attached in the appendix (Supplementary Figure 2, Supplementary Figure 3, Supplementary Figure 4, Supplementary Figure 5, Supplementary Figure 6 and (Supplementary Figure 7).

Table 13: Big Immune Cell panel used for analysis of different tissues (LP, IEL, spleen and blood)

Target	Host	Channel	µl	Manufacturer
CD3 (T cells)	hamster	YG602 (PE-CF594)	1	BD Biosciences, San José, USA

CD4 (CD4+ cells)	rat	V710 (BV711)	1	BD Biosciences, San José, USA
CD8 (CD8+ cells)	rat	V660 (BV650)	2	BD Biosciences, San José, USA
CD11b (monocytes)	rat	V510 (BV510)	0.5	BD Biosciences, San José, USA
CD11c (DC)	hamster	R730 (AF700)	0.5	BD Biosciences, San José, USA
CD14 (monocytes)	rat	YG585 (PE)	0.5	BD Biosciences, San José, USA
CD19 (B-cells)	rat	R780 (APC-Cy7)	1	BD Biosciences, San José, USA
CD25 (Tregs)	rat	YG780 (PE-Cy7)	2	BD Biosciences, San José, USA
CD36 (macrophages)	mouse	R675 (APC)	2	BD Biosciences, San José, USA
CD45 (immune cells)	rat	V427 (Vioblue/BV421)	2	Miltenyi Biotec, Mönchen-Gladbach
CD80 (monocytes, B cells)	hamster	B510 (FITC)	2	BD Biosciences, San José, USA
GITR (Tregs)	rat	B510 (FITC)	1	BD Biosciences, San José, USA
F4/80 (macrophages)	rat	YG780 (PE-Cy7)	0.5	BioLegend, San Diego, USA
Ly-6G (neutrophils)	rat	R780 (APC-Cy7)	1	BD Biosciences, San José, USA
Ly-6C (monocytes)	rat	B710 (PerCP-Cy55)	0.5	Thermo Scientific, Waltham, USA
MHC II (APCs)	rat	V595 (BV605)	0.5	BD Biosciences, San José, USA
NK1.1 (NK cells)	mouse	YG585 (PE)	2	BD Biosciences, San José, USA
7AAD	-	PE-Cy5	2	Miltenyi Biotec, Mönchen-Gladbach, Germany

Table 14: T cell panel

Target	Host	Channel	µl	Manufacturer
CD3 (T cells)	hamster	YG602 (PE-CF594)	1	BD Biosciences, San José, USA

CD4 (CD4+ cells)	rat	V710 (BV711)	1	BD Biosciences, San José, USA
CD8 (CD8+ cells)	rat	V660 (BV650)	2	Thermo Scientific, Waltham, USA
CD11b (monocytes)	rat	V510 (BV510)	0.5	BD Biosciences, San José, USA
CD25 (Tregs)	rat	YG780 (PE-Cy7)	2	BD Biosciences, San José, USA
CD45 (immune cells)	rat	R730 (AF700)	2	BD Biosciences, San José, USA
GITR (Tregs)	rat	B510 (FITC)	1	BD Biosciences, San José, USA
7AAD	-	PE-Cy5	2	Miltenyi Biotec, Mönchen-Gladbach, Germany

3.5.8 Cytometric Bead Array (CBA)

For simultaneous detection of multiple cytokines in the supernatant of treated cells, CBA was performed as instructed in the CBA Flex set kit. Supernatant of cells was centrifuged at 14000 rpm for 10 min at 4 °C. In a FACS tube, 25 µl of supernatant were mixed with 25 µl of antibody-CBA buffer mix. Per cytokine 0.5 µl of antibody beads (blue cap) were used and filled up to 25 µl with CBA buffer for each sample. The mixture was vortexed and incubated for 1 h at RT. After this incubation, the detection reagent (red cap) was prepared just like the antibody beads and 25 µl of the detection reagent mix was added to each sample and vortexed. After 2 h incubation at RT protected from light, 1 ml FACS flow was added to the samples to wash them (5 min, 500 x g). The supernatant was discarded and the pellet was resuspended in 300 µl of FACS flow. The samples were analysed via flow cytometry analysis and 300 events per cytokine were measured. For calibration of the concentration, a standard curve was also measured with standards provided in the kit. Samples were then analysed via FlowJo v10 software.

3.5.9 TNFα Enzyme-linked Assay (ELISA)

For detection of TNFα concentration in the supernatant of stimulated Jurkat cells, $1.7 * 10^7$ cells/ml were seeded and activated with CD2/3/28 activation beads in a 1:1 cell-to-bead ratio and 200 U/ml IL2. Cells were centrifuged at 1500 rpm for 5 min and

the supernatant was placed in a new tube and stored at − 20 °C until usage. 96-well plates were coated with 100 µl of TNFα Capture Antibody (1:250 diluted in Coating Buffer) overnight at 4 °C. On the next day, Capture Antibody was thrown away and the wells were washed thrice with 300 µl TNF ELISA wash buffer. Then unspecific binding sites were blocked with 200 µl Assay Diluent in every well for 1 h at RT. Assay Diluent was then replaced and the wells were washed thrice with 300 µ TNF ELISA wash buffer. Then 100 µl of standard or sample was added and incubated for 2 h at RT. Wells were washed five times with 300 µl TNF ELISA wash buffer. Then 100 µl Working Detector solution (1:250 TNFα Detection Antibody + 1:250 Streptavidin-Horseradishperoxidase (HRP) diluted in Assay Diluent) was added to every well and incubated for 1 h at RT. Working Detector solution was taken away and the wells were washed seven times with 300 µl TNF ELISA wash buffer for at least 30 s in each washing step. After the last washing step, 100 µl Substrate Solution (TMB and H_2O_2 1:1) was added to each well and incubated for 30 min at RT in the dark (wells should get a blue color). Reaction was stopped by adding 50 µl Stop solution (1 M H_3PO_4) and the absorption at 450 nm was measured immediately at the Tecan Reader (Tecan, Männedorf, Switzerland).

3.6 Lipid Methods

3.6.1 LC-MS/MS

Concentrations of cellular sphingolipids of different cell lines were determined by high-performance liquid chromatography coupled with tandem mass spectrometry (LC-MS/MS). Extraction, measurement and quantification of sphingolipids were performed by Sandra Trautmann, Viktoria Wagner, Dr. Dominique Thomas and Dr. Robert Gurke from the Analytics Department of the Institute of Clinical Pharmacology, Frankfurt am Main, Germany. The chemicals and reagents used for this method are therefore listed in the description of the method.

For the quantification of sphingolipids, lipids were extracted from cell pellets of $2.5*10^6$ cells each and quantified by LC-MS/MS [392, 393]. Several mass spectrometer units were connected in series, resulting in tandem MS (or MS/MS), a coupling option which is coupled with a liquid chromatograph. With this coupling, pure and also substance mixtures can be precisely identified and quantified.

Cell pellets were resuspended with 200 µl extraction buffer (30nM citric acid + 40 mM disodium hydrogen phosphate) and then mixed with 20 µl internal standard (mixture of SPH d18:1-d7, SPH d18:0-d7, S1P d18:1-d7, S1P d18:0-d7, Cer d18:1/16: 0-d7, Cer d18:1/18:0-d7, Cer d18:1/24:1-d7, GlcCer d18:1/18:0-d5, LacCer d18:1/16:0-d3, LacCer d18:1/17:0 (Avanti polar lipids, Alabaster, USA) Cer d18:0/18:0-d3 (Cayman Chemicals, Ann Arbor, USA), and Cer d18:1/24:0-d4 (Chiroblock GmbH, Wolfen, Germany). To separate the sphingolipids, 600 µl methanol/chloroform/HCl (15:83:2, v/v/v) was added to the mixture. After phase separation, the lower phase was divided into two new tubes and evaporated at 45 °C under a light stream of nitrogen. The sphingoid bases and ceramides were analysed separately. The calibration standards and quality control samples were prepared by pipetting 20 µl of a ceramide working solution and 20 µl of a sphingoid base working solution together, respectively, and processed using the same method as for the cells.

To analyse the ceramides, one of the aliquots was re-dissolved with 50 µl THF/water (9:1, v/v) containing 0.2 % formic acid and 10 mM ammonium formate shortly before measurement. Chromatographic separation was performed with an Agilent 1290 HPLC system using a Zorbax Eclipse Plus C18 UHPLC column (50 mm x 2.1 mm ID, 1.8 µm; Agilent technologies, Waldbronn, Germany). The column temperature was 60 °C and the injection volume 7.5 µl. Water containing 0.2 % formic acid and 10 mM ammonium formate (mobile phase A), and ACN/IPA/acetone (5:3:2, v/v/v) containing 0.2 % formic acid were used as mobile phases. The following gradient programme was performed: 50 % A (0.0 -0.2 min) - 10 % A (0.6 min) - 0 % A (4.0 - 5.5 min) - 50 % A (6.0 - 7.5 min), flow rate 0.35 ml/min.

In order to analyse the sphingoid bases, they were re-dissolved with 50 µl MeOH containing 5 % formic acid shortly before the measurement. Chromatographic separation was performed with an Agilent 1290 HPLC system using a Zorbax Eclipse Plus C8 UHPLC column (30 mm x 2.1 mm ID, 1.8 µm; Agilent technologies, Waldbronn, Germany). The column temperature was 55 °C and the injection volume was 5 µl. Water with 0.5 % formic acid (mobile phase A), and ACN/IPA/acetone (5:3:2, v/v/v) with 1 % formic acid were used as mobile phases. The following gradient programme was carried out: 55 % A (0.0 - 0.5 min) - 0 % A (1.5 - 3.0 min) - 55 % A (4.0 - 5.5 min) - 0 % A (3.1 - 4.5 min), flow rate 0.4 ml/min.

Tandem mass spectrometric analysis was performed for both measurements using a 5500QTRAP mass spectrometer (Sciex, Darmstadt, Germany) equipped with a Turbo V ion source in positive electrospray mode. The source parameters were set as follows (ceramides/sphingoid bases): Ionisation voltage 4500/4500 V, ion source temperature 450/500 °C, shielding gas 35/35 psi, collision gas 6/6 psi, nebulizer gas 55/50 psi and heating gas 50/70 psi. The analysis was performed in Multiple Reaction Monitoring (MRM) mode and two mass transitions were recorded for each analyte and internal standard.

Analyst software V 1.6.3 and MultiQuant software V 3.0.2 (Sciex, Darmstadt, Germany) were used to acquire and evaluate the data using the isotope dilution method. Calibration was performed for each analyte individually using linear regression and 1/x weighting or quadratic regression and 1/x2 weighting. Deviations in the accuracy of the calibration standards were less than 15 % over the whole calibration range, only for the smallest calibration standard a deviation of 20 % was accepted.

3.7 Human colon chip methods

To recreate natural physiological processes in the human body, many different models were established. A very well established model is the three-dimensional (3D) culture of cells in the form of organoids, in which specific tissue cells are kept in a matrix resembling their natural microenvironment. Cells in 3D culture behave differently and show more translational relevance in the clinics than cells in a 2D model. An organ-chip recreates the microenvironment of tissues even better, because it allows the co-cultivation of epithelial and endothelial cells as well as the application of mechanical forces that are normally present within the human body (e. g. peristaltic of the intestine, blood pressure differences).

The organ chip (S-1® Chip) (Emulatebio, Boston, USA) consists of polydimethylsiloxane (PDMS) that makes it flexible to be able to apply stretch. The chips has two microfluidic channels that extend parallel to each other and they are connected through a porous membrane of 7 µm to allow cell-cell interactions between the top and the bottom channel cells (Figure 5). The top channel is filled with the epithelial cells of the desired organ (in this case colon epithelial cells) and the bottom

channel is seeded with the endothelial cells that represent the respective blood vessel of the organ.
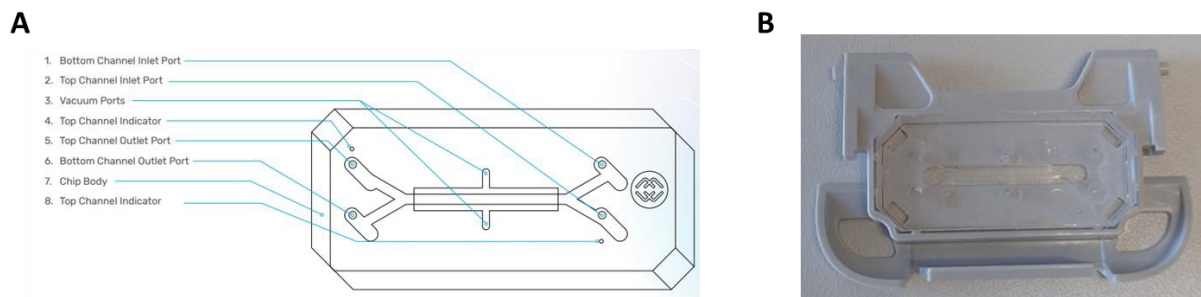
Figure 5: S-1® Chip. A) Schematic depicture of S-1 Chip with all features. Picture was obtained from Emulatebio.com **B)** Photo of S-1 Chip in Chip carrier.

Once the chip is activated, coated with extracellular matrix (ECM) proteins and the cells are seeded, chips can be connected to the pods (Pod-1® Portable Module (Emulatebio, Boston, USA)) (Figure 6). The pods supply media to the channels and allow collection of media that flow through the channels.
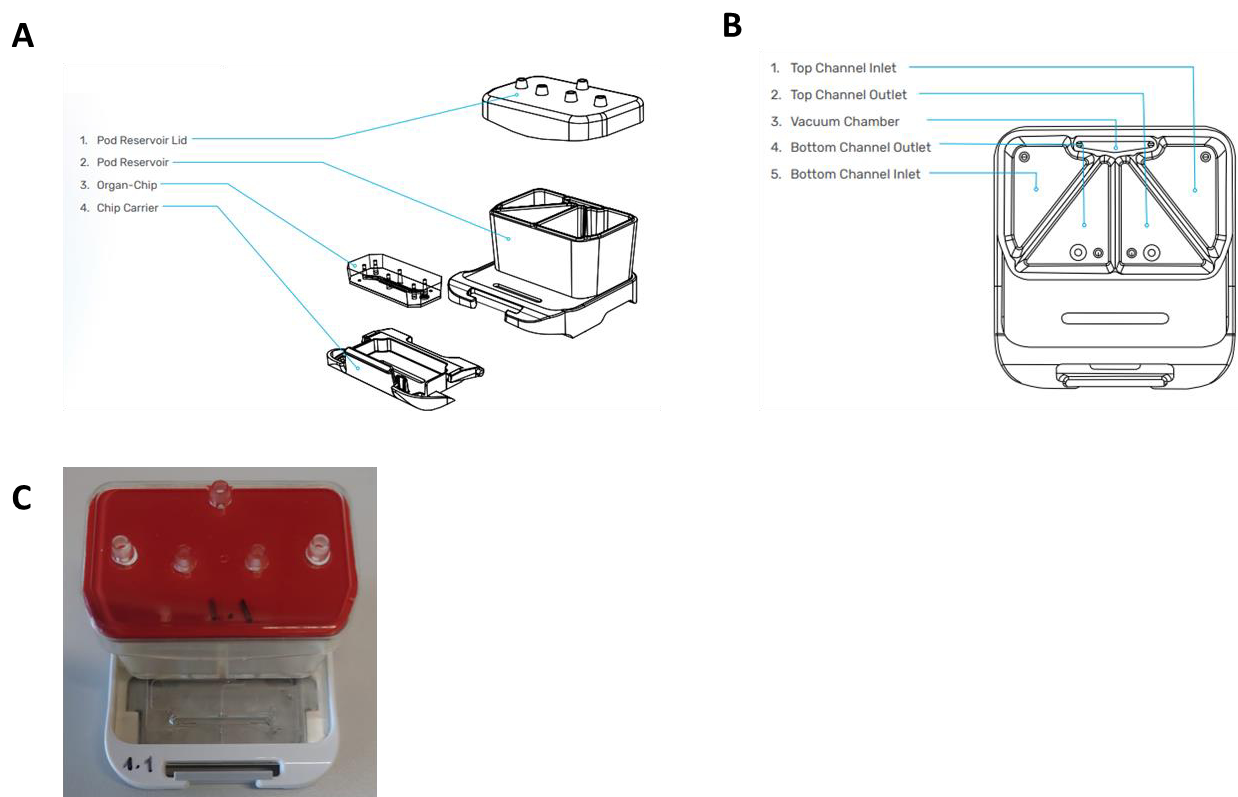
Figure 6: Pod-1® Portable Module. A) Schematic depicture of a Pod-1 Portable Module with all parts. Picture was obtained from Emulatebio.com **B)** Sketch of top and bottom inlet and outlet reservoirs for media of the pod. Picture was obtained from Emulatebio.com **C)** Photo of Pod-1 Portable Module with connected S-1 Chip.

3. Methods

Chips connected to the pod can be placed into the Zoë (Zoë® Culture Module) (Emulatebio, Boston, USA), a device that provides continuous medium flow for the channels and simultaneously applies mechanical forces in form of stretch to the chips (Figure 7). Up to twelve pods can be held in one Zoë under the same conditions in an incubator.

The Zoë is controlled by the Orb-HM1® Hub Module (Emulatebio, Boston, USA), a central hub that can connect up to four Zoë Culture Modules. It supplies the Zoë with 5 % CO_2, the vacuum needed for stretch and running power.
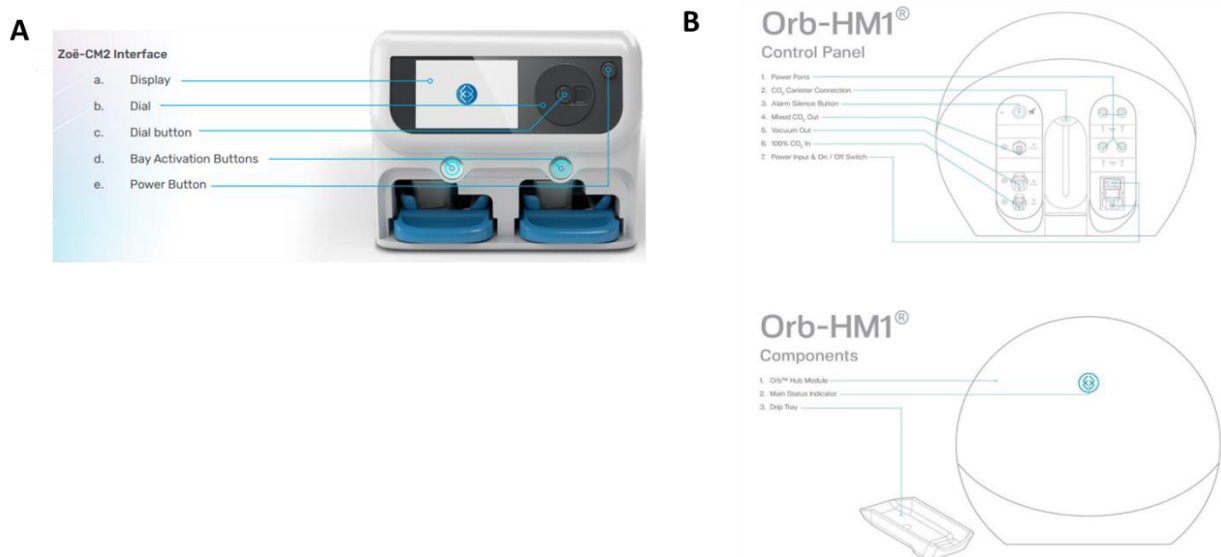
Figure 7: Zoe-CM2® Culture Module and Orb-HM1® Hub Module. A) Schematic depicture of Zoe-CM2® Culture Module all parts. Picture was obtained from Emulatebio.com **B)** Sketch Orb-HM1® Hub Module from front and back. Picture was obtained from Emulatebio.com

3.7.1 Chip activation and ECM coating

The PDMS material of the chip is hydrophobic and has to be turned hydrophilic to apply ECM for cell adhesion. For this, the chips in the carrier were placed into the chip cradle that can hold up to six chips at once. Before handling the chips, they were placed properly into the carrier by taking a 1000 µl pipet tip and pushing all four corners down to ensure proper stability. The chip was always orientated with the Emulate symbol to the right (Figure 8). For stability when working with the chip, it is recommended to hold the chip down with a pipet tip, so it does not move when operating on the inlets or outlets. Filter tips were used for every step.

For activation of the chip, ER-1 solution had to be prepared in the dark under a biosafety cabinet. ER-1 powder and ER-2 solution was equilibrated to RT for 15 to 20 min. After equilibration, 6 ml of ER-2 solution was pipetted into a dark falcon and 1 ml ER-2 solution was pipetted into the ER-1 vial. Without introducing any bubbles ER-1 powder was resuspended by adding one by one 1 ml of ER-2 solution until all the ER-1 powder was resolved in a total of 10 ml ER-2 (final concentration: 0.5 mg/ml). The solution was slightly inverted. To activate the chips, 200 µl of ER-1 solution was pipetted into the bottom inlet until there was a small droplet on the bottom outlet. Without pushing the plunger of the pipet, the pipet tip was removed from the bottom inlet and then the steps were repeated for the top channel. It is crucial not to introduce any bubbles into the channels, because this would disturb chip activation. The excess ER-1 solution on top of the chip had to be removed, because otherwise the surface of the chip would become hydrophilic. Chips in the chip cradle were placed into a square cell culture dish (Greiner BioOne, Frickenhausen, Germany) and then observed under the microscope to confirm the absence of bubbles. When all the chips were acceptable, the cell culture dish (without the lid) was placed under the UV light and incubated for 10 min. ER-1 solution was then completely removed from the channels (by placing an aspirator on the outlet ports). Again, 200 µl of ER-1 solution were placed into each channel and checked for bubbles before 5 min incubation under the UV light. After that, channels were washed with 200 µl ER-2 solution. Then 200 µl cold PBS was introduced into both channels, leaving little droplets on every inlet and outlet port, so that the channels would not dry out.

Immediately after chip activation, ECM coating had to be performed. For colon chips, a mixture of 100 µg/ml matrigel (Table 3) and 30 µg/ml collagen type I (Table 3) in cold PBS was prepared on ice, also with pre-chilled tips and Eppendorf tubes. Collagen Type I had to be pipetted very slowly (when pipet tip is in solution, at least 10 to 30 s should pass before taking it out). Then, the cold PBS of both channels was aspirated and replaced with 100 µl ECM solution forming a little droplet on the outlet and starting with the bottom channel. Then the chips were checked for bubbles. If bubbles had been introduced, channels would have been washed with ECM solution, until no bubbles were visible anymore. The reservoir on the chip cradle was filled with 1 ml PBS to avoid evaporation of liquids in the channels and then placed into the incubator for 2 h or overnight. It is also possible to seed cells after 4 h ECM coating at 37 °C.
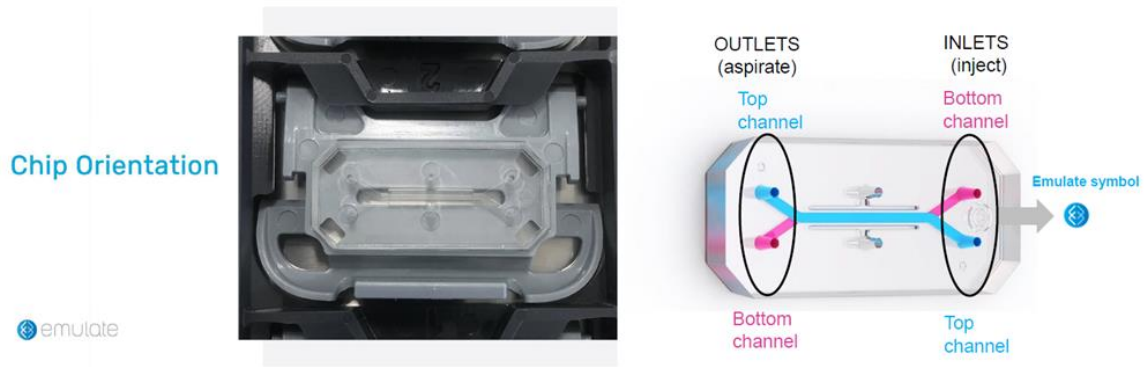
Figure 8: Chip Orientation. For chip handling, the chips were always placed with the Emulate symbol to the right, so the bottom channel inlet was on the right top, and the top channel inlet was on the right bottom. Picture obtained from Emulatebio.com

3.7.2 Cell seeding

Excess ECM solution of activated and ECM coated chips was removed and both channels were washed with 200 µl complete ECBM medium (ECBM + supplements (Table 4) + 2 % FBS + 1 % P/S). Channels were then filled with 200 µl complete HUVEC media leaving droplets on inlet and outlet ports of both channels. Chips were placed back into the incubator until HUVECs were fully prepared. HUVECs were trypsinized and centrifuged for 2 min at 1200 rpm. The cell pellet was resuspended in 300 µl of media and the cells were counted. For HUVEC seeding, cell density was adjusted to 6-8 $*10^6$ cells/ml. The chip cradle was then put under the biosafety bench. HUVEC suspension was mixed and then 15 to 20 µl of HUVEC suspension was pushed quickly into the bottom inlet by reverse pipetting while simultaneously aspirating the outflow of the outlet. Chips were then checked under the microscope for the right density (Figure 9). When cells were not at the right density in the channel, endothelial cells were washed twice with 200 µl complete ECBM medium to remove all the cells and then re-seeded. Chips were then flipped before being put into the incubator and incubated for 2 h at 37 °C. After incubation, the top channel inlet was filled with 200 µl complete Caco-2 medium leaving droplets at the inlet and outlet. For the bottom channel a gravity wash was performed. For this, an empty pipet tip was put on the bottom outlet and 200 µl complete HUVEC medium was put into the inlet. Then the pipet was released from the pipet tip, leaving the tip in the inlet. The gravity flow should allow flow through the channel into the tip on the outlet.

For preparation of Caco-2 cells, cells were trypsinized and centrifuged at 1200 rpm for 3 min. Cells were resuspended in 500 µl complete Caco-2 media (Table 4) before cell counting. Cell density was adjusted to 2.5 to 3 *10^6 cells/ml. Caco-2 suspension was mixed and then 35 to 50 µl was pushed quickly into the top inlet by reverse pipetting while simultaneously aspirating the outflow of the outlet. Chips were then checked under the microscope for the right density (Figure 9). When cells were not at the right density in the channel, epithelial cells were washed twice with 200 µl culture medium to remove all the cells and then re-seeded. The chip cradle reservoir was filled with 1 ml of PBS and the chips were incubated for 2 h at 37 °C. After incubation, a gravity wash for both channels was done starting with the bottom channel. The chips with the filter tips in the inlets and outlets of both channels were placed into the incubator for a minimum of 2 h at 37 °C and 5 % CO_2.
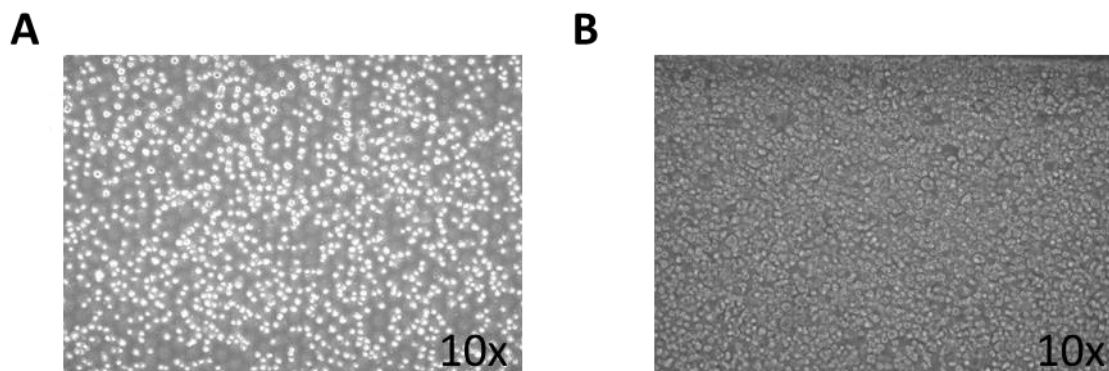
Figure 9: Seeding density of HUVEC and Caco-2 cells. A) HUVECs were seeded in a density of $6 - 8 * 10^6$ cells/ml into the bottom channel of the chip. **B)** Caco-2 cells were seeded in a density of $2.5 - 3 * 10^6$ cells/ml into the bottom channel of the chip.

3.7.3 Media preparation and pod priming

For placement of the medium into the pods, media had to be degassed. For this, 50 ml Complete HUVEC and Caco-2 medium was placed into a Falcon and a steriflip filter unit (Emulatebio, Boston, USA) was placed on top. Then vacuum was applied to the Steriflip unit for 5 min at 37 °C (in a water bath). If bubbles still persisted, vacuum was applied for additional 10 minutes. To inhibit regassing of the media, the media was placed with a loosened lid in the incubator at 37 °C until use.

Before chips were connected to the pod, first top and then bottom channel were washed with 200 µl warm complete Caco-2 medium leaving little droplets on the in-

and outlets of each channel. The chips were placed back into the incubator until they were put in the pods.

For pod priming, pods were placed on the blue tray from the Zoë. 3 ml of warm, degassed complete Caco-2 or complete ECBM medium was placed into the corner of each inlet reservoir above the VIA (port that connects inlet/outlet of pod with inlet/outlet of Chip). In the outlet reservoirs, 300 µl of equilibrated, warm medium was placed above the VIA. If bubbles were visible, they were removed. The blue tray with the pods was inserted into the Zoë and primed to ensure that media flow through the pod channels is given and no bubbles block the way (*Prime* program was selected and started). After a signal noise sounded, the pods were primed for one minute. After priming, the tray was taken out and the pods were checked for correct priming. There should be drops at each inlet and outlet port of every pod. If this was the case, pods were taken into the biosafety cabinet along with the chips. Chips were placed into the pods by sliding the chips in their carrier into the pod. When the chips were inserted correctly, excess media was removed from the chip surface.

When pods with chips were placed for the first time into the Zoë a *regulate cycle* was started to get rid of all remaining bubbles to guarantee correct media flow. For this the blue tray, with the chips connected to the pods, was placed into the Zoë, the flow rate was set to 30 µl/h, the *regulate* cycle was selected and started. The regulate cycle takes 2 h, after this Zoë resumes with the set flowrate.

After 24 h, pods were taken out of Zoë and a VIA wash was performed. For VIA wash, 100 µl medium was taken with reverse pipetting and pipetted up and down right above the respective VIA (but not *in* the VIA). This step was repeated for every reservoir (inlet and outlet). VIA wash was performed every time after media were added to the pod reservoirs. Then the pods were placed back into the Zoë and a second *regulate cycle* was done.

3.7.4 Chip maintenance

Chips that were connected to the pods, Zoë respectively, for 48 h were checked every 24 h for morphology of the cells. Representative pictures of the inlet and outlet junctions, as well from the centre were taken to track cell proliferation and 3D formation of the epithelial layer. Cell medium for the bottom channel was changed to ECBM

medium (with supplements) and 0.5 % FBS to prevent endothelial cells from over-growing. When pods were reconnected to the Zoë on the third day after cell seeding, the stretch was added. Stretch for colon chips are set to 10 % 0.15 Hz.

The top channel was checked daily for 3D growth of Caco-2 cells. After approximately six to seven days, Caco-2 cells had fully covered the channel and built a 3D structural epithelial barrier. When cells formed an epithelial barrier, the FBS in the complete Caco-2 media was reduced from 20 to 10 % to prevent overgrowth of cells.

If bubbles were introduced at any time during experiments, bubble troubleshoot was performed. For this, the chips must be removed from the pods, then channels would are washed with 200 µl ER-1, ECM or media solution, depending on the step. When chips were connected to the pods, flow rate was set to 600 µl/h for top and bottom channel and activated for 5 min. If bubbles still persisted, an attempt was made to remove them manually. A 1000 µl pipet tip was filled with 1 ml of media and the tip was placed directly on the VIA. The pipet was pushed down for at least 30 s up to 1 min.

3.7.5 Chip cell harvest

For cell harvesting, chips were disconnected from the pods and inserted into the chip cradle. Both channels were washed with 150 µl PBS. The top channel was blocked at the inlet and outlet with 200 µl tips. PBS from the bottom channel was aspirated and a 200 µl pipet tip was put on the outlet. 50 µl trypsin was inserted into the bottom channel and the pipet tip was released from the pipet. Chips were incubated for 5 min at 37 °C. After incubation, the pipet was put back on the pipet tip on the inlet and the liquid was pipetted up and down and then collected. Complete trypsinization of cells was checked under the microscope. The steps were repeated for the Caco-2 cells in the top channel, but they were incubated for 1 h with trypsin with repeated pipetting up and down every 10 min.

3.7.6 T cell recruitment to colon chip

For T cell recruitment to the epithelial barrier, the epithelial barrier had to be matured, building up a vili like 3D structure. On day one of the T cell recruitment, the bottom inlet pod reservoir was filled with at least 1.2 ml ECBM + supplements + 0.5 % FBS media

containing 50 ng/ml human TNFα to induce endothelial cell damage (priming). For stimulation of an inflammation in the colon (to simulate colitis), the top inlet pod reservoir was filled with at least 1.2 ml complete Caco-2 medium + 10 % FBS and 100 ng/ml of human IP10, MIP-3α, MEC, GPR14L, TECK, MCP-1, SDF-α and MIP-3β or 50 ng/ml IFNγ to induce epithelial barrier damage. Epithelial barrier disruption was induced with 50 ng/ml IFNγ in the bottom inlet pod (positive leak control). Resting controls were treated neither with TNFα, nor with the colitis chemokine cocktail or IFNγ. Dosing media treatment was done for 24 h. For tracking of T cells, cells were pre-stained with tracer dyes (s.3.2.5 Staining of T cells with tracer dyes). 4 *10^6 shNC and 4 *10^6 shCerS3 cells were centrifuged at 1200 rpm for 3 min and resuspended in 2 ml of Buoyancy medium and 2 ml of 2X RPMI medium (for a cell density of 2 *10^6 cells/ml). T cells in 4 ml 2X RPMI/ 2X Buoyancy medium were filled into the inlet pod reservoir of the bottom channel. Complete Caco-2 medium (10 % FBS) was filled into the inlet pod reservoir of the top channel. Pods were inserted into the Zoë and flow rate was set to 1000 μl/h for 4h. After this, media of pod outlets were collected and prepared for flow cytometry. Pod reservoirs were filled with their respective medium and flushed for 30 min at 1000 μl/h flow rate and afterwards incubated for another 24 h. After incubation, chips were checked under an Axio Primovert invert microscope with an integrated AxioCamERc5s with a Plan-Achromat 4x/0.10 objective (Carl Zeiss, Oberkochen, Germany) to detect fluorescent T cells attached to the epithelial or endothelial barrier. After pictures were obtained, cells were harvested from the chips and then analysed by flow cytometry. For flow cytomtery analysis cells were resuspended in 300 μl FACS flow and measured for 3 min each (Supplementary Figure 7).

3.8 Statistics

Statistical analyses were performed using GraphPad Prism software V9 (GraphPad Software Inc., La Jolla, USA). Data are presented as mean ± standard error (SEM) with a significance level of 95 %. Statistical significance of (adjusted) p-values was presented as follows: * $p<0.05$; ** $p<0.01$; *** $p<0.001$, **** $p<0.0001$. Data from two independent samples were compared by an unpaired, two-tailed t-test with a 95 % confidence interval. Dependent samples were compared by a paired t-test with a 95 % confidence interval. Statistical significances between groups of more than two

independent data sets were determined using a two-factorial or one-factorial analysis of variances (ANOVA) (two-way or one-way ANOVA), followed by a posthoc Tukey, Dunnett's multiple comparison test, Sidak's multiple comparison test or uncorrected Fisher's least significant difference (LSD) comparison, respectively. Differences in data collected over a period of time were analysed by comparison of areas under the curves (AUC) that were also calculated by the software.

4. Results

4.1 Effects of CerS1 and CerS3 on CD4+ Jurkat T cell signalling and function

CerS1 and CerS3 were significantly upregulated in WBC of human colitis patients in different disease status [363]. As $CD4^+$ T cells are the most prominent and abundant WBC type in colitis pathophysiology, the impact of CerS1 and CerS3 on those cells is of great interest. Therefore, stable knockdown and overexpression of both enzymes in a $CD4^+$ T cell line (Jurkat) was established and the role of CerS1 and CerS3 in T cells was investigated.

For stable knockdown of CerS1 and CerS3 in the $CD4^+$ Jurkat cell line, lentiviral transduction of shCerS1 and shCerS3 RNA or shNC (control) was performed. CerS3 overexpression was obtained by transfection of human CerS3 myc-tagged plasmid. Successful downregulation of CerS1 could be demonstrated by significant reduction of mRNA expression compared to the control (Figure 11 B). Unfortunately, CerS3 downregulation could not be shown via mRNA levels, but stable knockdown of CerS3 could be verified via WB analysis and reduction of dhCer and Cer products of CerS3 (very long-chain Cer) (Figure 10, Figure 14 A and Table 15). CerS3 overexpression was demonstrated by mRNA expression, CerS3 protein levels and increase of CerS3 dhCer and Cer products (Figure 13, Figure 10, Figure 15 A and Table 16).
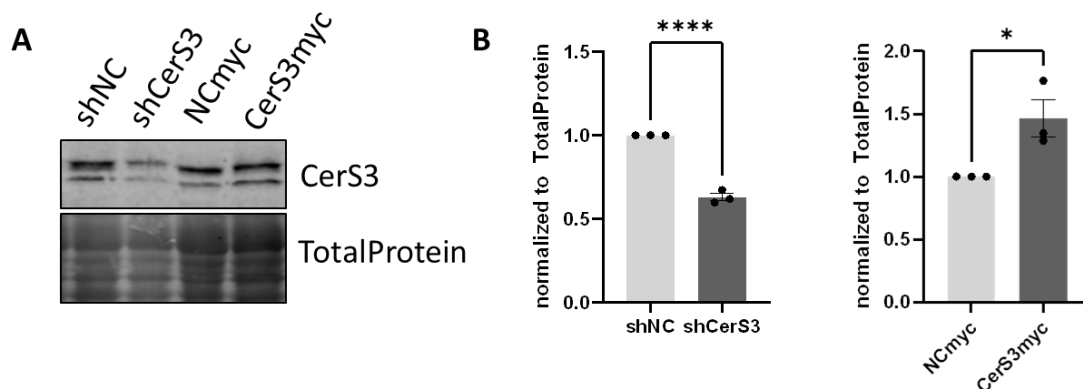
Figure 10: CerS3 protein levels in CerS3 knockdown and overexpression cells. CerS3 knockdown (shNC and shCerS3) and overexpression (NCmyc and CerS3myc) cells were harvested and total protein was isolated. 50 µg total protein was used for WB analysis. Blots were stained with TotalRevert700 stain for normalization and incubated overnight with CerS3 antibody. **A)** WB analysis of shNC, shCerS3, NCmyc and CerS3myc protein samples detected with CerS3 antibody. **B)** Relative CerS3 protein levels normalized to total protein on WB. Data are mean ± SEM. Statistical analysis was performed with an unpaired t-test (* p < 0.05, **** p < 0.0001) Group sizes: n=3

4.1.1 CerS1 and 3 expression increases after T cell stimulation

To confirm stable knockdown of CerS1 and CerS3 in Jurkat cells, but also to observe CerS expression levels after TCR activation, CerS1-6 expression levels were checked after 24 and 48 h of stimulation with CD2/3/28 activation beads and IL2. Control cells showed significant increase of CerS1 expression after activation, whereas after transduction of Jurkat cells with a virus containing GIPZ CerS1 V3LMM_432975 plasmid for CerS1 shRNA, cells could not restore CerS1 expression increase after stimulation (Figure 11). CerS1 knockdown was accompanied by CerS4, CerS5 and CerS6 decrease on a basal level, as well as a tendency of CerS3 downregulation (Figure 11). After stimulation of CerS1 knockdown cells, no CerS showed a significant increase and mRNA levels of CerS3 were significantly lower after stimulation compared to the controls (Figure 11).
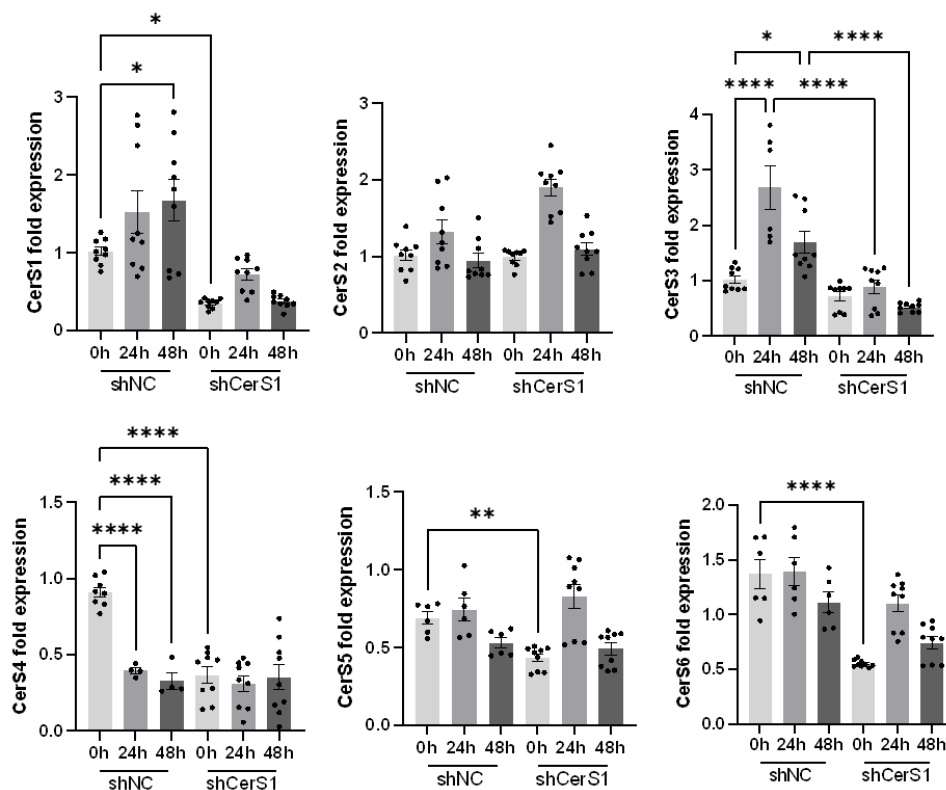
Figure 11: CerS expression after activation of CerS1 knockdown and control T cells. CerS1 knockdown (shCerS1) and control (shNC) cells were stimulated for 24 and 48 h with CD2/3/28 activation beads in a 1:1 cell-to-bead ratio and 200 U/ml human IL2. CerS expression was determined via qRT-PCR and related to expression of RPL13A. CerS1-6 mRNA levels in shNC and shCerS1 cells are shown. Data are mean ± SEM. Statistical analysis was performed with a one-way ANOVA with a posthoc Dunnett's multiple comparison test (* $p < 0.05$, ** $p < 0.01$, *** $p < 0.001$, **** $p < 0.0001$) Group sizes: n=3 measured in triplicates

CerS3 knockdown (accomplished by transduction of Jurkat cells with three viruses for CerS3 shRNA (GIPZ CerS3 V3LHS_ 373185, GIPZ CerS3 V3LHS_373159 and GIPZ CerS3 V3LHS_373183)) was accompanied by upregulation of CerS1 and downregulation of CerS5 and CerS6 on a basal level (Figure 12). Control cells showed significant increase of CerS3 after stimulation that could not be observed in the CerS3 knockdown cells (Figure 12).
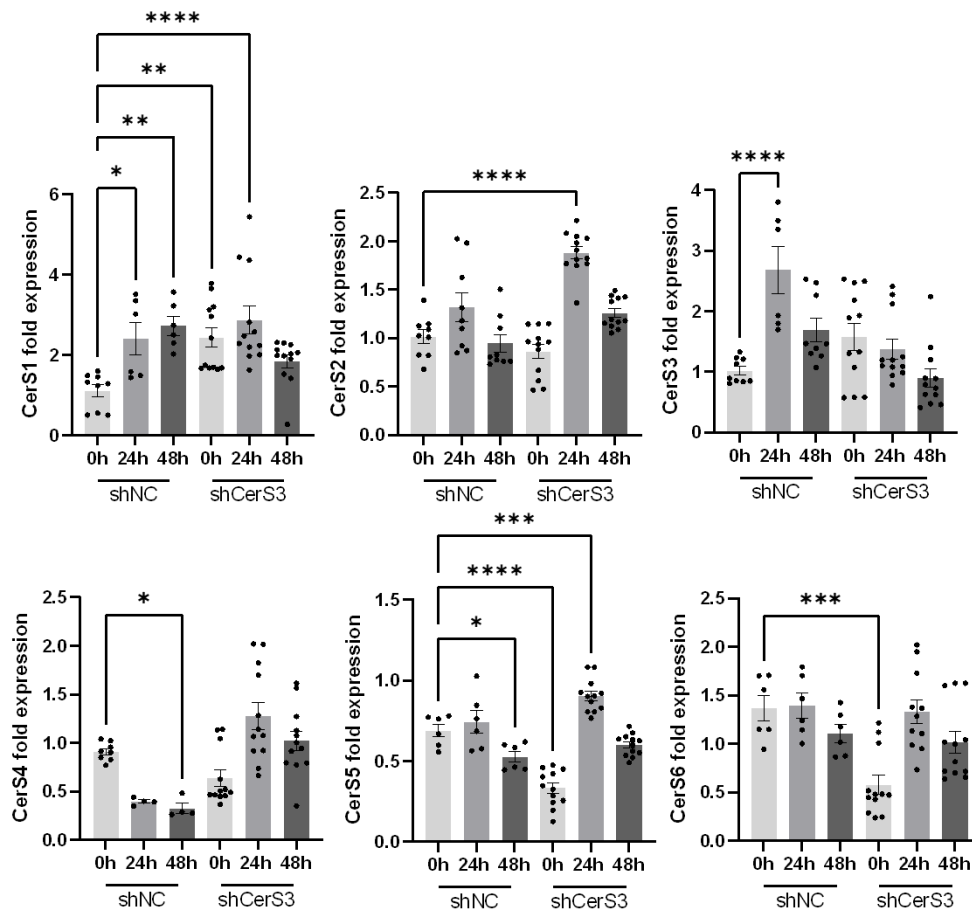
Figure 12: CerS expression after activation of CerS3 knockdown and control T cells. Knockdown (shCerS3) and control (shNC) cells were stimulated for 24 and 48 h with CD2/3/28 activation beads in a 1:1 cell-to-bead ratio and 200 U/ml human IL2. CerS expression was determined via qRT-PCR and related to expression of RPL13A. CerS1-6 mRNA levels in shNC and shCerS3 cells. Data are mean ± SEM. Statistical analysis was performed with a one-way ANOVA with a posthoc Dunnett's multiple comparison test (* $p < 0.05$, ** $p < 0.01$, *** $p < 0.001$, **** $p < 0.0001$) Group sizes: shNC n=3, shCerS3 n=4, measured in triplicates

Transfection of Jurkat cells with LASS3 Human Tagged ORF clone with pCMV6 promotor plasmid led to a 25-fold increase of CerS3 mRNA compared to the control, which remained after stimulation of cells (Figure 13). It also led to an increase of CerS1 and a decrease of CerS5 expression on a basal level (Figure 13). The expression

pattern of CerS1, CerS2, CerS4 and CerS6 did not differ between CerS1 knockdown cells and controls (Figure 13).
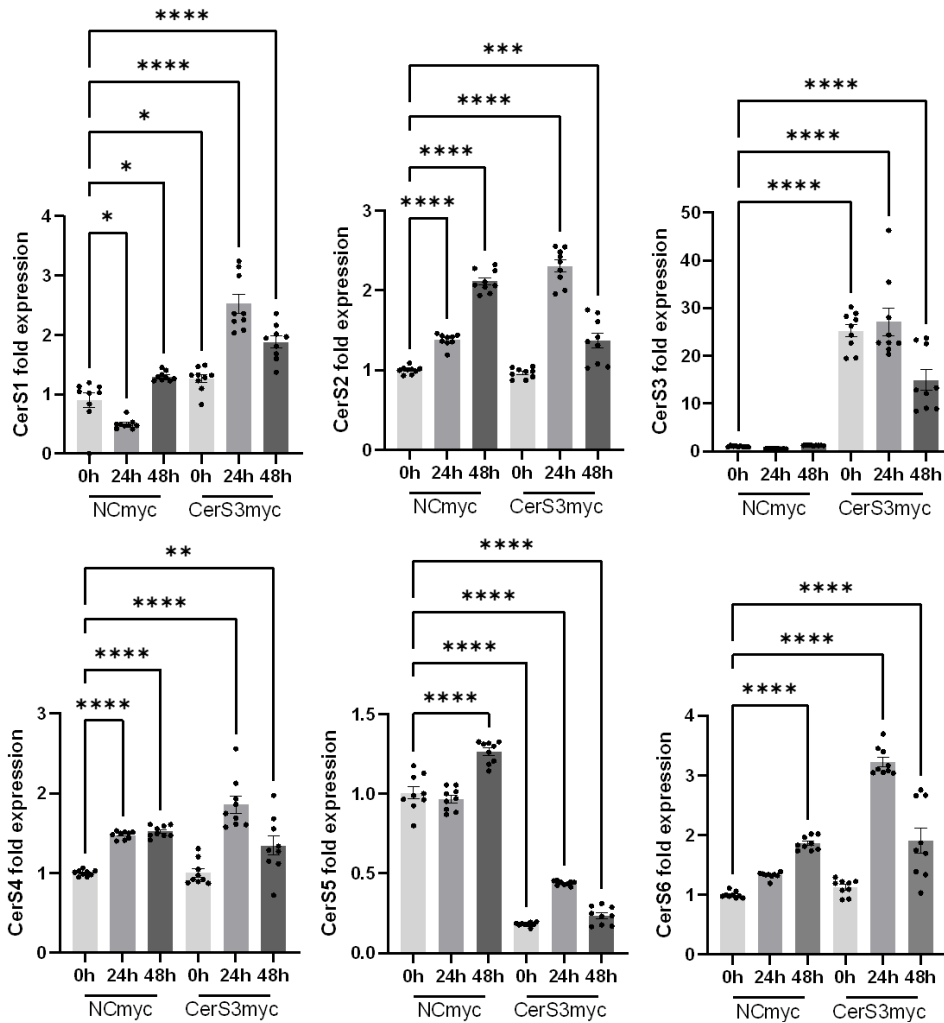
Figure 13: CerS expression after activation of Jurkat CerS3 overexpression or control cells. CerS3 overexpression (CerS3myc) and control (NCmyc) cells were stimulated for 24 and 48 h with CD2/3/28 activation beads in a 1:1 cell-to-bead ratio and 200 U/ml human IL2. CerS expression was determined via qRT-PCR and related to expression of RPL13A. CerS1-6 mRNA levels in NCmyc and CerS3myc cells are depicted in these graphs. Data are mean ± SEM. Statistical analysis was performed with a one-way ANOVA with a posthoc Dunnett's multiple comparison test (* $p < 0.05$, ** $p < 0.01$, *** $p < 0.001$, **** $p < 0.0001$) Group sizes: n=3 measured in triplicates

To sum it up, CerS1 and CerS3 expression was increased after activation of T cells. CerS1 knockdown cells failed to restore CerS1 increase after stimulation. CerS3 knockdown cells were also not able to restore CerS3 increase after stimulation. Overexpression of CerS3 maintained a high CerS3 expression over the stimulation time period.

4.1.2 Sphingolipid levels are reduced in CerS1 and CerS3 knockdown T cells and increased in CerS3 overexpression T cells

CerS expression was differently regulated after stimulation of cells. Thus it would be important to see the impact of CerS1 and CerS3 knockdown and CerS3 overexpression on a product level. For that, in addition to CerS mRNA expression after activation of TCR, cellular levels of dhCer and Cer, as well as levels of the corresponding complex sphingolipids like GlcCer, LacCer and S1P and the sphingoid bases (SPH) were measured in CerS1 knockdown cells, CerS3 knockdown (Figure 14, Table 15) and overexpression cells (Figure 15 A and Table 16) via LC-MS/MS measurement and compared to the controls.

The heat maps in Figure 15 A, B and C clearly depict an overall decrease of sphingolipids in untreated and stimulated (CD2/3/28 activation beads and IL2 for 24 and 48 h) CerS3 knockdown Jurkat cells in comparison to shNC cells.

There were no great differences in dhCer and Cer contents between control and CerS1 knockdown cells (Figure 14 A, Table 15). After stimulation, control and CerS1 cells displayed significantly lower concentrations of multiple Cer (C_{14}-, C_{18}-, $C_{18:1}$-, C_{20}-, C_{22}-, C_{24} and $C_{24:1}$-Cer).

Basal Glc- and LacCer concentrations in shCerS1 cells did not differ from control cell levels (Figure 14 A, Table 15). Glc-$C_{16:0}$-, -$C_{18:1}$- and -$C_{24:1}$-Cer concentrations were significantly increased in CerS1 knockdown cells after stimulation (Figure 14 B, Table 15).

For sphingoid bases, SPH-d$C_{18:1}$ and -d$C_{18:0}$ were significantly increased in an unstimulated and stimulated state in CerS1 knockdown cells, and S1P-d$C_{18:1}$ only showed significant increase in an unstimulated state (Figure 14 B, Table 15).
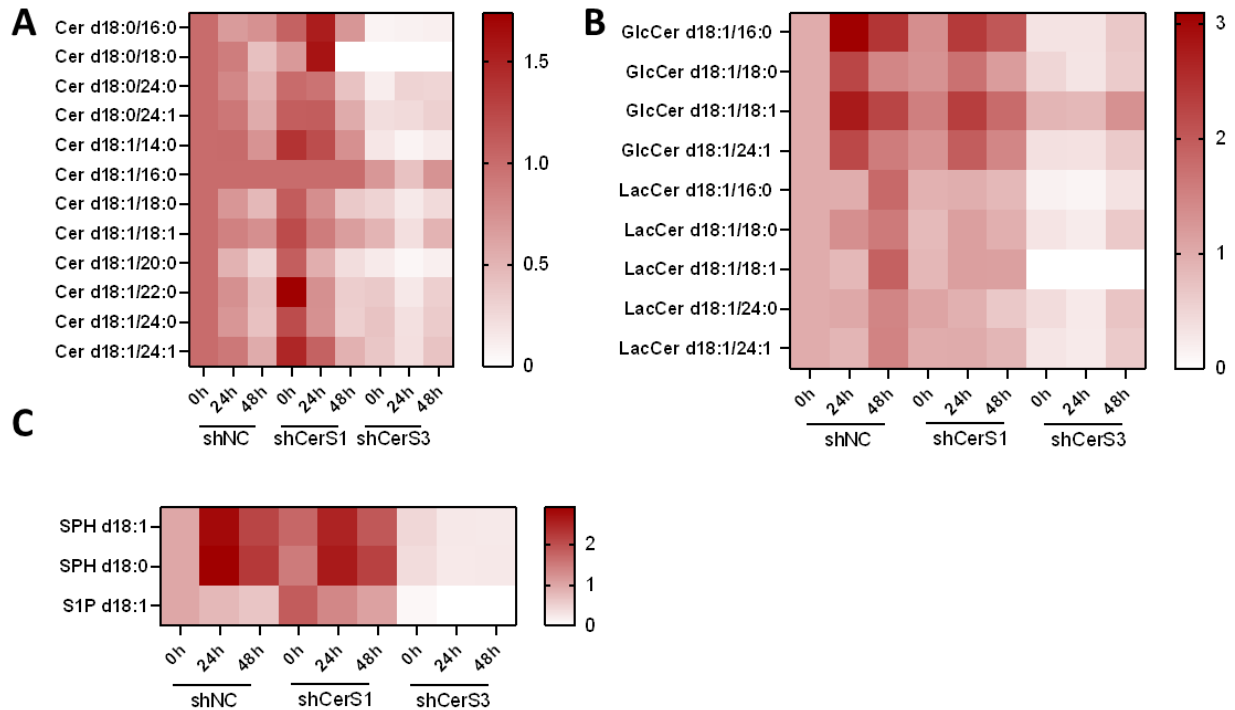
Figure 14: Sphingolipid levels of stimulated control and CerS1/CerS3 knockdown Jurkats. Control (shNC) and CerS1/CerS3 knockdown (shCerS1/shCerS3) cells were stimulated with CD2/3/28 activation beads in a 1:1 cell-to-bead ratio and 200 U/ml human IL2. **A)** Dihydro-Ceramide (dhCer) and ceramide (Cer) levels in shNC, shCerS1 and shCerS3 cells. **B)** Glycosyl- (GlcCer) and lactosyl-(LacCer) Ceramide levels in shNC, shCerS1 and shCerS3 cells. **C)** Detectable sphingoid bases (SPH, S1P) in shNC, shCerS1 and shCerS3 cells. Data are mean ± SEM. All values were compared to the unstimulated control. Group sizes: n=3

Basal levels of long-chain C_{14}-, C_{18}-, $C_{18:1}$, C_{20}-Cer, as well as very long-chain C_{22}-, C_{24}- and $C_{24:1}$-Cer levels were significantly lower in CerS3 knockdown cells compared to controls (Figure 14 A, Table 15). Long-chain and very long-chain dhCer (C_{18}-, C_{24}-, $C_{24:1}$-dhCer) and long-chain and very long-chain Cer (C_{18}-, C_{20}-, C_{22}-, C_{24}- and $C_{24:1}$-Cer) were significantly downregulated after 24 or 48 h of activation in shNC control cells (Figure 14 A, Table 15). But there was no significant upregulation of long-chain or very long-chain dhCer or Cer in CerS3 knockdown cells after stimulation (Figure 14 A, Table 15).

In control cells, Glc- and LacCer levels were elevated after activation, whereas in CerS3 knockdown cells there was no significant increase (Figure 14 B, Table 15). Glc- and LacCer levels in CerS3 knockdown cells stayed significantly lower after stimulation compared to control cells (Figure 14 B, Table 15).

Sphingoid bases SPH $-dC_{18:0}$ and $-dC_{18:1}$ increased after stimulation of control cells, whereas S1P-$dC_{18:1}$ (Sphingosine-1-Phosphate) levels dropped significantly after

stimulation of cells (Figure 14 C, Table 15). In CerS3 knockdown cells, no elevation of any sphingoid base after stimulation could be observed (Figure 14 C, Table 15).

Table 15: P-values for absolute sphingolipid levels of stimulated shNC, shCerS1 and shCerS3 cells. All values are related to shNC 0h. Statistical analysis was performed with an Oneway ANOVA and followed by Tukey's posthoc analysis (* $p < 0.05$, ** $p < 0.01$, *** $p < 0.001$, **** $p < 0.0001$). Data that could not be statistically evaluated are crossed out. Group sizes: n=3

Sphingolipids	shNC 24h	shNC 48h	shCerS1 0h	shCerS1 24h	shCerS1 48h	shCerS3 0h	shCerS3 24h	shCerS3 48h
Cer d18:0/16:0	0,8854	0,0299	0,0981	0,1407	0,0365	0,0063	0,0002	0,0031
Cer d18:0/18:0	0,5898	0,145	0,1454	0,9593	0,0225	0,0225	0,0225	0,0225
Cer d18:0/24:0	0,1434	0,0538	0,9999	0,9914	0,0207	0,0187	0,0129	<0,0001
Cer d18:0/24:1	0,9272	0,0063	0,6487	0,5456	0,0217	0,0308	0,006	0,0449
Cer d18:1/14:0	0,9999	0,5266	0,009	0,2972	0,001	0,0063	0,001	0,0047
Cer d18:1/16:0	-	-	-	-	-	-	-	-
Cer d18:1/18:0	0,0991	0,0061	0,0735	0,0364	0,0003	0,0352	0,0012	0,0103
Cer d18:1/18:1	0,3925	0,721	0,4675	0,3891	0,0389	0,186	0,0396	0,1521
Cer d18:1/20:0	0,3699	0,1387	0,9635	0,3656	0,1044	0,1008	0,0736	0,095
Cer d18:1/22:0	0,0339	0,0511	0,0544	0,2452	0,0398	0,0603	0,0219	0,0202
Cer d18:1/24:0	0,2874	0,0268	0,0779	0,1329	0,0118	0,1856	0,0144	0,0971
Cer d18:1/24:1	0,8555	0,007	0,0034	0,4843	0,0013	0,0757	0,0013	0,0436
GlcCer d18:1/16:0	0,033	0,1448	0,2256	0,0148	0,0121	0,0752	0,0234	0,2835
GlcCer d18:1/18:0	0,018	0,2693	0,0611	0,0814	0,4639	0,0985	0,0032	0,0802
GlcCer d18:1/18:1	0,0267	0,4612	0,0376	0,0025	0,0259	0,8802	0,6543	0,263
GlcCer d18:1/24:1	0,1107	0,028	0,1736	0,0229	0,0826	0,0967	0,0098	0,3839
LacCer d18:1/16:0	0,9999	0,5171	0,8253	0,9998	0,0024	0,019	0,0107	0,0554
LacCer d18:1/18:0	0,0633	0,1888	0,1381	0,5619	0,9933	0,2297	0,0438	0,1305
LacCer d18:1/18:1	0,5386	0,4634	0,6498	0,9626	0,8239	0,0187	0,0187	0,0187
LacCer d18:1/24:0	0,9962	0,4812	0,6284	0,9972	0,2457	0,198	0,0716	0,6013
LacCer d18:1/24:1	0,4074	0,5057	>0,9999	>0,9999	0,8589	0,0307	0,0093	0,0389
SPH d18:1	0,0386	0,1514	0,0022	0,0009	0,06	0,1436	0,0056	0,0194
SPH d18:0	0,0405	0,1859	0,0172	0,0006	0,0563	0,1384	0,0032	0,0183
S1P d18:1	0,3042	0,0497	0,0215	0,1057	0,8041	0,0275	0,0113	0,0113

In contrast to CerS3 knockdown cells, CerS3 overexpression cells showed higher basal levels of long-chain C_{18}-dhCer and very long-chain C_{24}- and $C_{24:1}$-dhCer compared to control cells (Figure 15 A, Table 16). Long-chain C_{14} and C_{18}-Cer and very long-chain C_{20}-, C_{24}- and $C_{24:1}$-Cer concentrations were also elevated in unstimulated CerS3 overexpression cells (Figure 15 A, Table 16). After stimulation of CerS3 overexpression cells, a significant increase of C_{18}-, C_{24}- and $C_{24:1}$- dhCer and C_{14}-, C_{18}-, C_{20}-, C_{22}-, C_{24}- and $C_{24:1}$-Cer could be observed (Figure 15 A, Table 16). After stimulation of control cells, C_{18}-, C_{24}- and $C_{24:1}$- dhCer and C_{18}-, C_{20}-, C_{22}-, C_{24}-

and $C_{24:1}$-Cer levels were significantly lower compared to stimulated CerS3myc cells (Figure 15 A, Table 16).
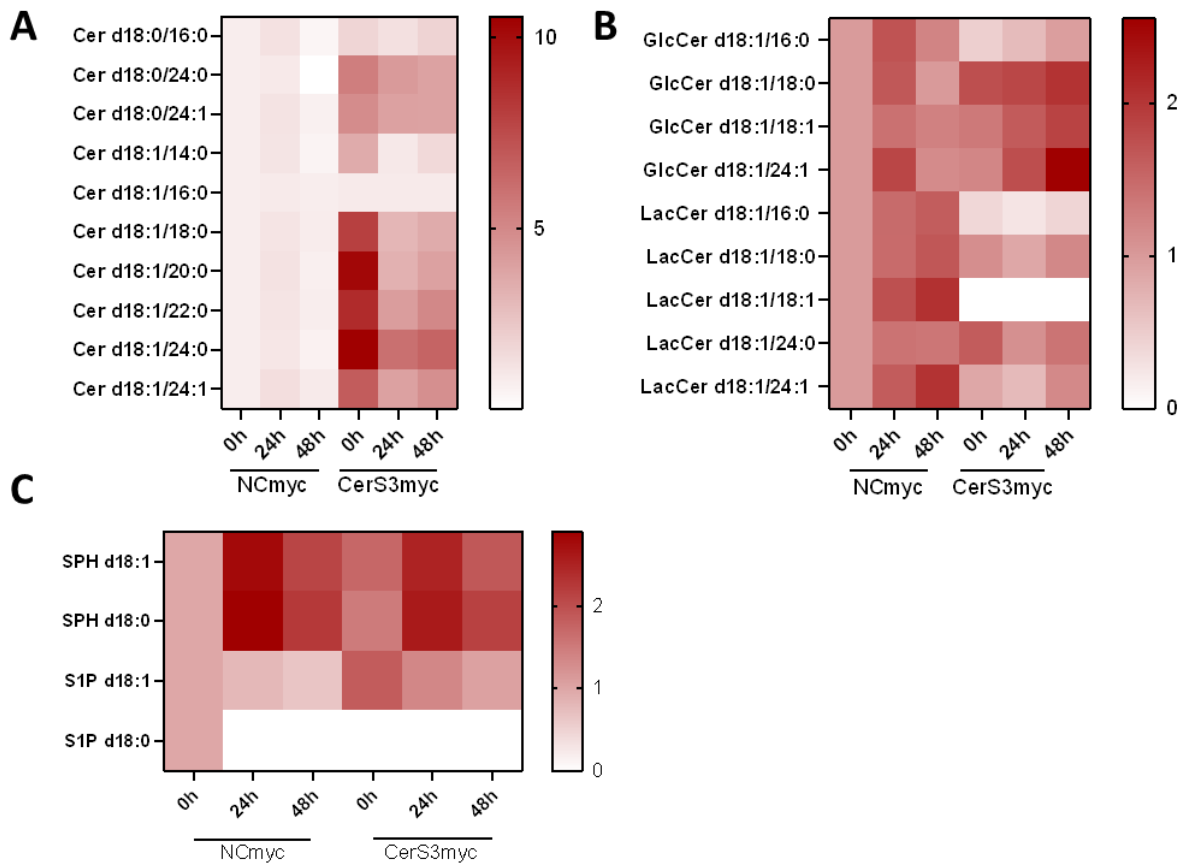
Figure 15: Sphingolipid levels of stimulated control and CerS3 overexpression Jurkats. Control (NCmyc) and CerS3 overexpression (CerS3myc) cells were stimulated with CD2/3/28 activation beads in a 1:1 cell-to-bead ratio and 200 U/ml human IL2. **A)** Dihydro-Ceramide (dhCer) and ceramide (Cer) levels in NCmyc and CerS3myc cells. **B)** Glycosyl- (GlcCer) and lactosyl-(LacCer) Ceramide levels in NCmyc and CerS3myc cells. **C)** Detectable sphingoid bases (SPH, S1P) in NCmyc and CerS3myc cells. Data are mean ± SEM. All values were compared to the unstimulated control. Group sizes: n=3

In control cells, levels of Lac-C_{18}-, -$C_{18:1}$- and –$C_{24:1}$-Cer were significantly increased after stimulation of T cells (Figure 15 B, Table 16). In CerS3 overexpression cells, on the other hand only Lac-$C_{24:1}$-Cer concentrations were elevated after activation of cells (Figure 15 B, Table 16).

SPH-d$C_{18:1}$ concentration was significantly higher in non-stimulated CerS3 overexpression cells compared to control (Figure 15 C, Table 16). In CerS3 overexpression cells, only S1P-d$C_{18:1}$ levels decreased significantly after stimulation (Figure 15 C, Table 16).

Table 16: P-values for absolute sphingolipid levels of stimulated NCmyc and CerS3myc cells. All values are related to NCmyc 0h. Statistical analysis was performed with an Oneway ANOVA and followed by Tukey's posthoc analysis (* $p < 0.05$, ** $p < 0.01$, *** $p < 0.001$, **** $p < 0.0001$). Data that could not be statistically evaluated are crossed out. Group sizes: n=3

Sphingolipids	NCmyc 24h	NCmyc 48h	CerS3myc 0h	CerS3myc 24h	CerS3myc 48h
Cer d18:0/16:0	-	-	-	-	-
Cer d18:0/24:0	0,9431	0,0062	0,0002	0,0144	0,0262
Cer d18:0/24:1	0,3203	0,7237	0,0016	0,0142	0,0205
Cer d18:1/14:0	0,3886	0,706	0,0398	0,405	0,4566
Cer d18:1/16:0	0,525	0,9999	0,525	0,525	0,525
Cer d18:1/18:0	0,3422	0,9919	0,0036	0,0028	0,0091
Cer d18:1/20:0	0,3548	0,9689	0,003	0,0246	0,0368
Cer d18:1/22:0	0,2255	0,9999	0,0029	0,001	0,0089
Cer d18:1/24:0	0,0928	0,775	0,0056	0,0154	0,0316
Cer d18:1/24:1	0,0962	0,862	0,0004	0,0083	0,0227
GlcCer d18:1/16:0	0,0354	0,94	0,6828	0,6953	>0,9999
GlcCer d18:1/18:0	0,063	>0,9999	0,1536	0,0227	0,2797
GlcCer d18:1/18:1	0,5341	0,9375	0,5725	0,4216	0,2893
GlcCer d18:1/24:1	0,0486	0,9953	0,9342	0,0142	0,1708
LacCer d18:1/16:0	0,4883	0,0962	0,2665	0,1434	0,3166
LacCer d18:1/18:0	0,266	0,0471	0,4429	0,7128	0,236
LacCer d18:1/18:1	0,1139	0,0025	0,0571	0,0571	0,0571
LacCer d18:1/24:0	0,5622	0,3476	0,0629	0,5834	0,7809
LacCer d18:1/24:1	0,1697	0,176	0,9089	0,2981	0,9479
SPH d18:1	0,0321	0,1269	0,0018	0,0008	0,0499
SPH d18:0	0,0336	0,1563	0,0143	0,0005	0,0469
S1P d18:1	0,2583	0,0413	0,0179	0,0882	0,7308
S1P d18:0	0,7831	0,7831	0,7831	0,7831	0,7831

All in all, CerS3 knockdown cells displayed a significant reduction of CerS3 products (very long-chain dhCer and Cer) and were unable to increase Glc- and Lac-Cer levels after stimulation compared to control cells. CerS3 overexpression showed a significant increase of very long-chain dhCer and Cer and a distinct pattern of Glc- and Lac-Cer compared to control cells. CerS1 knockdown cells did not show reduction of CerS1 products (C_{18}-Cer) and displayed less changes in sphingolipid levels compared to control.

4.1.3. TCR signalling is impaired in CerS3 knockdown T cells and not affected in CerS1 knockdown and CerS3 overexpression cells

TCR signalling takes places in lipid rafts, which show a high abundance of different glycosphingolipids [394]. After activation of T cells, glycosphingolipids were increased. Therefore the TCR signalling could be affected by the lipid content alterations in CerS1 and CerS3 knockdown cells and CerS3 overexpression cells. Activation of T cells is mediated through stimulation of the TCR via phosphorylation of Zap70 and co-stimulatory receptors like CD2, CD28 or IL2 at the plasma membrane [89, 90]. To activate the cells, they were treated with CD2/3/28 activation beads and IL2. Phosphorylation of Zap70 was assessed via WB analysis. Control cells were compared to CerS1 and CerS3 knockdown cells, as well as to CerS3 overexpression cells (Figure 16 and Figure 17).

TCR signalling occurs very fast in the T cells, therefore time points from 5, 15 and 30 min were chosen to observe Zap70 phosphorylation. After 5 to 15 min after activation with CD2/3/28 activation beads and IL2, significant phosphorylation of Zap70 could be observed in the control cells, as well as in the CerS1 knockdown cells (Figure 16). Both cell lines were capable to induce TCR signalling via Zap70 phosphorylation and after 30 min, phosphorylation decreased in control and CerS1 knockdown (Figure 16).
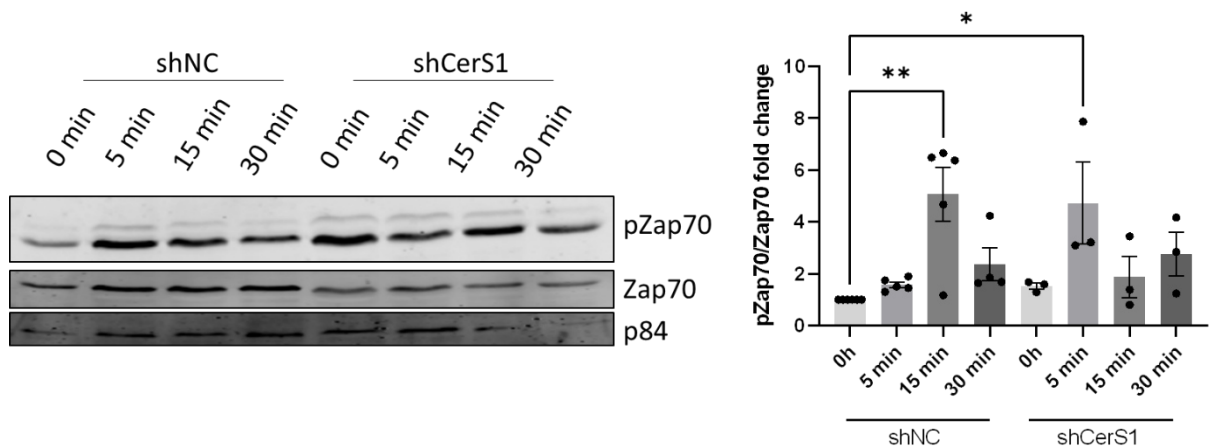
Figure 16: TCR signalling in CerS1 knockdown cells. Cells were stimulated for 5, 15 and 30 min with CD2/3/28 activation beads in a 1:1 cell-to-bead ratio and 200 U/ml human IL2. Whole protein was isolated and 50 µg total protein was used for WB analysis of Zap70 phosphorylation of shNC and shCerS1 samples. Protein levels were normalized to p84 protein levels. Data are mean ± SEM. Statistical analysis was performed with a one-way ANOVA and posthoc Tukey's test (* $p < 0.05$, ** $p < 0.01$) Group sizes: shNC n=5, shCerS1 n=3

CerS3 knockdown cells did not show significant phosphorylation of Zap70 after stimulation of the cells (Figure 17 A). Control cells showed an increase of Zap70 phosphorylation after 5 and 15 min, but shCerS3 cells were unable to increase Zap70 phosphorylation even after 30 min. In contrast to that, CerS3 overexpression cells showed significant increase of Zap70 phosphorylation after 5 and 15 min, similar to NCmyc control cells (Figure 17 B).

Figure 17: TCR signalling in CerS3 knockdown and overexpression cells. Knockdown (shNC and shCerS3) and overexpression (NCmyc and CerS3myc) cells were stimulated for 5, 15 and 30 min with CD2/3/28 activation beads in a 1:1 cell to bead ratio and 200 U/ml human IL2. Whole protein was isolated and 50 µg total protein was used for WB analysis. Protein levels were normalized to β-Actin protein levels. **A)** WB analysis of Zap70 phosphorylation of shNC and shCerS3 samples. **B)** WB analysis of Zap70 phosphorylation of NCmyc and CerS3myc samples. Data are mean ± SEM. Statistical analysis was performed with a one-way ANOVA and posthoc Tukey's test for A and B) and an unpaired t-test for B) (* $p < 0.05$, ** $p < 0.01$, *** $p < 0.001$, **** $p < 0.0001$) Group sizes: n=3

In summary, CerS1 knockdown did not affect TCR signalling in Jurkat cells via Zap70 phosphorylation and CerS3 overexpression in Jurkat cells showed similar TCR activation compared to control cells. Instead, TCR signalling was not activatable in CerS3 knockdown Jurkat cells.

4.1.4 NFAT1 activation in CerS3 knockdown T cells is reduced

TCR signalling was impaired in CerS3 knockdown cells and unaffected in CerS3 overexpression cells. TCR signalling leads to activation of a variety of transcription factors (AP-1, NFκB and NFAT1) that enhance gene expression of effector genes which are responsible for proliferation, migration and cytokine release in T cells [92, 93]. Therefore, activation of those transcription factors were studied in shCerS3, CerS3myc and control cells (shNC and NCmyc). CerS1 knockdown cells were not tested, since TCR signalling did not differ from the control.

AP-1 is a heterodimeric protein that consists of phosphorylated c-Jun and c-Fos. When phosphorylated c-Jun and c-Fos interact with each other, the complex translocates into the nucleus. Activation of AP-1 was investigated by phosphorylation of c-Jun and c-Fos expression via WB analysis (Figure 18).

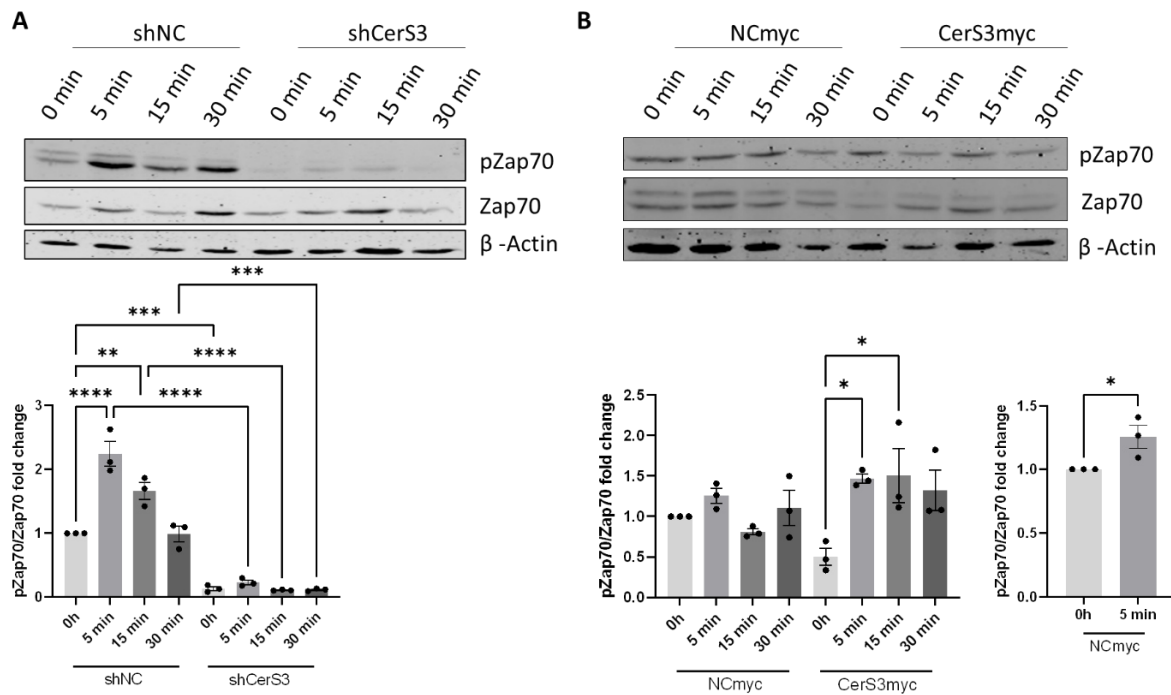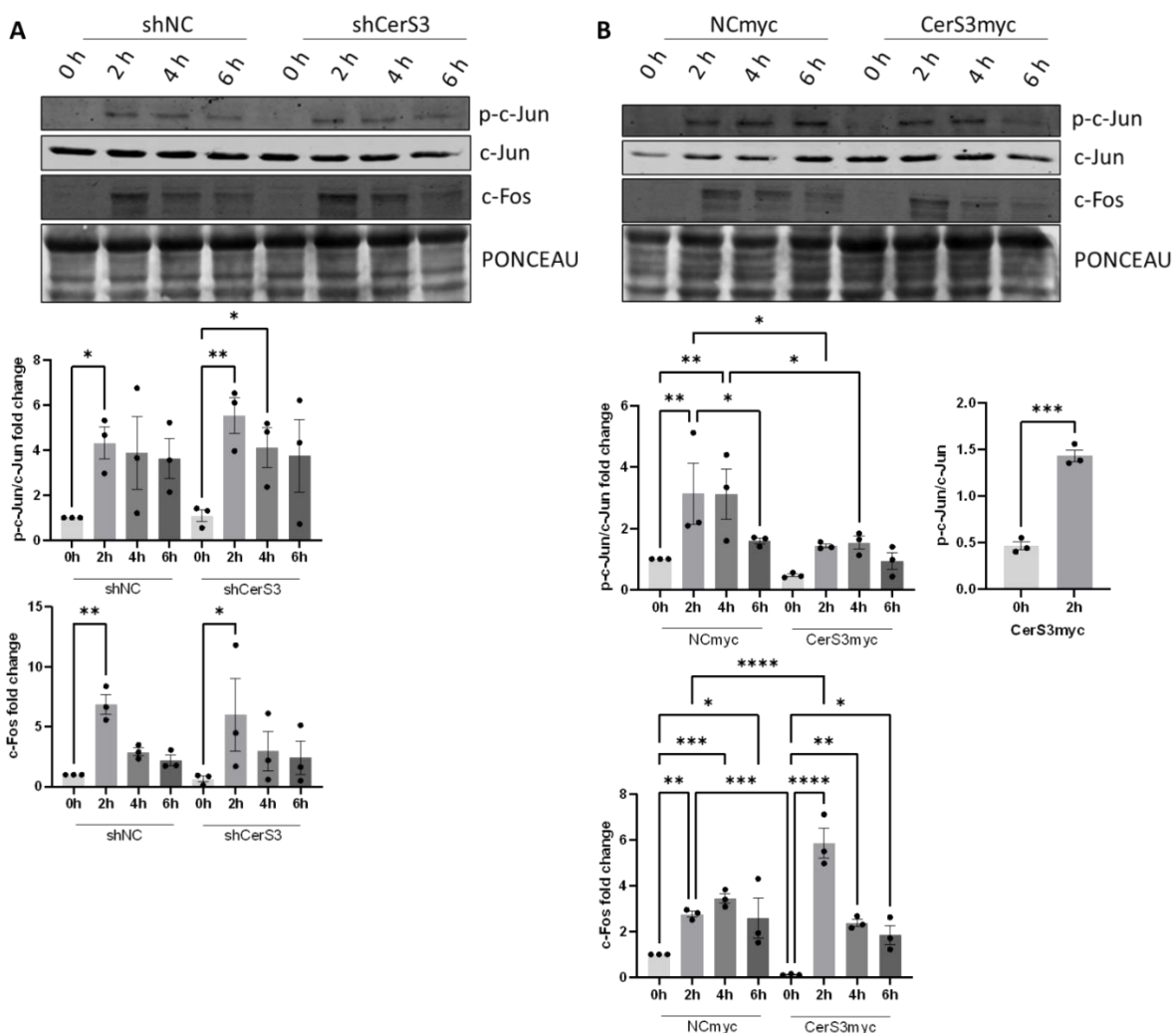**Figure 18: AP-1 complex in CerS3 knockdown and overexpression cells.** Knockdown (shNC and shCerS3) and overexpression (NCmyc and CerS3myc) cells were stimulated for 2, 4 and 6 h with CD2/3/28 activation beads in a 1:1 cell to bead ratio and 200 U/ml human IL2. Whole protein was

isolated and 50 μg total protein was used for WB analysis. Protein levels of phosphorylated c-Jun, c-Jun and c-Fos were normalized to PONCEAU staining of WB membranes. **A)** WB analysis of c-Jun phosphorylation and c-Fos of shNC and shCerS3 Jurkat cells. P-c-Jun and c-Fos fold expressions are related to unstimulated control cells. **B)** WB analysis of c-Jun phosphorylation and c-Fos of NCmyc and CerS3myc Jurkat cells. P-c-Jun and c-Fos fold expressions were related to unstimulated control cells. Data are mean ± SEM. Statistical analysis was performed with an ne-way ANOVA and uncorrected Fisher's LSD comparison for A) One-way ANOVA and uncorrected Fisher's LSD comparison and an unpaired t-test for B) (* $p < 0.05$, ** $p < 0.01$, *** $p < 0.001$, **** $p < 0.0001$) Group sizes: n=3

Significant phosphorylation of c-Jun after 2 h of stimulation could be observed in control cells as well as in CerS3 knockdown (Figure 18 A) and CerS3 overexpression cells (Figure 18 B). C-Fos expression was significantly upregulated after 2 h stimulation in both, CerS3 knockdown and control cells (Figure 18 A). There was no significant difference between phosphorylation state of c-Jun or c-Fos expression in CerS3 knockdown and control cells (Figure 18 A). On the other hand, CerS3 overexpression cells showed significant higher c-Fos expression after 2 h compared to the control (Figure 18 B). Phosphorylation state of c-Jun was significantly lower after 2 and 4 h in CerS3 overexpression cells compared to control (Figure 18 B).
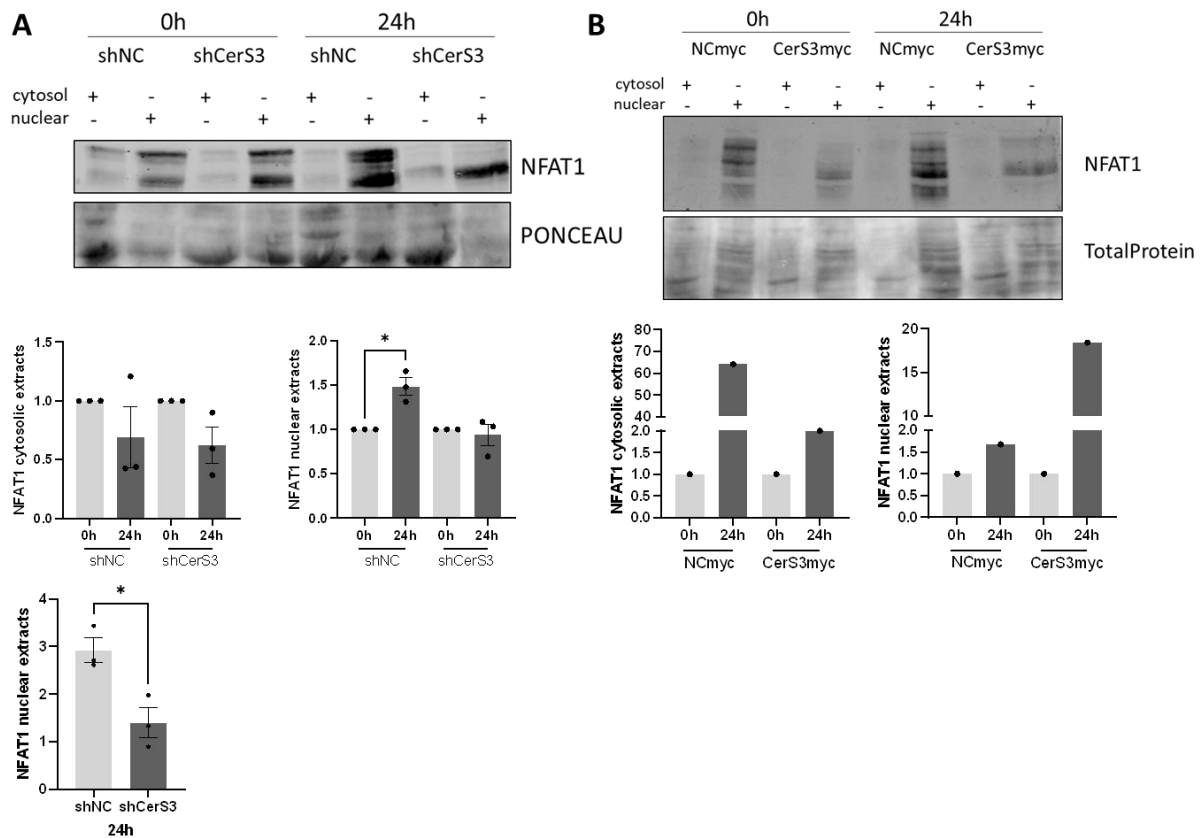
Figure 19: NFAT1 translocation into the nucleus in CerS3 knockdown and overexpression cells. CerS3 knockdown (shCerS3) and overexpression (CerS3myc) and control (shNC, NCmyc) cells were stimulated with CD2/3/28 activation beads in a 1:1 cell-to-bead ratio and 200 U/ml IL2 for 24 h. Afterwards cytosolic and nuclear proteins were extracted. 50 μg of cytosolic and nuclear extracts were

used for the WB analysis. **A)** NFAT1 protein levels in shNC and shCerS3 cells. Protein levels were normalized to PONCEAU staining. **B)** NFAT1 protein levels in NCmyc and CerS3myc cells. Protein levels were normalized to total protein. Data are mean for B) and ± SEM for A). Statistical analysis was performed with a one-way ANOVA and post-hoc Tukey's correction and unpaired t-test for A) (* p < 0.05) Group sizes: n=3 for A, n=1 for B

NFAT1 is activated when it is dephosphorylated. Dephosphorylation triggers the translocation of NFAT1 into the nucleus. To observe transcription factor activation, cytoplasmic and nucleic NFAT1 protein levels were compared in CerS3 knockdown and overexpression cells (Figure 19). In CerS3 knockdown cells, translocation of NFAT1 after 24 h into the nucleus was impaired and significantly decreased compared to the control cells (Figure 19 A). Since the data of CerS3 overexpression cells are preliminary, no statements about statistical significances for Figure 19 B can be made. It seems that in CerS3 overexpression Jurkat cells, NFAT1 translocation into the nucleus was increased compared to the increase in control cells after 24 h stimulation with CD2/3/28 activation beads and IL2 (Figure 19 B). Further experiments for CerS3myc cells are planned, but due to antibody delivery problems, the WBs could not be finished.

4.1.5 S1P1 is upregulated in CerS3 overexpression cells, and downregulated in CerS3 knockdown cells

Lipid concentrations were significantly altered in CerS1 and CerS3 knockdown Jurkat cells, as well as in CerS3 overexpression cells. Alterations in the sphingolipid contents can also alter plasma membrane composition and thereby affect membrane-bound receptors like S1P1 and 4 that play a crucial role in T cell effector function [385, 395]. So first, mRNA levels of S1P1 and S1P4 in activated shCerS1 and shCerS3 knockdown and CerS3 overexpression Jurkat cells and controls were tested (Figure 20 and Figure 21).

CerS1 and CerS3 knockdown cells showed significant less S1P1 expression in an unstimulated state compared to control cells (Figure 20). After activation of control cells, S1P1 expression decreased significantly after 24 and 48 h. CerS3 knockdown cells showed increased S1P1 expression after 24 h, but it was not as high as the expression in unstimulated control cells (Figure 20). For S1P4, the opposite could be observed. Expression levels were significantly higher in CerS1 and CerS3 knockdown

cells in comparison to shNC Jurkat cells and were reduced after activation of cells with CD2/3/28 activation beads and IL2 for 24 and 48 h in both cell lines (Figure 20). CerS3 knockdown cells even showed significantly higher S1P4 expression levels compared to CerS1 knockdown cells (Figure 20).
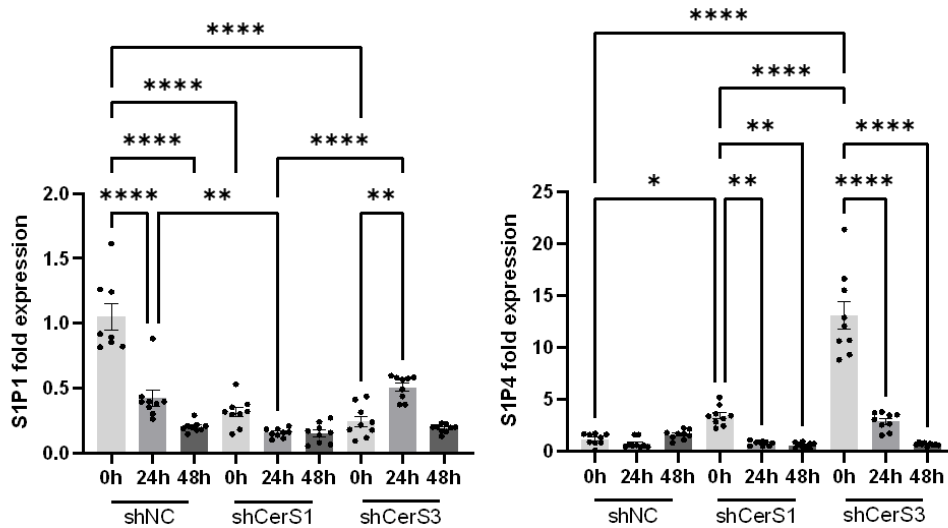
Figure 20: S1P1 and 4 expression after activation of CerS1 and CerS3 knockdown and control Jurkat cells. CerS1 (shCerS1) and CerS3 knockdown (shCerS3) and control (shNC) cells were stimulated for 24 and 48 h with CD2/3/28 activation beads in a 1:1 cell-to-bead ratio and 200 U/ml human IL2. S1P1 and 4 expression was determined via qRT-PCR and related to expression of RPL13A. Data are mean ± SEM. Statistical analysis was performed with a one-way ANOVA with a posthoc Tukey's comparison test (* $p < 0.05$, ** $p < 0.01$, **** $p < 0.0001$) Group sizes: n=3 measured in triplicates

For CerS3 overexpression cells, an upregulation of S1P1, but not S1P4, could be demonstrated on a basal level (Figure 21 B). After activation, there was no significant increase or decrease of S1P1 mRNA expression in control cells, but S1P4 mRNA levels were reduced (Figure 21 A). After stimulation, CerS3 overexpression Jurkat cells showed a significant elevation of S1P1 expression compared to the unstimulated control (Figure 21 A).
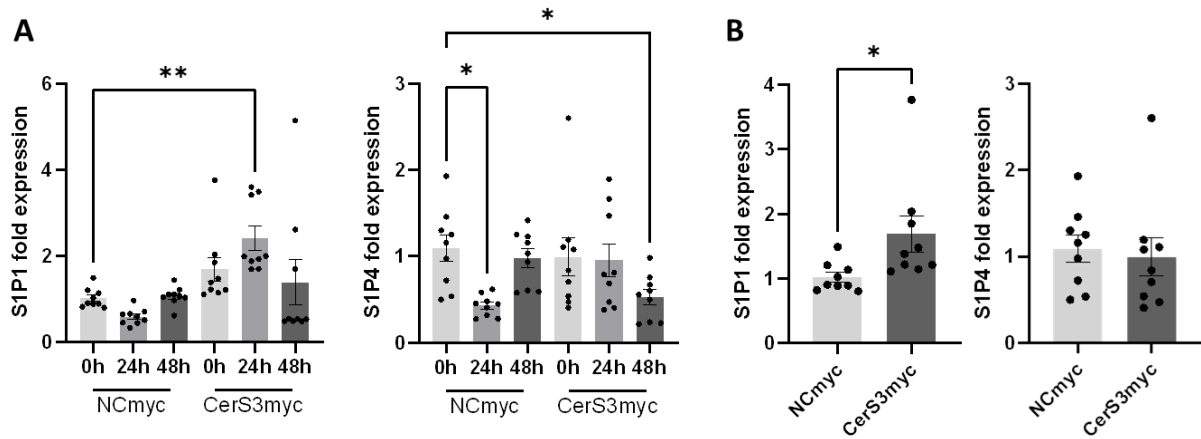
Figure 21: S1P1 and 4 expression after activation of CerS3 overexpression and control Jurkat cells. CerS3 overexpression (CerS3myc) and control (NCmyc) cells were stimulated for 24 and 48 h with CD2/3/28 activation beads in a 1:1 cell-to-bead ratio and 200 U/ml human IL2. S1P1 and 4 expression was determined via qRT-PCR and related to expression of RPL13A. **A)** S1P1 and 4 mRNA levels in NCmyc and CerS3myc cells are shown. **B)** S1P1 and 4 mRNA levels in unstimulated NCmyc and CerS3myc cells. Data are mean ± SEM. Statistical analysis was performed with a one-way ANOVA with a posthoc Tukey's test for A) and a Dunnett's multiple comparison test for B) and an unpaired t-test for C) (* p < 0.05, ** p < 0.01) Group sizes: n=3 measured in triplicates

To confirm mRNA expression data, protein levels of S1P1 were detected in total protein isolates of CerS1 and CerS3 knockdown Jurkat cells (Figure 22 A) and CerS3 overexpression cells (Figure 22 B). S1P1 protein levels were significantly reduced in shCerS1 and shCerS3 cells compared to the control (Figure 22 A). CerS3 overexpression cells showed a significant elevation of S1P1 protein levels compared to the control (Figure 22 B).
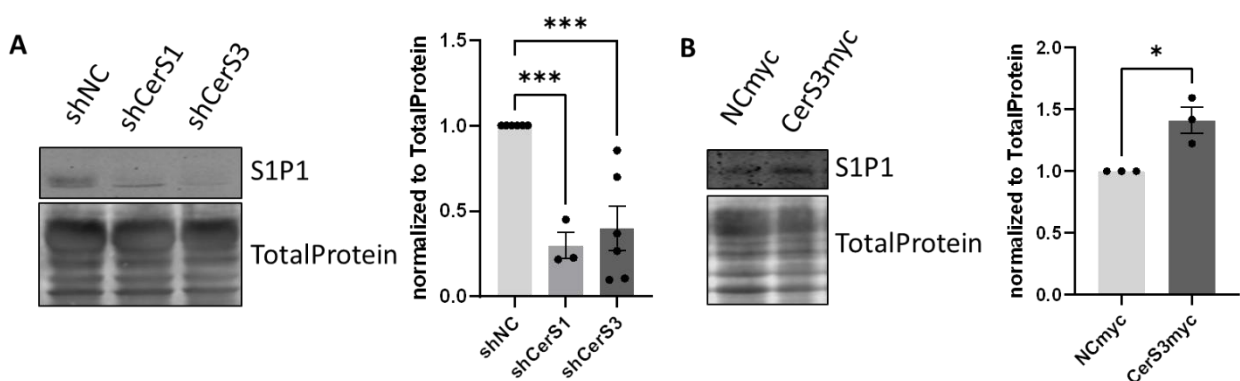
Figure 22: S1P1 protein levels in CerS1 and CerS3 knockdown and CerS3 overexpression cells. CerS1 knockdown (shCerS1), CerS3 knockdown (shCerS3) and control (shNC) and CerS3 overexpression (CerS3myc) and control (NCmyc) cells were harvested and total protein was isolated. 50 µg total protein was used for WB analysis. Blots were stained with TotalRevert700 stain for normalization and incubated overnight with S1P1 antibody. **A)** WB analysis of shNC, shCerS1 and shCerS3 cells protein samples detected with S1P1 antibody **B)** WB analysis of NCmyc and CerS3myc cell protein samples detected with S1P1 antibody ± SEM. Statistical analysis was performed with a one-

way ANOVA and a posthoc Tukey's comparison test for A) and an unpaired t-test for B) (* $p < 0.05$, *** $p < 0.001$) Group sizes: shNC n=6, shCerS3 n=6, shCerS1 n=3, NCmyc n=3, CerS3myc n=3

In summary, S1P1 mRNA expression was significantly reduced in CerS1, but more in CerS3 knockdown cells, which was also supported by protein levels. CerS3 overexpression cells displayed higher S1P1 mRNA and protein levels compared to control cells. S1P4 expression was significantly increased in unstimulated CerS1 and CerS3 knockdown cells, but not affected at all in CerS3 overexpression cells.

4.1.6 S1P induced [Ca^{2+}]$_i$ are decreased in CerS3 knockdown cells

Based on the altered S1P1 and 4 expression in CerS3 knockdown and control cells, S1P induced [Ca^{2+}]$_i$ were examined in fura-2 loaded CerS3 knockdown and control cells. Both cell lines showed an increase of [Ca^{2+}]$_i$ after stimulation with 1 µM S1P (Figure 23 A). CerS3 knockdown cells showed a lower response to S1P stimulation that is reflected in the deltaCa^{2+} values (Figure 23 A).
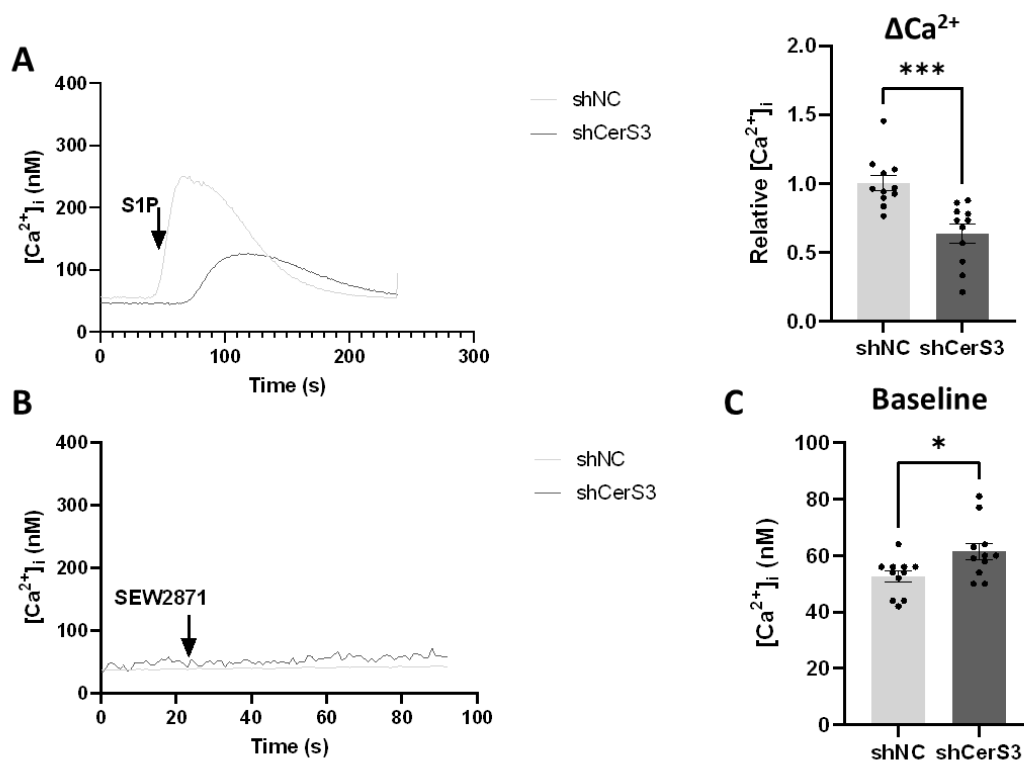
Figure 23: S1P- and S1P1 agonist- induced [Ca^{2+}]$_i$ increase in CerS3 knockdown and control T cells. Ca^{2+}$_i$ was labelled with fura-2 and emission was measured at 510 nm. **A)** CerS3 knockdown (shCerS3) and control (shNC) cells were stimulated with 1 µM S1P. Maximum [Ca^{2+}]$_i$ increase after S1P stimulation was calculated by substraction of the baseline from the highest peak (ΔCa^{2+}) and is depicted

in a graph. **B)** Stimulation of shCerS3 and shNC cells with 1 µM S1P1 agonist SEW2871. **C)** Baseline $[Ca^{2+}]_i$ of unstimulated shNC and shCerS3 cells. Data are mean ± SEM. Statistical analysis was performed with an unpaired t-test (* $p < 0.05$, *** $p < 0.001$) Group sizes: n=3: n=1-2 measured in triplicates and n=3 measured in quintuplicates

Since S1P stimulates every S1P receptor, a S1P1-specific agonist (SEW2871) was used for S1P1 dependent $[Ca^{2+}]_i$ increase. SEW2871 was not able to induce $[Ca^{2+}]_i$ increase in neither control nor CerS3 knockdown cells (Figure 23 B). There was also a significant difference in the $[Ca^{2+}]_i$ baseline of shNC and shCerS3 cells. CerS3 knockdown cells demonstrated a higher baseline compared to the control (Figure 23 C).

4.1.7 Migration is interrupted in CerS3 knockdown cells

S1P1 mRNA and protein levels were significantly reduced in CerS1 and CerS3 knockdown cells and S1P dependent $[Ca^{2+}]_i$ increase was decreased in CerS3 knockdown Jurkat T cells. Therefore migration capacity of T cells towards S1P was investigated. T cells were placed on a transwell with 8 µm pore sizes and were allowed to migrate for 4 h towards 100 nM S1P or 10 % FCS (positive control that naturally contains S1P) (Figure 24).

CerS1 and CerS3 knockdown cells migrated significantly less towards S1P and 10 % FCS compared to control cells (Figure 24 A and B). There was no significant difference in migration between shCerS1 and shCerS3 cells. CerS3 overexpression cells showed a significant faster migration towards S1P, but there was no difference in migration between control and CerS3 overexpression cells towards 10 % FCS (Figure 24 A and B).
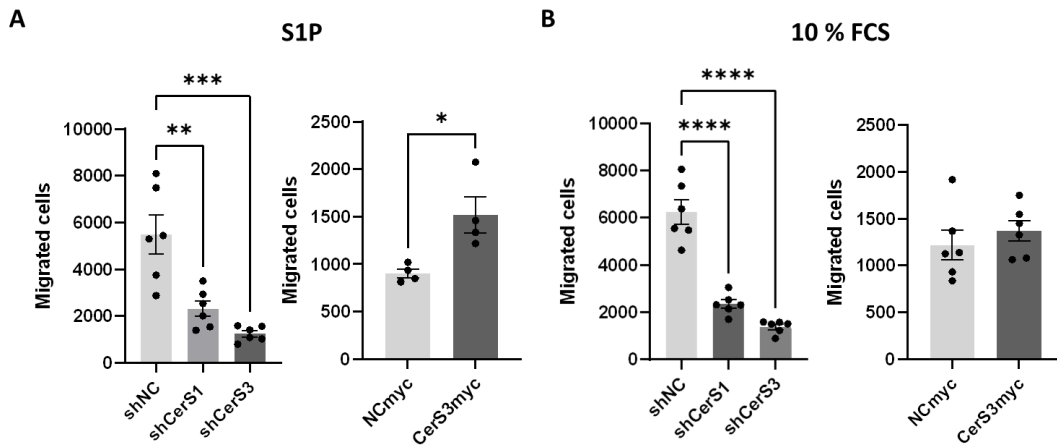
Figure 24: Migration of CerS1 and CerS3 knockdown and CerS3 overexpression cells towards S1P or 10 % FCS. CerS1 knockdown (shCerS1), CerS3 knockdown (shCerS3) and control (shNC) and CerS3 overexpression (CerS3myc) and control (NCmyc) cells were placed on 8 µm pore size transwell inserts and were given 4 h to migrate towards 100 nM S1P or 10 % FCS. Afterwards cells were harvested and measured for 1 min via flow cytometry. **A)** Migration assay of shNC, shCerS1, shCerS3, NCmyc and CerS3myc cells towards 100 nM S1P. **B)** Migration assay of shNC, shCerS1, shCerS3, NCmyc and CerS3myc cells towards 10 % FCS (positive control). Data are mean ± SEM. Statistical analysis was performed with a one-way ANOVA and posthoc Tukey's comparison test and unpaired t-test (* $p < 0.05$, ** $p < 0.01$, *** $p < 0.001$, **** $p < 0.0001$) Group sizes: shNC, shCerS1 and shCerS3 n=6, NCmyc and CerS3myc n=4-6

All in all, CerS1 and CerS3 cells migrated less towards S1P compared to the control. In contrast, CerS3 overexpression cells, migrated faster towards S1P.

4.1.8 T cell effector function is disturbed in CerS3 knockdown cells

As TCR signalling and subsequent activation of transcription factor NFAT1 is impaired in CerS3 knockdown cells, cytokine release could be also impacted. The release of the pro-inflammatory cytokine TNFα in activated CerS3 knockdown and overexpression cells was measured by ELISA (Figure 25).

Control Jurkat cells as well as CerS3 knockdown and CerS3 overexpression cells showed an enhanced TNFα release after 24 h of activation (Figure 25 A). There was a significant difference between control cells and CerS3 knockdown cells, as shCerS3 cells had significantly less TNFα in their supernatant (Figure 25 B). CerS3 overexpression cells also released significantly less TNFα into the medium compared to the control cells (Figure 25 B).
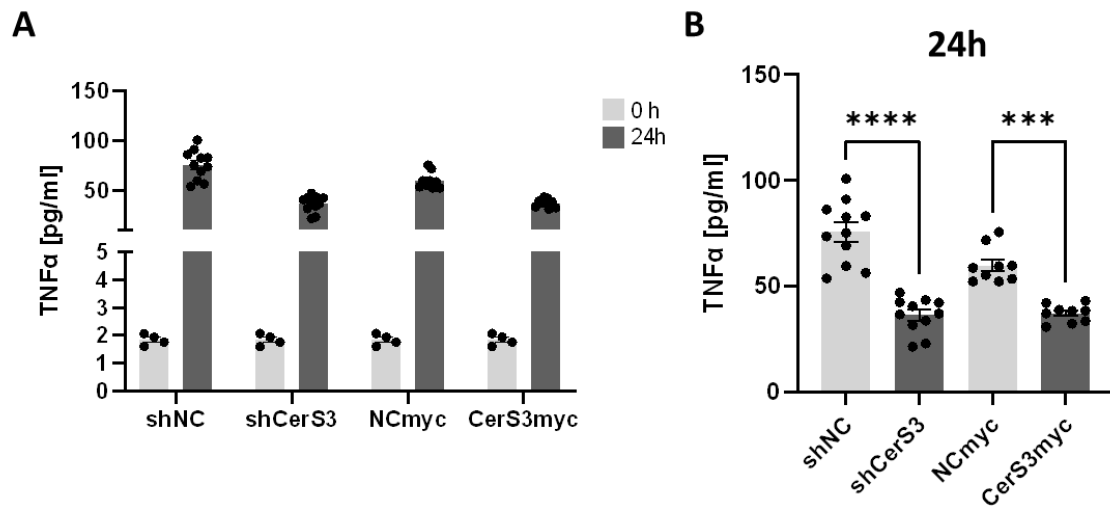
Figure 25: TNFα secretion in CerS3 knockdown and overexpression Jurkat cells. CerS3 knockdown (shCerS3) and control (shNC) and CerS3 overexpression (CerS3myc) and control (NCmyc) cells were stimulated at a density of 1.6 *10^7 cells/ml for 24 h with CD2/3/28 activation beads in a 1:1 cell-to-bead ratio and 200 U/ml IL2. Supernatant of cells was taken and TNFα concentration was measured via ELISA. **A)** TNFα concentrations in unstimulated and 24 h stimulated cells. **B)** Pairwise comparison of TNF levels after 24 h stimulation. Data are mean ± SEM. Statistical analysis was performed with a one-way ANOVA with a posthoc Tukey's test (*** $p < 0.001$, **** $p < 0.0001$) Group sizes: n=3 measured in triplicates

To exclude proliferation effects on T cell effector function of CerS3 knockdown and overexpression cells, proliferation of cells was observed by assessment of intracellular CellTrace Violet staining (Figure 26). CellTrace Violet concentration was measured every 24 h via flow cytometry. Neither CerS3 knockdown, nor overexpression Jurkat cells showed a different proliferation behaviour compared to their control cells (Figure 26 A and B). CellTrace Violet concentrations decreased over time indicating normal proliferation of cells.
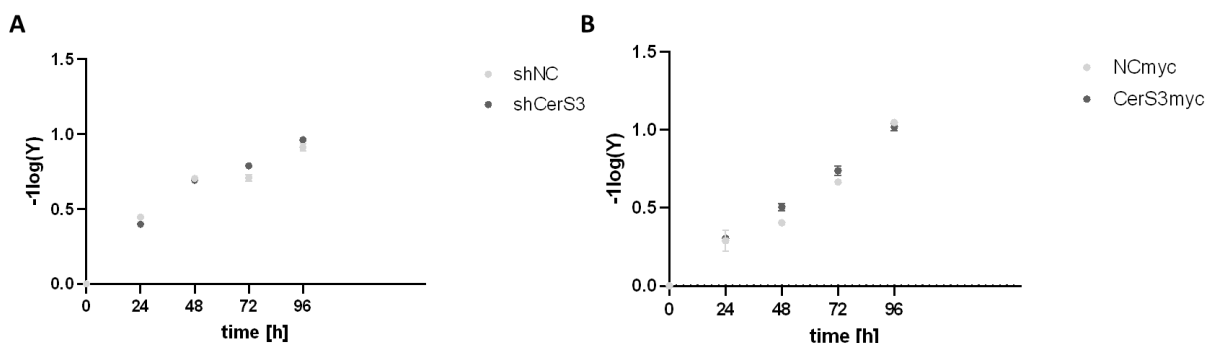
Figure 26: Proliferation of CerS3 knockdown and overexpression Jurkat cells. CerS3 knockdown (shCerS3) and control (shNC) and CerS3 overexpression (CerS3myc) and control (NCmyc) cells were stained with CellTrace Violet and CellTrace Violet concentration was measured via flow cytometry every 24 h (0 to 96 h). **A)** Proliferation assay of shNC and shCerS3 for 96 h. **B)** Proliferation assay of NCmyc

87

and CerS3myc cells for 96 h. Y-values were transformed to -1log(Y). Data are mean ± SEM. Group sizes: n=4

4.2 Influence of CerS3 downregulation in primary CD4^{+} cells

To confirm the effects of CerS3 knockdown on T cell function observed in the CD4^{+} Jurkat cell line, primary T cells were isolated from healthy donors. CD4^{+} and CD8^{+} T cells were activated by CD2/3/28 activation beads and IL2 stimulation for 24 and 48 h and CerS expression data were measured (Figure 27 and Figure 28).

In primary CD4^{+} cells, all CerS mRNA levels increased significantly after 48 h of stimulation (Figure 27). CerS2 and CerS4 expressions were already upregulated after 24 h (Figure 27).
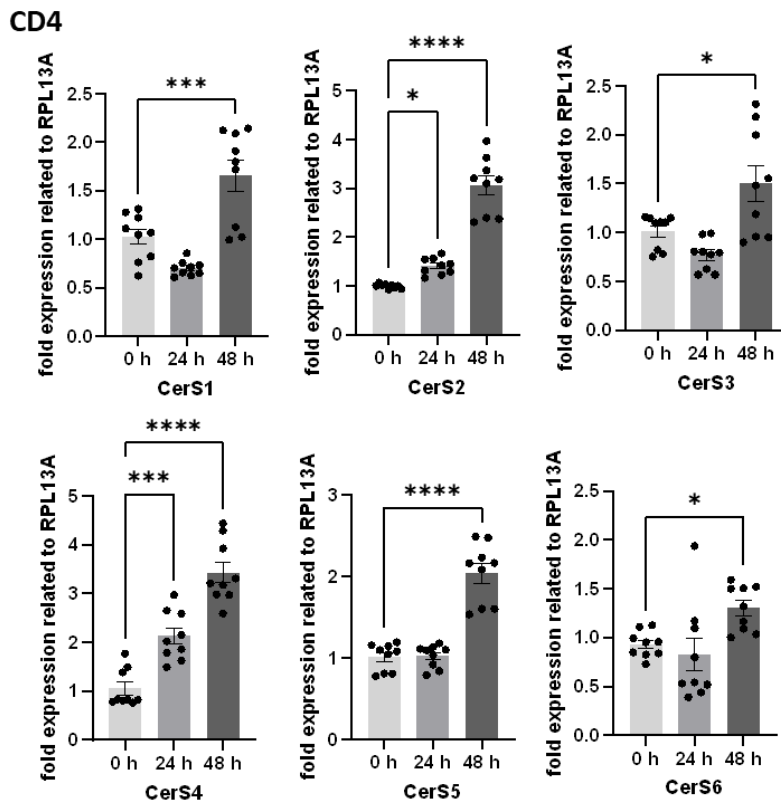
Figure 27: CerS expression after activation of primary human CD4^{+} T cells. Primary human CD4^{+} T cells were isolated from Buffycoats and activated for 24 and 48 h with CD2/3/28 activation beads in a 1:1 cell-to-bead ratio and 200 U/ml human IL2. RNA was isolated from samples, cDNA synthesis performed and CerS expressions were determined via qRT-PCR and related to RPL13A mRNA expression. Data are mean ± SEM. Statistical analysis was performed with a one-way ANOVA with a posthoc Dunnett's multiple comparison test (* $p < 0.05$, *** $p < 0.001$, **** $p < 0.0001$) Group sizes: n=3 measured in triplicates

In contrast to CD4$^+$ cells, CerS1 and CerS3 expression significantly decreased in primary CD8$^+$ T cells after 24 and 48 h of stimulation (Figure 28). CerS2 levels were upregulated after 24 h and 48 h similar to the CD4$^+$ cells, but CerS4 expression was only elevated after 24 h and decreased again after 48 h (Figure 28). CerS5 and CerS6 expressions were not altered after stimulation of CD8$^+$ cells.
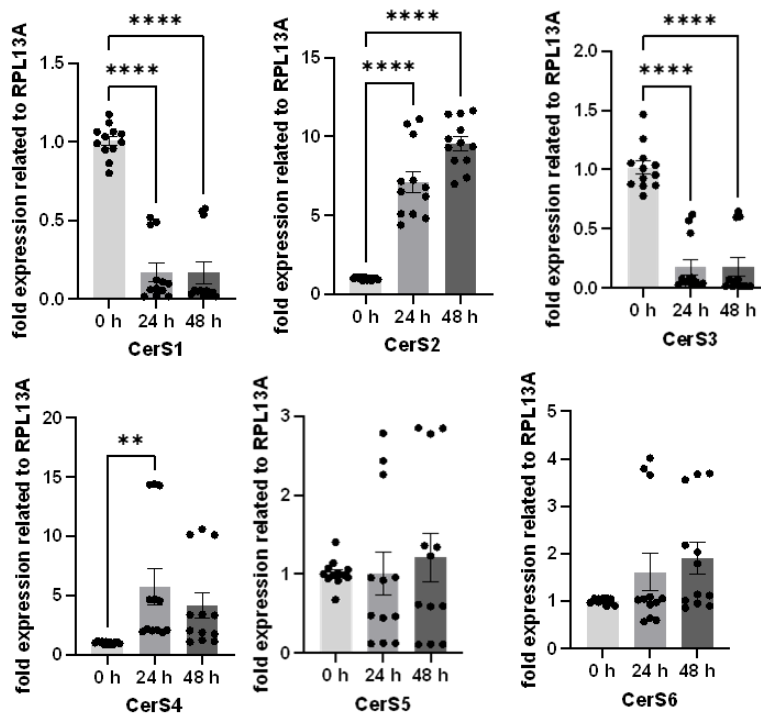
Figure 28: CerS expression after activation of primary human CD8$^+$ T cells. Primary human CD8$^+$ T cells were isolated from Buffycoats and activated for 24 and 48 h with CD2/3/28 activation beads in a 1:1 cell-to-bead ratio and 200 U/ml human IL2. After RNA isolation and cDNA synthesis, CerS1-6 expression was determined via qRT-PCR and related to RPL13A mRNA expression. Data are mean ± SEM. Statistical analysis was performed with a one-way ANOVA with a posthoc Dunnett's multiple comparison test (** $p < 0.01$, **** $p < 0.0001$) Group sizes: n=4 measured in triplicates

In regard to CerS1 and CerS3 expression after T cell stimulation, CD4$^+$ and CD8$^+$ cells reacted in opposite ways. CD4$^+$ cells upregulated CerS1 and CerS3 expression after stimulation, while CD8$^+$ cells downregulated both enzymes after activation. As CD8$^+$ cells only play a minor role in colitis development, and stimulation of CD8$^+$ cells already resulted in a decrease of CerS1 and CerS3 expression, these cells were excluded from the following investigations on the influence of CerS3 knockdown on primary T cell activation.

4.2.1 siRNA treatment of primary CD4$^+$ cells

To study the influence of CerS3 knockdown on primary T cells and to confirm *in vitro* data in the CD4$^+$ Jurkat cell line, primary CD4$^+$ cells from the blood of healthy donors were treated with a CerS3 siRNA-pool for CerS3 downregulation. Primary T cells were treated for 48 h with CerS3 or control siRNA and IL2, before they were activated with CD2/3/28 activation beads and IL2 for 24 and 48 h (Figure 29).

After activation of primary CD4$^+$ cells treated with scrambled siRNA (siCtrl), all CerS increased significantly after 48 h (Figure 29). Downregulation of CerS3 with CerS3 siRNA was accompanied by CerS1 and CerS5 downregulation in an unstimulated state (Figure 29). CerS2 mRNA levels were significantly upregulated in unstimulated CerS3 siRNA treated cells (Figure 29). CerS3 expression was also increased after 48 h stimulation of primary CD4$^+$ cell treated with CerS3 siRNA (Figure 29).
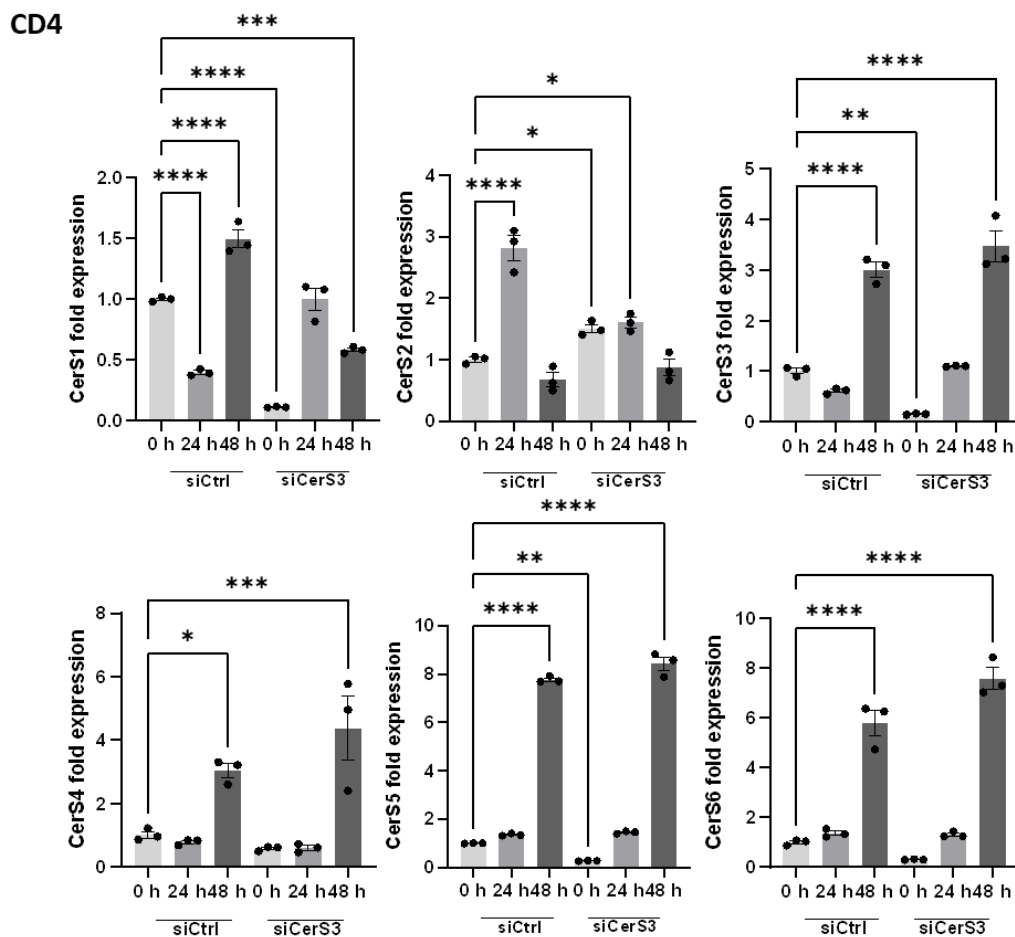
Figure 29: CerS expression in primary CD4$^+$ T cells treated with scrambled or CerS3 siRNA. Primary CD4$^+$ T cells were isolated from Whole Blood of healthy volunteers. CD4$^+$ T cells were treated with either control or CerS3 siRNA and 200 U/ml IL2 for 48 h. Afterwards cells were activated for 24 and 48 h with CD2/3/28 activation beads in a 1:1 cell-to-bead ratio and 200 U/ml IL2. RNA was isolated and qRT-PCR was performed for CerS1-6. mRNA expression levels were normalized to RPL13A levels. Data are mean ± SEM. Statistical analysis was performed with a one-way ANOVA with a Dunnett's

90

multiple comparison test (* p < 0.05, ** p < 0.01, *** p < 0.001, **** p < 0.0001) Group sizes: n=3 measured in triplicates, one representative n is shown in this figure.

4.2.2 Effector function is disturbed in siCerS3 treated primary CD4+ cells

Besides migration capacity, release of cytokines is a crucial effector function of T cells that also affects the pathophysiology of colitis [17, 24]. Primary T cells isolated from the blood of healthy donors and treated with scrambled siRNA (siCtrl) or CerS3 siRNA (siCerS3) were activated for 24 and 48 h with CD2/3/28 activation beads and IL2. The supernatants of the cells were tested for multiple pro-inflammatory cytokines (IFNγ, IL17, IL6 and TNFα) via CBA (Figure 30).
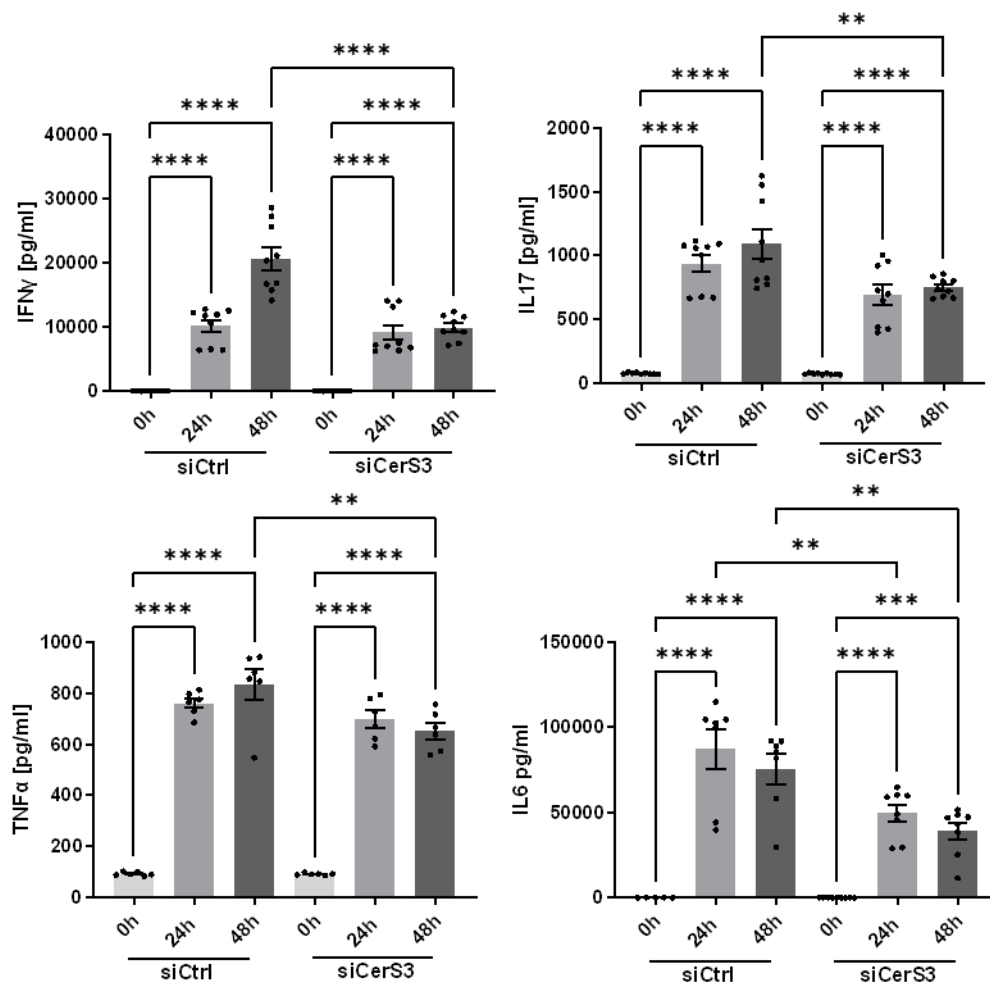
Figure 30: Pro-inflammatory cytokine profile of primary CD4+ T cells treated with scrambled or CerS3 siRNA. Primary CD4+ T cells were isolated from the blood of healthy donors and treated with scrambled (siCtrl) or CerS3 siRNA (siCerS3) and 200 U/ml IL2 for 48 h. Afterwards cells were activated with CD2/3/28 activation beads in a 1:1 cell-to-bead ratio and 200 U/ml for 24 and 48 h. Supernatants were collected and pro-inflammatory cytokines (IFNγ, IL17, TNFα and IL6) concentrations were measured via CBA. Data are mean ± SEM. Statistical analysis was performed with a one-way ANOVA and a Tukey's posthoc test (** p < 0.01, *** p < 0.001, **** p < 0.0001) Group sizes: n=3 measured in triplicates, for TNFα n=2 measured in triplicates

Control cells (siCtrl) showed significant increase of IFNγ, IL17, IL6 and TNFα after 24 and 48 h of stimulation (Figure 30). CD4$^+$ T cells treated with CerS3 siRNA also showed significant increase of all four pro-inflammatory cytokines (Figure 30) but in comparison to control cells, CerS3 siRNA cells released significantly less amounts of IFNγ, IL17, IL6 and TNFα after stimulation (Figure 30).

In summary, both, control and CerS3 siRNA treated primary CD4$^+$ T cells, released pro-inflammatory cytokines after activation. In CerS3 siRNA treated CD4$^+$ cells, the release of pro-inflammatory cytokines after stimulation was significantly reduced in comparison to control cells.

4.3 Impact of T cell specific CerS3 knockout on DSS induced acute colitis

To investigate the impact of CerS3 on T cell function *in vivo* in mice, CerS3 expression was downregulated only in T cells by crossing CerS3$^{fl/fl}$ mice with LCK-Cre mice, leading to a knockdown of CerS3 only in mature T cells (Supplementary Figure 1). For induction of acute colitis, CerS3 LCK Cre and WT mice were treated for 5 days with 2 % DSS in their drinking water. Mice displayed similar symptoms to human patients in the clinic such as diarrhoea, bloody stool and weight loss. After replacement of the drinking water, both mice groups showed significant weight loss until the last day of the experiment (Figure 31 B). Disease score of mice that contained assessment of physical health during the experiment also changed significantly after replacement of drinking water (Figure 31 A). When WT mice and CerS3 LCK Cre treated with DSS were compared, WT mice showed a significantly higher disease score, as well as more weight loss over time (Figure 31 A and B).
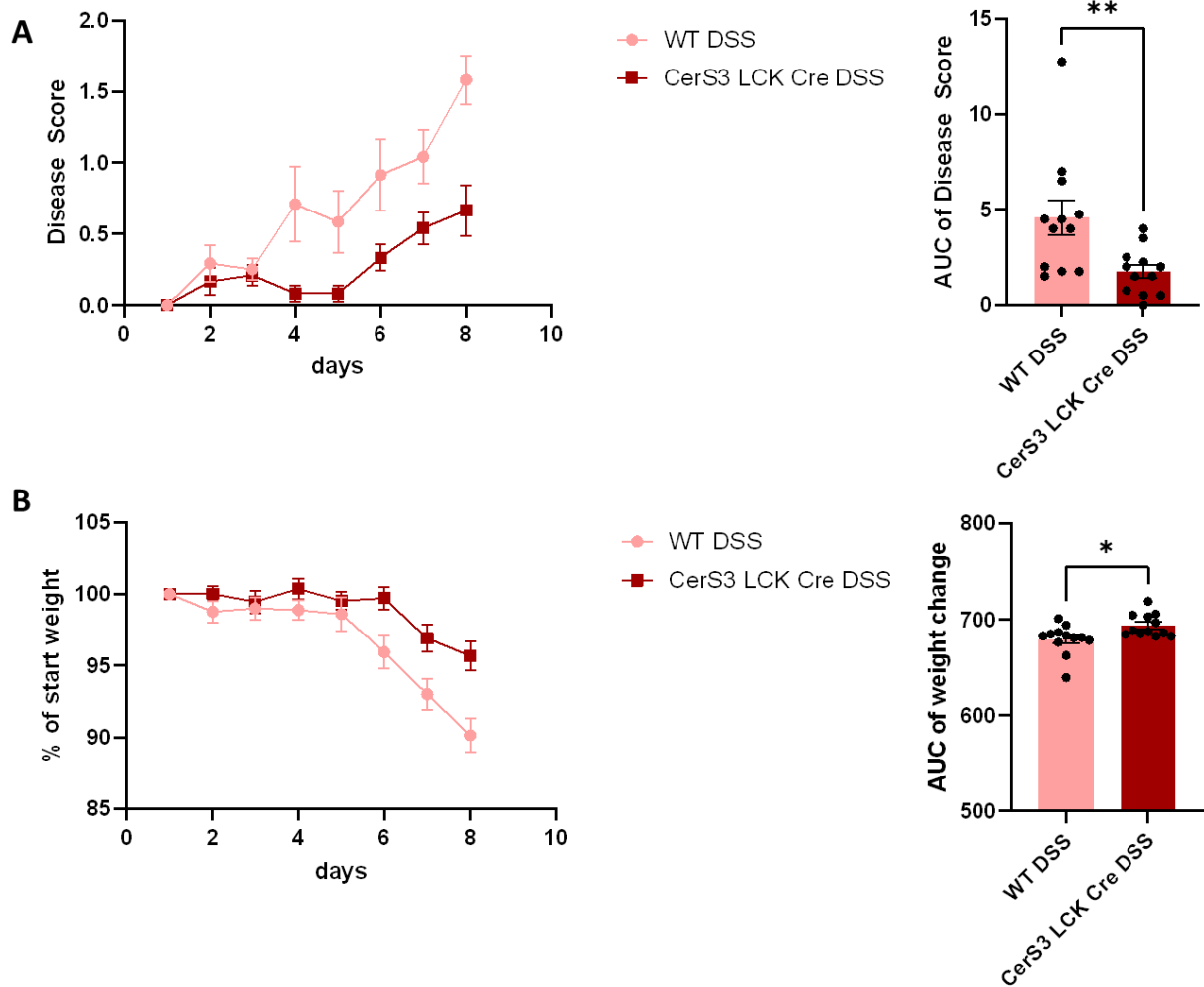
Figure 31: Disease score and weight change of WT and CerS3 LCK Cre mice during dextran sodium sulfate (DSS) induced acute colitis. Mice were treated with 2 % DSS in their drinking water for 5 days and observed for 8 days in total. **A)** Disease Score of DSS treated mice during experiment. **B)** Body weight change of DSS treated mice. Data are mean ±SEM. Statistical analysis was performed with an unpaired t-test (* $p < 0.05$, ** $p < 0.01$) Group sizes of CerS3 LCK Cre and WT mice: n=12

DSS-induced colitis led to a shortening of the colon during persisting inflammation. Measurement of the colon showed a significant decrease in colon length in both DSS-treated groups, WT and CerS3 LCK Cre mice (Figure 32 A and B). Nevertheless, when both DSS groups were compared, colon length of WT mice showed a significantly stronger shortening compared to CerS3 LCK Cre mice (Figure 32 A).
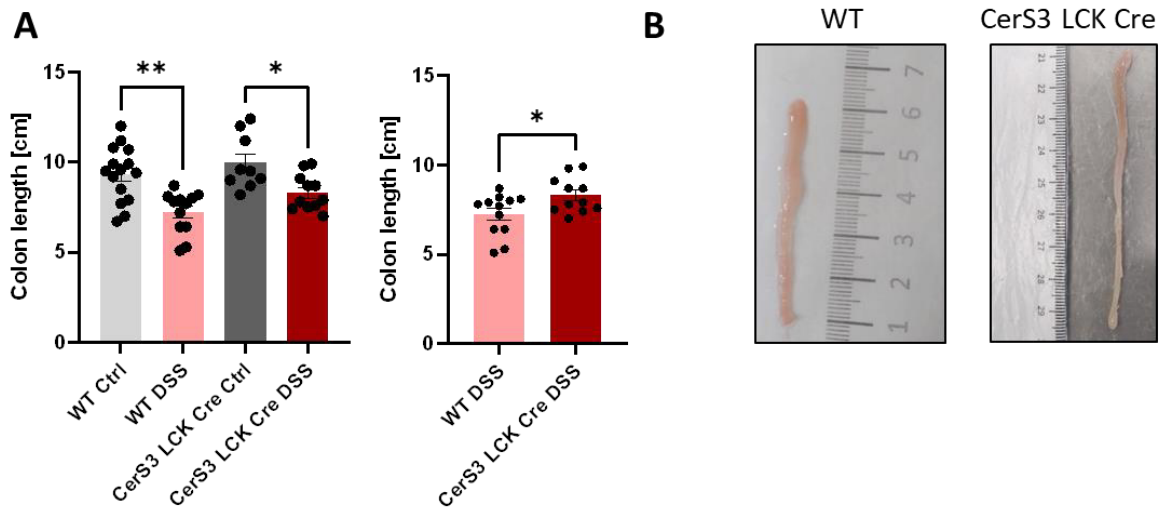
Figure 32: Colon length of DSS treated mice. A) Colon lengths of DSS treated mice compared to controls. **B)** Representative pictures of DSS treated colons from WT and CerS3 LCK Cre mice. Data are mean ± SEM. Statistical analysis was performed with an unpaired t-test (* $p < 0.05$, ** $p < 0.01$) Group sizes of control and DSS mice: WT n = 11-12; CerS3 LCK Cre n=9-12

In general, WT mice reacted more sensitive to the DSS-treatment and had more severe colitis than the CerS3 LCK Cre mice.

4.3.1 Immune cell distribution not in LP, but in IEL is affected by DSS-induced colitis in WT and CerS3 LCK Cre mice

To further characterize the inflammation status in WT and CerS3 LCK Cre mice after DSS treatment, immune cell distribution in blood and different tissues was measured via flow cytometry (Figure 33 and Figure 34). Both mice groups showed a significant increase of neutrophils in their blood after DSS treatment (Figure 33 A). Activated monocytes or DCs were not altered in the blood. T cell populations in the blood were also not changed after DSS treatment, but CerS3 LCK Cre control mice displayed a significant reduction in CD3$^+$ populations compared to WT controls (Figure 33 A). In the spleen, macrophages were significantly upregulated in both DSS treated mice groups (Figure 33 B). Overall, T cell populations in the spleen did not change after DSS treatment.
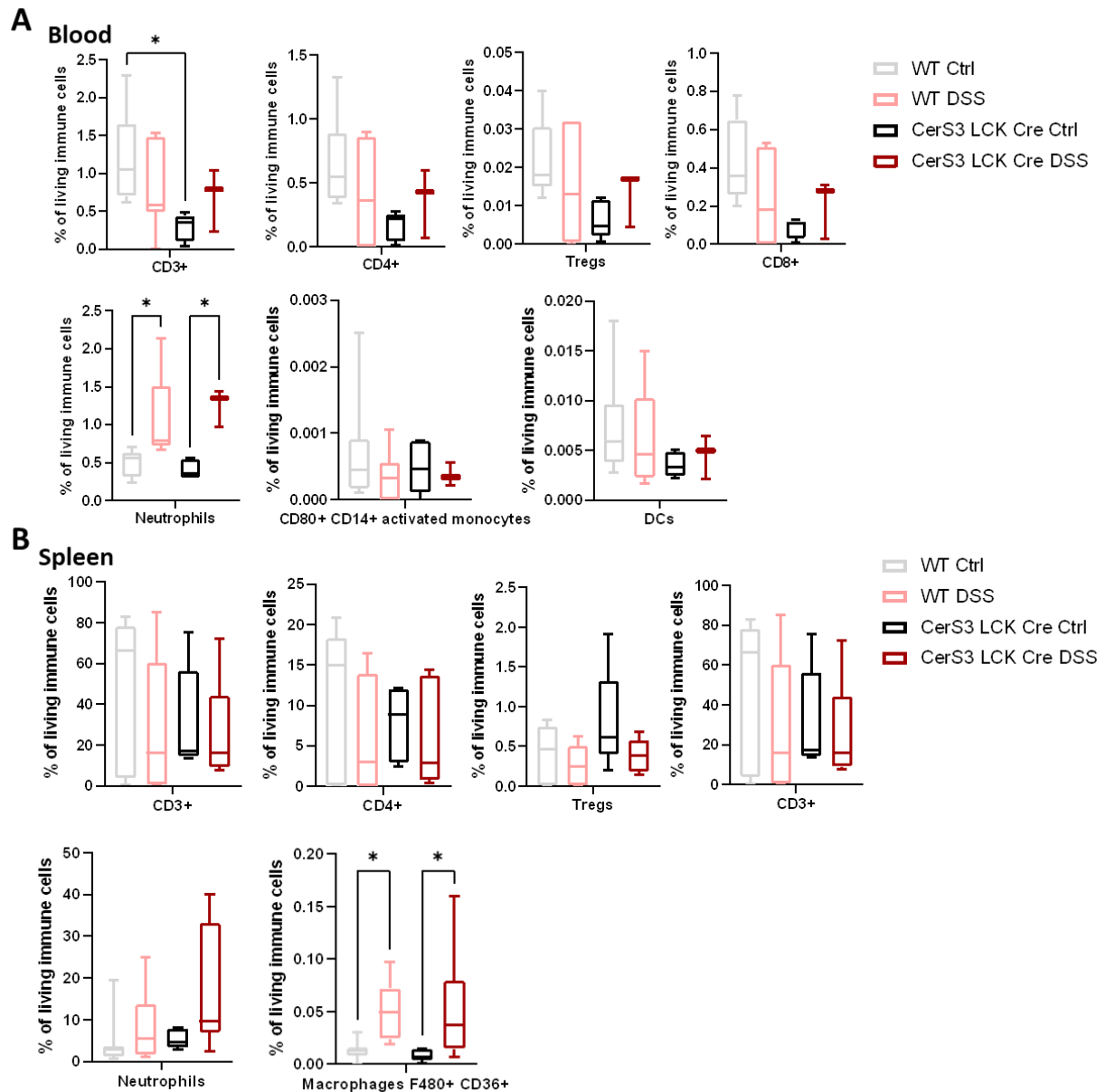
Figure 33: Immune cell populations in WT and CerS3 LCK Cre mice in blood and spleen tissue. Mice were either in the control group or treated with 2 % DSS in their drinking water for 5 days before water replacement. Mice were sacrificed after 8 days. Immune cells isolated from blood and spleen were stained according to the Immune Cell panel and analysed by flow cytometry (Supplementary Figure 3 and Supplementary Figure 5). **A)** T cell populations from the blood are depicted, as well as neutrophils, activated monocytes and DCs**. B)** T cell populations from spleen tissue are depicted, as well as neutrophils and macrophages isolated from the spleen. Data are mean ± SEM. Statistical analysis was performed with a one-way ANOVA followed by Tukey's Test (* p < 0.05) Group sizes: A) For WT Ctrl n=8, WT DSS n= 7, CerS3 LCK Cre Ctrl n=5, CerS3 LCK Cre DSS n=3 B) For WT Ctrl n=11, WT DSS n= 9, CerS3 LCK Cre Ctrl n=5, CerS3 LCK Cre DSS n=8

Immune cell assessment in the lamina propria (LP) fraction of WT and CerS3 LCK Cre colon did not show any differences (Figure 34 A). Neither T cell populations nor other immune cells (neutrophils or macrophages) were significantly upregulated. Only by tendency there were more neutrophils and macrophages in the LP fraction after DSS

treatment in both mice groups (both not significant) (Figure 34 A). Thus, in the intra epithelial lymphocyte (IEL) fraction of WT and CerS3 LCK Cre colon, there was an increase of neutrophils after DSS treatment (Figure 34 B). Macrophages, as well as CD4+ T cells, were also increased, but only in the IEL fraction of WT DSS colon (Figure 34 B). CerS3 LCK Cre DSS mice showed a significant increase of CD8+ populations only in the IEL fraction of the colon (Figure 34 B).
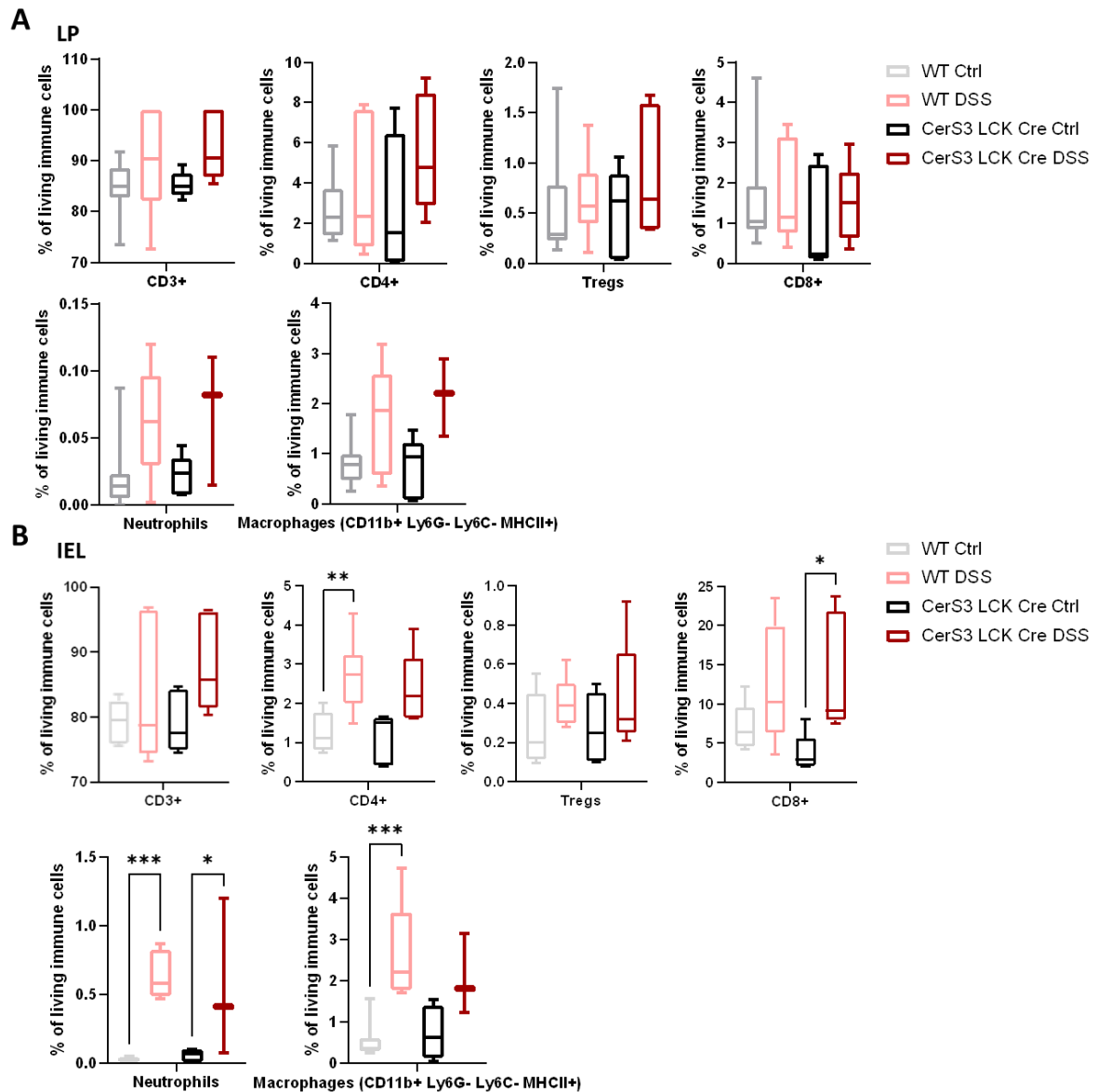
Figure 34: Immune cell populations in WT and CerS3 LCK Cre mice in colon IEL and LP fractions. Mice were either untreated (Ctrl) or treated with 2 % DSS in their drinking water for 5 days before water replacement. Mice were sacrificed after 8 days. Immune cells isolated from the IEL and LP colon fractions were stained according to the Immune Cell panel and analysed by flow cytometry (Supplementary Figure 2). **A)** T cell populations (CD3+, CD4+, CD8+, Tregs), neutrophils and macrophages from the LP fraction are depicted. **B)** T cell populations (CD3+, CD4+, CD8+, and Tregs), neutrophils and macrophages from the IEL fraction are depicted. Data are mean ± SEM. Statistical analysis was performed with a one-way ANOVA followed by Tukey's Test (* p < 0.05, ** p < 0.01, *** p

< 0.001) Group sizes: For WT Ctrl n=9, WT DSS n= 5, CerS3 LCK Cre Ctrl n=5, CerS3 LCK Cre DSS n=3

In summary, WT and CerS3 LCK Cre mice showed a significant increase of various immune cells in different tissues after DSS treatment without significant differences between WT and CerS3 LCK Cre mice. But untreated CerS3 LCK Cre mice had significant less CD3$^+$ cells in the blood than WT mice.

4.3.2 CerS3 LCK Cre mice show less inflammation in the colon after DSS treatment

To analyse inflammation in the colon, tissue slices from colon swiss rolls of WT and CerS3 LCK Cre mice treated with DSS were prepared and stained with Hemacolor (Figure 35). Histological analysis of colon tissue from DSS treated mice, showed massive inflammation in WT mice (Figure 35 A and B). WT colon tissue disclosed substantial swelling of the submucosa and disruption of the epithelial layer, especially at the top of the crypts in the distal part (black arrows in Figure 35 B). In contrast, CerS3 LCK Cre mice showed only mild inflammation with less submucosa swelling and few disrupted crypts (Figure 35 C, D).
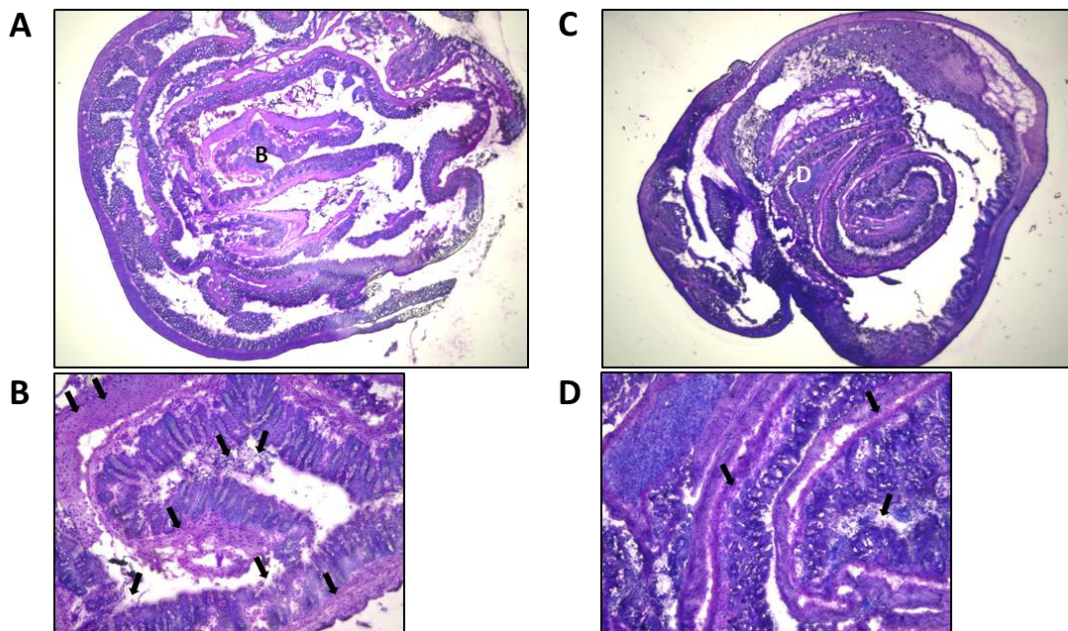
Figure 35: Histological analysis of representative colon swiss rolls after DSS treatment of WT and CerS3 LCK Cre mice. Tissue was embedded in Tissue-Tek and stained with Hemacolor. Pictures were obtained with a 2X or 10X objective. Swiss rolls were rolled from the distal to proximal part, meaning the distal part of the colon resides in the middle of the roll. **A)** Overview of colon tissue from WT mice after DSS treatment with 2X magnification. **B)** 10X magnification of an inflamed colon section from T mice after DSS treatment. Black arrows indicate thicker LP area filled with immune cells and

disrupted crypts. **C)** Overview of CerS3 LCK Cre DSS colon swiss roll in 2X magnifiation **D)** 10X magnification pictures of an inflamed area of CerS3 LCK Cre colon tissue after DSS treatment. Black arrows indicate disrupted crypts and areas with some more immune cells.

In summary, according to the disease score and immune cell data, colon tissue from WT mice showed more inflammation compared to the CerS3 LCK Cre colon tissue after DSS treatment.

4.3.3 CerS3 LCK Cre mice show less T cells in blood, spleen and thymus, but more in lymph nodes

As T cells of CerS3 LCK Cre control mice were reduced in the blood, all T cell populations were studied in the WT and CerS3 LCK Cre controls (Figure 36). In the blood, all three T cell subtypes (CD4$^+$, Treg and CD8$^+$) were significantly reduced in the CerS3 LCK Cre control mice compared to the WT (Figure 36 A). In the thymus, Tregs were reduced only in the CerS3 LCK Cre mice controls (Figure 36 B). CerS3 LCK Cre control mice also displayed a significant reduction of CD4$^+$ and CD8$^+$ cells in the spleen compared to WT mice (Figure 36 C). In the lymph nodes CD3$^+$ populations were significantly enhanced in the CerS3 LCK Cre mice compared to the WT mice (Figure 36 D). By tendency, all three subpopulations seemed to be increased in the lymph nodes of CerS3 LCK Cre mice (not significant), but not in the WT (Figure 36 D).
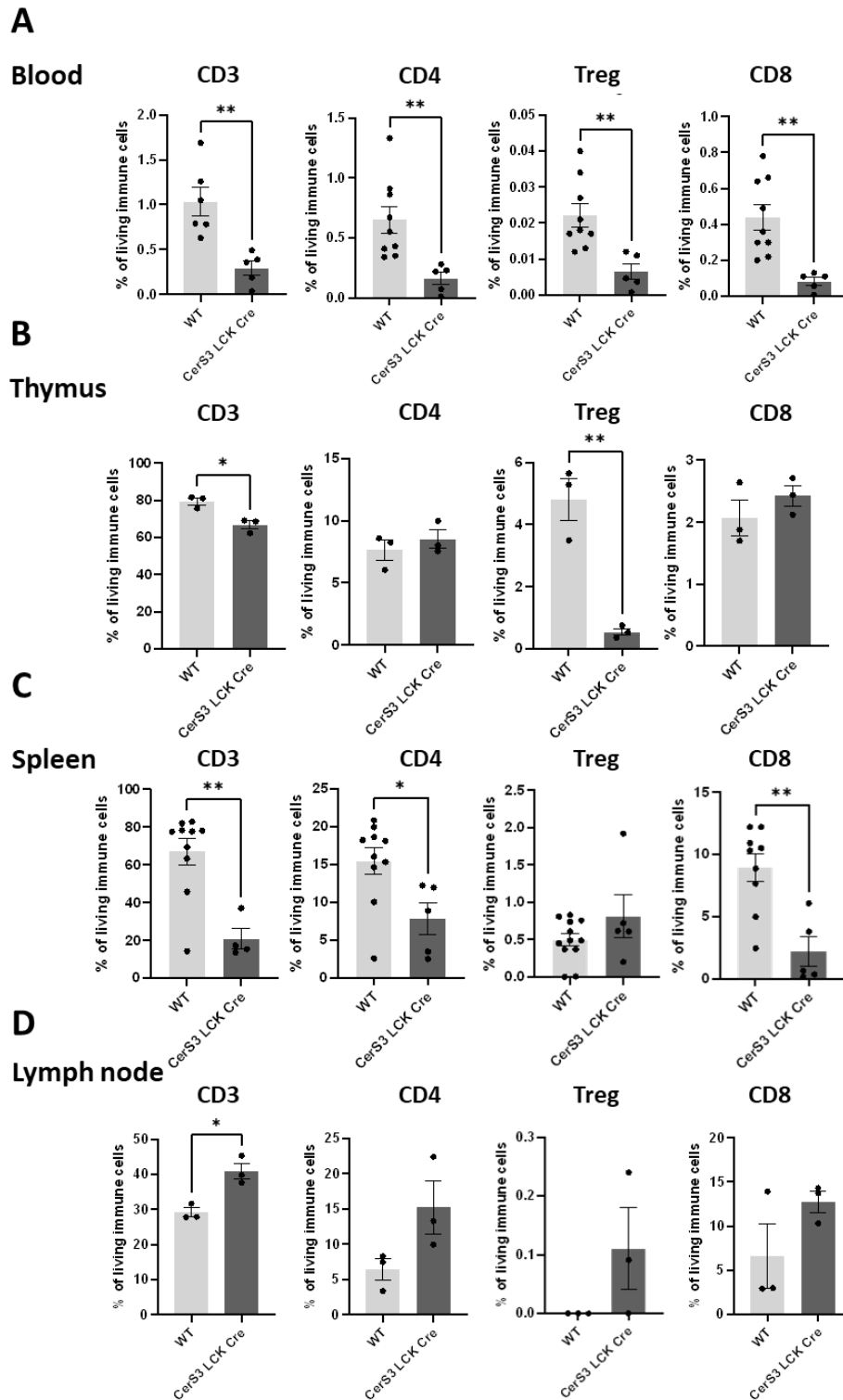
Figure 36: T cell populations in Ctrl WT and Ctrl CerS3 LCK Cre mice in blood and various tissues. A) T cell populations measured by flow cytometry from blood samples of WT and CerS3 LCK Ctrl mice. **B)** Flow cytometry analysis of T cell populations from thymus. **C)** Flow cytometry analysis of T cells from the spleen. **D)** Lymph node T cell populations analysed by flow cytometry. Data are mean ± SEM. Statistical analysis was performed with an unpaired t-test (* p < 0.05, ** p < 0.01) Group sizes: For A) WT= 6-9; CerS3 LCK Cre. For B) WT= 3; CerS3 LCK Cre n=3. C) WT= 10; CerS3 LCK Cre n=4. For D) WT= 3; CerS3 LCK Cre n=3

In a nutshell, WT mice showed higher CD3$^+$ populations in blood, spleen and thymus, while CerS3 LCK Cre mice had more CD3$^+$ cells in the lymph nodes.

4.3.4 CerS3 LCK Cre T cells differentiate worse than WT T cells

The differences in the amount of T cell populations in CerS3 LCK Cre and WT mice tissue, could be due to migration or differentiation differences. In order to investigate the capacity of CerS3 LCK Cre and WT T cells to differentiate into the three T cell subtypes, T cells were isolated from the thymus of WT and CerS3 LCK Cre mice and differentiated into TH, Tregs and cytotoxic CD8$^+$ cells for 10 d (Figure 37). T cells derived from CerS3 LCK Cre mice showed an impaired differentiation potential to the TH and Treg subtypes compared to WT controls (Figure 37 A and B). Differentiation of T cells into CD8$^+$ cells was not affected in CerS3 LCK Cre mice (Figure 37 C).
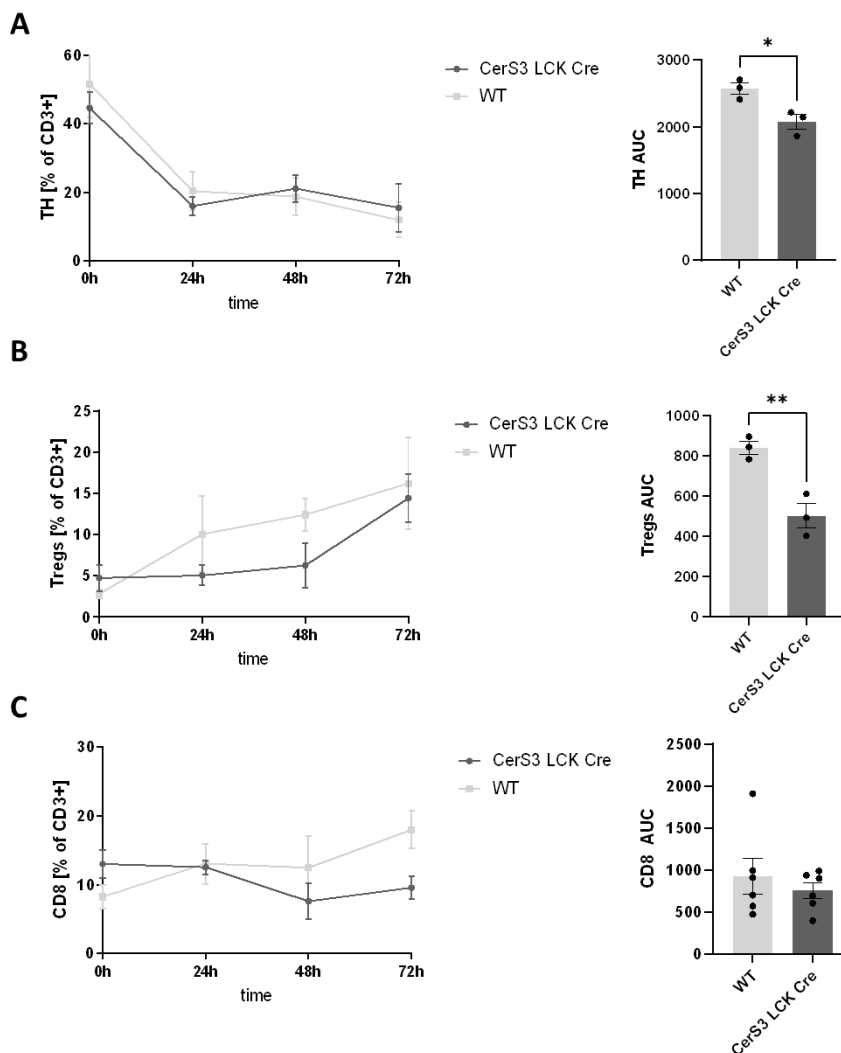
Figure 37: Differentiation of WT and CerS3 LCK Cre T cells. T cells isolated from thymus were differentiated into the different T cell subtypes (TH, Treg and CD8$^+$), followed by activation with CD3/28

activation beads, 200 U/ml IL2, 50 nM β-mercaptoethanol and 20 ng/ml IL7 every two days. **A)** Thymocytes were stimulated with 10 ng/ml murine IFNγ and 6 ng/ml murine IL12 to be differentiated into the TH subtype and then activated and cultivated for 10 d. **B)** Thymocytes were stimulated with 60 ng/ml of human IL15 to be differentiated into the Treg subtype and then activated and cultivated for 10 d**. C)** Thymocytes were stimulated with 60 ng/ml human TGFβ to be differentiated into the CD8$^+$ subtype and then activated and cultivated for 10 d. Data are mean SEM. Statistical analysis was performed with an unpaired t-test (* p < 0.05, ** p < 0.01) Group sizes: n=6, representative ns are shown in the figure.

T cells develop into single-positive (CD4$^+$ or CD8$^+$) T cells in the thymus from double-positive (CD4$^+$CD8$^+$CD3$^-$) progenitor cells. To see if differentiation effects were due to a change in progenitor cell amount in the thymus, all CD3$^+$ and progenitor cells were investigated (Figure 38). Over the time span of 10 d there was a significant difference between WT and CerS3 LCK Cre CD3$^+$ differentiated cells (Figure 38 A). CerS3 LCK Cre cells differentiated worse than WT cells. But this was not due to less progenitor cells as indicated in Figure 38 B, where no difference was shown between WT and CerS3 LCK Cre progenitor cells.
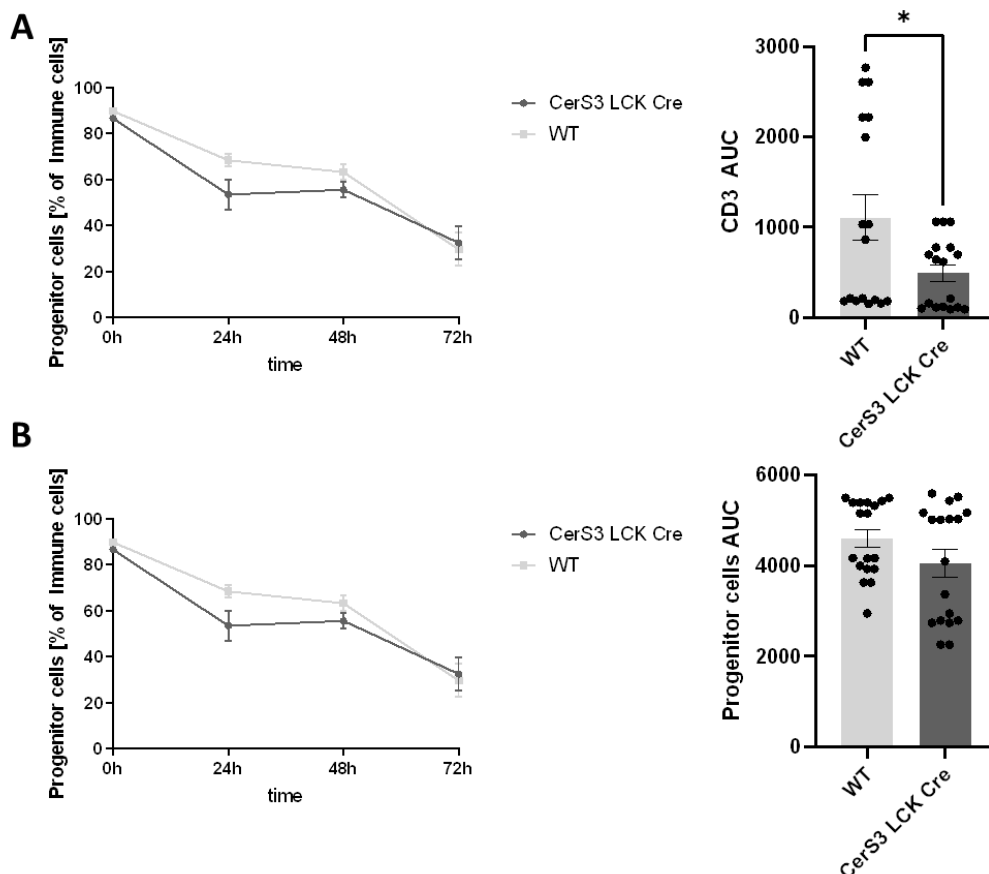
Figure 38: CD3$^+$ and progenitor cells from WT and CerS3 LCK Cre T cells. T cells isolated from thymus were differentiated into the three different T cell subtypes (TH, Treg and CD8$^+$) for 10 days. Every day cells were taken out and stained for the T cell panel and analysed via flow cytometry. **A)** Percentage of all T cell subtypes from CD3$^+$ cells from WT and CerS3 LCK Cre are compared. **B)** Double-negative T cell progenitors from all differentiation assays between WT and CerS3 LCK Cre cells.

Data are mean ± SEM. Statistical analysis was performed with an unpaired t-test (* p < 0.05) Group sizes: n=18

In summary, the differentiation potential of CerS3 LCK Cre T cells to TH and Treg cells was impaired in comparison to WT T cells.

4.3.5 Reduced cytokine release by CerS3 LCK Cre T cells

In order to see effector function of WT and CerS3 LCK Cre T cells, premature thymocytes were differentiated into the three different subtypes and activated for 24 and 48 h. Cytokine release was assessed via CBA (Figure 39). WT and CerS3 LCK Cre TH cells showed a significant increase of pro-inflammatory cytokine IFNγ after 48 h stimulation with CD3/28 activation beads and IL2 (Figure 39 A). There was no significant difference between WT and CerS3 LCK Cre in respect to their IFNγ release. IL17 and TNFα release in WT TH cells were significantly upregulated after stimulation, whereas there was no significant increase of IL17 release in CerS3 LCK Cre TH cells (Figure 39 A). The amount of IL17 and TNFα release from CerS3 LCK Cre TH cells was significantly lower compared to WT TH cells after stimulation of cells for 48 h with CD3/28 activation beads and IL2 (Figure 39 A).

Figure 39 B shows the cytokine release of WT and CerS3 LCK Cre Tregs. IFNγ production was significantly upregulated in both groups after 48 h stimulation of cells with CD3/28 activation beads and IL2, but there was no difference between CerS3 LCK Cre and WT Tregs (Figure 39 B). IL17 release tended to be increased after 48 h in WT cells and after 24 and 48 h in CerS3 LCK Cre Tregs (Figure 39 B). The anti-inflammatory cytokine IL10 was only significantly increased in WT cells after 48 h and was significantly higher compared to the amount of IL10 released by CerS3 LCK Cre cells after stimulation (Figure 39 B).

For CD8^{+} effector function, release of IFNγ and TNFα was tested (Figure 39 C). The release of the pro-inflammatory cytokines IFNγ and TNFα increased significantly after stimulation of WT cells for 48 h (Figure 39 C). IFNγ release from CerS3 LCK Cre CD8^{+} cells was not significant (Figure 39 C). TNFα production was also upregulated in CerS3 LCK Cre cells after stimulation for 48 h, but the concentration was significantly lower compared to TNFα concentration of WT cells (Figure 39 C).
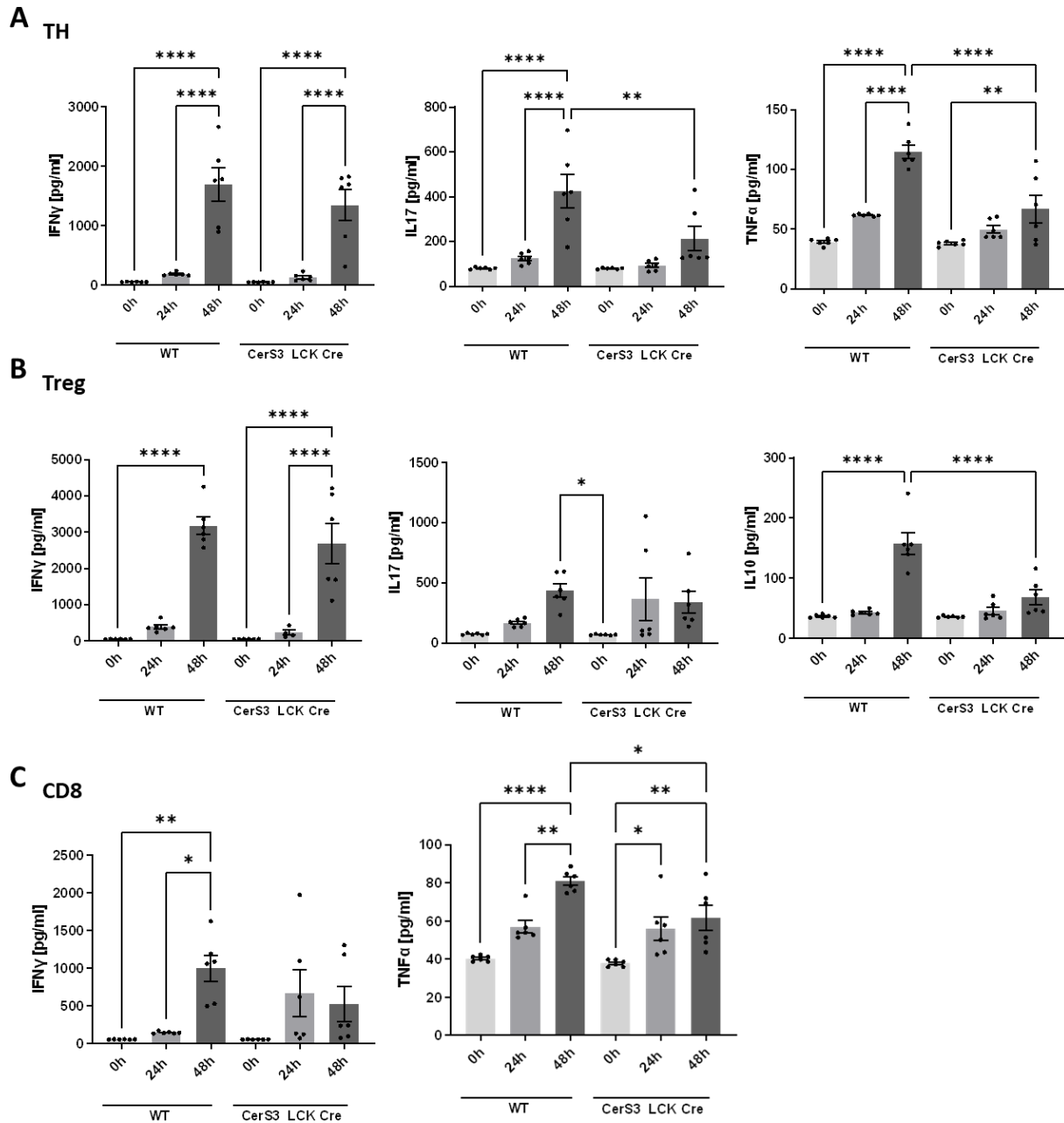
Figure 39: Cytokine release from activated WT and CerS3 LCK Cre T cells. Premature T cells were isolated from the thymus of WT and CerS3 LCK Cre T cells and differentiated into TH, Treg or CD8^{+} cells. T cells were then activated with CD3/28 activation beads, 200 U/ml IL2, 50 nM β-mercaptoethanol and 20 ng/ml IL7 for 0 to 48 h and the cytokine concentrations of the supernatants were determined via CBA. **A)** Cytokine profile of TH cells (IFNγ, IL17 and TNFα) stimulated with 10 ng/ml murine IFNγ and 6 ng/ml murine IL12. **B)** IFNγ, IL17 and IL10 release by Tregs stimulated with 60 ng/ml human IL15. **C)** Cytokine profile (IFNγ and TNFα) of CD8^{+} cells stimulated with 60 ng/ml human TGFβ. Data are mean ± SEM. Group sizes: n=6

Cytokine levels in plasma from DSS treated CerS3 LCK Cre and WT mice did not differ significantly (Figure 40).
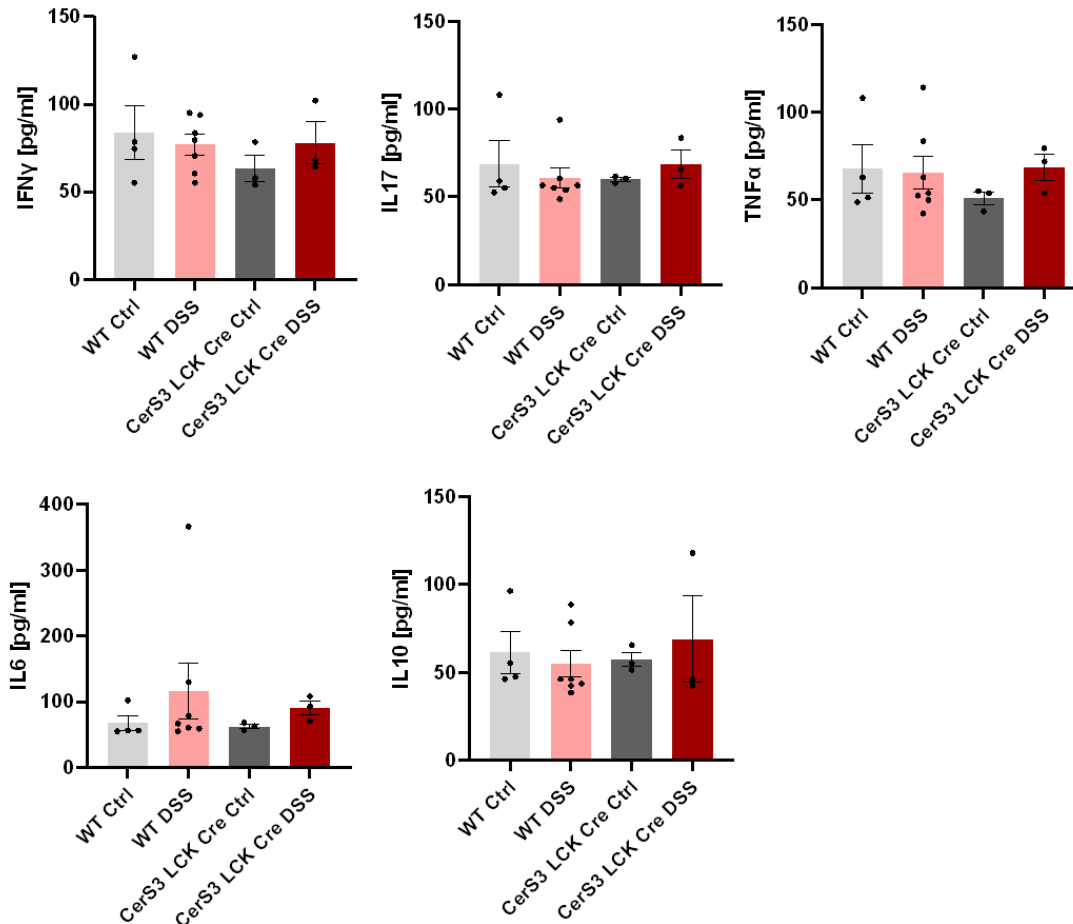
Figure 40: Cytokine levels in plasma of WT and CerS3 LCK Cre Ctrl and DSS treated mice. Mice were either untreated or treated with 2 % DSS in their drinking water for 5 days before water was replaced. After 8 days mice were sacrificed and blood was taken and the plasma was obtained. Cytokine concentrations of IFNγ, IL17, TNFα, IL6 and IL10 in the plasma of WT and CerS3 LCK Cre mice were measured via CBA. Data are mean ± SEM. Group sizes: WT Ctrl n=4, WT DSS n=7, CerS3 LCK Cre Ctrl n=3, CerS3 LCK Cre DSS n=3

In general, CerS3 LCK Cre T cells released less cytokines after stimulation compared to WT T cells.

4.4 Establishment of human colon chip

The transfer of mice data to the human system is often problematic because mice disclose a different immune cell status in comparison to humans and the disease models are only under certain conditions comparable to the human disease. Therefore humanized disease models are of urgent need to make a reliable statement about molecular mechanisms and drug efficacy. For this purpose a physiologically-close system was established using a human organ on a chip system. The here used *Emulate* chip enables the development of a 3D colon epithelial-like structure that

resembles the human colon and could further be connected to human endothelial cells that form a vessel-like structure. By adding physiological stretch and flow to both tissues, the complexity of the colon is much better represented than in traditional 2D cell culture or even 3D organoid cultures.

4.4.1 Formation of epithelial and endothelial barrier in colon chip

In order to get the physiologically relevant colon chips, chips had to be activated and coated with ECM proteins resembling the physiological ECM and for a better attachment of epithelial colon (Caco-2) and endothelial (HUVEC) cells to the chip channels. When endothelial cells were seeded into the bottom channel, they quickly started to form a monolayer with a vessel-like structure. 48 h after seeding, they received serum-reduced media (from 2 % to 0.5 % FBS) to avoid overgrowth of endothelial cells in the chip (Figure 41 A). Caco-2 cells were seeded into the top channel of the chip and after 24 h cells attached to the ECM (Figure 41 A and B). After 48 h, Caco-2 cells proliferated, but still did not form a layer without holes (Figure 41 B). 72 h post-seeding, Caco-2 cells formed a sufficient layer, spreading through the whole area of the top channel (Figure 41 B). Six days after seeding and under continuous stretch (resembling the colon peristaltic) and medium flow, Caco-2 cells formed a tight and matured 3D structure in the chip with strong tight junctions and barrier function (Figure 41 B). With matured epithelial barrier, further experiments could be conducted.
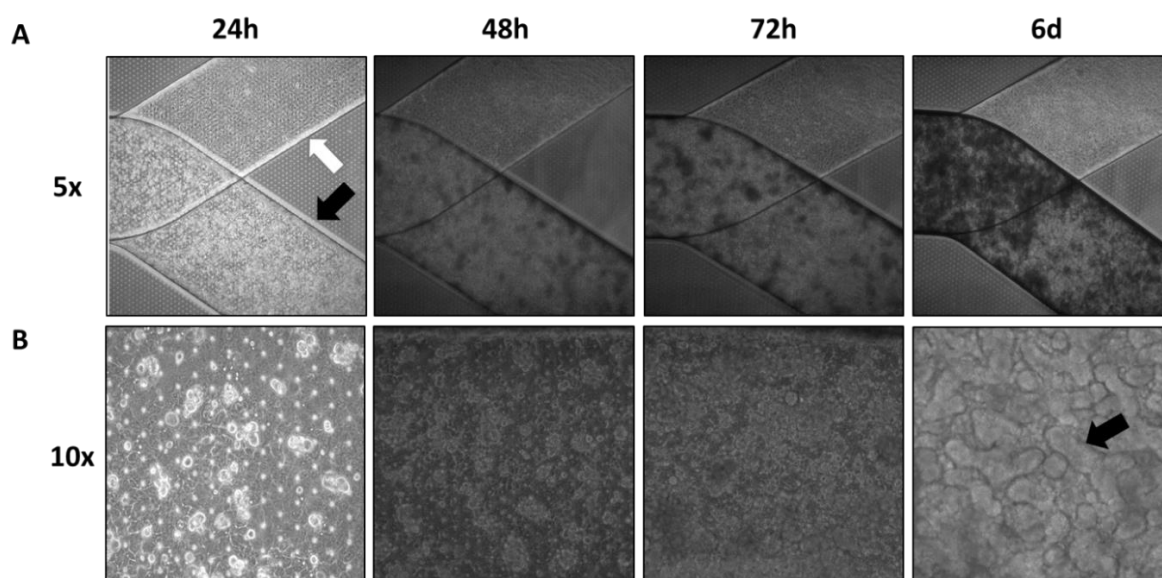
Figure 41: Development of epithelial and endothelial barrier in colon intestine chip. HUVECs were seeded in a density of 7 * 10^6 cells/ml into the bottom channel (depicted in the inlet above with a white

arrow) and Caco-2 cells were seeded in a density of 3 * 10^6 cells/ml into the top channel (depicted in the inlet below with a black arrow) of the chips. Cell growth was controlled via microscopy pictures every day after seeding. Pictures were obtained on the inlet and outlet of the chips, as well as in the middle (in between the vacuum ports). **A)** 5X magnification of inlets of colon chips 24 h to 6 d after seeding containing HUVEC and Caco-2 cells. **B)** 10X magnification of middle part of colon chips 24 to 6 d after seeding containing Caco-2 cells. Black arrow indicates 3D villi-like structure of Caco-2 cells

4.4.2 T cell recruitment to inflamed tissue

To investigate if CerS3 plays also a role in human colitis, inflammation-specific attachment and migration of control and CerS3 knockdown Jurkat T cells and, T cell recruitment to the epithelial layer was established. Human colon chips, that were cultured for 6 days and had already developed their 3D structure, were perfused for 4 h with a mixture of pre-stained control (shNC) and CerS3 knockdown (shCerS3) Jurkat T cells in a physiological density of 2*10^6 cells/ml with a 1000 µl/h flow rate in the vascular channel. Afterwards chips were incubated for an additional 24 h at normal flow rate and stretch. Control Jurkat cells were pre-stained with green-fluorescent (PK67) and shCerS3 Jurkat cells were stained with red-fluorescent (PKH26) dyes. Control and CerS3 knockdown cells both express GFP, so only red-green co-stained cells were accounted for shCerS3 cells. Attachment of the cells to the endothelial and epithelial layer after 24 h was controlled by microscopy (Figure 42). Outflow after 4 h T cell perfusion and trypsinized cells from top and bottom channel after 24 h were checked via flow cytometry. Data from T cell recruitment are preliminary and can not be statistically evaluated.
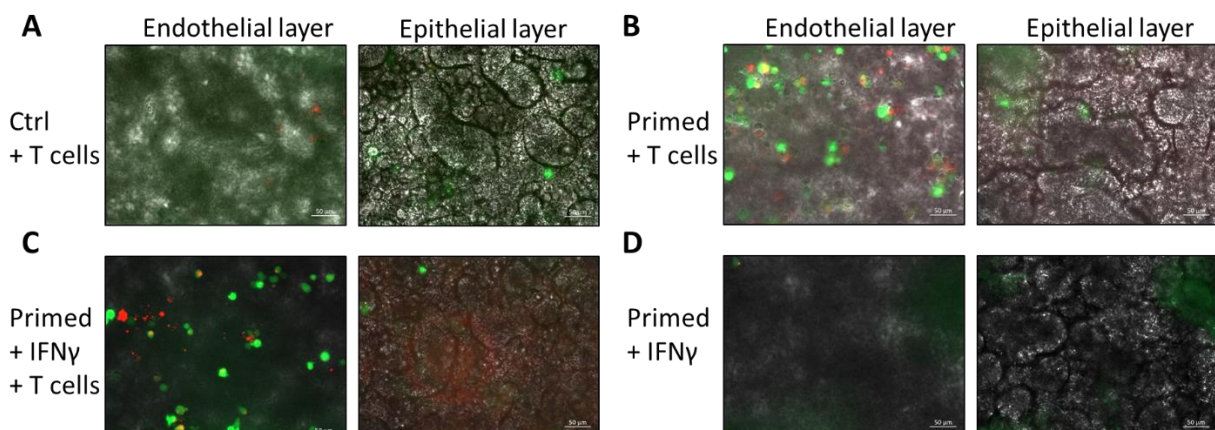
Figure 42: T cell attachment to epithelial and endothelial layer in colon chips. Endothelial (HUVEC) and colonic epithelial (Caco-2) cells were seeded on chips and let grow for 6 days to allow growth of endothelial monolayer and epithelial 3D structure. On day 6, chips were either primed with 50 ng/ml TNFα in the bottom channel and/or primed with IFNγ in the bottom and top channel for induction of colitis and epithelial barrier disruption. After 24 h of priming, a mixture of each 4 * 10^6 pre-stained shNC (PK67, green) and shCerS3 (PKH26, red) cells in a gel-like medium were introduced into the bottom

channel for 4 h at a flow rate of 1000 µl/h. Pictures of attachment of T cells on the endothelial and epithelial layer were obtained with a 20X magnification with a Zeiss fluorescence microscope. **A)** Chip was not primed with cytokines, but perfused with pre-stained T cells. **B)** Chip was primed with 50 ng/ml TNFα in the bottom channel and perfused with pre-stained T cells. **C)** Chip was primed with 50 ng/ml TNFα in the bottom channel and 50 ng/ml IFNγ in the top and bottom channel. Chip was also perfused with pre-stained T cells. **D)** Chip was primed with 50 ng/ml TNFα in the bottom channel and 50 ng/ml IFNγ in the bottom and top channel. n=1 for every condition

For resting control, chips were not primed with TNFα nor treated with cytokines, but perfused with pre-stained T cells (Figure 42 A). There were almost no fluorescent T cells visible in the endothelial or epithelial layer of this chip (Figure 42 A). For T cell control, the chip was only primed with 50 ng/ml TNFα in the bottom channel and perfused with pre-stained T cells (Figure 42 B). It was clearly visible that many T cells had attached to the endothelial layer, but not many to the epithelial layer (Figure 42 B). Additionally, more shNC cells were visible on the endothelial layer. To induce migration of T cells into the inflamed epithelial layer, the chip was primed with 50 ng/ml TNFα in the bottom channel and treated with 50 ng/ml IFNγ in the bottom and top channel and then perfused with pre-stained T cells (Figure 42 C). T cells had attached to the endothelial layer, but there were also few T cells detectable in the epithelial layer (Figure 42 C). More control cells had attached to the endothelial layer. For priming control, chip was primed with 50 ng/ml TNFα in the bottom channel and as chemoattractant for T cell migration bottom and top channel were treated with 50 ng/ml IFNγ. There were no T cells visible in either layer (Figure 42 D). A green-fluorescent background could be observed in each layer of each chip (Figure 42).

In further experiments a more physiological chemokine cocktail containing IP10, MIP-3α, MEC, GPR14L, TECK, MCP-1, SDF-α and MIP-3β was used as chemoattractant for T cell migration.

In order to quantify T cells attached to the endothelial or epithelial layer, the outflow after 4 h T cell perfusion as well as harvested cells from bottom and top channel after 24 h were checked via flow cytometry. In this case, chips were primed with 50 ng/ml TNFα in the bottom channel and treated with a 100 ng/ml chemokine cocktail (IP10, MIP-3α, MEC, GPR14L, TECK, MCP-1, SDF-α, MIP-3β) in the top channel to mimick cytokine state in human colitis patients. In this experiment, shNC cells were stained red-fluorescent and shCerS3 cells were stained green-fluorescent. Following data are preliminary, and therefore can not be statistically validated.
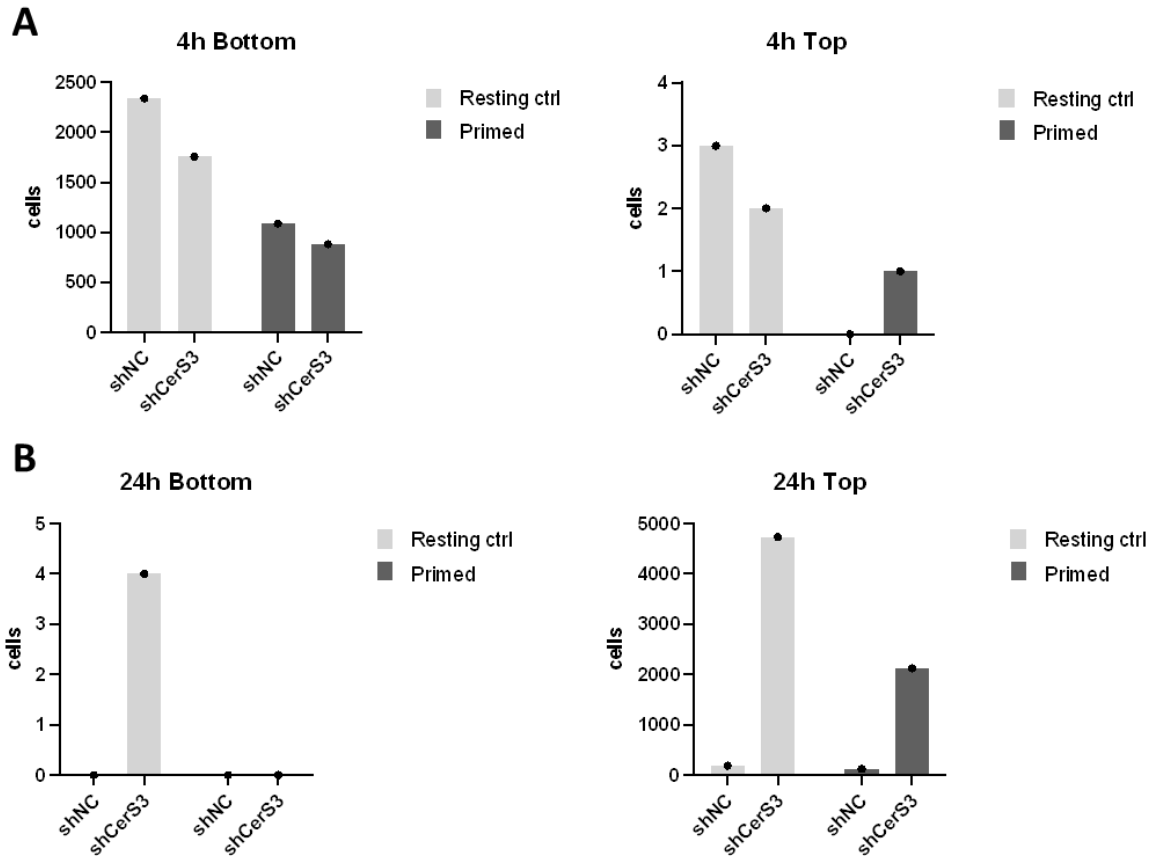
Figure 43: T cell count in outflow after 4 h and trypsinized cells after 24 h in colon chip. Endothelial (HUVEC) and colonic epithelial (Caco-2) cells were seeded on chips and let grow for 6 days to allow growth of endothelial monolayer and epithelial 3D structure. On day 6, chips were either primed with 50 ng/ml TNFα in the bottom channel and a 100 ng/ml chemokine cocktail (IP10, MIP-3α, MEC, GPR14L, TECK, MCP-1, SDF-α, MIP-3β) in the top channel for induction of colitis or not treated at all. After 24h of priming, a mixture of each $4 * 10^6$ pre-stained shNC (PKH26, red) and shCerS3 (PK67, green) cells in a gel-like medium were introduced into the bottom channel for 4 h at a flow rate of 1000 µl/h. After this, chips were incubated for an additional 24 h under normal flow rate and stretch conditions. **A)** Outflow of chips after 4 h T cell perfusion was analysed via flow cytometry. **B)** Cells from top and bottom channel were trypsinized after 24 h incubation and analysed via flow cytometry. Data are mean ± SEM. n=1 for every condition

After 4 h perfusion of T cells, there were more control cells than CerS3 knockdown cells in the outflow of the bottom channel of the resting control and the primed chip (Figure 43 A). In the 4 h outflow of the top channel, there were more control cells than CerS3 knockdown cells in the resting control, but more shCerS3 cells in the primed chip. After 24 h incubation of T cells, there were no T cells detectable in the bottom channels of the primed chip and only a few shCerS3 cells in the resting control (Figure 43 B). In the top channel, there were almost 5000 shCerS3 cells in the resting control and over 2000 shCerS3 cells in the primed chip (Figure 43 B). There were fewer control cells in both chips. (Figure 43 B).

In summary, T cell attachment to the endothelial and epithelial layer was detectable. Quantification of attached T cells after 24 h via flow cytometry showed more CerS3 knockdown cells in the epithelial layer compared to control cells, but also more T cells in the resting control.

5. Discussion

In this work, the role of CerS1 and 3 in T cells and colitis was elucidated. T cells, mainly THs, display a pathologically raised immune response in UC. This leads to a vicious cycle of recurrent immune cell recruitment and activation as well as cytokine release that promotes inflammation and UC development [123, 124]. It is known that bioactive sphingolipids are not only important structural elements of the plasma membrane, but can also interfere with signalling pathways important for T cell function [335]. Since CerS1 and CerS3 are significantly upregulated in the WBC of human colitis patients, and there is evidence for influence of CerS and their products on T cell function, the role of both enzymes was the main focus in this work [361, 363, 382, 384].

5.1 CerS expression in primary T cells and CerS1 and CerS3 knockdown and overexpression cells

To study the role of CerS1 and 3 in T cells, both enzymes were downregulated or overexpressed in a CD4$^+$ Jurkat cell line.

Control cells showed a significant upregulation of CerS1 and CerS3 after stimulation of cells, indicating an important role for both enzymes in T cell function. In CerS1 knockdown cells, there was a significant downregulation of CerS3 expression after stimulation compared to the control and a significant CerS3 to 6 downregulation in unstimulated shCerS1 cells. In previous studies of our group, it was already established that activity of CerS2 is enhanced by co-activation of CerS4 and CerS6 in a human colon tumor (HCT) cell line [396]. When CerS4 was co-activated with CerS6 in HCT 116 cells, CerS4 was inhibited and the effects could not be reversed with addition of the CerS4 substrate $C_{16:0}$-CoA substrate showing that protein-protein interactions between CerS could be possible [396]. Additionally, we were able to demonstrate that Cer content elevation alone does not lead to induction of apoptosis and CerS activity is also responsible for this [396]. The equilibrium between Cer or CerS is therefore very important. Our group already showed for various cell lines that loss or gain of different CerS led not only to co-regulation but also to compensatory up- or downregulation of CerS. CerS5 and CerS6, for example, were co-regulated in CerS4 knockdown Jurkat cells [384]. In a different study, our group showed, that CerS1 and 3 expression was upregulated when CerS5 was downregulated in control Jurkat

cells [361]. CerS2 and CerS5 KO in MCF-7 breast cancer cells reacted with upregulation of CerS4 expression and in CerS2 KO mice, CerS6 was upregulated to compensate for the loss of long-chain Cer [397, 398]. In the case of CerS3 knockdown cells, CerS1 was compensatory and significantly upregulated in the unstimulated and stimulated cells, whereas CerS5 and CerS6 expression was downregulated in the unstimulated cells. These findings suggest a more important role for CerS3 than CerS1, since CerS1 upregulation in shCerS3 cells fails to compensate for the downregulation of CerS3. Additionally, the more mild effects of CerS1 downregulation on migration behaviour and the non-affected TCR signalling also indicate a co-effect of CerS3 downregulation in CerS1 knockdown cells that is not as severe as in CerS3 knockdown cells. CerS3 overexpression was accompanied by a slight increase of CerS1 in an unstimulated state, as well as CerS5 mRNA decrease. Even though Cer contents are higher in CerS3 overexpression cells, there is no compensatory decrease of other CerS. This could indicate that cells do not have to counter-regulate CerS3 increase.

Interestingly, in activated primary CD4$^+$ T cells the expression of every CerS is upregulated after at least 48 h. In contrast, CD8$^+$ T cells only show an upregulation of CerS2 and CerS4, while CerS1 and CerS3 are significantly decreased. This hints at differing roles of CerS in CD4$^+$ and CD8$^+$ T cells. CD4 is a homodimeric receptor, whereas CD8 is a disulfide-linked heterodimer [84, 85, 399]. Both proteins are post-translationally palmitoylated and engage with LCK upon stimulation [86, 400–402]. Localization of CD4 in lipid rafts is necessary for the co-stimulatory effects of CD4 on the TCR activation [403]. Hence, for CD8$^+$ cell proliferation and activation, CD8 does not have to engage in lipid rafts [404]. Since upregulation of CerS3 leads to an increase of glycosphingolipids that are necessary for lipid raft formation and also for CD3/CD4 activation, it is obvious that CerS3 expression is downregulated in CD8$^+$ T cells when lipid raft formation is not needed for CD8 activation. And since expression of CerS1 and CerS3 was upregulated in the WBC of human colitis patients, and CD8$^+$ cells play a minor role in UC development, it was decided to only focus on the CD4$^+$ cell function for this project.

In primary CD4$^+$ T cells, downregulation of CerS3 via siRNA led to a significant downregulation of CerS3 accompanied by CerS1 and 5 downregulation and CerS2 upregulation. Surprisingly, CerS3 mRNA expression was increased upon stimulation,

similar to CerS3 increase in control cells. This increase could be a compensatory effect by the cells. A possible reason for this effect could be the interference of siRNA with mRNA translation, thereby impairing protein increase [405]. Since T cells upregulate CerS3 upon activation, CerS3 siRNA treated cells may produce more CerS3 mRNA to compensate the loss of the protein. This hypothesis is supported by the results of the effector function assay, in which pro-inflammatory cytokine release was decreased in CerS3 siRNA treated cells. For confirmation, CerS3 protein levels should be checked to fully prove loss of function of CerS3 in CerS3 siRNA treated primary CD4$^+$ T cells.

This chapter discussed the importance of a balanced CerS expression and Cer contents in T cells. CerS1 upregulation fails to compensate for the loss of CerS3 in CerS3 knockdown meaning, CerS3 activity cannot be compensated and is of uttermost importance for T cell activation and signalling.

5.2 Influence of CerS1 and CerS3 on TCR activation

One important feature of T cells is their characteristic TCR. It is stimulated by the presentation of antigens from APCs and co-stimulants to trigger downstream effects in the cell to induce survival, proliferation, migration and cytokine release [113]. Activation of TCR leads to phosphorylation of LCK, which then phosphorylates Zap70 and promotes LAT recruitment to the plasma membrane as well as co-localization of LCK and LAT [334, 406]. There are reports that demonstrated the requirement of CerS6 for optimal TCR activation, in particular for Zap70 phosphorylation [382]. Furthermore, our group showed impairment of Zap70 phosphorylation in CerS5 knockdown Jurkat cells [361].

In this project, phosphorylation of Zap70 was investigated as it is a key step for TCR activation. Since CerS1 and CerS3 are both increased after activation of control Jurkat cells or primary CD4$^+$ cells, it was proposed that knockdown of either CerS1 or CerS3 would lead to TCR signalling inhibition. TCR signalling of CerS3 overexpression was suspected to be already activated without any stimulus, since the unstimulated CerS3 overexpression resembled the activated state of control cells. WB analysis of Zap70 phosphorylation revealed CerS1 knockdown did not affect TCR signalling, whereas CerS3 knockdown cells were not able to phosphorylate Zap70 upon stimulation. Surprisingly, CerS3 overexpression did not lead to a higher phosphorylation of Zap70

upon stimulation and was not already activated on a basal level. This effect differed from observations from CerS4 knockdown in Jurkat cells. CerS4 was downregulated when control T cells were activated and constitutive downregulation of CerS4 led to a steady-state activation without any external stimulus [384].

One possible explanation for this missing effect in CerS3 overexpression cells could lie in the sphingolipid contents. As TCR signalling takes place in lipid rafts, lipid order and composition in the plasma membrane is of undoubtable importance [407, 408]. Lipid rafts are normally enriched in cholesterols and glycosphingolipids and display parts of the membrane in which recruitment of receptors and proteins is facilitated for signalling processes [324]. TCR signalling therefore can be influenced by glycosphingolipid content. The lipid surrounding is crucial for receptors to engage or reside in the plasma membrane [409]. Transmembrane (TM) domains are usually in alpha-helices topological conformation with TM-unique amino acid composition [410]. There is already evidence that sphingolipids can bind to TM domains of receptors [411]. $C_{18:0}$ SM can directly bind to the TM domain of coat protein complex (COP) I vesicle machinery protein p24 [412]. The specific interaction of $C_{18:0}$ SM with the VXXTLXXIY motif within the TM domain has an influence on the activation state of p24 [412]. Unfortunately the TCR TM domains do not contain this specific motif. Nevertheless, there is evidence for the role of two amino acids (Arg521 and Lys256) in the confirmation change upon antigen binding on the TCR α chain [413]. Brazin et al. showed that these amino acids control immersion depth when antigens bind to the TCR in the lipid bilayer [413]. With interference to the lipid order and composition in the plasma membrane these necessary confirmation changes might be disturbed leading to inhibited TCR downstream signalling.

In previous studies, it was already shown that LCK activity is increased when glycosphingolipid species are increased in T cells [414]. Hyperactive T cells derived from SLE patients could be re-normalized after decreasing glycosphingolipid contents in the cells [415]. In this work it could be observed that CerS1 and 3 expression is upregulated after activation, indicating a higher production of long-chain C_{18}-Cer by CerS1 and very long-chain C_{22-24}-Cer by CerS3 in activated T cells. In contrast to that a general decrease of dhCer and Cer species could be observed in the shNC T cells accompanied by an increase of glycosphingolipids and some sphingoid bases. Higher production of dhCer and Cer after T cell activation is supported by the findings of Hose

et al., who observed increase of Cer species after activation of WT cells and even more Cer in acid Ceramidase deficient T cells, contradicting the findings of this work [369]. Nevertheless, Hose et al. did not directly compare un-activated and activated WT cells to have statistical data on this finding. Furthermore they were working with murine cells, which can differ from primary human cells or cell lines. However, in this work, activated NCmyc cells showed by tendency slight increases of long-chain and very long-chain dhCer (C_{16}-, C_{24}- and $C_{24:1}$-dhCer) and Cer (C_{14}-, C_{16}-, C_{18}-, C_{20}-, C_{22}-, C_{24}- and $C_{24:1}$-Cer) after activation. Notably, a decrease of dhCer and Cer in control cells could be caused by SM-synthase or UGCG producing more glycosphingolipids (GlcCer and LacCer) when T cells are activated. This is strongly supported by evidence that glycosphingolipids are needed for lipid raft formation [324, 326, 416].

Zap70 phosphorylation happened after 5 to 15 min of activation in control cells, when glycosphingolipid species were also elevated. CerS1 knockdown cells did not show any disturbance in TCR signalling. This was also reflected in the increase of C_{16}-, C_{18}- and $C_{24:1}$-GlcCer after activation of these cells. In contrast to that, CerS3 knockdown cells that had no elevation of Glc- or Lac-Cer after activation did not show any phosphorylation of Zap70 upon stimulation, highlighting the importance of CerS3 dependent upregulation of glycosphingolipids in TCR activation. CerS3 overexpression cells showed similar Zap70 phosphorylation compared to the control, which is also reflected in the glycosphingolipid content pattern that resembles the pattern of activated NCmyc control cells. Only $C_{24:1}$-GlcCer were significantly elevated in the CerS3 overexpression after 48 h stimulation compared to the controls, while $C_{24:1}$-LacCer was increased only in the control cells after stimulation. Notably, CerS3myc cells showed higher S1P-$dC_{18:1}$ contents on a basal level compared to control cells, as well as increase in numerous dhCer (C_{18}-, C_{24}-, $C_{24:1}$-dhCer) and Cer (C_{14}-, C_{18}-, C_{20}-, C_{22}-, C_{24}- and $C_{24:1}$-Cer) species. This could mean that CerS3 overexpression does not lead to an excessive TCR activation.

Composition of the plasma membrane is not the only factor contributing to lipid raft formation. Lipid order and the subsequent membrane condensation is necessary to maintain the highly dynamic nature of lipid raft formation [417]. Glycosphingolipids with saturated FA chains have higher transition temperatures and display a more ordered and less fluid phase of the membrane [418]. When lipid raft formation is prohibited, different signalling complexes cannot come together to be formed properly [419].

114

Studies showed that higher membrane orders were found at the periphery of immunological synapses, exactly where the proximal signalling happens [420]. By interfering with the composition of sphingolipid contents, lipid order can also be affected. CerS1 knockdown cells showed increase of saturated Glc- and LacCer (C_{16}- and C_{18}-GlcCer and C_{18}-LacCer), whereas CerS3 knockdown cells did not show any increase of saturated Glc- and LacCer after activation. This indicates a differential membrane order impacting TCR signalling. There is also evidence for a direct influence of Cer in the plasma membrane. ASMase activity leads to Cer production via the salvage pathway and aCDase leads to Cer breakdown [283, 421]. In aSMase deficient mice, T cells showed impaired activation with less Cer, while aCDase deficient murine T cells showed more Cer and elevated T cell activation [369]. Co-staining of TCR and C_{16}-Cer showed a strong co-localization in the plasma membrane, indicating a role for Cer-enriched platforms in TCR signalling [369]. A study showed that neutral Sphingomyelinase (nSM) 2 deficient T cells failed to phosphorylate LCK after stimulation, and CD3 polarization to the immunological synapse was not possible [368, 422]. Reports of non T cells showed promotion of membrane recruitment and activation of PKC ξ by nSM2, which was rescued in a nSM2 deficient model, where exogenously applied Cer could activate PKC ξ [423, 424]. These findings support a role for Cer-enriched membranes in TCR signalling. In this regard, it would be interesting to investigate co-localization of Cer and TCR in CerS1 and CerS3 knockdown and overexpression cells to verify the importance of Cer in the signalling hubs of the TCR.

Since T cells were not only activated via the TCR itself, but also via IL2 and CD28 activation, these receptors and their signalling can also be impaired by disrupted lipid rafts. IL2 receptor localization into the membrane is affected when glycosphingolipids are immobilized [425]. CD28 is a co-stimulatory receptor for TCR signalling and is activated by binding of CD80 and CD86 [119]. CD28 translocation into the plasma membrane is IL2R signalling-dependent [426], indicating that a change in glycosphingolipids in the lipid rafts can also affect co-stimulation of TCR with IL2 and CD28. CD28 is also responsible for LCK recruitment to the immunological synapse, enabling TCR signalling and also promoting TCR activation [427, 428]. In further experiments, IL2 and CD28 signalling pathways should be studied in detail in CerS1 knockdown and CerS3 knockdown and overexpression cells.

In conclusion, interaction of sphingolipids with TM domains or changes in lipid composition and order in the plasma membrane affects lipid raft formation and receptor recruitment. Decrease of glycosphingolipids after activation of CerS3 knockdown T cells led to disturbance of lipid raft formation and proper TCR activation via Zap70 phosphorylation. CerS1 knockdown did not show any TCR activation impairment and since mRNA expression showed that CerS1 upregulation failed to compensate for the loss of CerS3 in CerS3 knockdown, it was decided to conduct further experiments only in CerS3 knockdown and overexpression cells.

5.3 Impact of CerS3 on TCR signalling

TCR signalling triggers a variety of pathways that lead to transcription factor activation with subsequent promotion of proliferation, differentiation and migration [91–94]. Zap70 phosphorylation also activates, among other transcription factors, NFAT, NFκB and AP-1 [95, 96, 102, 103, 112, 113]. There is evidence for the effects of Cer on transcription factors. Human hepcidin gene expression, for example, can be induced by Cer through Stat3, c-Jun terminal kinase (JNK) and NFκB phosphorylation and surfactant protein B1 (SP-B1) in lung epithelial cells is decreased via transcriptional control through Cer [429, 430]. To investigate which transcription factors are impacted by the inhibited TCR signalling in CerS3 knockdown cells, AP-1 and NFAT1 expression were studied.

AP-1 is a heterodimeric protein consisting of phosphorylated c-Jun and c-Fos [112, 113]. In CerS3 knockdown and control cells phosphorylation of c-Jun and c-Fos expression was observed after 2 h. This showed that CerS3 knockdown had no effect on AP-1. CerS3 overexpression and control cells also showed significant activation of c-Jun and c-Fos after 2 h activation. Nevertheless, phosphorylation state of c-Jun was significantly lower in CerS3 overexpression cells compared to the control, while c-Fos expression was significantly higher in CerS3 overexpression cells. Neither higher c-Fos expression nor lower c-Jun phosphorylation can be explained by TCR signalling, since CerS3 overexpression cells showed similar Zap70 phosphorylation upon stimulation to control cells. A possible explanation for this could be the TCR co-receptor CD28, since AP-1 activation is heavily dependent on CD28 signalling [431–433]. Nevertheless, the results from this dissertation do not provide enough information on

CD28 receptor signalling. Therefore, further investigations on AP-1 activation should include CD28 pathway analysis.

NFAT1 is regulated by calcium increase in the cell upon TCR signalling [100]. Calcium increase leads to calcineurin activation which dephosphorylates NFAT1. To better understand the impact of CerS3 on NFAT1 transcription activation, $[Ca^{2+}]_i$ in stimulated Jurkat cells were studied. Since S1P1 can activate PLC-dependent Ca^{2+} pathways, it was decided to stimulate cells with S1P [434, 435]. But the investigations on S1P-induced $[Ca^{2+}]_i$, in this work, revealed a minor role for S1P1 in $[Ca^{2+}]_i$ increase. $[Ca^{2+}]_i$ levels in control cells increased significantly more compared to CerS3 knockdown cells. When cells were stimulated with a specific S1P1 agonist (SEW2871) [436–439], no $[Ca^{2+}]_i$ increase was detectable in control or CerS3 knockdown cells. Therefore, the difference in the S1P induced $[Ca^{2+}]_i$ response between CerS3 knockdown and control cells might be associated with a different S1P receptor. Besides S1P1, S1P4 displays an important S1PR in T cells. If S1P4 was responsible for the S1P induced $[Ca^{2+}]_i$ increase in control cells, this would contradict mRNA data which showed higher expression of S1P4 in CerS3 knockdown T cells compared to control cells. Nevertheless, investigations of $[Ca^{2+}]_i$ levels with a specific S1P4 agonist like CYM50308 [440] would shed more light on this research question. The higher $[Ca^{2+}]_i$ baseline of CerS3 knockdown Jurkat cells could also be a reason for the lower response to the S1P stimulation, however the difference in the baseline are minimal (only approximately 10 nM), which can not compensate for the approximately 40 % lower $[Ca^{2+}]_i$ in CerS3 knockdown cells after S1P stimulation.

Since $[Ca^{2+}]_i$ were reduced after S1P stimulation in CerS3 knockdown cells, it would be interesting to study $[Ca^{2+}]_i$ after TCR activation via CD2/3/28 stimulation. Moreover, $[Ca^{2+}]_i$ should also be studied in CerS3 overexpression cells to see if CerS3 overexpression shows opposite effects to CerS3 knockdown cells.

Based on the reduced $[Ca^{2+}]_i$ after S1P stimulation in CerS3 knockdown cells, it was assumed that NFAT1 translocation could be affected too. NFAT1 translocation to the nucleus in CerS3 knockdown was decreased compared to the controls. CerS3 overexpression showed increase of NFAT1 translocation in preliminary experiments. NFAT1 activation can be inhibited by GSK3β through additional phosphorylation of NFAT1 [441]. Simultaneously, GSK3β promotes JNK activation and subsequent c-Jun phosphorylation [441]. GSK3β is activated by PP2A [442, 443]. It could already be

shown that Cer has an influence on PP2A activation and saturated FAs were able to activate PP2A in hepatocytes during lipoapoptosis, which is triggered by exposure to excess FAs [444, 445]. When Cer influence PP2A activation, they could thereby indirectly affect GSK3β activation. After T cell activation, there is a significant decrease in Cer and dhCer species, which could lead to less PP2A and GSK3β activation. One would expect that less GSK3β activity leads to more NFAT1 activation when Cer are downregulated. However, CerS3 knockdown cells did not show an increase of NFAT1 activation, even though less Cer species were present in these cells. In contrast, this would also mean that NFAT1 activation should have been decreased in CerS3 overexpression cells, which was also not the case in the preliminary data. Therefore another pathway must be responsible for the observed effects.

Another regulatory mechanism for GSK3β is inhibition by Akt [446, 447]. Akt phosphorylates GSK3β and impairs nuclear export of NFAT1. Stimulation of TCR co-receptor CD28 activates Akt pathway [448, 449]. T cells in this dissertation were activated via CD2/3 and 28 activation beads. CD28 stimulation could have had an impact on Akt activation, which would inhibit GSK3β activation and promote NFAT1 activation. Therefore it would be interesting to study Akt and GSK3β activity in CerS3 knockdown and overexpression cells. If changes in the lipid rafts also affected CD28 receptor function, Akt pathway could be impaired in CerS3 knockdown cells, promoting GSK3β dependent inhibition of NFAT1.

NFAT1 can also act in quaternary complexes with other transcription factors, like AP-1 [450, 451]. The interaction of NFAT1 with other transcription factors has an important role in differentiation processes in T cells [100]. TH2 lineage differentiation, for example, is strongly dependent on GATA3 and NFAT1 mediated IL4 release which promotes TH2 differentiation [178, 452]. Additionally, NFAT1 interaction with STAT4 promotes TH1 lineage differentiation by increase of IFNγ production [155, 156, 453]. Differentiation assay of murine thymocytes into TH cells, revealed impaired differentiation into the TH lineage in CerS3 LCK Cre mice. Since NFAT1 translocation was reduced in CerS3 knockdown T cells, this can also influence effector function (like TNFα production), and differentiation potential into TH1 or TH2 cells.

These results demonstrated a special role for CerS3 in TCR and co-receptor activation caused by changes in the lipid status. AP-1 activation is not affected by CerS3. It was shown that NFAT1 activation is impaired in CerS3 knockdown cells thereby affecting

118

cytokine gene expression (effector function) and differentiaton processes in T cells. Since NFκB is one of the transcription factors activated by TCR signalling, it should be included in future experiments.

5.4 Impact of CerS1 and 3 on T cell migration

T cell activity is usually assessed by the capacity of T cells to release cytokines and to migrate towards specific chemokines. It was already shown in mice, that CerS2, but not CerS4, has a direct influence on S1P mediated thymocyte egress, as it is responsible for the formation of S1P by extra thymic cells [454]. To see the effects of CerS1 and CerS3 on T cell function, T cells were tested in a migration assay, where they had to migrate towards 100 nM S1P, the most prominent chemokine for T cell migration [347].

As expected, CerS1 and CerS3 knockdown cells both showed impaired migration capacity towards S1P compared to the control cells but also towards the positive control (FBS), which naturally contains S1P. In contrast, CerS3 overexpression showed better migration towards S1P compared to the control. These findings are in line with the mRNA expression pattern of S1P1, the receptor mainly responsible for the S1P-dependent migration [385], as well as with mRNA levels of S1P4, which is also important for lymphocyte migration [395]. S1P1 mRNA was decreased in unstimulated CerS3 and CerS1 knockdown cells compared to their controls, while being significantly upregulated in the unstimulated overexpression cells. This could also be verified on protein level, where S1P1 protein levels were decreased in CerS1 and CerS3 knockdown cells and increased in CerS3 overexpression cells on a basal level. Interestingly, S1P4 was highly expressed in CerS1 and CerS3 knockdown cells on a basal level, but not decreased in CerS3 overexpression cells. This may be a compensatory effect of the cells, trying to upregulate a different S1PR for S1P sensing and subsequent migration. Nevertheless, upregulation of S1P4 failed to compensate properly for S1P1 decrease and does not lead to a restored migration capacity in CerS1 and CerS3 knockdown cells.

But how do CerS impact S1P dependent migration and what is the underlying mechanism? S1PR expression on the membrane is a very complex process which is influenced by many factors, including other receptors such as CCR7 [273, 455, 456].

Ligand-binding of S1P1 leads to the internalisation of the receptor and loss of function [385]. Internalisation of receptors in the cell is highly dependent on endosome formation. Studies have shown that sphingolipids take part in endosome formation and inhibition of *de novo* synthesis of Cer in *Drosophila melanogaster* led to impairment of endosome formation and protein trafficking [457, 458]. Control T cells showed a decrease in S1P1 mRNA expression after activation. Meanwhile CerS1 and CerS3 knockdown cells showed the opposite effect: an increase after stimulation, indicating a disturbed internalisation of S1P1 upon stimulation. Interestingly, CerS3 overexpression cells showed a significant increase of S1P1 after stimulation in contrast to the downregulation by tendency in the control cells. This findings implicates an important role of sphingolipid composition and balance in the cells for proper S1P1 internalisation and signalling.

As already stated, lipid raft formation is crucial for different receptor signalling pathways, including S1P1 [337, 338]. Membrane fluidity is controlled by sphingolipids and cholesterol, causing them to have a great impact on lipid raft formation [459, 460]. Internalisation of S1P1 is proposed to happen in non-lipid raft domains [336]. This would fit well with the CerS3 overexpression data, that showed increase in all glycosphingolipids indicating more lipid raft formation and subsequently less S1P1 internalisation upon stimulation of the TCR like the mRNA data was showing. In regard to the dysregulated lipid contents in CerS1 and CerS3 knockdown cells, it fits well, that S1P1 dependent migration is downregulated in both cell lines, when the signalling hubs necessary for S1P1 signalling at the plasma membrane are missing. Of course, it is still necessary to investigate the effects of CerS1 and CerS3 knockdown and CerS3 overexpression on the S1PR internalisation process in more detail, since the experiments in this work do not provide enough information on this process.

Other receptors responsible for migration in T cells are also thought to be organized in lipid rafts and therefore affected by changes in sphingolipids. CXCR4, for example, is activated by binding of CXCL12 and promotes migration in T cells [461]. The receptor is organized in lipid nanoclusters and this organization is crucial for T cell migration [462]. Gardeta et al. showed that by reducing Cer species by aSMase depletion, lipid nanoclusters were not able to form and CXCL12-CXCR4 mediated migration was inhibited in T cells [462]. This is in line with findings from Limatola et al., who could

demonstrate that CXCR4-dependet migration was impaired by pharmacological inhibition of glycosphingolipid synthesis [463].

CerS1 and 3 knockdown led to reduced S1P-dependent migration, whereas CerS3 overexpression cells showed better migration. This demonstrates how important sphingolipid balance is to maintain T cell migration. To confirm *in vitro* data generated from Jurkat cells, it would be interesting to test S1P dependent migration on primary CD4$^+$ ^{T} cells treated with CerS3 siRNA.

5.5 Impact of CerS3 on T cell function

In previous chapters it was already demonstrated that CerS3 knockdown and overexpression influence sphingolipid contents and membrane properties thereby affecting TCR activation and signalling. It was also shown, that S1P dependent migration is influenced by CerS3 knockdown and overexpression. In this chapter the influence of CerS3 on effector function like proliferation and cytokine release is discussed.

Based on the fact that sphingolipids and Cer regulate cell proliferation, it was postulated that T cell proliferation could be impacted if the TCR was disturbed [464]. A previous study demonstrated that Cer accumulation in CD4$^+$ cells in aging mice showed less proliferation capacity for these cells [465]. In the case of CerS3 knockdown or overexpression, no effect on proliferation could be observed.

TCR activation and signalling leads to the expression of several genes, including genes for cytokine release [466]. NFAT1 is a regulator of TNFα gene expression [467] and since the preliminary data for NFAT1 activation showed impairment, cytokine release in T cells was assessed. The control, CerS3 knockdown and overexpression cells showed an increase of TNFα after stimulation. It was expected that TNFα production is impaired in CerS3 downregulated T cells and indeed CerS3 knockdown had significant lower TNFα levels compared to the control. This fits well with the impaired TCR signalling and the assumed reduced NFAT1 activation. The mechanisms behind cytokine release are not fully understood yet. Some cytokines are released via extracellular vesicles [468]. Newly synthesized cytokines are firstly inserted into the ER and soluble or transmembrane precursors are trafficked in vesicles to the Golgi [468]. Trans Golgi network loads them into vesicles or carriers for transport

to the plasma membrane [468]. The vesicle formation is extremely dependent on an asymmetric lipid distribution in the vesicles [469]. Cholesterols and Cer play the most important role in this process. While SM breakdown increases cholesterol levels and therefore enhances membrane fluidity, increase of Cer leads to more curved membranes, as the conical shape of Cer promote the curving nature of membranes [470–472]. Trajkovic et al. could demonstrate that Cer are essential for exosome formation and that exosomes could not be formed when SMase activity was inhibited [322]. Additionally other groups were able to demonstrate that blockade of Cer conversion to SM promotes exosome formation [314, 473]. Studies in macrophages and granulocytes showed that cytokine release in form of vesicles was also dependent on soluble N-ethylmaleimide-sensitive factor attachment receptor (SNARE) proteins [26, 474–476]. Darios et al. found, that sphingosine was necessary for synaptobrevin activation in neuro-synaptic vesicles for SNARE complex formation [477]. It was already shown that SNAP-23 and 25 are located in sphingolipid- and cholesterol-enriched lipid rafts [478]. This again supports the role of CerS in lipid raft formation and dysregulation of sphingolipid contents, like in the case of CerS3 knockdown, can strongly interfere with membrane properties.

It was surprising that TNFα release was also decreased in CerS3 overexpression cells, since preliminary data hinted at an increase of TNFα-inducing transcription factor NFAT1. However, TCR signalling was not elevated and showed similar Zap70 phosphorylation compared to the control. This could be an explanation for TNFα production similar to control cells, but this was not the case in the CerS3 overexpression cells. So what could cause a decrease in TNFα release of CerS3 overexpressing cells? TNFα is built in T cells as a transmembrane protein that is cleaved by the TNFα converting enzyme (TACE) metalloproteinase at the plasma membrane to soluble TNFα [479]. Indeed, there is evidence for direct influence of sphingolipids on TACE activity. It was also shown that sphingolipid alterations in aSMase-deficient macrophages led to enhanced TACE activity while administration of exogenous aSMase to those cells compensated this phenotype and inhibited TACE activity [480]. It could already be demonstrated that Ceramide-1-Phosphate (C1P) directly binds to TACE and inhibits its activity [481]. In a LPS induced sepsis model in CerS2 knockout mice, higher TNFα levels were detectable due to elevated TACE activity [482]. This showed that very long-chain Cer had a direct influence on TACE activity. TACE is regulated by membrane composition and lipid raft depletion leads to

enhanced TACE activity [483]. CerS3 overexpression in Jurkat T cells resulted in enhanced glycosphingolipid levels in these cells, indicating more lipid raft formation that could disturb TACE activity and therefore lead to less TNFα release. Transmembrane TNFα is palmitoylated in order to get into the membrane [483]. As there is a reduction of C_{16}-dhCer and C_{16}-Cer in CerS3 knockdown cells, there might be a general imbalance of C_{16}-acyl-CoA in the cell which is also a substrate for palmitoyltransferases to palmitoylate certain transmembrane proteins, like TNFα. Palmitoylation of TNFα is a prerequisite to translocate to the plasma membrane which might be impaired in our cells. But further experiments have to be done to proof these hypotheses.

For confirmation of *in vitro* cell line data, cytokine release of primary CD4$^+$ T cells treated with either control or CerS3 siRNA was investigated. Control cells showed significant increase of pro-inflammatory cytokines IFNγ, TNFα, IL6 and IL17 after 24 and 48 h of stimulation with activation beads and IL2. Notably, IFNγ and IL6 concentrations were very high (around 30000 - 50000 pg/ml) compared to the other cytokines (around 800 – 1100 pg/ml). This indicates a high population of pro-inflammatory TH1 and TH2 cells in the pool of isolated CD4$^+$ T cells that are prone to secrete IFNγ, but also IL6 [484, 485]. However, the composition of the CD4$^+$ cells is donor dependent and could only accurately be determined by surface marker analysis via flow cytometry. Therefore, the primary data are in general more variable and could vary from Jurkat T cell data. Nevertheless, in CerS3 siRNA treated primary T cells pro-inflammatory cytokines significantly increased after 24 or 48 h stimulation. Cytokine concentrations were significantly lower after 48 h in CerS3 siRNA treated cells compared to control. These findings confirm the data generated in Jurkat cells.

All in all, the results discussed in this chapter show that effector function of CD4$^+$ T cells is clearly affected by CerS3 downregulation. Inhibited vesicle formation for cytokine release or reduced TACE activity caused by the disturbance of the Cer and CerS equilibrium might be involved in the reduced effector function of CerS3 knockdown T cells.

5.6 Effects of CerS3 on DSS-induced acute colitis

Other studies could already show the importance of several CerS in colitis development and T cell function. An AOM/DSS induced colitis associated colon cancer model in CerS4 LCK Cre mice showed an enhanced pancolitis with extensive hyperplasia and tumor-burden in comparison to WT mice [384]. Interestingly, CerS6 deficient mice were protected from T cell mediated colitis, while in the DSS induced model, CerS6 deficiency aggravated disease progression and symptoms [360]. These different findings suggest a special role for each CerS on colitis development and in the effector cells involved in the pathophysiology.

The effects of CerS3 on TCR signalling, migration and effector function were successfully investigated *in vitro*. To study the effects *in vivo*, especially in the context of colitis, a T cell specific knockout of CerS3 (CerS3 LCK Cre) in mice was conducted and acute colitis was induced with DSS.

CerS3 LCK Cre and WT mice showed an increase of disease score and weight loss during the experiment. Comparing both groups, WT mice developed a significant higher disease score, as well as significantly more weight loss. Together with immune-histological data of the colon, it was obvious that WT mice had more severe colitis and reacted more sensitive to the DSS treatment than CerS3 LCK Cre mice. CerS3 LCK Cre mice were not completely protected from DSS induced colitis, but showed less symptoms and disease progression compared to the WT. This is in line with the human data that showed an increase in CerS3 expression in the WBC of colitis patients in dependency of the disease stage [363].

Looking at the immune cell distribution of different tissues in the control and DSS treated mice, both mice groups showed a significant increase of neutrophils and macrophages in the blood and spleen. Immune cells were isolated from the LP and the IEL fraction of the colon. LP fraction did not show any significant difference between control and DSS treated mice, but by tendency neutrophils and macrophages were increased. However, in the IEL fraction neutrophils significantly increased in DSS treated WT and CerS3 LCK Cre mice, whereas an increase of CD4$^+$ cells and macrophages could only be observed in the WT mice. In contrast to that, only in CerS3 LCK Cre DSS treated mice CD8$^+$ population increased. These findings provide evidence for the overall colonic inflammation in both groups, but also show more inflammatory immune cell populations in the IEL fraction of WT mice.

A stronger inflammation in WT mice after DSS treatment was also reflected in the immune-histological stainings of colon swiss rolls showing more substantial swelling of the submucosa and disruption of the epithelial layer in comparison to CerS3 LCK Cre colon tissue. Chronic colon inflammation is also characterized by immune cell recruitment that is mediated by cytokines. Especially cytokines, like TNFα and IL6, promote immune cell recruitment, migration and function [486, 487]. TNFα is already in use as a target for UC treatment showing the importance of attenuation of cytokine effects [19, 488]. TH cells derived from CerS3 LCK Cre mice showed less pro-inflammatory cytokine release (including TNFα). This was also the case in CerS3 downregulated human primary CD4$^+$ T cells and cell line CD4$^+$ Jurkat cells. So reduced TNFα secretion could be one reason for the milder colitis symptoms in CerS3 LCK Cre mice.

Since effector function in human CD4$^+$ cells was decreased, cytokines in the plasma of control and DSS WT and CerS3 LCK Cre mice were compared. Colitis patients show increased IL1β, IL4, IL5, IL8, Il12p40, IFNγ and TNFα expression [17], but in the DSS WT and CerS3 LCK Cre mice no increase of cytokines in the plasma could be observed. Only IL6 showed a tendency to increase in the plasma of DSS treated mice. This might be due to the short observation time of these mice or the time point, when the blood was taken from the mice, which might be not in the acute inflammation phase. Usually, cytokines are very stable in EDTA-blood [489], but as inflammation occurs in the colon, cytokine concentrations in this tissue or released directly from effectors cells would be more conclusive. Therefore, cytokine release of murine WT and CerS3 LCK Cre cells was compared after their differentiation into the three subtypes (TH, Treg and cytotoxic CD8$^+$). Indeed, in both groups (WT and CerS3 LCK Cre) all three subtypes showed an increase of cytokines after stimulation. CerS3 LCK Cre T cells produced significantly lower amounts of pro-inflammatory cytokines IL17 and TNFα and anti-inflammatory IL-10 compared to the WT T cells. This also fits well with the inflammatory state of the mice, because Tregs do not have to release as much IL10 to regulate inflammation, when inflammation is not severe.

Notably, there were differences in T cell populations of control WT and CerS3 LCK Cre mice. Blood, thymus, spleen and lymph nodes were examined for CD3$^+$ cells and their subpopulations (CD4$^+$, Treg and CD8$^+$). It was observed that in CerS3 LCK Cre mice CD3$^+$ populations were significantly decreased in blood, thymus and spleen whereas

in the lymph nodes they were significantly increased. T cell egress out of the lymph nodes is highly dependent on S1P gradients. S1P concentrations are high in the blood and low in the lymph nodes, to promote egress into the blood [273, 455]. The human *in vitro* data showed, that S1P dependent migration was disturbed in CerS3 knockdown Jurkat cells. This could be one reason why T cells are trapped in the lymph node in CerS3 LCK Cre mice and are unable to egress into the blood. S1P levels in the plasma of WT and CerS3 LCK Cre control and DSS mice were unaltered (data not shown), giving no hint to actual differences in S1P gradient. S1PR are not the only receptors promoting migration of T cells. As already stated, CXCR4 is involved in T cell migration and also affected by sphingolipid contents [462, 463]. There is a second receptor, CCR7, that is especially responsible for retention of T cells in the lymph node [490, 491]. CCR7 expression on the plasma membrane promotes T cells to stay in the lymph node and S1P signalling has to overcome this signalling [492]. CCR7 ligands are mainly expressed in the endothelial venules and the lymph node parenchym [493]. Further investigations could focus on CCR7 ligands (CCL19 and CCL21) in the lymph nodes to see if there are differences between the WT and CerS3 LCK Cre lymph nodes, as well as CCR7 expression differences between WT and CerS3 LCK Cre T cells.

Lower incidence of T cells in the periphery could also be an effect of impaired differentiation. Reports showed that changes in Cer can have an impact on differentiation behaviour. One study showed that less Cer contents in thymocytes supported Treg differentiation [369]. Therefore, thymocytes isolated from WT and CerS3 LCK Cre mice, were differentiated for 10 d into the three main CD3$^+$ cell groups: TH, Tregs and cytotoxic CD8$^+$. Analysing the AUC of the time course of differentiation, TH and Tregs of CerS3 LCK Cre mice showed less differentiation capacity compared to the WT. This was not due to less progenitor cells, as analysis of progenitor cells from all samples of the differentiation assay showed no significant difference between both groups. But overall, differentiation into CD3$^+$ cells was less effective in CerS3 LCK Cre T cells. Findings by Sen et al. showed an important role for Cer *de novo* synthesis in TH17 differentiation [377]. Differentiation into the different TH subsets is connected to metabolic changes and a constant Cer accumulation was observed during TH17 polarization [377]. However, a previous report stated that Treg differentiation was supported with Cer content decrease [369]. Cer contents dropped in activated Jurkat

T cells, so it would be interesting to check if this was also the case for TH and Treg cells.

These results show that lack of CerS3 in T cells protects mice from severe DSS induced colitis, attenuates disease progression and leads to a milder disease progression. Changes in the lipid status of CerS3 LCK Cre cells might have influenced naïve T cell polarization into the TH and Treg subtype, but also cytokine release. S1P dependent egress of CerS3 LCK Cre T cells might be disturbed leading to retention of the cells in the lymph node.

5.7 CerS3 influence in a human colitis model

2D cell cultures are great models for studying different mechanisms, pathways and effects of different genes, proteins or drugs on cells. They are very easy to handle and the use of immortalized cell lines enable high-throughput research with reproducable data. Nevertheless, there are some disadvantages. One important disadvantage: Cell lines lack the diversity of the tissues they come from. In the colon, for example, epithelial colon cells are generated from stem cells and differentiate into goblet or paneth cells, and are surrounded by fibroblasts, immune cells and endothelial cells. Interaction between different cell types by direct contact or protein exchange is very important for cell function [494, 495]. The complexity of these tissues is poorly represented in the 2D culture. For better representation of tissues, cells were embedded in ECM that resembles the matrix of tissue in the body to allow the cells to grow three dimensional into the ECM [496]. Nowadays it is even possible to grow organoids consisting of different cell types from primary tissues obtained from mice or humans [497, 498]. These 3D cultures differ from 2D cultures in morphology and are more representative of the actual tissue in the body [499–501]. They are already used in a variety of studies, including cancer and colitis research [502–504]. Organoids are also in use for more physiological representation of organ systems in research, while also giving researchers a pool of biobanks for different cancer entities or inflammatory diseases [505, 506]. For every study that goes into more detail about functions of the body, animal experiments are necessary. For a long time, animal experiments were irreplaceable for drug development, especially for testing toxicity of different substances and possible systemic side effects of different drugs. The animal models represent a whole body system with all organs and tissues working together.

5. Discussion

Nevertheless, besides obvious major ethical problems, animal models sometimes lack the translationality into the human system. Li et al., for example, found enhanced T-cell antitumor immunity against a Lass5-epitope in mice [507]. Unfortunately, the part of Lass5 that was presented as antigen only exists in the murine protein, and not in humans.

A new law signed in the U.S. in December 2022 stipulates that new drugs do not have to be tested on animals before they are approved by the U.S. Food and Drug Administration (FDA). This new law will have a huge impact on drug development and could break ground for new methods. Since the FDA and the European Medicines Agency (EMA) work closely together, it is expected that the EMA follows the decision of the FDA. New methods that go beyond 2D culture and revolutionize 3D culture are so-called organ on a chip models. These microfluidic models allow the 3D growth of epithelial cells next to endothelial cells that form a vessel, mimicking physiological conditions present in the human body. Chips can be seeded with different cell types that are common for the organ of interest, for example epithelial colon cells for colon chips or hepatocytes for liver chips. In a study in liver chips that tested 27 known hepatotoxic and non-toxic drugs, a sensitivity of 87 % with 100 % specificity has been obtained [508].

In this dissertation, I established a human colon chip to build the grounds for better physiological and human relevant colitis research. The PDSM chip contains two channels (top and bottom) that are connected through a porous membrane (7 µm pores). Cells are seeded into ECM coated channels to form blood vessel-like structure or epithelial layer, respectively. Chips can be connected to medium reservoirs allowing individual medium flow through each channel. Chips can be placed into a regulatory unit that controls and provides flow rate of medium through the channels and applies physiological stretch to the chip for natural intestinal peristalsis.

For the colon intestine chip, Caco-2 cells were used for the epithelial layer and HUVECs for the endothelial layer. Caco-2 cells formed a 3D structure within five days after seeding into the channel.

The colon chip was also used to mimick human colitis. Epithelial cells were treated with IFNγ, a colitis-related cytokine, whereas endothelial cells were treated with TNFα to imply inflammation to endothelial cell barrier and to display pro-inflammatory stimulus,

like in the colitis patients. Afterwards the vascular channel was perfused with T cells, T cell attachment to the endothelium, as well as migration of T cells into the inflammatory tissue induced by cytokines in the colon channel could be observed. Control and CerS3 downregulated Jurkat T cells were dyed with two different cell tracers to differ between them.

Attachment of both, control and CerS3 knockdown cells, to the endothelial layer could be observed in TNFα primed chips. Resting control showed a minimal attachment of T cells to the endothelial layer. Interestingly, more green-fluorescent cells (shNC) were attached to the endothelial and the epithelial layer of all T cell perfused chips. This fits well with the *in vitro* migration assay data, showing less migration capacity for CerS3 knockdown cells. But also with murine *in vivo* data which showed more T cells in the lymph node of CerS3 LCK Cre mice and less T cells in blood, thymus and spleen compared to WT mice hinting on a possible migration effect.

Nevertheless, few cells migrated to the epithelial layer in any chip. The IFNγ stimulus was probably not enough to induce T cell migration. Because of this, it was decided to use a more physiological stimulus in the top channel, consisting of eight different chemokines typical in human colitis (IP10, MIP-3α, MEC, GPR14L, TECK, MCP-1, SDF-α and MIP-3β) for further experiments.

Quantification of T cell attachment to the endothelial and epithelial layers showed that Jurkat T cells migrated from the endothelial into the epithelial layer regardless of the given stimulus. Resting control and primed chips showed both T cell migration. In this preliminary experiment more CerS3 knockdown Jurkat cells migrated to the epithelium compared to the control Jurkat cells, contradicting the data of the first T cell recruitment experiment conducted with the IFNγ migration stimulus. Taking into consideration that control cells, as well as CerS3 knockdown cells, are GFP⁺, successfully red-fluorescent-dyed cells should appear green- and red-fluorescent. There were no T cells visible that were co-stained for red and green, which might indicate that staining of the cells was not good enough or that the fluorescence dyes are not good enough (data not shown). As CerS3 knockdown cells were not distinguishable from control cells, the flow cytometry preliminary data should be interpreted with caution.

The first attachment and migration to inflamed colon experiments were successful. Further experiments with physiological conditions should be conducted to confirm

already generated data. It would also be interesting to include cytokine analysis of bottom and top channel effluents after TNFα and chemokine cocktail treatment, as well as after T cell introduction, to see if CerS3 knockdown cells release less pro-inflammatory cytokines. If shCerS3 cells really migrated less to the inflamed epithelial layer, research on possible receptors and surface markers would be of great interest. Cells could be pre-treated with different antagonists for receptors like S1P1 before being perfused into the chips to see possible effects on migration. In more advanced experiments, Caco-2 cells could be replaced by patient-derived organoids to form epithelial layer. HUVECs could be replaced by human intestinal microvascular endothelial cells (HIMECs) to enhance physiological resemblance of the experiment. This method is already established for small intestine on a chip by Emulatebio and could be transferred to colon chips [509]. Jurkat cells could be replaced by patient-derived primary T cells and treated with siRNA to downregulate CerS3 and study the effects on patient-derived organ chips.

5.8 CerS3 as therapeutic target

For many years, CerS have been discussed as therapeutic targets for different conditions [510]. Studies have looked at Fumonisin B1, which is a mycotoxin acting as a general CerS inhibitor by competitive inhibition towards sphinganine and acyl-CoA [511, 512]. However, Fumonisin B1 is not used in the clinic because of the high hepato- and renal toxicity and risk of edema development [513–515]. Additionally, *in vivo* inhibition of CerS is relatively weak compared to *in vitro* effects [516]. Other CerS inhibitors, like australifungin, are more potent, but are too toxic [516]. S1PR agonist, fingolimod, primarily acts on S1PR and is in clinical use for MS treatment as well as having a potent effect on lymphocyte retention [517]. Fingolimod is also able to inhibit CerS by non-competetive inhibition towards sphinganine and acylCoA [518]. There are no pharmacological inhibitors that are specific for only one CerS in particular, but as CerS and their products contribute to different disease progressions, targeting CerS could be beneficial for patients.

CerS3 is the most overlooked CerS of all six isoforms. From 1993 to June 2023 only 69 publications turn up when "CerS3" is searched on pubmed.com. CerS3 is predominantly expressed in the skin and testis. Ultra long-chain Cer, as well as very long-chain Cer are important for good skin barrier, as well as for spermatogenesis [300,

130

519]. Mutations in CerS3 or lack of CerS3 in humans can lead to autosomal recessive congenital ichthyosis, skin disorders characterized by dry and scaled skin [520]. In a human colitis study, it was shown that CerS3 is overexpressed in WBC of human colitis patients, indicating an important role for CerS3 in T cells [363].

Taking together human *in vitro* and murine *in vivo* data from this dissertation, it is evident that CerS3 downregulation in colitis has a protective role and leads to impaired TCR signalling, decreased migration and reduced T cell effector function. A proposed role for the mechanism behind these effects is depicted in Figure 44. CerS3 downregulation leads to decrease in dhCer, Cer and glycosphingolipids that cannot be incorporated into the plasma membrane for lipid raft recruitment. Failed lipid raft formation leads to a disrupted TCR signalling with inhibition of Zap70 phosphorylation that leads to decreased $[Ca^{2+}]_i$. Less TCR activation decreases translocation of NFAT1 into the nucleus and leads to reduced TNFα release by the cells. S1P1 might not home properly into the plasma membrane, due to the lack of proper lipid raft formation. S1P dependent migration is therefore decreased in CerS3 downregulated T cells. In murine CerS3 KO T cells, differentiation into the TH subtype is disturbed and T cells are trapped in the lymph node. In DSS induced colitis in mice, where high TH response leads to disease progression, CerS3 depletion in T cells shows a protective role, with less inflammation in the colon and less colitis symptoms and therefore better outcome for mice.
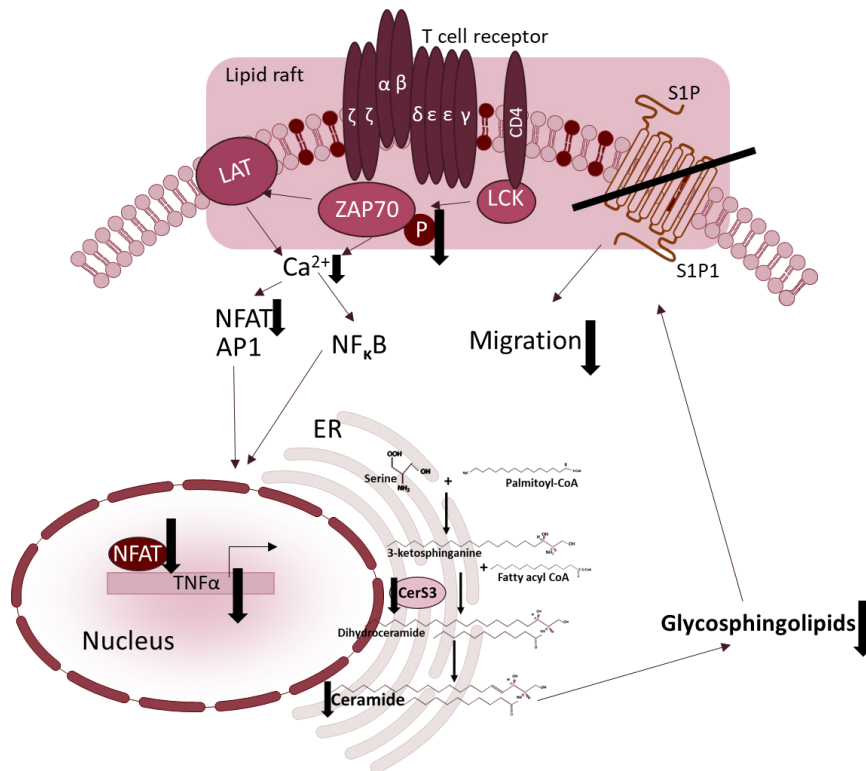
Figure 44: Proposed mechanism of CerS3 downregulation effects. CerS3 downregulation leads to less Cer production and less glycosphingolipids. If there are not enough glycosphingolipids, proper lipid raft formation is impaired and S1P1 probably cannot reside at the plasma membrane. S1P dependent migration is therefore decreased. Upon stimulation of the TCR, Zap70 phosphorylation is inhibited and leads to less $[Ca^{2+}]_i$ and affects NFAT1 translocation into the nucleus. NFAT1 dependent TNFα gene expression is downregulated and T cells release less TNFα.

Even though CerS3 seems to be a good target in T cells, mechanistically, it still has to be discussed if CerS3 is a good target in general. As CerS3 is largely not expressed in any tissue except for skin and testis, most organs should not be affected by CerS3 downregulation. In naïve, M1 and M2 macrophages, CerS3 mRNA expression is very low (data not shown). Notably, CerS3 expression in T cells only becomes important when cells are activated and with CerS3 downregulation T cell function is attenuated, but not completely diminished. This indicates that CerS3 downregulation will only affect stimulated and activated T cells, lowering possible side effects coming from unactivated cells. Targeting CerS3 seems beneficial for early stages of colitis, when disease progression is still ongoing and damage is not high enough to stop T cells from migrating into the inflammatory tissue and to avoid high cytokine levels for immune cell recruitment. Nevertheless, CerS3 might be a new target that can ameliorate colitis symptoms and be beneficial for the general well-being of patients.

A possible way to introduce CerS3 downregulation in target cells would be siRNA treatment. Small interfering RNAs degrade mRNA expression and impair protein translation of target mRNAs by activation of the RNA-induced silencing complex. It is very promising, because there is the possibility to directly target genes that are responsible for diseases and conditions. The clinical use of siRNAs is limited due to poor stability of siRNA and possible off-target effects [521]. However, stability can be enhanced by chemical modifications [522–524]. Off-target effects can also be lowered by chemical modifications or different transporters to the target cells [525–527]. Naked siRNA is too heavy (13-16 kDA) and negatively charged for entrance through the plasma membrane of most cell types. In order to transport siRNA to the target cell type, carriers, like lipid-nanoparticles, are needed [528, 529]. They do not only transport the siRNA, but they also help with stability of the siRNA. So far since 2018, five siRNAs were approved by the FDA and EMA for rare metabolic conditions [530]. CerS3 siRNA treatment of primary CD4$^+$ T cells showed significant decrease of CerS3 mRNA expression in an unstimulated state with minimal effects on the expression of other CerS. Unfortunately, cells increased CerS3 mRNA expression upon stimulation similar to control cells. This effect may be corrected with different siRNA concentrations or incubation times. Nevertheless, cytokine release in CerS3 siRNA treated cells, showed a significant lower amount of pro-inflammatory cytokines, indicating that CerS3 protein levels were also reduced. In future experiments, siRNA treatment of primary CD4$^+$ cells should be optimized.

Summarizing all the generated data in this dissertation, a clear influence of CerS3 on TCR activation and signalling, T cell function and migration and colitis could be demonstrated. This work provides evidence for a beneficial use of CerS3 as therapeutic target and lays the ground for more detailed and profound research on this topic.

6. Outlook

In this work, a potential new role for CerS3 as a therapeutic target has been proposed. Since CerS3 knockdown impairs TCR signalling and attenuates cytokine release and migration of cells, targeting CerS3 in T cell driven colitis could be beneficial for patients. Further tests of CerS3 knockdown in other cells must be conducted to ensure specific targeting of T cells, but also to avoid side effects that can be caused by other immune cells. As monocytes or neutrophils play vital roles in inflammatory bowel diseases and their off-set, CerS3 knockdown in these cells should be established and the effects on these cell functions investigated.

TCR signalling takes place in lipid rafts that are enriched in glycosphingolipids. As the TCR signalling in CerS3 knockdown cells was impaired and sphingolipid species were reduced in activated T cells, changes in the lipid status of lipid raft fractions could be of great interest. Membrane fractions of unstimulated and stimulated cells should be isolated and then checked for their lipid content. It would be also very interesting to see if there is a re-translocation of the TCR in CerS3 knockdown cells. When lipid species are downregulated in activated CerS3 knockdown cells, there is a possibility that the TCR cannot reside in the lipid rafts anymore. This could be analysed via WB analysis of TCR proteins in the lipid raft fractions and by co-staining of lipid raft regions and TCR proteins at the plasma membrane. This could also be very interesting for S1P1, since migration in shCerS3 cells was also affected. The pathway downstream of S1P1 should also be elucidated, as well as upstream protein and complexes of the NFAT1 pathway, to unravel every detail of the interaction of the inhibition of NFAT activation by CerS3 knockdown.

For proof of principle, CerS3 knockdown cells should be transfected with CerS3 overexpression plasmid to rescue the CerS3 knockdown phenotype and check if TCR signalling and effector function can be restored. It would also be possible to try to rescue the CerS3 knockdown phenotype by treatment with different ceramide species. This would shed light on the question which Cer in particular is responsible for the effects on TCR signalling inhibition at the plasma membrane.

CD8^{+} cells may seem less important in the light of UC, but nevertheless, they are very important effector T cells in other diseases. In GvHD, cytotoxic CD8^{+} effector function is the main driver of the disease. This work showed that CerS3 expression is downregulated when CD8^{+} cells are activated. Maybe overexpression of CerS3 in

these cells would lead to impaired effector function. This could be a possible target for attenuation of CD8$^+$ effector function in inflammatory diseases.

Optimization of CerS3 siRNA treatment for primary T cells would also be very important. Concentrations and incubation times can be improved, as well as different siRNAs should be tested to ensure the least possible off-target effects in the T cells.

With establishment of the physiologically-relevant human colon chip, a variety of new opportunities arises for colitis research. The co-culture of epithelial and endothelial cells allows to include more naturally occuring conditions to the cell culture and to investigate the interaction of different cell types *in vitro*. It is also possible to culture patient derived organoids and patient derived colon-endothelial cells in the chips. This would create a system with the possibility of testing individual drugs on the cells of a patient, making personalized medicine more applicable. Personalized cell therapy could also be tested with patient derived colon organoid chips, since there is no need for a high amount of cells. Primary T cells could be isolated directly from the patient's blood and then treated and stimulated *in vitro* prior to perfusion into the chip. In regard to CerS3 as a new therapeutic target, isolated T cells could be treated with CerS3 siRNA and then placed into the chip. Thus recruitment and effects of CerS3 siRNA treated T cells compared to control siRNA T cells on the patient's colon chip can be tested.

7. Summary

Kolitis Ulzerosa ist eine chronisch entzündliche Darmerkrankung des Kolons, die mehr als 170000 Menschen in Deutschland betrifft. Patienten leiden an Symptomen wie Durchfall, rektalen Blutungen, blutigem Stuhl, abdominalen Schmerzen und Krämpfen, Fieber und Erschöpfung [3]. Bisher ist Kolitis Ulzerosa zwar behandelbar, aber nicht heilbar. Im gesunden Zustand ist das Darmepithel mit einer Mukusschicht benetzt, die nicht nur eine physische Barriere darstellt, sondern auch eine antimikrobielle Funktion aufweist [7, 8]. In Kolitis Patienten ist die Mukusproduktion stark beeinträchtigt und dies führt zu einer erhöhten Permeabilität und dem verstärkten Eintreten von Pathogenen, die das Immunsystem aktivieren [9].

Die Pathophysiologie der Kolitis Ulzerosa ist sehr komplex und kann nicht auf einen einzigen Mechanismus zurückgeführt werden. Pathogene, die die erste Barriere des Darms durchbrochen haben, werden von dendritischen Zellen (DCs), aber auch von Makrophagen und T Zellen durch *Toll Like* Rezeptoren (TLR) erkannt [11]. TLR Signalwege aktivieren Transkriptionsfaktoren, die die Ausschüttung von Interleukinen wie IL12 und 23 oder *Tumor Necrosis Factor* (TNF) α fördern [14]. Aktivierte T Zellen schütten Zytokine aus, um weitere Immunzellen zu rekrutieren. Die Infiltration des bereits entzündeten Gewebes durch neue Immunzellen führt zur Entwicklung einer chronischen Entzündung, die immer weiter gefördert wird [24].

T Zellen sind Teil des adaptiven Immunsystems und werden über den T Zell Rezeptor (TZR) aktiviert. Dieser erkennt Antigene, die von Antigen-präsentierenden Zellen (APZ) präsentiert werden [68, 74]. Der TZR wird ebenfalls durch Co-Rezeptoren stimuliert, wie *Cluster of Differentiation* (CD) 4 und 8 [84]. Diese Co-Rezeptoren sorgen für eine räumliche Nähe der Proteine, um die Signaltransduktion der TZR Aktivierung weiterzuleiten [86]. Ein wichtiger Schritt bei der Aktivierung des TZR ist die Phosphorylierung der *Zeta-Chain-Associated-Protein Kinase 70* (Zap70), die zur Aktivierung mehrere Transkriptionsfaktoren wie *Nuclear Factor Kappa B* (NFκB), *Activating Protein* (AP-1) oder *Nuclear Factor of activated T Cells* (NFAT) führt. Die Aktivierung dieser Transkriptionsfaktoren führt zu einer Translokation in den Nukleus und daraufhin werden Gene angeschaltet, die Proliferation, Überleben, Differenzierung und Effektorfunktion der Zelle steuern [89–94]. Den größten Beitrag zur Kolitis leisten T Helfer (TH) Zellen. Sie sind definiert durch die Expression des CD4 Rezeptors und nehmen eine unterstützende Rolle ein, in der sie Zytokine zur

136

Rekrutierung und Regulierung anderer Immunzellen ausschütten. Die Anzahl der aktivierten T Zellen ist in Kolitis Patienten erhöht, sowie die Menge der Zytokine, die sie ausschütten [166, 186]. Dementsprechend ist es wichtig, verschiedene Faktoren zu untersuchen, die die Aktivierung von T Zellen beeinflussen.

Sphingolipide sind nicht nur strukturgebende Elemente der Zellmembran, sondern sind auch in verschiedene Signalwege involviert und können als aktive Biomoleküle verschiedene Signalwege in der Zelle aktivieren [283]. Die einfachsten Sphingolipide und das Grundgerüst für komplexere Sphingolipide sind die Ceramide (Cer), die aus einem Sphingosin und einer über N-Acylierung angehängten Fettsäure variierender Kettenlänge (C_{6-32}) bestehen [279]. Sie werden entweder *de novo* im Endoplasmatischen Retikulum (ER) synthetisiert oder über den *Salvage Pathway* aus Sphingomyelin (SM) zu Cer abgebaut [283]. Die Schlüsselenzyme für die *de novo* Synthese sind die Ceramidsynthasen (CerS) [286]. Diese binden durch N-Acylierung verschieden langkettige Fettsäuren kovalent an ein Sphinganin oder Sphingosin und bilden somit DihydroCer bzw. Cer [285, 286]. Es gibt sechs verschiedene Isoformen der CerS, die Spezifität gegenüber Fettsäuren verschiedener Kettenlängen aufweisen [287]. CerS1 etwa weist eine Spezifität gegenüber C_{18} auf, während CerS3 Fettsäuren der Kettenlänge C_{18}-C_{32} favorisiert [287]. CerS werden nicht in jedem Gewebe gleich exprimiert. CerS3 ist vor allem in der Haut, in Prostata und Hoden exprimiert, während CerS1 am meisten in Hirngewebe nachgewiesen wird [287]. Cer können direkt in die Zellmembran eingebaut werden oder sie werden zu komplexeren Sphingolipiden wie Sphingomyelin oder Glykosphingolipde verstoffwechselt und in die Zellmembranen eingebaut [304]. Bereiche der Plasmamembran, die eine hohe Konzentration an Cholesterol und Glykosphingolipiden aufweisen, nennt man *Lipid rafts* [324, 325]. *Lipid rafts* dienen als Signalplattformen für verschiedene Rezeptoren, darunter auch der TZR, dessen Aktivierung nur dann stattfinden kann, wenn er in *Lipid Rafts* lokalisiert ist [334, 335]. Durch Vorarbeiten wurde bereits ein Einfluss von CerS auf die T Zell Funktion nachgewiesen [361, 384]. CerS4 *Knockdown* in CD4$^+$ Jurkatzellen führte zu einer Aktivierung der Zellen ohne externen Stimulus und CerS5 *Knockdown* in Jurkat Zellen inhibierte die TZR Aktivierung [361, 384].

In einer Studie mit humanen Kolitis Patienten konnte eine Überexpression von CerS1 und CerS3 in weißen Blutzellen nachgewiesen werden [363]. Basierend auf dieser Erkenntnis und den bereits bestehenden Vorarbeiten zum Einfluss von CerS4 und

CerS5 auf die T Zell Funktion, wurde in dieser Dissertation der Einfluss von CerS1 und CerS3 auf die T Zell Funktion und Colitis untersucht.

Hierfür wurden CerS1 und CerS3 durch lenti-virale Transduktion in der CD4$^+$ Jurkatzelllinie runterreguliert, während CerS3 durch Transfektion eines CerS3 Überexpressionsplasmids ebenso überexprimiert wurde. Es stellte sich heraus, dass die mRNA Expression von CerS1 und CerS3 nach Aktivierung der T Zellen mit CD2/3/28 Aktivierungsbeads und IL2 hochreguliert wurde. In CerS1 *Knockdown* Zellen konnte neben der erfolgreichen Runterregulierung der CerS1 ebenfalls eine Runterregulierung von CerS3, CerS4, CerS5 und CerS6 im unaktivierten Status beobachtet werden und eine signifikante Reduzierung der CerS3 Expression nach Aktivierung der Zellen. Im Gegensatz dazu konnte in nicht aktivierten CerS3 *Knockdown* Zellen eine erhöhte CerS1 und reduzierte CerS5 und CerS6 Expression gemessen werden. Die erhöhte CerS1 Expression könnte auf einen kompensatorischen Effekt der CerS1 hinweisen. Allerdings reicht die Expression von CerS1 in CerS3 *Knockdown* Zellen nicht aus, um den CerS3 *Knockdown* zu kompensieren, was man anhand der Sphingolipidkonzentrationen in diesen Zellen erkennen kann. In CerS3 *Knockdown* Zellen waren alle dhCer und Cer, sowie Glykosphingolipide signifikant reduziert im Vergleich zu den Kontrollzellen, während in CerS1 *Knockdown* Zellen kaum Veränderungen in den Sphingolipiden zu erkennen waren. Dies weist auf eine mögliche untergeordnete Rolle von CerS1 gegenüber CerS3 in Jurkat Zellen hin. Kontrollzellen zeigten nach der Aktivierung eine Reduzierung der dhCer und Cer, während Glykosphingolipide anstiegen. Möglicherweise werden nach Aktivierung der T Zellen mehr Glykosphingolipide in die Zellmembran eingebaut, da diese für *Lipid Rafts* essentiell sind [324, 326, 416].

Falls diese Hypothese zutrifft, sollte in CerS3 *Knockdown* Zellen der TZR Signalweg beeinflusst werden. Hierfür untersuchte ich die TZR Aktivierung anhand der Phosphorylierung von Zap70. In CerS3 *Knockdown* Zellen war die Phosphorylierung von Zap70 nach Aktivierung der Zellen deutlich gehemmt im Vergleich zu Kontrollzellen, nicht jedoch in CerS1 *Knockdown* Zellen. CerS3 Überexpressionszellen zeigten keine erhöhte TZR Aktivierung auf.

Eine weitere Zellfunktion von T Zellen, die durch *Lipid Raft* Formation beeinflusst werden kann, ist die Sphingosin-1-Phosphat (S1P) abhängige Migration [337, 338, 347]. Im Migrations*assay* zeigten CerS1 und CerS3 *Knockdown* Zellen signifikant

schlechteres S1P-abhängiges Migrationsverhalten als die Kontrollzellen. CerS3 Überexpressionszellen hingegen zeigten ein erhöhtes S1P-abhängigges Migrationsverhalten im Vergleich zu Kontrollzellen. Daraufhin wurde die Expression des S1P1 und S1P4 in den Zellen bestimmt. Sowohl CerS1 als auch CerS3 *Knockdown* Zellen zeigten eine niedrigere S1P1 mRNA Expression im unstimulierten Zustand, während in diesen Zellen die S1P4 Expression erhöht war. CerS3 Überexpressionzellen wiesen eine erhöhte S1P1 Expression im unaktivierten Zustand auf und keine Veränderung in der S1P4 Expression.

Da CerS1 *Knockdown* Zellen keine Veränderung in der TZR Aktivierung zeigten, wurden Untersuchungen zu nachgeschalteten Signalwegen wie der Aktivierung von Transkriptionsfaktoren nur in CerS3 *Knockdown* und Überexpression Zellen durchgeführt. Zap70 Phosphorylierung führt zu einer Aktivierung des Transkriptionsfaktors AP-1, der unter anderem aus den Proteinen c-Jun und c-Fos gebildet wird, sowie einer Translokation von NFκB und NFAT1 in den Nukleus. Während AP-1 in CerS3 *Knockdown* und Überexpression Zellen ähnlich wie in den Kontrollzellen aktiviert wurde, zeigte NFAT1 in CerS3 *Knockdown* Zellen eine verminderte Translokation in den Nukleus. NFAT1 ist für die transkriptionelle Aktivierung verschiedener Zytokine verantwortlich. In CerS3 *Knockdown* Zellen konnte dann im Vergleich zu Kontrollzellen eine verminderte TNFα Ausschüttung nach Stimulation gemessen werden.

Diese *in vitro* Daten in Jurkat Zellen konnten durch Untersuchungen anhand von primären CD4 Zellen bestätigt werden. Primäre CD4$^+$ T-Zellen wurden aus dem Blut von gesunden Probanden isoliert und dann mit einer siRNA gegen CerS3 behandelt, welches zu einer Runterregulation der CerS3, CerS1 und CerS5 Expression in diesen Zellen führte. Die mit siRNA behandelten primären CD4$^+$ T-Zellen wiesen ebenfalls eine verminderte Zytokinproduktion im Vergleich zu den Kontrollzellen auf nach Aktivierung.

Um den Einfluss von CerS3 auf den Prozess der Kolitis zu untersuchen, wurde in WT und in einem T Zell spezifischen CerS3 *Knockout* (CerS3 LCK Cre) Mäusen mithilfe von Dextran-Sodium-Sulfat (DSS) Kolitis induziert. Die Mäuse wurden für fünf Tage mit 2 % DSS im Trinkwasser behandelt und nach acht Tagen wurde das Experiment beendet. Der Krankheitsverlauf, sowie die Gewichtsabnahme wurden während des Versuchs beobachtet und anschließend wurden Immunzellen aus Blut, Milz, Thymus,

Darm und Lymphknoten entnommen, um den Krankheitsverlauf in beiden Mauslinien zu vergleichen. Die WT Tiere zeigten eine höhere Gewichtsabnahme, einen erhöhten Krankheitsscore (mehr Kolitis Symptome) sowie eine stärkere entzündungsbedingte Verkürzung des Kolons im Vergleich zu den CerS3 LCK Cre Mäusen. Die WT Mäuse zeigten somit einen deutlich schwereren Kolitisverlauf als CerS3 LCK Cre Mäuse. Dies spiegelte sich auch in der Immunzellverteilung in der intraepithelialen Lymphozytenfraktion wieder, welche in DSS behandelten WT Tieren deutlich mehr CD4 Zellen aufwies als DSS behandelte CerS3 LCK Cre Mäuse. In den CerS3 LCK Cre Kontrollmäusen wurden außerdem weniger CD3$^+$ T Zellen in Blut, Thymus und Milz beobachtet, während im Lymphknoten mehr CD3$^+$ T Zellen zu finden waren. Diese Daten passen gut zu den humanen *in vitro* Daten, die zeigten, dass in CerS3 runterregulierten Zellen die S1P-abhängige Migration gestört ist, die für den Austritt der T Zellen aus dem Lymphknoten verantwortlich ist [273, 385, 455]. Aus dem Thymusgewebe der Maus isolierte CerS3 LCK Cre T Zellen zeigten *in vitro* im Vergleich zu WT T Zellen eine verminderte Differenzierung in TH und regulatorische T Zellen (Treg) und eine signifikant verringerte Produktion von pro-inflammatorischem Zytokinen.

Des Weiteren konnte ein humanes *organ-on-a-chip in vitro* System etabliert werden, in dem Caco-2 Zellen als Kolon-Epithelzellen und HUVECs als Endothelzellen gewebeähnlich co-kultiviert wurden. Die Chips wurden zuerst mit einer extrazellulären Matrix beschichtet und anschließend wurden die Zellen darauf ausgesät. Hierbei entwickelten Caco-2 Zellen eine kryptenähnliche 3D-Struktur aus und HUVECs formten eine Endothelschicht. Epithel- und Endothelschicht waren durch eine poröse Membran miteinander verbunden. Epithel- und Endothelzellgewebe wurden mit unterschiedlichen Medien in einem stetigen Flüssigkeitsstrom und unter mechanischen Dehnungsreizen, die der natürlichen Darmperistaltik ähneln, inkubiert. Im Rahmen dieser Arbeit wurde dieses System, sowie die Handhabung der Chips in der Arbeitsgruppe etabliert. Zur Untersuchung des Einflusses von CerS3 auf die Migration von T Zellen in entzündetes Gewebe wurde das Epithelgewebe mit pro-inflammatorischen Zytokinen, sowie einem Gemisch aus verschiedenen Zytokinen und Chemokinen behandelt, während im vaskulären Kanal Kontroll-, sowie CerS3 *Knockdown* T Zellen perfundiert wurden. Erste Voruntersuchungen zeigten ein erhöhtes Adhäsionsverhalten von Kontrollzellen im Endothelkanal im Vergleich zu

CerS3 *Knockdown* Zellen, was auf ein verringertes Migrationsverhalten oder Adhäsionspotential der CerS3 *Knockdown* Zellen hinweist.

Zusammenfassend kann gesagt werden, dass in dieser Dissertation eine wichtige Rolle für die CerS3 in der T Zellfunktion aufgezeigt wurde. Die Hemmung der CerS3 in T Zellen hat einen positiven Effekt auf die Entwicklung der Kolitis in Mäusen und hemmt die TZR Aktivierung und S1P-abhängige Migration in humanen T Zellen. Somit könnte die CerS3 ein neues *Target* für T Zell abhängige Erkrankungen wie die Kolitis Ulzerosa, aber auch Multiple Sklerose oder Rheumatoide Arthritis darstellen.

8. References

1. **Fabián O, Kamaradová K**. Morphology of inflammatory bowel diseases (IBD). Cesk Patol (2022) 58:27–37.

2. **Ng SC, Shi HY, Hamidi N, Underwood FE, Tang W, Benchimol EI**, et al. Worldwide incidence and prevalence of inflammatory bowel disease in the 21st century: a systematic review of population-based studies. Lancet (2017) 390:2769–78.

3. **Zeitz M, Schmidt HH, Bojarski C, editors.** Harrisons Gastroenterologie und Hepatologie. [London], Berlin: McGraw-Hill; ABW, Wiss.-Verl. (2011). 790 p.

4. **Lamb CA, Kennedy NA, Raine T, Hendy PA, Smith PJ, Limdi JK**, et al. British Society of Gastroenterology consensus guidelines on the management of inflammatory bowel disease in adults. Gut (2019) 68:s1-s106.

5. **Lakatos P-L, Lakatos L**. Risk for colorectal cancer in ulcerative colitis: changes, causes and management strategies. World J Gastroenterol (2008) 14:3937–47.

6. **Campos Silva EF** de, **Baima JP, Barros JR** de, **Tanni SE, Schreck T, Saad-Hossne R**, et al. Risk factors for ulcerative colitis-associated colorectal cancer: A retrospective cohort study. Medicine (Baltimore) (2020) 99:e21686.

7. **Boltin D, Perets TT, Vilkin A, Niv Y**. Mucin function in inflammatory bowel disease: an update. J Clin Gastroenterol (2013) 47:106–11.

8. **Syed ZA, Zhang L, Hagen KG** ten. In vivo models of mucin biosynthesis and function. Adv Drug Deliv Rev (2022) 184:114182.

9. **van Klinken BJ, van der Wal JW, Einerhand AW, Büller HA, Dekker J**. Sulphation and secretion of the predominant secretory human colonic mucin MUC2 in ulcerative colitis. Gut (1999) 44:387–93.

10. **Bertin B, Dubuquoy L, Colombel J-F, Desreumaux P**. PPAR-gamma in ulcerative colitis: a novel target for intervention. Curr Drug Targets (2013) 14:1501–7.

11. **Steinman RM, Hawiger D, Nussenzweig MC**. Tolerogenic dendritic cells. Annu Rev Immunol (2003) 21:685–711.

12. **Zeng Q, Jewell CM**. Directing toll-like receptor signaling in macrophages to enhance tumor immunotherapy. Curr Opin Biotechnol (2019) 60:138–45.

13. **Kabelitz D**. Expression and function of Toll-like receptors in T lymphocytes. Curr Opin Immunol (2007) 19:39–45.

14. **Agbanoma G, Li C, Ennis D, Palfreeman AC, Williams LM, Brennan FM**. Production of TNF-α in macrophages activated by T cells, compared with lipopolysaccharide, uses distinct IL-10-dependent regulatory mechanism. J Immunol (2012) 188:1307–17.

15. **Cario E, Podolsky DK**. Differential alteration in intestinal epithelial cell expression of toll-like receptor 3 (TLR3) and TLR4 in inflammatory bowel disease. Infect Immun (2000) 68:7010–7.

16. **Vamadevan AS, Fukata M, Arnold ET, Thomas LS, Hsu D, Abreu MT**. Regulation of Toll-like receptor 4-associated MD-2 in intestinal epithelial cells: a comprehensive analysis. Innate Immun (2010) 16:93–103.

17. **Sawa Y, Oshitani N, Adachi K, Higuchi K, Matsumoto T, Arakawa T**. Comprehensive analysis of intestinal cytokine messenger RNA profile by real-time quantitative polymerase chain reaction in patients with inflammatory bowel disease. Int J Mol Med (2003) 11:175–9.

18. **Liu C, Chu D, Kalantar-Zadeh K, George J, Young HA, Liu G**. Cytokines: From Clinical Significance to Quantification. Adv Sci (Weinh) (2021) 8:e2004433.

19. **Nakase H, Sato N, Mizuno N, Ikawa Y**. The influence of cytokines on the complex pathology of ulcerative colitis. Autoimmun Rev (2022) 21:103017.

20. **Sands BE, Kaplan GG**. The role of TNFalpha in ulcerative colitis. J Clin Pharmacol (2007) 47:930–41.

21. **van Heel DA, Udalova IA, Silva AP** de, **McGovern DP, Kinouchi Y, Hull J**, et al. Inflammatory bowel disease is associated with a TNF polymorphism that affects an interaction between the OCT1 and NF(-kappa)B transcription factors. Hum Mol Genet (2002) 11:1281–9.

22. **Louis E**. The immuno-inflammatory reaction in Crohn's disease and ulcerative colitis: characterisation, genetics and clinical application. Focus on TNF alpha. Acta Gastroenterol Belg (2001) 64:1–5.

23. **Stucchi A, Reed K, O'Brien M, Cerda S, Andrews C, Gower A**, et al. A new transcription factor that regulates TNF-alpha gene expression, LITAF, is increased in intestinal tissues from patients with CD and UC. Inflamm Bowel Dis (2006) 12:581–7.

24. **Chen ML, Sundrud MS**. Cytokine Networks and T-Cell Subsets in Inflammatory Bowel Diseases. Inflamm Bowel Dis (2016) 22:1157–67.

25. **Walker AM, Szneke P, Bianchi LA, Field LG, Sutherland LR, Dreyer NA**. 5-Aminosalicylates, sulfasalazine, steroid use, and complications in patients with ulcerative colitis. Am J Gastroenterol (1997) 92:816–20.

26. **Murray A, Nguyen TM, Parker CE, Feagan BG, MacDonald JK**. Oral 5-aminosalicylic acid for maintenance of remission in ulcerative colitis. Cochrane Database Syst Rev (2020) 8:CD000544.

27. **Iida T, Onodera K, Nakase H**. 5-Aminosalicylic acid. Nihon Rinsho (2017) 75:392–7.

28. **Le Berre C, Roda G, Nedeljkovic Protic M, Danese S, Peyrin-Biroulet L**. Modern use of 5-aminosalicylic acid compounds for ulcerative colitis. Expert Opin Biol Ther (2020) 20:363–78.

29. **Buchman AL**. Side effects of corticosteroid therapy. J Clin Gastroenterol (2001) 33:289–94.

30. **Berends SE, Strik AS, Löwenberg M, D'Haens GR, Mathôt RAA**. Clinical Pharmacokinetic and Pharmacodynamic Considerations in the Treatment of Ulcerative Colitis. Clin Pharmacokinet (2019) 58:15–37.

31. **Timmer A, McDonald JWD, Macdonald JK**. Azathioprine and 6-mercaptopurine for maintenance of remission in ulcerative colitis. Cochrane Database Syst Rev (2007) CD000478.

32. **Timmer A, McDonald JWD, Tsoulis DJ, MacDonald JK**. Azathioprine and 6-mercaptopurine for maintenance of remission in ulcerative colitis. Cochrane Database Syst Rev (2012) CD000478.

33. **Loftus CG, Loftus EV, Sandborn WJ**. Cyclosporin for refractory ulcerative colitis. Gut (2003) 52:172–3.

34. **Lichtiger S**. The Role of Cyclosporine Therapy in Ulcerative Colitis Treatment. Gastroenterol Hepatol (N Y) (2006) 2:624–6.

8. References

35. **Szemes K, Soós A, Hegyi P, Farkas N, Erős A, Erőss B**, et al. Comparable Long-Term Outcomes of Cyclosporine and Infliximab in Patients With Steroid-Refractory Acute Severe Ulcerative Colitis: A Meta-Analysis. Front Med (Lausanne) (2019) 6:338.

36. **Hanauer S, Panaccione R, Danese S, Cheifetz A, Reinisch W, Higgins PDR**, et al. Tofacitinib Induction Therapy Reduces Symptoms Within 3 Days for Patients With Ulcerative Colitis. Clin Gastroenterol Hepatol (2019) 17:139–47.

37. **Bhattacharya A, Osterman MT**. Biologic Therapy for Ulcerative Colitis. Gastroenterol Clin North Am (2020) 49:717–29.

38. **Feagan BG, Rutgeerts P, Sands BE, Hanauer S, Colombel J-F, Sandborn WJ**, et al. Vedolizumab as induction and maintenance therapy for ulcerative colitis. N Engl J Med (2013) 369:699–710.

39. **Sandborn WJ, Baert F, Danese S, Krznarić Ž, Kobayashi T, Yao X**, et al. Efficacy and Safety of Vedolizumab Subcutaneous Formulation in a Randomized Trial of Patients With Ulcerative Colitis. Gastroenterology (2020) 158:562-572.e12.

40. **Strober W, Fuss IJ**. Proinflammatory cytokines in the pathogenesis of inflammatory bowel diseases. Gastroenterology (2011) 140:1756–67.

41. **Roda G, Marocchi M, Sartini A, Roda E**. Cytokine Networks in Ulcerative Colitis. Ulcers (2011) 2011:1–5.

42. **Hemperly A, Vande Casteele N**. Clinical Pharmacokinetics and Pharmacodynamics of Infliximab in the Treatment of Inflammatory Bowel Disease. Clin Pharmacokinet (2018) 57:929–42.

43. **Guo C, Wu K, Liang X, Liang Y, Li R**. Infliximab clinically treating ulcerative colitis: A systematic review and meta-analysis. Pharmacol Res (2019) 148:104455.

44. **Yuan A, Yang H, Qi H, Cui J, Hua W, Li C**, et al. IL-9 antibody injection suppresses the inflammation in colitis mice. Biochem Biophys Res Commun (2015) 468:921–6.

45. **Sandborn WJ, Ferrante M, Bhandari BR, Berliba E, Feagan BG, Hibi T**, et al. Efficacy and Safety of Mirikizumab in a Randomized Phase 2 Study of Patients With Ulcerative Colitis. Gastroenterology (2020) 158:537-549.e10.

46. **Wong U, Cross RK**. Expert opinion on interleukin-12/23 and interleukin-23 antagonists as potential therapeutic options for the treatment of inflammatory bowel disease. Expert Opin Investig Drugs (2019) 28:473–9.

47. **Bouhnik Y, Carbonnel F, Laharie D, Stefanescu C, Hébuterne X, Abitbol V**, et al. Efficacy of adalimumab in patients with Crohn's disease and symptomatic small bowel stricture: a multicentre, prospective, observational cohort (CREOLE) study. Gut (2018) 67:53–60.

48. **Sands BE, Sandborn WJ, Panaccione R, O'Brien CD, Zhang H, Johanns J**, et al. Ustekinumab as Induction and Maintenance Therapy for Ulcerative Colitis. N Engl J Med (2019) 381:1201–14.

49. **Seiderer J, Elben I, Diegelmann J, Glas J, Stallhofer J, Tillack C**, et al. Role of the novel Th17 cytokine IL-17F in inflammatory bowel disease (IBD): upregulated colonic IL-17F expression in active Crohn's disease and analysis of the IL17F p.His161Arg polymorphism in IBD. Inflamm Bowel Dis (2008) 14:437–45.

50. **Yang XO, Chang SH, Park H, Nurieva R, Shah B, Acero L**, et al. Regulation of inflammatory responses by IL-17F. J Exp Med (2008) 205:1063–75.

51. **O'Connor W, Kamanaka M, Booth CJ, Town T, Nakae S, Iwakura Y**, et al. A protective function for interleukin 17A in T cell-mediated intestinal inflammation. Nat Immunol (2009) 10:603–9.

52. **Zhang Z, Zheng M, Bindas J, Schwarzenberger P, Kolls JK**. Critical role of IL-17 receptor signaling in acute TNBS-induced colitis. Inflamm Bowel Dis (2006) 12:382–8.

53. **Leppkes M, Becker C, Ivanov II, Hirth S, Wirtz S, Neufert C**, et al. RORgamma-expressing Th17 cells induce murine chronic intestinal inflammation via redundant effects of IL-17A and IL-17F. Gastroenterology (2009) 136:257–67.

54. **Ogawa A, Andoh A, Araki Y, Bamba T, Fujiyama Y**. Neutralization of interleukin-17 aggravates dextran sulfate sodium-induced colitis in mice. Clin Immunol (2004) 110:55–62.

55. **Eskandari-Nasab E, Moghadampour M, Tahmasebi A**. Meta-Analysis of Risk Association Between Interleukin-17A and F Gene Polymorphisms and Inflammatory Diseases. J Interferon Cytokine Res (2017) 37:165–74.

56. **Dragasevic S, Stankovic B, Sokic-Milutinovic A, Milosavljevic T, Milovanovic T, Lukic S**, et al. Importance of TLR9-IL23-IL17 axis in inflammatory bowel disease development: Gene expression profiling study. Clin Immunol (2018) 197:86–95.

57. **Heller F, Florian P, Bojarski C, Richter J, Christ M, Hillenbrand B**, et al. Interleukin-13 is the key effector Th2 cytokine in ulcerative colitis that affects epithelial tight junctions, apoptosis, and cell restitution. Gastroenterology (2005) 129:550–64.

58. **Martini E, Krug SM, Siegmund B, Neurath MF, Becker C**. Mend Your Fences: The Epithelial Barrier and its Relationship With Mucosal Immunity in Inflammatory Bowel Disease. Cell Mol Gastroenterol Hepatol (2017) 4:33–46.

59. **Wollenberg A, Weidinger S, Worm M, Bieber T**. Tralokinumab in atopic dermatitis. J Dtsch Dermatol Ges (2021) 19:1435–42.

60. **Danese S, Rudziński J, Brandt W, Dupas J-L, Peyrin-Biroulet L, Bouhnik Y**, et al. Tralokinumab for moderate-to-severe UC: a randomised, double-blind, placebo-controlled, phase IIa study. Gut (2015) 64:243–9.

61. **Privitera G, Pugliese D, Onali S, Petito V, Scaldaferri F, Gasbarrini A**, et al. Combination therapy in inflammatory bowel disease - from traditional immunosuppressors towards the new paradigm of dual targeted therapy. Autoimmun Rev (2021) 20:102832.

62. **Vermeire S**. Combination biologic therapy for ulcerative colitis. Lancet Gastroenterol Hepatol (2023) 8:288–90.

63. **Sonnenberg GF, Hepworth MR**. Functional interactions between innate lymphoid cells and adaptive immunity. Nat Rev Immunol (2019) 19:599–613.

64. **Handfield C, Kwock J, MacLeod AS**. Innate Antiviral Immunity in the Skin. Trends Immunol (2018) 39:328–40.

65. **Smith NC, Rise ML, Christian SL**. A Comparison of the Innate and Adaptive Immune Systems in Cartilaginous Fish, Ray-Finned Fish, and Lobe-Finned Fish. Front Immunol (2019) 10:2292.

66. **Hirayama D, Iida T, Nakase H**. The Phagocytic Function of Macrophage-Enforcing Innate Immunity and Tissue Homeostasis. Int J Mol Sci (2017) 19.

67. **Crinier A, Narni-Mancinelli E, Ugolini S, Vivier E**. SnapShot: Natural Killer Cells. Cell (2020) 180:1280-1280.e1.

8. References

68. **Wieczorek M, Abualrous ET, Sticht J, Álvaro-Benito M, Stolzenberg S, Noé F**, et al. Major Histocompatibility Complex (MHC) Class I and MHC Class II Proteins: Conformational Plasticity in Antigen Presentation. Front Immunol (2017) 8:292.

69. **Bradley P, Thomas PG**. Using T Cell Receptor Repertoires to Understand the Principles of Adaptive Immune Recognition. Annu Rev Immunol (2019) 37:547–70.

70. **Wang Y, Liu J, Burrows PD, Wang J-Y**. B Cell Development and Maturation. Adv Exp Med Biol (2020) 1254:1–22.

71. **Treanor B**. B-cell receptor: from resting state to activate. Immunology (2012) 136:21–7.

72. **Pouw RB, Ricklin D**. Tipping the balance: intricate roles of the complement system in disease and therapy. Semin Immunopathol (2021) 43:757–71.

73. **Conigliaro P, Triggianese P, Ballanti E, Perricone C, Perricone R, Chimenti MS**. Complement, infection, and autoimmunity. Curr Opin Rheumatol (2019) 31:532–41.

74. **Szeto C, Lobos CA, Nguyen AT, Gras S**. TCR Recognition of Peptide-MHC-I: Rule Makers and Breakers. Int J Mol Sci (2020) 22.

75. **Wang J, Lim K, Smolyar A, Teng M, Liu J, Tse AG**, et al. Atomic structure of an alphabeta T cell receptor (TCR) heterodimer in complex with an anti-TCR fab fragment derived from a mitogenic antibody. EMBO J (1998) 17:10–26.

76. **Morath A, Schamel WW**. αβ and γδ T cell receptors: Similar but different. J Leukoc Biol (2020) 107:1045–55.

77. **Akamatsu Y, Oettinger MA**. Distinct roles of RAG1 and RAG2 in binding the V(D)J recombination signal sequences. Mol Cell Biol (1998) 18:4670–8.

78. **Roth DB**. V(D)J Recombination: Mechanism, Errors, and Fidelity. Microbiol Spectr (2014) 2.

79. **Srivastava SK, Robins HS**. Palindromic nucleotide analysis in human T cell receptor rearrangements. PLoS One (2012) 7:e52250.

80. **Birnbaum ME, Berry R, Hsiao Y-S, Chen Z, Shingu-Vazquez MA, Yu X**, et al. Molecular architecture of the αβ T cell receptor-CD3 complex. Proc Natl Acad Sci U S A (2014) 111:17576–81.

81. **Call ME, Pyrdol J, Wiedmann M, Wucherpfennig KW**. The organizing principle in the formation of the T cell receptor-CD3 complex. Cell (2002) 111:967–79.

82. **Dushek O, Goyette J, van der Merwe PA**. Non-catalytic tyrosine-phosphorylated receptors. Immunol Rev (2012) 250:258–76.

83. **Hennecke J, Wiley DC**. T cell receptor-MHC interactions up close. Cell (2001) 104:1–4.

84. **Leahy DJ**. A structural view of CD4 and CD8. FASEB J (1995) 9:17–25.

85. **Cole DK, Laugel B, Clement M, Price DA, Wooldridge L, Sewell AK**. The molecular determinants of CD8 co-receptor function. Immunology (2012) 137:139–48.

86. **Stepanek O, Prabhakar AS, Osswald C, King CG, Bulek A, Naeher D**, et al. Coreceptor scanning by the T cell receptor provides a mechanism for T cell tolerance. Cell (2014) 159:333–45.

87. **Bergman M, Mustelin T, Oetken C, Partanen J, Flint NA, Amrein KE**, et al. The human p50csk tyrosine kinase phosphorylates p56lck at Tyr-505 and down regulates its catalytic activity. EMBO J (1992) 11:2919–24.

88. **Bommhardt U, Schraven B, Simeoni L**. Beyond TCR Signaling: Emerging Functions of Lck in Cancer and Immunotherapy. Int J Mol Sci (2019) 20.

89. **Gascoigne NRJ, Casas J, Brzostek J, Rybakin V**. Initiation of TCR phosphorylation and signal transduction. Front Immunol (2011) 2:72.

90. **Isakov N, Wange RL, Burgess WH, Watts JD, Aebersold R, Samelson LE**. ZAP-70 binding specificity to T cell receptor tyrosine-based activation motifs: the tandem SH2 domains of ZAP-70 bind distinct tyrosine-based activation motifs with varying affinity. J Exp Med (1995) 181:375–80.

91. **Naito T, Tanaka H, Naoe Y, Taniuchi I**. Transcriptional control of T-cell development. Int Immunol (2011) 23:661–8.

92. **Hosokawa H, Rothenberg EV**. How transcription factors drive choice of the T cell fate. Nat Rev Immunol (2021) 21:162–76.

93. **Conley JM, Gallagher MP, Berg LJ**. T Cells and Gene Regulation: The Switching On and Turning Up of Genes after T Cell Receptor Stimulation in CD8 T Cells. Front Immunol (2016) 7:76.

94. **Hough KP, Chisolm DA, Weinmann AS**. Transcriptional regulation of T cell metabolism. Mol Immunol (2015) 68:520–6.

95. **Beach D, Gonen R, Bogin Y, Reischl IG, Yablonski D**. Dual role of SLP-76 in mediating T cell receptor-induced activation of phospholipase C-gamma1. J Biol Chem (2007) 282:2937–46.

96. **Zhong X-P, Guo R, Zhou H, Liu C, Wan C-K**. Diacylglycerol kinases in immune cell function and self-tolerance. Immunol Rev (2008) 224:249–64.

97. **Berridge MJ**. Inositol trisphosphate and calcium signalling mechanisms. Biochim Biophys Acta (2009) 1793:933–40.

98. **Oh-hora M, Rao A**. Calcium signaling in lymphocytes. Curr Opin Immunol (2008) 20:250–8.

99. **Kania E, Roest G, Vervliet T, Parys JB, Bultynck G**. IP3 Receptor-Mediated Calcium Signaling and Its Role in Autophagy in Cancer. Front Oncol (2017) 7:140.

100. **Macian F**. NFAT proteins: key regulators of T-cell development and function. Nat Rev Immunol (2005) 5:472–84.

101. **Olenchock BA, Guo R, Carpenter JH, Jordan M, Topham MK, Koretzky GA**, et al. Disruption of diacylglycerol metabolism impairs the induction of T cell anergy. Nat Immunol (2006) 7:1174–81.

102. **Lin X, O'Mahony A, Mu Y, Geleziunas R, Greene WC**. Protein kinase C-theta participates in NF-kappaB activation induced by CD3-CD28 costimulation through selective activation of IkappaB kinase beta. Mol Cell Biol (2000) 20:2933–40.

103. **Sun Z, Arendt CW, Ellmeier W, Schaeffer EM, Sunshine MJ, Gandhi L**, et al. PKC-theta is required for TCR-induced NF-kappaB activation in mature but not immature T lymphocytes. Nature (2000) 404:402–7.

104. **Lu HY, Bauman BM, Arjunaraja S, Dorjbal B, Milner JD, Snow AL**, et al. The CBM-opathies-A Rapidly Expanding Spectrum of Human Inborn Errors of Immunity Caused by Mutations in the CARD11-BCL10-MALT1 Complex. Front Immunol (2018) 9:2078.

105. **Matsumoto R, Wang D, Blonska M, Li H, Kobayashi M, Pappu B**, et al. Phosphorylation of CARMA1 plays a critical role in T Cell receptor-mediated NF-kappaB activation. Immunity (2005) 23:575–85.

8. References

106. **Sun L, Deng L, Ea C-K, Xia Z-P, Chen ZJ**. The TRAF6 ubiquitin ligase and TAK1 kinase mediate IKK activation by BCL10 and MALT1 in T lymphocytes. Mol Cell (2004) 14:289–301.

107. **Zhou H, Wertz I, O'Rourke K, Ultsch M, Seshagiri S, Eby M**, et al. Bcl10 activates the NF-kappaB pathway through ubiquitination of NEMO. Nature (2004) 427:167–71.

108. **Oeckinghaus A, Ghosh S**. The NF- B Family of Transcription Factors and Its Regulation. Cold Spring Harb Perspect Biol (2009) 1:a000034-a000034.

109. **Hoffmann A, Natoli G, Ghosh G**. Transcriptional regulation via the NF-kappaB signaling module. Oncogene (2006) 25:6706–16.

110. **Hayden MS, West AP, Ghosh S**. NF-kappaB and the immune response. Oncogene (2006) 25:6758–80.

111. **So T, Croft M**. Regulation of the PKCθ-NF-κB Axis in T Lymphocytes by the Tumor Necrosis Factor Receptor Family Member OX40. Front Immunol (2012) 3:133.

112. **Ebinu JO, Bottorff DA, Chan EY, Stang SL, Dunn RJ, Stone JC**. RasGRP, a Ras guanyl nucleotide- releasing protein with calcium- and diacylglycerol-binding motifs. Science (1998) 280:1082–6.

113. **Smith-Garvin JE, Koretzky GA, Jordan MS**. T cell activation. Annu Rev Immunol (2009) 27:591–619.

114. **Lapinski PE, King PD**. Regulation of Ras signal transduction during T cell development and activation. Am J Clin Exp Immunol (2012) 1:147–53.

115. **Janknecht R, Ernst WH, Pingoud V, Nordheim A**. Activation of ternary complex factor Elk-1 by MAP kinases. EMBO J (1993) 12:5097–104.

116. **Kolch W**. Coordinating ERK/MAPK signalling through scaffolds and inhibitors. Nat Rev Mol Cell Biol (2005) 6:827–37.

117. **Bertin S, Lozano-Ruiz B, Bachiller V, García-Martínez I, Herdman S, Zapater P**, et al. Dual-specificity phosphatase 6 regulates CD4+ T-cell functions and restrains spontaneous colitis in IL-10-deficient mice. Mucosal Immunol (2015) 8:505–15.

118. **Damasio MP, Marchingo JM, Spinelli L, Hukelmann JL, Cantrell DA, Howden AJM**. Extracellular signal-regulated kinase (ERK) pathway control of CD8+ T cell differentiation. Biochem J (2021) 478:79–98.

119. **Riha P, Rudd CE**. CD28 co-signaling in the adaptive immune response. Self Nonself (2010) 1:231–40.

120. **Genot EM, Arrieumerlou C, Ku G, Burgering BM, Weiss A, Kramer IM**. The T-cell receptor regulates Akt (protein kinase B) via a pathway involving Rac1 and phosphatidylinositide 3-kinase. Mol Cell Biol (2000) 20:5469–78.

121. **Abdullah L, Hills LB, Winter EB, Huang YH**. Diverse Roles of Akt in T cells. Immunometabolism (2021) 3.

122. **Ohteki T, Parsons M, Zakarian A, Jones RG, Nguyen LT, Woodgett JR**, et al. Negative regulation of T cell proliferation and interleukin 2 production by the serine threonine kinase GSK-3. J Exp Med (2000) 192:99–104.

123. **Imam T, Park S, Kaplan MH, Olson MR**. Effector T Helper Cell Subsets in Inflammatory Bowel Diseases. Front Immunol (2018) 9:1212.

124. **Smids C, Horjus Talabur Horje CS, Drylewicz J, Roosenboom B, Groenen MJM, van Koolwijk E**, et al. Intestinal T Cell Profiling in Inflammatory Bowel Disease: Linking T Cell Subsets to Disease Activity and Disease Course. J Crohns Colitis (2018) 12:465–75.

125. **Kratky W, Reis e Sousa C, Oxenius A, Spörri R**. Direct activation of antigen-presenting cells is required for CD8+ T-cell priming and tumor vaccination. Proc Natl Acad Sci U S A (2011) 108:17414–9.

126. **Cox MA, Zajac AJ**. Shaping successful and unsuccessful CD8 T cell responses following infection. J Biomed Biotechnol (2010) 2010:159152.

127. **Novy P, Quigley M, Huang X, Yang Y**. CD4 T cells are required for CD8 T cell survival during both primary and memory recall responses. J Immunol (2007) 179:8243–51.

128. **Laidlaw BJ, Craft JE, Kaech SM**. The multifaceted role of CD4(+) T cells in CD8(+) T cell memory. Nat Rev Immunol (2016) 16:102–11.

129. **Curtsinger JM, Lins DC, Mescher MF**. Signal 3 determines tolerance versus full activation of naive CD8 T cells: dissociating proliferation and development of effector function. J Exp Med (2003) 197:1141–51.

130. **Henry CJ, Ornelles DA, Mitchell LM, Brzoza-Lewis KL, Hiltbold EM**. IL-12 produced by dendritic cells augments CD8+ T cell activation through the production of the chemokines CCL1 and CCL17. J Immunol (2008) 181:8576–84.

131. **Joshi NS, Cui W, Chandele A, Lee HK, Urso DR, Hagman J**, et al. Inflammation directs memory precursor and short-lived effector CD8(+) T cell fates via the graded expression of T-bet transcription factor. Immunity (2007) 27:281–95.

132. **Takemoto N, Intlekofer AM, Northrup JT, Wherry EJ, Reiner SL**. Cutting Edge: IL-12 inversely regulates T-bet and eomesodermin expression during pathogen-induced CD8+ T cell differentiation. J Immunol (2006) 177:7515–9.

133. **Rao RR, Li Q, Odunsi K, Shrikant PA**. The mTOR kinase determines effector versus memory CD8+ T cell fate by regulating the expression of transcription factors T-bet and Eomesodermin. Immunity (2010) 32:67–78.

134. **Groom JR, Luster AD**. CXCR3 ligands: redundant, collaborative and antagonistic functions. Immunol Cell Biol (2011) 89:207–15.

135. **Voskoboinik I, Whisstock JC, Trapani JA**. Perforin and granzymes: function, dysfunction and human pathology. Nat Rev Immunol (2015) 15:388–400.

136. **Trapani JA**. Granzymes: a family of lymphocyte granule serine proteases. Genome Biol (2001) 2:REVIEWS3014.

137. **Aouad SM, Cohen LY, Sharif-Askari E, Haddad EK, Alam A, Sekaly R-P**. Caspase-3 is a component of Fas death-inducing signaling complex in lipid rafts and its activity is required for complete caspase-8 activation during Fas-mediated cell death. J Immunol (2004) 172:2316–23.

138. **Sobrido-Cameán D, Barreiro-Iglesias A**. Role of Caspase-8 and Fas in Cell Death After Spinal Cord Injury. Front Mol Neurosci (2018) 11:101.

139. **Kourtzelis I, Hajishengallis G, Chavakis T**. Phagocytosis of Apoptotic Cells in Resolution of Inflammation. Front Immunol (2020) 11:553.

8. References

140. **Reiser J, Banerjee A**. Effector, Memory, and Dysfunctional CD8(+) T Cell Fates in the Antitumor Immune Response. J Immunol Res (2016) 2016:8941260.

141. **Bhat P, Leggatt G, Waterhouse N, Frazer IH**. Interferon-γ derived from cytotoxic lymphocytes directly enhances their motility and cytotoxicity. Cell Death Dis (2017) 8:e2836.

142. **Murthy AK, Li W, Chaganty BKR, Kamalakaran S, Guentzel MN, Seshu J**, et al. Tumor necrosis factor alpha production from CD8+ T cells mediates oviduct pathological sequelae following primary genital Chlamydia muridarum infection. Infect Immun (2011) 79:2928–35.

143. **Casalegno Garduño R, Däbritz J**. New Insights on CD8+ T Cells in Inflammatory Bowel Disease and Therapeutic Approaches. Front Immunol (2021) 12:738762.

144. **Galiano-Landeira J, Torra A, Vila M, Bové J**. CD8 T cell nigral infiltration precedes synucleinopathy in early stages of Parkinson's disease. Brain (2020) 143:3717–33.

145. **Oshi M, Asaoka M, Tokumaru Y, Yan L, Matsuyama R, Ishikawa T**, et al. CD8 T Cell Score as a Prognostic Biomarker for Triple Negative Breast Cancer. Int J Mol Sci (2020) 21.

146. **Philip M, Schietinger A**. CD8+ T cell differentiation and dysfunction in cancer. Nat Rev Immunol (2022) 22:209–23.

147. **Lee Y, Awasthi A, Yosef N, Quintana FJ, Xiao S, Peters A**, et al. Induction and molecular signature of pathogenic TH17 cells. Nat Immunol (2012) 13:991–9.

148. **Funderburg NT, Stubblefield Park SR, Sung HC, Hardy G, Clagett B, Ignatz-Hoover J**, et al. Circulating CD4(+) and CD8(+) T cells are activated in inflammatory bowel disease and are associated with plasma markers of inflammation. Immunology (2013) 140:87–97.

149. **Schenkel JM, Masopust D**. Tissue-resident memory T cells. Immunity (2014) 41:886–97.

150. **Roosenboom B, Wahab PJ, Smids C, Groenen MJM, van Koolwijk E, van Lochem EG**, et al. Intestinal CD103+CD4+ and CD103+CD8+ T-Cell Subsets in the Gut of Inflammatory Bowel Disease Patients at Diagnosis and During Follow-up. Inflamm Bowel Dis (2019) 25:1497–509.

151. **Noble A, Durant L, Hoyles L, Mccartney AL, Man R, Segal J**, et al. Deficient Resident Memory T Cell and CD8 T Cell Response to Commensals in Inflammatory Bowel Disease. J Crohns Colitis (2020) 14:525–37.

152. **Romagnani S**. Th1/Th2 cells. Inflamm Bowel Dis (1999) 5:285–94.

153. **Kaplan MH, Sun YL, Hoey T, Grusby MJ**. Impaired IL-12 responses and enhanced development of Th2 cells in Stat4-deficient mice. Nature (1996) 382:174–7.

154. **Powell MD, Read KA, Sreekumar BK, Jones DM, Oestreich KJ**. IL-12 signaling drives the differentiation and function of a TH1-derived TFH1-like cell population. Sci Rep (2019) 9:13991.

155. **Afkarian M, Sedy JR, Yang J, Jacobson NG, Cereb N, Yang SY**, et al. T-bet is a STAT1-induced regulator of IL-12R expression in naïve CD4+ T cells. Nat Immunol (2002) 3:549–57.

156. **Smeltz RB, Chen J, Ehrhardt R, Shevach EM**. Role of IFN-gamma in Th1 differentiation: IFN-gamma regulates IL-18R alpha expression by preventing the negative effects of IL-4 and by inducing/maintaining IL-12 receptor beta 2 expression. J Immunol (2002) 168:6165–72.

157. **Nakanishi K, Yoshimoto T, Tsutsui H, Okamura H**. Interleukin-18 regulates both Th1 and Th2 responses. Annu Rev Immunol (2001) 19:423–74.

158. **Tripp RA, Jones L, Anderson LJ, Brown MP**. CD40 ligand (CD154) enhances the Th1 and antibody responses to respiratory syncytial virus in the BALB/c mouse. J Immunol (2000) 164:5913–21.

159. **Mackay F, Loetscher H, Stueber D, Gehr G, Lesslauer W**. Tumor necrosis factor alpha (TNF-alpha)-induced cell adhesion to human endothelial cells is under dominant control of one TNF receptor type, TNF-R55. J Exp Med (1993) 177:1277–86.

160. **Rastogi S, Rizwani W, Joshi B, Kunigal S, Chellappan SP**. TNF-α response of vascular endothelial and vascular smooth muscle cells involve differential utilization of ASK1 kinase and p73. Cell Death Differ (2012) 19:274–83.

161. **Elkington PT, Green JA, Friedland JS**. Analysis of matrix metalloproteinase secretion by macrophages. Methods Mol Biol (2009) 531:253–65.

162. **Shapouri-Moghaddam A, Mohammadian S, Vazini H, Taghadosi M, Esmaeili S-A, Mardani F**, et al. Macrophage plasticity, polarization, and function in health and disease. J Cell Physiol (2018) 233:6425–40.

163. **Palmieri EM, McGinity C, Wink DA, McVicar DW**. Nitric Oxide in Macrophage Immunometabolism: Hiding in Plain Sight. Metabolites (2020) 10.

164. **Okamura H, Kashiwamura S, Tsutsui H, Yoshimoto T, Nakanishi K**. Regulation of interferon-gamma production by IL-12 and IL-18. Curr Opin Immunol (1998) 10:259–64.

165. **Klose CSN, Flach M, Möhle L, Rogell L, Hoyler T, Ebert K**, et al. Differentiation of type 1 ILCs from a common progenitor to all helper-like innate lymphoid cell lineages. Cell (2014) 157:340–56.

166. **Petagna L, Antonelli A, Ganini C, Bellato V, Campanelli M, Divizia A**, et al. Pathophysiology of Crohn's disease inflammation and recurrence. Biol Direct (2020) 15:23.

167. **Wallace KL, Zheng L-B, Kanazawa Y, Shih DQ**. Immunopathology of inflammatory bowel disease. World J Gastroenterol (2014) 20:6–21.

168. **Kamali AN, Noorbakhsh SM, Hamedifar H, Jadidi-Niaragh F, Yazdani R, Bautista JM**, et al. A role for Th1-like Th17 cells in the pathogenesis of inflammatory and autoimmune disorders. Mol Immunol (2019) 105:107–15.

169. **Tosolini M, Kirilovsky A, Mlecnik B, Fredriksen T, Mauger S, Bindea G**, et al. Clinical impact of different classes of infiltrating T cytotoxic and helper cells (Th1, th2, treg, th17) in patients with colorectal cancer. Cancer Res (2011) 71:1263–71.

170. **Lu X**. Impact of IL-12 in Cancer. Curr Cancer Drug Targets (2017) 17:682–97.

171. **Nava P, Koch S, Laukoetter MG, Lee WY, Kolegraff K, Capaldo CT**, et al. Interferon-gamma regulates intestinal epithelial homeostasis through converging beta-catenin signaling pathways. Immunity (2010) 32:392–402.

172. **Neurath MF, Weigmann B, Finotto S, Glickman J, Nieuwenhuis E, Iijima H**, et al. The transcription factor T-bet regulates mucosal T cell activation in experimental colitis and Crohn's disease. J Exp Med (2002) 195:1129–43.

173. **Krausgruber T, Schiering C, Adelmann K, Harrison OJ, Chomka A, Pearson C**, et al. T-bet is a key modulator of IL-23-driven pathogenic CD4(+) T cell responses in the intestine. Nat Commun (2016) 7:11627.

8. References

174. **Garrett WS, Lord GM, Punit S, Lugo-Villarino G, Mazmanian SK, Ito S**, et al. Communicable ulcerative colitis induced by T-bet deficiency in the innate immune system. Cell (2007) 131:33–45.

175. **Muzaki ARBM, Tetlak P, Sheng J, Loh SC, Setiagani YA, Poidinger M**, et al. Intestinal CD103(+)CD11b(-) dendritic cells restrain colitis via IFN-γ-induced anti-inflammatory response in epithelial cells. Mucosal Immunol (2016) 9:336–51.

176. **Allen JE, Sutherland TE**. Host protective roles of type 2 immunity: parasite killing and tissue repair, flip sides of the same coin. Seminars in Immunology (2014) 26:329–40.

177. **Lozano-Ojalvo D, Tyler SR, Aranda CJ, Wang J, Sicherer S, Sampson HA**, et al. Allergen recognition by specific effector Th2 cells enables IL-2-dependent activation of regulatory T-cell responses in humans. Allergy (2023) 78:697–713.

178. **Stark JM, Tibbitt CA, Coquet JM**. The Metabolic Requirements of Th2 Cell Differentiation. Front Immunol (2019) 10:2318.

179. **Zhu J**. T helper 2 (Th2) cell differentiation, type 2 innate lymphoid cell (ILC2) development and regulation of interleukin-4 (IL-4) and IL-13 production. Cytokine (2015) 75:14–24.

180. **Rael EL, Lockey RF**. Interleukin-13 signaling and its role in asthma. World Allergy Organ J (2011) 4:54–64.

181. **Minty A, Chalon P, Derocq JM, Dumont X, Guillemot JC, Kaghad M**, et al. Interleukin-13 is a new human lymphokine regulating inflammatory and immune responses. Nature (1993) 362:248–50.

182. **Zhu J, Paul WE**. CD4 T cells: fates, functions, and faults. Blood (2008) 112:1557–69.

183. **Fallon PG, Jolin HE, Smith P, Emson CL, Townsend MJ, Fallon R**, et al. IL-4 induces characteristic Th2 responses even in the combined absence of IL-5, IL-9, and IL-13. Immunity (2002) 17:7–17.

184. **Matsuda S, Kotani T, Kuwabara H, Suzuka T, Kiboshi T, Wada Y**, et al. Association of M2 Macrophages, Th2, and B Cells With Pathomechanism in Microscopic Polyangiitis Complicated by Interstitial Lung Disease. J Rheumatol (2022) 49:913–21.

185. **Mi L-L, Guo W-W**. Crosstalk between ILC2s and Th2 CD4+ T Cells in Lung Disease. J Immunol Res (2022) 2022:8871037.

186. **León B**. Understanding the development of Th2 cell-driven allergic airway disease in early life. Front Allergy (2022) 3:1080153.

187. **Kałużna A, Olczyk P, Komosińska-Vassev K**. The Role of Innate and Adaptive Immune Cells in the Pathogenesis and Development of the Inflammatory Response in Ulcerative Colitis. J Clin Med (2022) 11.

188. **Protti MP, Monte L** de. Thymic Stromal Lymphopoietin and Cancer: Th2-Dependent and -Independent Mechanisms. Front Immunol (2020) 11:2088.

189. **Griseri T, Arnold IC, Pearson C, Krausgruber T, Schiering C, Franchini F**, et al. Granulocyte Macrophage Colony-Stimulating Factor-Activated Eosinophils Promote Interleukin-23 Driven Chronic Colitis. Immunity (2015) 43:187–99.

190. **Lampinen M, Carlson M, Sangfelt P, Taha Y, Thörn M, Lööf L**, et al. IL-5 and TNF-alpha participate in recruitment of eosinophils to intestinal mucosa in ulcerative colitis. Dig Dis Sci (2001) 46:2004–9.

191. **Lampinen M, Backman M, Winqvist O, Rorsman F, Rönnblom A, Sangfelt P**, et al. Different regulation of eosinophil activity in Crohn's disease compared with ulcerative colitis. J Leukoc Biol (2008) 84:1392–9.

192. **Okamura M, Yoh K, Ojima M, Morito N, Takahashi S**. Overexpression of GATA-3 in T cells accelerates dextran sulfate sodium-induced colitis. Exp Anim (2014) 63:133–40.

193. **Rosen MJ, Frey MR, Washington MK, Chaturvedi R, Kuhnhein LA, Matta P**, et al. STAT6 activation in ulcerative colitis: a new target for prevention of IL-13-induced colon epithelial cell dysfunction. Inflamm Bowel Dis (2011) 17:2224–34.

194. **Shih T-C, Hsieh S-Y, Hsieh Y-Y, Chen T-C, Yeh C-Y, Lin C-J**, et al. Aberrant activation of nuclear factor of activated T cell 2 in lamina propria mononuclear cells in ulcerative colitis. World J Gastroenterol (2008) 14:1759–67.

195. **Weigmann B, Lehr HA, Yancopoulos G, Valenzuela D, Murphy A, Stevens S**, et al. The transcription factor NFATc2 controls IL-6-dependent T cell activation in experimental colitis. J Exp Med (2008) 205:2099–110.

196. **Liu Z, Lee J, Krummey S, Lu W, Cai H, Lenardo MJ**. The kinase LRRK2 is a regulator of the transcription factor NFAT that modulates the severity of inflammatory bowel disease. Nat Immunol (2011) 12:1063–70.

197. **Fuss IJ, Heller F, Boirivant M, Leon F, Yoshida M, Fichtner-Feigl S**, et al. Nonclassical CD1d-restricted NK T cells that produce IL-13 characterize an atypical Th2 response in ulcerative colitis. J Clin Invest (2004) 113:1490–7.

198. **Fuss IJ, Joshi B, Yang Z, Degheidy H, Fichtner-Feigl S, Souza H** de, et al. IL-13Rα2-bearing, type II NKT cells reactive to sulfatide self-antigen populate the mucosa of ulcerative colitis. Gut (2014) 63:1728–36.

199. **Harrington LE, Hatton RD, Mangan PR, Turner H, Murphy TL, Murphy KM**, et al. Interleukin 17-producing CD4+ effector T cells develop via a lineage distinct from the T helper type 1 and 2 lineages. Nat Immunol (2005) 6:1123–32.

200. **Dong C**. Genetic controls of Th17 cell differentiation and plasticity. Exp Mol Med (2011) 43:1–6.

201. **Ivanov II, Atarashi K, Manel N, Brodie EL, Shima T, Karaoz U**, et al. Induction of intestinal Th17 cells by segmented filamentous bacteria. Cell (2009) 139:485–98.

202. **Castro G, Liu X, Ngo K, Leon-Tabaldo A** de, **Zhao S, Luna-Roman R**, et al. RORγt and RORα signature genes in human Th17 cells. PLoS One (2017) 12:e0181868.

203. **Yang XO, Pappu BP, Nurieva R, Akimzhanov A, Kang HS, Chung Y**, et al. T helper 17 lineage differentiation is programmed by orphan nuclear receptors ROR alpha and ROR gamma. Immunity (2008) 28:29–39.

204. **Chen K, Eddens T, Trevejo-Nunez G, Way EE, Elsegeiny W, Ricks DM**, et al. IL-17 Receptor Signaling in the Lung Epithelium Is Required for Mucosal Chemokine Gradients and Pulmonary Host Defense against K. pneumoniae. Cell Host Microbe (2016) 20:596–605.

205. **Conti HR, Bruno VM, Childs EE, Daugherty S, Hunter JP, Mengesha BG**, et al. IL-17 Receptor Signaling in Oral Epithelial Cells Is Critical for Protection against Oropharyngeal Candidiasis. Cell Host Microbe (2016) 20:606–17.

8. References

206. **Yuan S, Zhang S, Zhuang Y, Zhang H, Bai J, Hou Q**. Interleukin-17 Stimulates STAT3-Mediated Endothelial Cell Activation for Neutrophil Recruitment. Cell Physiol Biochem (2015) 36:2340–56.

207. **Carbone ML, Failla CM**. Interleukin role in the regulation of endothelial cell pathological activation. Vasc Biol (2021) 3:R96-R105.

208. **Wohlrab J, Gerloff D, Gebhardt K**. Expression and activity of IL-17 receptor subunits in human cutaneous cells as targets for anti-IL-17 therapeutic antibodies. Biomed Pharmacother (2022) 146:112569.

209. **Zheng Y, Danilenko DM, Valdez P, Kasman I, Eastham-Anderson J, Wu J**, et al. Interleukin-22, a T(H)17 cytokine, mediates IL-23-induced dermal inflammation and acanthosis. Nature (2007) 445:648–51.

210. **Zhao J, Lu Q, Liu Y, Shi Z, Hu L, Zeng Z**, et al. Th17 Cells in Inflammatory Bowel Disease: Cytokines, Plasticity, and Therapies. J Immunol Res (2021) 2021:8816041.

211. **Yasuda K, Takeuchi Y, Hirota K**. The pathogenicity of Th17 cells in autoimmune diseases. Semin Immunopathol (2019) 41:283–97.

212. **Yang J, Sundrud MS, Skepner J, Yamagata T**. Targeting Th17 cells in autoimmune diseases. Trends Pharmacol Sci (2014) 35:493–500.

213. **Moser T, Akgün K, Proschmann U, Sellner J, Ziemssen T**. The role of TH17 cells in multiple sclerosis: Therapeutic implications. Autoimmun Rev (2020) 19:102647.

214. **Knochelmann HM, Dwyer CJ, Bailey SR, Amaya SM, Elston DM, Mazza-McCrann JM**, et al. When worlds collide: Th17 and Treg cells in cancer and autoimmunity. Cell Mol Immunol (2018) 15:458–69.

215. **Salazar Y, Zheng X, Brunn D, Raifer H, Picard F, Zhang Y**, et al. Microenvironmental Th9 and Th17 lymphocytes induce metastatic spreading in lung cancer. J Clin Invest (2020) 130:3560–75.

216. **Lee J-Y, Hall JA, Kroehling L, Wu L, Najar T, Nguyen HH**, et al. Serum Amyloid A Proteins Induce Pathogenic Th17 Cells and Promote Inflammatory Disease. Cell (2020) 180:79-91.e16.

217. **Frank DN, St Amand AL, Feldman RA, Boedeker EC, Harpaz N, Pace NR**. Molecular-phylogenetic characterization of microbial community imbalances in human inflammatory bowel diseases. Proc Natl Acad Sci U S A (2007) 104:13780–5.

218. **Fuss IJ, Neurath M, Boirivant M, Klein JS, La Motte C** de, **Strong SA**, et al. Disparate CD4+ lamina propria (LP) lymphokine secretion profiles in inflammatory bowel disease. Crohn's disease LP cells manifest increased secretion of IFN-gamma, whereas ulcerative colitis LP cells manifest increased secretion of IL-5. J Immunol (1996) 157:1261–70.

219. **Rovedatti L, Kudo T, Biancheri P, Sarra M, Knowles CH, Rampton DS**, et al. Differential regulation of interleukin 17 and interferon gamma production in inflammatory bowel disease. Gut (2009) 58:1629–36.

220. **Fujino S, Andoh A, Bamba S, Ogawa A, Hata K, Araki Y**, et al. Increased expression of interleukin 17 in inflammatory bowel disease. Gut (2003) 52:65–70.

221. **Olsen T, Rismo R, Cui G, Goll R, Christiansen I, Florholmen J**. TH1 and TH17 interactions in untreated inflamed mucosa of inflammatory bowel disease, and their potential to mediate the inflammation. Cytokine (2011) 56:633–40.

222. **Jiang W, Su J, Zhang X, Cheng X, Zhou J, Shi R**, et al. Elevated levels of Th17 cells and Th17-related cytokines are associated with disease activity in patients with inflammatory bowel disease. Inflamm Res (2014) 63:943–50.

223. **Kempski J, Brockmann L, Gagliani N, Huber S**. TH17 Cell and Epithelial Cell Crosstalk during Inflammatory Bowel Disease and Carcinogenesis. Front Immunol (2017) 8:1373.

224. **Brazil JC, Louis NA, Parkos CA**. The role of polymorphonuclear leukocyte trafficking in the perpetuation of inflammation during inflammatory bowel disease. Inflamm Bowel Dis (2013) 19:1556–65.

225. **Iwakura Y, Ishigame H, Saijo S, Nakae S**. Functional specialization of interleukin-17 family members. Immunity (2011) 34:149–62.

226. **Ishigame H, Kakuta S, Nagai T, Kadoki M, Nambu A, Komiyama Y**, et al. Differential roles of interleukin-17A and -17F in host defense against mucoepithelial bacterial infection and allergic responses. Immunity (2009) 30:108–19.

227. **Ho S, Pothoulakis C, Koon HW**. Antimicrobial peptides and colitis. Curr Pharm Des (2013) 19:40–7.

228. **Kumar P, Monin L, Castillo P, Elsegeiny W, Horne W, Eddens T**, et al. Intestinal Interleukin-17 Receptor Signaling Mediates Reciprocal Control of the Gut Microbiota and Autoimmune Inflammation. Immunity (2016) 44:659–71.

229. **Kinugasa T, Sakaguchi T, Gu X, Reinecker HC**. Claudins regulate the intestinal barrier in response to immune mediators. Gastroenterology (2000) 118:1001–11.

230. **Dardalhon V, Awasthi A, Kwon H, Galileos G, Gao W, Sobel RA**, et al. IL-4 inhibits TGF-beta-induced Foxp3+ T cells and, together with TGF-beta, generates IL-9+ IL-10+ Foxp3(-) effector T cells. Nat Immunol (2008) 9:1347–55.

231. **Veldhoen M, Uyttenhove C, van Snick J, Helmby H, Westendorf A, Buer J**, et al. Transforming growth factor-beta 'reprograms' the differentiation of T helper 2 cells and promotes an interleukin 9-producing subset. Nat Immunol (2008) 9:1341–6.

232. **Ma CS, Tangye SG, Deenick EK**. Human Th9 cells: inflammatory cytokines modulate IL-9 production through the induction of IL-21. Immunol Cell Biol (2010) 88:621–3.

233. **Goswami R, Kaplan MH**. Gcn5 is required for PU.1-dependent IL-9 induction in Th9 cells. J Immunol (2012) 189:3026–33.

234. **Chang H-C, Sehra S, Goswami R, Yao W, Yu Q, Stritesky GL**, et al. The transcription factor PU.1 is required for the development of IL-9-producing T cells and allergic inflammation. Nat Immunol (2010) 11:527–34.

235. **Staudt V, Bothur E, Klein M, Lingnau K, Reuter S, Grebe N**, et al. Interferon-regulatory factor 4 is essential for the developmental program of T helper 9 cells. Immunity (2010) 33:192–202.

236. **Stassen M, Müller C, Arnold M, Hültner L, Klein-Hessling S, Neudörfl C**, et al. IL-9 and IL-13 production by activated mast cells is strongly enhanced in the presence of lipopolysaccharide: NF-kappa B is decisively involved in the expression of IL-9. J Immunol (2001) 166:4391–8.

237. **Perumal NB, Kaplan MH**. Regulating Il9 transcription in T helper cells. Trends Immunol (2011) 32:146–50.

8. References

238. **Angkasekwinai P, Chang SH, Thapa M, Watarai H, Dong C**. Regulation of IL-9 expression by IL-25 signaling. Nat Immunol (2010) 11:250–6.

239. **Jäger A, Dardalhon V, Sobel RA, Bettelli E, Kuchroo VK**. Th1, Th17, and Th9 effector cells induce experimental autoimmune encephalomyelitis with different pathological phenotypes. J Immunol (2009) 183:7169–77.

240. **Nowak EC, Weaver CT, Turner H, Begum-Haque S, Becher B, Schreiner B**, et al. IL-9 as a mediator of Th17-driven inflammatory disease. J Exp Med (2009) 206:1653–60.

241. **Li H, Nourbakhsh B, Ciric B, Zhang G-X, Rostami A**. Neutralization of IL-9 ameliorates experimental autoimmune encephalomyelitis by decreasing the effector T cell population. J Immunol (2010) 185:4095–100.

242. **Angkasekwinai P**. Th9 Cells in Allergic Disease. Curr Allergy Asthma Rep (2019) 19:29.

243. **Vyas SP, Goswami R**. A Decade of Th9 Cells: Role of Th9 Cells in Inflammatory Bowel Disease. Front Immunol (2018) 9:1139.

244. **Chen HY, Bao Y, Zou JJ, Cong XL, Zhang XX, Zheng JY**, et al. Activated Th9 cells in diabetic coronary heart disease. J Biol Regul Homeost Agents (2021) 35:1137–44.

245. **Elyaman W, Bradshaw EM, Uyttenhove C, Dardalhon V, Awasthi A, Imitola J**, et al. IL-9 induces differentiation of TH17 cells and enhances function of FoxP3+ natural regulatory T cells. Proc Natl Acad Sci U S A (2009) 106:12885–90.

246. **Gerlach K, Hwang Y, Nikolaev A, Atreya R, Dornhoff H, Steiner S**, et al. TH9 cells that express the transcription factor PU.1 drive T cell-mediated colitis via IL-9 receptor signaling in intestinal epithelial cells. Nat Immunol (2014) 15:676–86.

247. **Defendenti C, Sarzi-Puttini P, Saibeni S, Bollani S, Bruno S, Almasio PL**, et al. Significance of serum Il-9 levels in inflammatory bowel disease. Int J Immunopathol Pharmacol (2015) 28:569–75.

248. **Nalleweg N, Chiriac MT, Podstawa E, Lehmann C, Rau TT, Atreya R**, et al. IL-9 and its receptor are predominantly involved in the pathogenesis of UC. Gut (2015) 64:743–55.

249. **Ono M**. Control of regulatory T-cell differentiation and function by T-cell receptor signalling and Foxp3 transcription factor complexes. Immunology (2020) 160:24–37.

250. **Shi H, Chi H**. Metabolic Control of Treg Cell Stability, Plasticity, and Tissue-Specific Heterogeneity. Front Immunol (2019) 10:2716.

251. **Da Figliuolo Paz VR, Jamwal DR, Kiela PR**. Intestinal Regulatory T Cells. Adv Exp Med Biol (2021) 1278:141–90.

252. **Li C, Spallanzani RG, Mathis D**. Visceral adipose tissue Tregs and the cells that nurture them. Immunol Rev (2020) 295:114–25.

253. **Wan YY, Flavell RA**. 'Yin-Yang' functions of transforming growth factor-beta and T regulatory cells in immune regulation. Immunol Rev (2007) 220:199–213.

254. **Iyer SS, Cheng G**. Role of interleukin 10 transcriptional regulation in inflammation and autoimmune disease. Crit Rev Immunol (2012) 32:23–63.

255. **Nielsen OH, Ciardelli T, Wu Z, Langholz E, Kirman I**. Circulating soluble interleukin-2 receptor alpha and beta chain in inflammatory bowel disease. Am J Gastroenterol (1995) 90:1301–6.

256. **Poussier P, Ning T, Chen J, Banerjee D, Julius M**. Intestinal inflammation observed in IL-2R/IL-2 mutant mice is associated with impaired intestinal T lymphopoiesis. Gastroenterology (2000) 118:880–91.

257. **Elson CO, Cong Y, McCracken VJ, Dimmitt RA, Lorenz RG, Weaver CT**. Experimental models of inflammatory bowel disease reveal innate, adaptive, and regulatory mechanisms of host dialogue with the microbiota. Immunol Rev (2005) 206:260–76.

258. **Veltkamp C, Anstaett M, Wahl K, Möller S, Gangl S, Bachmann O**, et al. Apoptosis of regulatory T lymphocytes is increased in chronic inflammatory bowel disease and reversed by anti-TNFα treatment. Gut (2011) 60:1345–53.

259. **Yan J-B, Luo M-M, Chen Z-Y, He B-H**. The Function and Role of the Th17/Treg Cell Balance in Inflammatory Bowel Disease. J Immunol Res (2020) 2020:8813558.

260. **Bai A, Lu N, Guo Y, Liu Z, Chen J, Peng Z**. All-trans retinoic acid down-regulates inflammatory responses by shifting the Treg/Th17 profile in human ulcerative and murine colitis. J Leukoc Biol (2009) 86:959–69.

261. **Luo S, Wen R, Wang Q, Zhao Z, Nong F, Fu Y**, et al. Rhubarb Peony Decoction ameliorates ulcerative colitis in mice by regulating gut microbiota to restoring Th17/Treg balance. J Ethnopharmacol (2019) 231:39–49.

262. **Li L, Boussiotis VA**. The role of IL-17-producing Foxp3+ CD4+ T cells in inflammatory bowel disease and colon cancer. Clin Immunol (2013) 148:246–53.

263. **Ueno A, Jijon H, Chan R, Ford K, Hirota C, Kaplan GG**, et al. Increased prevalence of circulating novel IL-17 secreting Foxp3 expressing CD4+ T cells and defective suppressive function of circulating Foxp3+ regulatory cells support plasticity between Th17 and regulatory T cells in inflammatory bowel disease patients. Inflamm Bowel Dis (2013) 19:2522–34.

264. **Harrison OJ, Srinivasan N, Pott J, Schiering C, Krausgruber T, Ilott NE**, et al. Epithelial-derived IL-18 regulates Th17 cell differentiation and Foxp3$^+$ Treg cell function in the intestine. Mucosal Immunol (2015) 8:1226–36.

265. **Eastaff-Leung N, Mabarrack N, Barbour A, Cummins A, Barry S**. Foxp3+ regulatory T cells, Th17 effector cells, and cytokine environment in inflammatory bowel disease. J Clin Immunol (2010) 30:80–9.

266. **Mizoguchi A**. Animal models of inflammatory bowel disease. Prog Mol Biol Transl Sci (2012) 105:263–320.

267. **Voskens CJ, Fischer A, Roessner S, Lorenz C, Hirschmann S, Atreya R**, et al. Characterization and Expansion of Autologous GMP-ready Regulatory T Cells for TREG-based Cell Therapy in Patients with Ulcerative Colitis. Inflamm Bowel Dis (2017) 23:1348–59.

268. **Liu Y-J, Tang B, Wang F-C, Tang L, Lei Y-Y, Luo Y**, et al. Parthenolide ameliorates colon inflammation through regulating Treg/Th17 balance in a gut microbiota-dependent manner. Theranostics (2020) 10:5225–41.

269. **Chang Y, Zhai L, Peng J, Wu H, Bian Z, Xiao H**. Phytochemicals as regulators of Th17/Treg balance in inflammatory bowel diseases. Biomed Pharmacother (2021) 141:111931.

270. **Wen S, He L, Zhong Z, Zhao R, Weng S, Mi H**, et al. Stigmasterol Restores the Balance of Treg/Th17 Cells by Activating the Butyrate-PPARγ Axis in Colitis. Front Immunol (2021) 12:741934.

8. References

271. **Liu C, Li Y, Chen Y, Huang S, Wang X, Luo S**, et al. Baicalein Restores the Balance of Th17/Treg Cells via Aryl Hydrocarbon Receptor to Attenuate Colitis. Mediators Inflamm (2020) 2020:5918587.

272. **Dingjan T, Futerman AH**. The role of the 'sphingoid motif' in shaping the molecular interactions of sphingolipids in biomembranes. Biochim Biophys Acta Biomembr (2021) 1863:183701.

273. **Cartier A, Hla T**. Sphingosine 1-phosphate: Lipid signaling in pathology and therapy. Science (2019) 366.

274. **Obinata H, Hla T**. Sphingosine 1-phosphate and inflammation. Int Immunol (2019) 31:617–25.

275. **Argollo M, Furfaro F, Gilardi D, Roda G, Allocca M, Peyrin-Biroulet L**, et al. Modulation of sphingosine-1-phosphate in ulcerative colitis. Expert Opin Biol Ther (2020) 20:413–20.

276. **Bravo GÁ, Cedeño RR, Casadevall MP, Ramió-Torrentà L**. Sphingosine-1-Phosphate (S1P) and S1P Signaling Pathway Modulators, from Current Insights to Future Perspectives. Cells (2022) 11.

277. **Chen H, Wang J, Zhang C, Ding P, Tian S, Chen J**, et al. Sphingosine 1-phosphate receptor, a new therapeutic direction in different diseases. Biomed Pharmacother (2022) 153:113341.

278. **Verstockt B, Vetrano S, Salas A, Nayeri S, Duijvestein M, Vande Casteele N**. Sphingosine 1-phosphate modulation and immune cell trafficking in inflammatory bowel disease. Nat Rev Gastroenterol Hepatol (2022) 19:351–66.

279. **Castro BM, Prieto M, Silva LC**. Ceramide: a simple sphingolipid with unique biophysical properties. Prog Lipid Res (2014) 54:53–67.

280. **Grösch S, Schiffmann S, Geisslinger G**. Chain length-specific properties of ceramides. Prog Lipid Res (2012) 51:50–62.

281. **Ho QWC, Zheng X, Ali Y**. Ceramide Acyl Chain Length and Its Relevance to Intracellular Lipid Regulation. Int J Mol Sci (2022) 23.

282. **Mandon EC, Ehses I, Rother J, van Echten G, Sandhoff K**. Subcellular localization and membrane topology of serine palmitoyltransferase, 3-dehydrosphinganine reductase, and sphinganine N-acyltransferase in mouse liver. J Biol Chem (1992) 267:11144–8.

283. **Hannun YA, Obeid LM**. Sphingolipids and their metabolism in physiology and disease. Nat Rev Mol Cell Biol (2018) 19:175–91.

284. **Merrill AH**. De novo sphingolipid biosynthesis: a necessary, but dangerous, pathway. J Biol Chem (2002) 277:25843–6.

285. **Pewzner-Jung Y, Ben-Dor S, Futerman AH**. When do Lasses (longevity assurance genes) become CerS (ceramide synthases)? Insights into the regulation of ceramide synthesis. J Biol Chem (2006) 281:25001–5.

286. **Lahiri S, Lee H, Mesicek J, Fuks Z, Haimovitz-Friedman A, Kolesnick RN**, et al. Kinetic characterization of mammalian ceramide synthases: determination of K(m) values towards sphinganine. FEBS Lett (2007) 581:5289–94.

287. **Levy M, Futerman AH**. Mammalian ceramide synthases. IUBMB Life (2010) 62:347–56.

288. **Gomez-Larrauri A, Presa N, Dominguez-Herrera A, Ouro A, Trueba M, Gomez-Muñoz A**. Role of bioactive sphingolipids in physiology and pathology. Essays Biochem (2020) 64:579–89.

289. **Backman APE, Mattjus P**. Who moves the sphinx? An overview of intracellular sphingolipid transport. Biochim Biophys Acta Mol Cell Biol Lipids (2021) 1866:159021.

290. **Riboni L, Giussani P, Viani P**. Sphingolipid transport. Adv Exp Med Biol (2010) 688:24–45.

291. **Airola MV, Hannun YA**. Sphingolipid metabolism and neutral sphingomyelinases. Handb Exp Pharmacol (2013) 57–76.

292. **Kitatani K, Idkowiak-Baldys J, Hannun YA**. The sphingolipid salvage pathway in ceramide metabolism and signaling. Cell Signal (2008) 20:1010–8.

293. **Henry B, Ziobro R, Becker KA, Kolesnick R, Gulbins E**. Acid sphingomyelinase. Handb Exp Pharmacol (2013) 77–88.

294. **Parveen F, Bender D, Law S-H, Mishra VK, Chen C-C, Ke L-Y**. Role of Ceramidases in Sphingolipid Metabolism and Human Diseases. Cells (2019) 8.

295. **Hartel JC, Merz N, Grösch S**. How sphingolipids affect T cells in the resolution of inflammation. Front Pharmacol (2022) 13:1002915.

296. **Mullen TD, Hannun YA, Obeid LM**. Ceramide synthases at the centre of sphingolipid metabolism and biology. Biochem J (2012) 441:789–802.

297. **Wegner M-S, Schiffmann S, Parnham MJ, Geisslinger G, Grösch S**. The enigma of ceramide synthase regulation in mammalian cells. Prog Lipid Res (2016) 63:93–119.

298. **Wang Z, Wen L, Zhu F, Wang Y, Xie Q, Chen Z**, et al. Overexpression of ceramide synthase 1 increases C18-ceramide and leads to lethal autophagy in human glioma. Oncotarget (2017) 8:104022–36.

299. **Godeiro Junior CdO, Vale TC, Afonso COdM, Kok F, Pedroso JL, Barsottini OG**. Progressive Myoclonic Epilepsy Type 8 Due to CERS1 Deficiency: A Novel Mutation with Prominent Ataxia. Mov Disord Clin Pract (2018) 5:330–2.

300. **Jennemann R, Rabionet M, Gorgas K, Epstein S, Dalpke A, Rothermel U**, et al. Loss of ceramide synthase 3 causes lethal skin barrier disruption. Hum Mol Genet (2012) 21:586–608.

301. **Radner FPW, Marrakchi S, Kirchmeier P, Kim G-J, Ribierre F, Kamoun B**, et al. Mutations in CERS3 cause autosomal recessive congenital ichthyosis in humans. PLoS Genet (2013) 9:e1003536.

302. **Youssefian L, Vahidnezhad H, Saeidian AH, Sotoudeh S, Mahmoudi H, Daneshpazhooh M**, et al. Autosomal recessive congenital ichthyosis: CERS3 mutations identified by a next generation sequencing panel targeting ichthyosis genes. Eur J Hum Genet (2017) 25:1282–5.

303. **Sassa T, Hirayama T, Kihara A**. Enzyme Activities of the Ceramide Synthases CERS2-6 Are Regulated by Phosphorylation in the C-terminal Region. J Biol Chem (2016) 291:7477–87.

304. Huwiler A., Kolter T., Pfeilschifter J., Sandhoff K. Physiology and pathophysiology of sphingolipid metabolism and signaling. Biochimica et Biophysica (2000) 63–99.

305. **Eich C, Manzo C, Keijzer S** de, **Bakker G-J, Reinieren-Beeren I, García-Parajo MF**, et al. Changes in membrane sphingolipid composition modulate dynamics and adhesion of integrin nanoclusters. Sci Rep (2016) 6:20693.

306. **Montes L-R, López DJ, Sot J, Bagatolli LA, Stonehouse MJ, Vasil ML**, et al. Ceramide-enriched membrane domains in red blood cells and the mechanism of sphingomyelinase-induced hot-cold hemolysis. Biochemistry (2008) 47:11222–30.

307. **Hinkovska-Galcheva V, Boxer LA, Kindzelskii A, Hiraoka M, Abe A, Goparju S**, et al. Ceramide 1-phosphate, a mediator of phagocytosis. J Biol Chem (2005) 280:26612–21.

8. References

308. **Contreras F-X, Sánchez-Magraner L, Alonso A, Goñi FM**. Transbilayer (flip-flop) lipid motion and lipid scrambling in membranes. FEBS Lett (2010) 584:1779–86.

309. **Stahlberg S, Školová B, Madhu PK, Vogel A, Vávrová K, Huster D**. Probing the role of the ceramide acyl chain length and sphingosine unsaturation in model skin barrier lipid mixtures by (2)H solid-state NMR spectroscopy. Langmuir (2015) 31:4906–15.

310. **Imokawa G, Abe A, Jin K, Higaki Y, Kawashima M, Hidano A**. Decreased level of ceramides in stratum corneum of atopic dermatitis: an etiologic factor in atopic dry skin? J Invest Dermatol (1991) 96:523–6.

311. **Janssens M, van Smeden J, Gooris GS, Bras W, Portale G, Caspers PJ**, et al. Increase in short-chain ceramides correlates with an altered lipid organization and decreased barrier function in atopic eczema patients. J Lipid Res (2012) 53:2755–66.

312. **Ishikawa J, Narita H, Kondo N, Hotta M, Takagi Y, Masukawa Y**, et al. Changes in the ceramide profile of atopic dermatitis patients. J Invest Dermatol (2010) 130:2511–4.

313. **van Smeden J, Janssens M, Kaye ECJ, Caspers PJ, Lavrijsen AP, Vreeken RJ**, et al. The importance of free fatty acid chain length for the skin barrier function in atopic eczema patients. Exp Dermatol (2014) 23:45–52.

314. **Dinkins MB, Dasgupta S, Wang G, Zhu G, Bieberich E**. Exosome reduction in vivo is associated with lower amyloid plaque load in the 5XFAD mouse model of Alzheimer's disease. Neurobiology of Aging (2014) 35:1792–800.

315. **Dinkins MB, Enasko J, Hernandez C, Wang G, Kong J, Helwa I**, et al. Neutral Sphingomyelinase-2 Deficiency Ameliorates Alzheimer's Disease Pathology and Improves Cognition in the 5XFAD Mouse. J. Neurosci. (2016) 36:8653–67.

316. **Crivelli SM, Giovagnoni C, Zhu Z, Tripathi P, Elsherbini A, Quadri Z**, et al. Function of ceramide transfer protein for biogenesis and sphingolipid composition of extracellular vesicles. J Extracell Vesicles (2022) 11:e12233.

317. **Stanley AC, Lacy P**. Pathways for cytokine secretion. Physiology (Bethesda) (2010) 25:218–29.

318. **Grange C, Bussolati B**. Extracellular vesicles in kidney disease. Nat Rev Nephrol (2022) 18:499–513.

319. **Huang C, Neupane YR, Lim XC, Shekhani R, Czarny B, Wacker MG**, et al. "Extracellular vesicles in cardiovascular disease". In: Makowski GS, editor. Advances in clinical chemistry. Cambridge, MA: Academic Press, is an imprint of Elsevier (2021). p. 47–95.

320. **Carnino JM, Lee H**. Extracellular vesicles in respiratory disease. Adv Clin Chem (2022) 108:105–27.

321. **Menck K, Sönmezer C, Worst TS, Schulz M, Dihazi GH, Streit F**, et al. Neutral sphingomyelinases control extracellular vesicles budding from the plasma membrane. J Extracell Vesicles (2017) 6:1378056.

322. **Trajkovic K, Hsu C, Chiantia S, Rajendran L, Wenzel D, Wieland F**, et al. Ceramide Triggers Budding of Exosome Vesicles into Multivesicular Endosomes. Science (2008) 319:1244–7.

323. **Skotland T, Hessvik NP, Sandvig K, Llorente A**. Exosomal lipid composition and the role of ether lipids and phosphoinositides in exosome biology. J Lipid Res (2019) 60:9–18.

324. **Levental I, Levental KR, Heberle FA**. Lipid Rafts: Controversies Resolved, Mysteries Remain. Trends Cell Biol (2020) 30:341–53.

325. **Lingwood D, Simons K**. Lipid rafts as a membrane-organizing principle. Science (2010) 327:46–50.

326. **van Meer G, Voelker DR, Feigenson GW**. Membrane lipids: where they are and how they behave. Nat Rev Mol Cell Biol (2008) 9:112–24.

327. **Miyagawa-Yamaguchi A, Kotani N, Honke K**. Each GPI-anchored protein species forms a specific lipid raft depending on its GPI attachment signal. Glycoconj J (2015) 32:531–40.

328. **Taruno A, Sun H, Nakajo K, Murakami T, Ohsaki Y, Kido MA**, et al. Post-translational palmitoylation controls the voltage gating and lipid raft association of the CALHM1 channel. J Physiol (2017) 595:6121–45.

329. **Dai G**. Neuronal KCNQ2/3 channels are recruited to lipid raft microdomains by palmitoylation of BACE1. J Gen Physiol (2022) 154.

330. **Stalder D, Gershlick DC**. Direct trafficking pathways from the Golgi apparatus to the plasma membrane. Semin Cell Dev Biol (2020) 107:112–25.

331. **Fujita M, Kinoshita T**. GPI-anchor remodeling: potential functions of GPI-anchors in intracellular trafficking and membrane dynamics. Biochim Biophys Acta (2012) 1821:1050–8.

332. **Wang Y, Lu H, Fang C, Xu J**. Palmitoylation as a Signal for Delivery. Adv Exp Med Biol (2020) 1248:399–424.

333. **Jansen M, Beaumelle B**. How palmitoylation affects trafficking and signaling of membrane receptors. Biol Cell (2022) 114:61–72.

334. **Kapoor-Kaushik N, Hinde E, Compeer EB, Yamamoto Y, Kraus F, Yang Z**, et al. Distinct Mechanisms Regulate Lck Spatial Organization in Activated T Cells. Front Immunol (2016) 7:83.

335. **Luo C, Wang K, Liu DQ, Li Y, Zhao QS**. The functional roles of lipid rafts in T cell activation, immune diseases and HIV infection and prevention. Cell Mol Immunol (2008) 5:1–7.

336. **D'Aprile C, Prioni S, Mauri L, Prinetti A, Grassi S**. Lipid rafts as platforms for sphingosine 1-phosphate metabolism and signalling. Cell Signal (2021) 80:109929.

337. **Singleton PA, Dudek SM, Ma S-F, Garcia JGN**. Transactivation of sphingosine 1-phosphate receptors is essential for vascular barrier regulation. Novel role for hyaluronan and CD44 receptor family. J Biol Chem (2006) 281:34381–93.

338. **Zhao J, Singleton PA, Brown ME, Dudek SM, Garcia JGN**. Phosphotyrosine protein dynamics in cell membrane rafts of sphingosine-1-phosphate-stimulated human endothelium: role in barrier enhancement. Cell Signal (2009) 21:1945–60.

339. **Bartke N, Hannun YA**. Bioactive sphingolipids: metabolism and function. J Lipid Res (2009) 50 Suppl:S91-6.

340. **Mukhopadhyay A, Saddoughi SA, Song P, Sultan I, Ponnusamy S, Senkal CE**, et al. Direct interaction between the inhibitor 2 and ceramide via sphingolipid-protein binding is involved in the regulation of protein phosphatase 2A activity and signaling. FASEB J (2009) 23:751–63.

341. **Thompson JJ, Williams CS**. Protein Phosphatase 2A in the Regulation of Wnt Signaling, Stem Cells, and Cancer. Genes (Basel) (2018) 9.

8. References

342. **Allen-Petersen BL, Risom T, Feng Z, Wang Z, Jenny ZP, Thoma MC**, et al. Activation of PP2A and Inhibition of mTOR Synergistically Reduce MYC Signaling and Decrease Tumor Growth in Pancreatic Ductal Adenocarcinoma. Cancer Res (2019) 79:209–19.

343. **Grethe S, Pörn-Ares MI**. p38 MAPK regulates phosphorylation of Bad via PP2A-dependent suppression of the MEK1/2-ERK1/2 survival pathway in TNF-alpha induced endothelial apoptosis. Cell Signal (2006) 18:531–40.

344. **Wlodarchak N, Xing Y**. PP2A as a master regulator of the cell cycle. Crit Rev Biochem Mol Biol (2016) 51:162–84.

345. **Banday ZZ**. S1P-S1PR1 signaling switch: a new paradigm of tyrosine phosphorylation. Hum Cell (2022) 35:2020–1.

346. **Wang H, Huang H, Ding S-F**. Sphingosine-1-phosphate promotes the proliferation and attenuates apoptosis of Endothelial progenitor cells via S1PR1/S1PR3/PI3K/Akt pathway. Cell Biol Int (2018) 42:1492–502.

347. **Baeyens A, Fang V, Chen C, Schwab SR**. Exit Strategies: S1P Signaling and T Cell Migration. Trends Immunol (2015) 36:778–87.

348. **Liu G, Yang K, Burns S, Shrestha S, Chi H**. The S1P(1)-mTOR axis directs the reciprocal differentiation of T(H)1 and T(reg) cells. Nat Immunol (2010) 11:1047–56.

349. **Kornhuber J, Rhein C, Müller CP, Mühle C**. Secretory sphingomyelinase in health and disease. Biol Chem (2015) 396:707–36.

350. **Bock J, Liebisch G, Schweimer J, Schmitz G, Rogler G**. Exogenous sphingomyelinase causes impaired intestinal epithelial barrier function. World J Gastroenterol (2007) 13:5217–25.

351. **Li Z, Kabir I, Tietelman G, Huan C, Fan J, Worgall T**, et al. Sphingolipid de novo biosynthesis is essential for intestine cell survival and barrier function. Cell Death Dis (2018) 9:173.

352. **Xiong Y, Zhu X-D, Wan P, Ren Y-P, Wang C, Yan R-W**, et al. Inhibition of ASM activity ameliorates DSS-induced colitis in mice. Prostaglandins Other Lipid Mediat (2019) 140:26–30.

353. **Meiners J, Palmieri V, Klopfleisch R, Ebel J-F, Japtok L, Schumacher F**, et al. Intestinal Acid Sphingomyelinase Protects From Severe Pathogen-Driven Colitis. Front Immunol (2019) 10:1386.

354. **Aflaki E, Doddapattar P, Radović B, Povoden S, Kolb D, Vujić N**, et al. C16 ceramide is crucial for triacylglycerol-induced apoptosis in macrophages. Cell Death Dis (2012) 3:e280.

355. **Blaess M, Le HP, Claus RA, Kohl M, Deigner H-P**. Stereospecific induction of apoptosis in tumor cells via endogenous C16-ceramide and distinct transcripts. Cell Death Discov (2015) 1:15013.

356. **Nakagawa T, Morotomi A, Tani M, Sueyoshi N, Komori H, Ito M**. C18:3-GM1a induces apoptosis in Neuro2a cells: enzymatic remodeling of fatty acyl chains of glycosphingolipids. J Lipid Res (2005) 46:1103–12.

357. **Hartmann D, Lucks J, Fuchs S, Schiffmann S, Schreiber Y, Ferreirós N**, et al. Long chain ceramides and very long chain ceramides have opposite effects on human breast and colon cancer cell growth. Int J Biochem Cell Biol (2012) 44:620–8.

358. **Novotný J, Janůsová B, Novotný M, Hrabálek A, Vávrová K**. Short-chain ceramides decrease skin barrier properties. Skin Pharmacol Physiol (2009) 22:22–30.

359. **Oertel S, Scholich K, Weigert A, Thomas D, Schmetzer J, Trautmann S**, et al. Ceramide synthase 2 deficiency aggravates AOM-DSS-induced colitis in mice: role of colon barrier integrity. Cell Mol Life Sci (2017) 74:3039–55.

360. **Helke K, Angel P, Lu P, Garrett-Mayer E, Ogretmen B, Drake R**, et al. Ceramide Synthase 6 Deficiency Enhances Inflammation in the DSS model of Colitis. Sci Rep (2018) 8:1627.

361. **El-Hindi K, Brachtendorf S, Hartel JC, Oertel S, Birod K, Trautmann S**, et al. Ceramide Synthase 5 Deficiency Aggravates Dextran Sodium Sulfate-Induced Colitis and Colon Carcinogenesis and Impairs T-Cell Activation. Cancers (Basel) (2020) 12.

362. **Miklavcic JJ, Li Q, Skolnick J, Thomson ABR, Mazurak VC, Clandinin MT**. Ganglioside Alters Phospholipase Trafficking, Inhibits NF-κB Assembly, and Protects Tight Junction Integrity. Front Nutr (2021) 8:705172.

363. **Bazarganipour S, Hausmann J, Oertel S, El-Hindi K, Brachtendorf S, Blumenstein I**, et al. The Lipid Status in Patients with Ulcerative Colitis: Sphingolipids are Disease-Dependent Regulated. J Clin Med (2019) 8.

364. **Filimoniuk A, Blachnio-Zabielska A, Imierska M, Lebensztejn DM, Daniluk U**. Sphingolipid Analysis Indicate Lactosylceramide as a Potential Biomarker of Inflammatory Bowel Disease in Children. Biomolecules (2020) 10.

365. **Magee T, Pirinen N, Adler J, Pagakis SN, Parmryd I**. Lipid rafts: cell surface platforms for T cell signaling. Biol Res (2002) 35:127–31.

366. **Zumerle S, Molon B, Viola A**. Membrane Rafts in T Cell Activation: A Spotlight on CD28 Costimulation. Front Immunol (2017) 8:1467.

367. **Bi K, Tanaka Y, Coudronniere N, Sugie K, Hong S, van Stipdonk MJ**, et al. Antigen-induced translocation of PKC-theta to membrane rafts is required for T cell activation. Nat Immunol (2001) 2:556–63.

368. **Börtlein C, Schumacher F, Kleuser B, Dölken L, Avota E**. Role of Neutral Sphingomyelinase-2 (NSM 2) in the Control of T Cell Plasma Membrane Lipid Composition and Cholesterol Homeostasis. Front Cell Dev Biol (2019) 7:226.

369. **Hose M, Günther A, Naser E, Schumacher F, Schönberger T, Falkenstein J**, et al. Cell-intrinsic ceramides determine T cell function during melanoma progression. Elife (2022) 11.

370. **Hose M, Günther A, Abberger H, Begum S, Korencak M, Becker KA**, et al. T Cell-Specific Overexpression of Acid Sphingomyelinase Results in Elevated T Cell Activation and Reduced Parasitemia During Plasmodium yoelii Infection. Front Immunol (2019) 10:1225.

371. **Li Y, Xiao B, Qiu W,** Le Yang, **Hu B, Tian X**, et al. Altered expression of CD4(+)CD25(+) regulatory T cells and its 5-HT(1a) receptor in patients with major depression disorder. J Affect Disord (2010) 124:68–75.

372. **Himmerich H, Milenović S, Fulda S, Plümäkers B, Sheldrick AJ, Michel TM**, et al. Regulatory T cells increased while IL-1β decreased during antidepressant therapy. J Psychiatr Res (2010) 44:1052–7.

373. **Schneider-Schaulies J, Beyersdorf N**. CD4+ Foxp3+ regulatory T cell-mediated immunomodulation by anti-depressants inhibiting acid sphingomyelinase. Biol Chem (2018) 399:1175–82.

8. References

374. **Apostolidis SA, Rodríguez-Rodríguez N, Suárez-Fueyo A, Dioufa N, Ozcan E, Crispín JC**, et al. Phosphatase PP2A is requisite for the function of regulatory T cells. Nat Immunol (2016) 17:556–64.

375. **Komuro M, Nagane M, Endo R, Nakamura T, Miyamoto T, Niwa C**, et al. Glucosylceramide in T cells regulates the pathology of inflammatory bowel disease. Biochem Biophys Res Commun (2022) 599:24–30.

376. **Zhu Y, Gumlaw N, Karman J, Zhao H, Zhang J, Jiang J-L**, et al. Lowering glycosphingolipid levels in CD4+ T cells attenuates T cell receptor signaling, cytokine production, and differentiation to the Th17 lineage. J Biol Chem (2011) 286:14787–94.

377. **Sen P, Andrabi SBA, Buchacher T, Khan MM, Kalim UU, Lindeman TM**, et al. Quantitative genome-scale metabolic modeling of human CD4+ T cell differentiation reveals subset-specific regulation of glycosphingolipid pathways. Cell Rep (2021) 37:109973.

378. **Allen MJ, Fan Y-Y, Monk JM, Hou TY, Barhoumi R, McMurray DN**, et al. n-3 PUFAs reduce T-helper 17 cell differentiation by decreasing responsiveness to interleukin-6 in isolated mouse splenic CD4$^+$ T cells. J Nutr (2014) 144:1306–13.

379. **Zuo W, Chen Y-G**. Specific activation of mitogen-activated protein kinase by transforming growth factor-beta receptors in lipid rafts is required for epithelial cell plasticity. Mol Biol Cell (2009) 20:1020–9.

380. **Le Roy C, Wrana JL**. Clathrin- and non-clathrin-mediated endocytic regulation of cell signalling. Nat Rev Mol Cell Biol (2005) 6:112–26.

381. **Sofi MH, Heinrichs J, Dany M, Nguyen H, Dai M, Bastian D**, et al. Ceramide synthesis regulates T cell activity and GVHD development. JCI Insight (2017) 2.

382. **Sofi MH, Tian L, Schutt S, Khan I, Choi H-J, Wu Y**, et al. Ceramide synthase 6 impacts T-cell allogeneic response and graft-versus-host disease through regulating N-RAS/ERK pathway. Leukemia (2022) 36:1907–15.

383. **Moreno DF, Cid J**. Graft-versus-host disease. Medicina Clínica (2019) 152:22–8.

384. **El-Hindi K, Brachtendorf S, Hartel JC, Oertel S, Birod K, Merz N**, et al. T-Cell-Specific CerS4 Depletion Prolonged Inflammation and Enhanced Tumor Burden in the AOM/DSS-Induced CAC Model. Int J Mol Sci (2022) 23.

385. **Schwab SR, Cyster JG**. Finding a way out: lymphocyte egress from lymphoid organs. Nat Immunol (2007) 8:1295–301.

386. **Garris CS, Wu L, Acharya S, Arac A, Blaho VA, Huang Y**, et al. Defective sphingosine 1-phosphate receptor 1 (S1P1) phosphorylation exacerbates TH17-mediated autoimmune neuroinflammation. Nat Immunol (2013) 14:1166–72.

387. **Berdyshev EV, Gorshkova IA, Garcia JGN, Natarajan V, Hubbard WC**. Quantitative analysis of sphingoid base-1-phosphates as bisacetylated derivatives by liquid chromatography-tandem mass spectrometry. Anal Biochem (2005) 339:129–36.

388. **Kharel Y, Huang T, Salamon A, Harris TE, Santos WL, Lynch KR**. Mechanism of sphingosine 1-phosphate clearance from blood. Biochem J (2020) 477:925–35.

389. **Debes GF, Arnold CN, Young AJ, Krautwald S, Lipp M, Hay JB**, et al. Chemokine receptor CCR7 required for T lymphocyte exit from peripheral tissues. Nat Immunol (2005) 6:889–94.

390. **Eken A, Duhen R, Singh AK, Fry M, Buckner JH, Kita M**, et al. S1P1 deletion differentially affects TH17 and Regulatory T cells. Sci Rep (2017) 7:12905.

391. **Bradford MM**. A rapid and sensitive method for the quantitation of microgram quantities of protein utilizing the principle of protein-dye binding. Anal Biochem (1976) 72:248–54.

392. **Merrill AH, Sullards MC, Allegood JC, Kelly S, Wang E**. Sphingolipidomics: high-throughput, structure-specific, and quantitative analysis of sphingolipids by liquid chromatography tandem mass spectrometry. Methods (2005) 36:207–24.

393. **Bielawski J, Pierce JS, Snider J, Rembiesa B, Szulc ZM, Bielawska A**. Sphingolipid analysis by high performance liquid chromatography-tandem mass spectrometry (HPLC-MS/MS). Adv Exp Med Biol (2010) 688:46–59.

394. **Kabouridis PS**. Lipid rafts in T cell receptor signalling. Mol Membr Biol (2006) 23:49–57.

395. **Olesch C, Sirait-Fischer E, Berkefeld M, Fink AF, Susen RM, Ritter B**, et al. S1PR4 ablation reduces tumor growth and improves chemotherapy via CD8+ T cell expansion. J Clin Invest (2020) 130:5461–76.

396. **Hartmann D, Wegner M-S, Wanger RA, Ferreirós N, Schreiber Y, Lucks J**, et al. The equilibrium between long and very long chain ceramides is important for the fate of the cell and can be influenced by co-expression of CerS. Int J Biochem Cell Biol (2013) 45:1195–203.

397. **Mullen TD, Spassieva S, Jenkins RW, Kitatani K, Bielawski J, Hannun YA**, et al. Selective knockdown of ceramide synthases reveals complex interregulation of sphingolipid metabolism. J Lipid Res (2011) 52:68–77.

398. **Raichur S, Wang ST, Chan PW, Li Y, Ching J, Chaurasia B**, et al. CerS2 haploinsufficiency inhibits β-oxidation and confers susceptibility to diet-induced steatohepatitis and insulin resistance. Cell Metab (2014) 20:687–95.

399. **Li Y, Yin Y, Mariuzza RA**. Structural and biophysical insights into the role of CD4 and CD8 in T cell activation. Front Immunol (2013) 4:206.

400. **Crise B, Rose JK**. Identification of palmitoylation sites on CD4, the human immunodeficiency virus receptor. Journal of Biological Chemistry (1992) 267:13593–7.

401. **Arcaro A, Grégoire C, Boucheron N, Stotz S, Palmer E, Malissen B**, et al. Essential role of CD8 palmitoylation in CD8 coreceptor function. J Immunol (2000) 165:2068–76.

402. **Turner JM, Brodsky MH, Irving BA, Levin SD, Perlmutter RM, Littman DR**. Interaction of the unique N-terminal region of tyrosine kinase p56lck with cytoplasmic domains of CD4 and CD8 is mediated by cysteine motifs. Cell (1990) 60:755–65.

403. **Schieffer D, Naware S, Bakun W, Bamezai AK**. Lipid raft-based membrane order is important for antigen-specific clonal expansion of CD4(+) T lymphocytes. BMC Immunol (2014) 15:58.

404. **Kovacs B, Maus MV, Riley JL, Derimanov GS, Koretzky GA, June CH**, et al. Human CD8+ T cells do not require the polarization of lipid rafts for activation and proliferation. Proc Natl Acad Sci U S A (2002) 99:15006–11.

405. **Neumeier J, Meister G**. siRNA Specificity: RNAi Mechanisms and Strategies to Reduce Off-Target Effects. Front Plant Sci (2020) 11:526455.

406. **Lo W-L, Shah NH, Ahsan N, Horkova V, Stepanek O, Salomon AR**, et al. Lck promotes Zap70-dependent LAT phosphorylation by bridging Zap70 to LAT. Nat Immunol (2018) 19:733–41.

8. References

407. **Miceli MC, Moran M, Chung CD, Patel VP, Low T, Zinnanti W**. Co-stimulation and counter-stimulation: lipid raft clustering controls TCR signaling and functional outcomes. Seminars in Immunology (2001) 13:115–28.

408. **Harder T**. Lipid raft domains and protein networks in T-cell receptor signal transduction. Curr Opin Immunol (2004) 16:353–9.

409. **Sunshine H, Iruela-Arispe ML**. Membrane lipids and cell signaling. Curr Opin Lipidol (2017) 28:408–13.

410. **Mall S, Malcolm East J, Lee AG**. "Transmembrane α helices". In: Simon SA, McIntosh TJ, editors. Current topics in membranes. San Diego, London: Academic Press (2002). p. 339–70.

411. **Fantini J**. How sphingolipids bind and shape proteins: molecular basis of lipid-protein interactions in lipid shells, rafts and related biomembrane domains. Cell Mol Life Sci (2003) 60:1027–32.

412. **Contreras F-X, Ernst AM, Haberkant P, Björkholm P, Lindahl E, Gönen B**, et al. Molecular recognition of a single sphingolipid species by a protein's transmembrane domain. Nature (2012) 481:525–9.

413. **Brazin KN, Mallis RJ, Boeszoermenyi A, Feng Y, Yoshizawa A, Reche PA**, et al. The T Cell Antigen Receptor α Transmembrane Domain Coordinates Triggering through Regulation of Bilayer Immersion and CD3 Subunit Associations. Immunity (2018) 49:829-841.e6.

414. **Jury EC, Kabouridis PS, Flores-Borja F, Mageed RA, Isenberg DA**. Altered lipid raft-associated signaling and ganglioside expression in T lymphocytes from patients with systemic lupus erythematosus. J Clin Invest (2004) 113:1176–87.

415. **McDonald G, Deepak S, Miguel L, Hall CJ, Isenberg DA, Magee AI**, et al. Normalizing glycosphingolipids restores function in CD4+ T cells from lupus patients. J Clin Invest (2014) 124:712–24.

416. **Komatsuya K, Kaneko K, Kasahara K**. Function of Platelet Glycosphingolipid Microdomains/Lipid Rafts. Int J Mol Sci (2020) 21.

417. **Lindblom G, Orädd G**. Lipid lateral diffusion and membrane heterogeneity. Biochim Biophys Acta (2009) 1788:234–44.

418. **Sonnino S, Prinetti A, Mauri L, Chigorno V, Tettamanti G**. Dynamic and structural properties of sphingolipids as driving forces for the formation of membrane domains. Chem Rev (2006) 106:2111–25.

419. **Rentero C, Zech T, Quinn CM, Engelhardt K, Williamson D, Grewal T**, et al. Functional implications of plasma membrane condensation for T cell activation. PLoS One (2008) 3:e2262.

420. **Owen DM, Oddos S, Kumar S, Davis DM, Neil MAA, French PMW**, et al. High plasma membrane lipid order imaged at the immunological synapse periphery in live T cells. Mol Membr Biol (2010) 27:178–89.

421. **Gault CR, Obeid LM, Hannun YA**. An overview of sphingolipid metabolism: from synthesis to breakdown. Adv Exp Med Biol (2010) 688:1–23.

422. **Bai A, Kokkotou E, Zheng Y, Robson SC**. Role of acid sphingomyelinase bioactivity in human CD4+ T-cell activation and immune responses. Cell Death Dis (2015) 6:e1828.

423. **Bieberich E**. Ceramide in stem cell differentiation and embryo development: novel functions of a topological cell-signaling lipid and the concept of ceramide compartments. J Lipids (2011) 2011:610306.

424. **Krishnamurthy K, Wang G, Silva J, Condie BG, Bieberich E**. Ceramide regulates atypical PKCzeta/lambda-mediated cell polarity in primitive ectoderm cells. A novel function of sphingolipids in morphogenesis. J Biol Chem (2007) 282:3379–90.

425. **Marmor MD, Julius M**. Role for lipid rafts in regulating interleukin-2 receptor signaling. Blood (2001) 98:1489–97.

426. **Sadra A, Cinek T, Imboden JB**. Translocation of CD28 to lipid rafts and costimulation of IL-2. Proc Natl Acad Sci U S A (2004) 101:11422–7.

427. **Tavano R, Gri G, Molon B, Marinari B, Rudd CE, Tuosto L**, et al. CD28 and lipid rafts coordinate recruitment of Lck to the immunological synapse of human T lymphocytes. J Immunol (2004) 173:5392–7.

428. **Abrahamsen H, Baillie G, Ngai J, Vang T, Nika K, Ruppelt A**, et al. TCR- and CD28-mediated recruitment of phosphodiesterase 4 to lipid rafts potentiates TCR signaling. J Immunol (2004) 173:4847–58.

429. **Lu S, Natarajan SK, Mott JL, Kharbanda KK, Harrison-Findik DD**. Ceramide Induces Human Hepcidin Gene Transcription through JAK/STAT3 Pathway. PLoS One (2016) 11:e0147474.

430. **Sparkman L, Chandru H, Boggaram V**. Ceramide decreases surfactant protein B gene expression via downregulation of TTF-1 DNA binding activity. Am J Physiol Lung Cell Mol Physiol (2006) 290:L351-8.

431. **Macián F, García-Cózar F, Im S-H, Horton HF, Byrne MC, Rao A**. Transcriptional mechanisms underlying lymphocyte tolerance. Cell (2002) 109:719–31.

432. **Kriegel MA, Rathinam C, Flavell RA**. E3 ubiquitin ligase GRAIL controls primary T cell activation and oral tolerance. Proc Natl Acad Sci U S A (2009) 106:16770–5.

433. **Rochman Y, Yukawa M, Kartashov AV, Barski A**. Functional characterization of human T cell hyporesponsiveness induced by CTLA4-Ig. PLoS One (2015) 10:e0122198.

434. **Meyer zu Heringdorf D, Lass H, Alemany R, Laser KT, Neumann E, Zhang C**, et al. Sphingosine kinase-mediated Ca2+ signalling by G-protein-coupled receptors. EMBO J (1998) 17:2830–7.

435. **Mattie M, Brooker G, Spiegel S**. Sphingosine-1-phosphate, a putative second messenger, mobilizes calcium from internal stores via an inositol trisphosphate-independent pathway. Journal of Biological Chemistry (1994) 269:3181–8.

436. **Beckham TH, Lu P, Cheng JC, Zhao D, Turner LS, Zhang X**, et al. Acid ceramidase-mediated production of sphingosine 1-phosphate promotes prostate cancer invasion through upregulation of cathepsin B. Int J Cancer (2012) 131:2034–43.

437. **O'Sullivan MJ, Hirota N, Martin JG**. Sphingosine 1-phosphate (S1P) induced interleukin-8 (IL-8) release is mediated by S1P receptor 2 and nuclear factor κB in BEAS-2B cells. PLoS One (2014) 9:e95566.

438. **Matsushima-Nishiwaki R, Yamada N, Fukuchi K, Kozawa O**. Sphingosine 1-phosphate (S1P) reduces hepatocyte growth factor-induced migration of hepatocellular carcinoma cells via S1P receptor 2. PLoS One (2018) 13:e0209050.

8. References

439. **Zhang G, Xu S, Qian Y, He P**. Sphingosine-1-phosphate prevents permeability increases via activation of endothelial sphingosine-1-phosphate receptor 1 in rat venules. Am J Physiol Heart Circ Physiol (2010) 299:H1494-504.

440. Guerrero M, Urbano M, Velaparthi S, Schaeffer M-T, Brown SJ, Crisp M, et al. Probe Reports from the NIH Molecular Libraries Program: Identification of a Novel Agonist of the Sphingosine 1-phosphate Receptor 4 (S1P4). Bethesda (MD) (2010).

441. **Neal JW, Clipstone NA**. Glycogen synthase kinase-3 inhibits the DNA binding activity of NFATc. J Biol Chem (2001) 276:3666–73.

442. **Mott DM, Stone K, Gessel MC, Bunt JC, Bogardus C**. Palmitate action to inhibit glycogen synthase and stimulate protein phosphatase 2A increases with risk factors for type 2 diabetes. Am J Physiol Endocrinol Metab (2008) 294:E444-50.

443. **Mora A, Sabio G, Risco AM, Cuenda A, Alonso JC, Soler G**, et al. Lithium blocks the PKB and GSK3 dephosphorylation induced by ceramide through protein phosphatase-2A. Cell Signal (2002) 14:557–62.

444. **Dobrowsky RT, Kamibayashi C, Mumby MC, Hannun YA**. Ceramide activates heterotrimeric protein phosphatase 2A. J Biol Chem (1993) 268:15523–30.

445. **Barreyro FJ, Kobayashi S, Bronk SF, Werneburg NW, Malhi H, Gores GJ**. Transcriptional regulation of Bim by FoxO3A mediates hepatocyte lipoapoptosis. J Biol Chem (2007) 282:27141–54.

446. **Diehn M, Alizadeh AA, Rando OJ, Liu CL, Stankunas K, Botstein D**, et al. Genomic expression programs and the integration of the CD28 costimulatory signal in T cell activation. Proc Natl Acad Sci U S A (2002) 99:11796–801.

447. **Appleman LJ, van Puijenbroek AAFL, Shu KM, Nadler LM, Boussiotis VA**. CD28 costimulation mediates down-regulation of p27kip1 and cell cycle progression by activation of the PI3K/PKB signaling pathway in primary human T cells. J Immunol (2002) 168:2729–36.

448. **Kane LP, Weiss A**. The PI-3 kinase/Akt pathway and T cell activation: pleiotropic pathways downstream of PIP3. Immunol Rev (2003) 192:7–20.

449. **Okkenhaug K, Bilancio A, Emery JL, Vanhaesebroeck B**. Phosphoinositide 3-kinase in T cell activation and survival. Biochem Soc Trans (2004) 32:332–5.

450. **Macián F, López-Rodríguez C, Rao A**. Partners in transcription: NFAT and AP-1. Oncogene (2001) 20:2476–89.

451. **Jain J, McCaffrey PG, Valge-Archer VE, Rao A**. Nuclear factor of activated T cells contains Fos and Jun. Nature (1992) 356:801–4.

452. **Yagi R, Zhu J, Paul WE**. An updated view on transcription factor GATA3-mediated regulation of Th1 and Th2 cell differentiation. Int Immunol (2011) 23:415–20.

453. **Hermann-Kleiter N, Baier G**. NFAT pulls the strings during CD4+ T helper cell effector functions. Blood (2010) 115:2989–97.

454. **Rieck M, Kremser C, Jobin K, Mettke E, Kurts C, Gräler M**, et al. Ceramide synthase 2 facilitates S1P-dependent egress of thymocytes into the circulation in mice. Eur. J. Immunol. (2017) 47:677–84.

168

455. **Garris CS, Blaho VA, Hla T, Han MH**. Sphingosine-1-phosphate receptor 1 signalling in T cells: trafficking and beyond. Immunology (2014) 142:347–53.

456. **Pham THM, Okada T, Matloubian M, Lo CG, Cyster JG**. S1P1 receptor signaling overrides retention mediated by G alpha i-coupled receptors to promote T cell egress. Immunity (2008) 28:122–33.

457. **Pepperl J, Reim G, Lüthi U, Kaech A, Hausmann G, Basler K**. Sphingolipid depletion impairs endocytic traffic and inhibits Wingless signaling. Mech Dev (2013) 130:493–505.

458. **Young MM, Wang H-G**. Sphingolipids as Regulators of Autophagy and Endocytic Trafficking. Adv Cancer Res (2018) 140:27–60.

459. **Avota E, Lira MN** de, **Schneider-Schaulies S**. Sphingomyelin Breakdown in T Cells: Role of Membrane Compartmentalization in T Cell Signaling and Interference by a Pathogen. Front Cell Dev Biol (2019) 7:152.

460. **La Bernardino de Serna J, Schütz GJ, Eggeling C, Cebecauer M**. There Is No Simple Model of the Plasma Membrane Organization. Front Cell Dev Biol (2016) 4:106.

461. **Contento RL, Molon B, Boularan C, Pozzan T, Manes S, Marullo S**, et al. CXCR4-CCR5: a couple modulating T cell functions. Proc Natl Acad Sci U S A (2008) 105:10101–6.

462. **Gardeta SR, García-Cuesta EM, D'Agostino G, Soler Palacios B, Quijada-Freire A, Lucas P**, et al. Sphingomyelin Depletion Inhibits CXCR4 Dynamics and CXCL12-Mediated Directed Cell Migration in Human T Cells. Front Immunol (2022) 13:925559.

463. **Limatola C, Massa V, Lauro C, Catalano M, Giovanetti A, Nuccitelli S**, et al. Evidence for a role of glycosphingolipids in CXCR4-dependent cell migration. FEBS Lett (2007) 581:2641–6.

464. **Geilen CC, Wieder T, Orfanos CE**. Ceramide signalling: regulatory role in cell proliferation, differentiation and apoptosis in human epidermis. Arch Dermatol Res (1997) 289:559–66.

465. **Molano A, Huang Z, Marko MG, Azzi A, Wu D, Wang E**, et al. Age-dependent changes in the sphingolipid composition of mouse CD4+ T cell membranes and immune synapses implicate glucosylceramides in age-related T cell dysfunction. PLoS One (2012) 7:e47650.

466. **Leiden JM**. Transcriptional regulation of T cell receptor genes. Annu Rev Immunol (1993) 11:539–70.

467. **Kaminuma O, Kitamura F, Kitamura N, Hiroi T, Miyoshi H, Miyawaki A**, et al. Differential contribution of NFATc2 and NFATc1 to TNF-alpha gene expression in T cells. J Immunol (2008) 180:319–26.

468. **Lacy P, Stow JL**. Cytokine release from innate immune cells: association with diverse membrane trafficking pathways. Blood (2011) 118:9–18.

469. **Verderio C, Gabrielli M, Giussani P**. Role of sphingolipids in the biogenesis and biological activity of extracellular vesicles. J Lipid Res (2018) 59:1325–40.

470. **Slotte JP, Hedström G, Rannström S, Ekman S**. Effects of sphingomyelin degradation on cell cholesterol oxidizability and steady-state distribution between the cell surface and the cell interior. Biochim Biophys Acta (1989) 985:90–6.

471. **Neufeld EB, Cooney AM, Pitha J, Dawidowicz EA, Dwyer NK, Pentchev PG**, et al. Intracellular trafficking of cholesterol monitored with a cyclodextrin. Journal of Biological Chemistry (1996) 271:21604–13.

8. References

472. **Jarsch IK, Daste F, Gallop JL**. Membrane curvature in cell biology: An integration of molecular mechanisms. J Cell Biol (2016) 214:375–87.

473. **Yuyama K, Sun H, Mitsutake S, Igarashi Y**. Sphingolipid-modulated exosome secretion promotes clearance of amyloid-β by microglia. J Biol Chem (2012) 287:10977–89.

474. **Pagan JK, Wylie FG, Joseph S, Widberg C, Bryant NJ, James DE**, et al. The t-SNARE syntaxin 4 is regulated during macrophage activation to function in membrane traffic and cytokine secretion. Curr Biol (2003) 13:156–60.

475. **Suzuki K, Verma IM**. Phosphorylation of SNAP-23 by IkappaB kinase 2 regulates mast cell degranulation. Cell (2008) 134:485–95.

476. **Manderson AP, Kay JG, Hammond LA, Brown DL, Stow JL**. Subcompartments of the macrophage recycling endosome direct the differential secretion of IL-6 and TNFalpha. J Cell Biol (2007) 178:57–69.

477. **Darios F, Wasser C, Shakirzyanova A, Giniatullin A, Goodman K, Munoz-Bravo JL**, et al. Sphingosine facilitates SNARE complex assembly and activates synaptic vesicle exocytosis. Neuron (2009) 62:683–94.

478. **Salaün C, Gould GW, Chamberlain LH**. The SNARE proteins SNAP-25 and SNAP-23 display different affinities for lipid rafts in PC12 cells. Regulation by distinct cysteine-rich domains. Journal of Biological Chemistry (2005) 280:1236–40.

479. **Moss ML, Jin SL, Milla ME, Bickett DM, Burkhart W, Carter HL**, et al. Cloning of a disintegrin metalloproteinase that processes precursor tumour-necrosis factor-alpha. Nature (1997) 385:733–6.

480. **Rozenova KA, Deevska GM, Karakashian AA, Nikolova-Karakashian MN**. Studies on the role of acid sphingomyelinase and ceramide in the regulation of tumor necrosis factor alpha (TNFalpha)-converting enzyme activity and TNFalpha secretion in macrophages. J Biol Chem (2010) 285:21103–13.

481. **Lamour NF, Wijesinghe DS, Mietla JA, Ward KE, Stahelin RV, Chalfant CE**. Ceramide kinase regulates the production of tumor necrosis factor α (TNFα) via inhibition of TNFα-converting enzyme. J Biol Chem (2011) 286:42808–17.

482. **Ali M, Saroha A, Pewzner-Jung Y, Futerman AH**. LPS-mediated septic shock is augmented in ceramide synthase 2 null mice due to elevated activity of TNFα-converting enzyme. FEBS Lett (2015) 589:2213–7.

483. **Utsumi T, Takeshige T, Tanaka K, Takami K, Kira Y, Klostergaard J**, et al. Transmembrane TNF (pro-TNF) is palmitoylated. FEBS Lett (2001) 500:1–6.

484. **Mosmann TR, Coffman RL**. TH1 and TH2 cells: different patterns of lymphokine secretion lead to different functional properties. Annu Rev Immunol (1989) 7:145–73.

485. **Zubiaga AM, Munoz E, Merrow M, Huber BT**. Regulation of interleukin 6 production in T helper cells. Int Immunol (1990) 2:1047–54.

486. **Jang D-I, Lee A-H, Shin H-Y, Song H-R, Park J-H, Kang T-B**, et al. The Role of Tumor Necrosis Factor Alpha (TNF-α) in Autoimmune Disease and Current TNF-α Inhibitors in Therapeutics. Int J Mol Sci (2021) 22.

487. **Tanaka T, Narazaki M, Kishimoto T**. IL-6 in inflammation, immunity, and disease. Cold Spring Harb Perspect Biol (2014) 6:a016295.

488. **Pugliese D, Felice C, Papa A, Gasbarrini A, Rapaccini GL, Guidi L**, et al. Anti TNF-α therapy for ulcerative colitis: current status and prospects for the future. Expert Rev Clin Immunol (2017) 13:223–33.

489. **Aziz N, Detels R, Quint JJ, Li Q, Gjertson D, Butch AW**. Stability of cytokines, chemokines and soluble activation markers in unprocessed blood stored under different conditions. Cytokine (2016) 84:17–24.

490. **Worbs T, Mempel TR, Bölter J, Andrian UH** von, **Förster R**. CCR7 ligands stimulate the intranodal motility of T lymphocytes in vivo. J Exp Med (2007) 204:489–95.

491. **Asperti-Boursin F, Real E, Bismuth G, Trautmann A, Donnadieu E**. CCR7 ligands control basal T cell motility within lymph node slices in a phosphoinositide 3-kinase-independent manner. J Exp Med (2007) 204:1167–79.

492. **Benechet AP, Menon M, Xu D, Samji T, Maher L, Murooka TT**, et al. T cell-intrinsic S1PR1 regulates endogenous effector T-cell egress dynamics from lymph nodes during infection. Proc Natl Acad Sci U S A (2016) 113:2182–7.

493. **Förster R, Davalos-Misslitz AC, Rot A**. CCR7 and its ligands: balancing immunity and tolerance. Nat Rev Immunol (2008) 8:362–71.

494. **Chowdhury F, Howat WJ, Phillips GJ, Lackie PM**. Interactions between endothelial cells and epithelial cells in a combined cell model of airway mucosa: effects on tight junction permeability. Exp Lung Res (2010) 36:1–11.

495. **Zhang M, Wu C**. The relationship between intestinal goblet cells and the immune response. Biosci Rep (2020) 40.

496. **Kim J, Koo B-K, Knoblich JA**. Human organoids: model systems for human biology and medicine. Nat Rev Mol Cell Biol (2020) 21:571–84.

497. **Wilson SS, Mayo M, Melim T, Knight H, Patnaude L, Wu X**, et al. Optimized Culture Conditions for Improved Growth and Functional Differentiation of Mouse and Human Colon Organoids. Front Immunol (2020) 11:547102.

498. **Aslam MN, McClintock SD, Attili D, Pandya S, Rehman H, Nadeem DM**, et al. Ulcerative Colitis-Derived Colonoid Culture: A Multi-Mineral-Approach to Improve Barrier Protein Expression. Front Cell Dev Biol (2020) 8:577221.

499. **Benya PD, Shaffer JD**. Dedifferentiated chondrocytes reexpress the differentiated collagen phenotype when cultured in agarose gels. Cell (1982) 30:215–24.

500. **Nelson CM, Bissell MJ**. Modeling dynamic reciprocity: engineering three-dimensional culture models of breast architecture, function, and neoplastic transformation. Semin Cancer Biol (2005) 15:342–52.

501. **Baharvand H, Hashemi SM, Kazemi Ashtiani S, Farrokhi A**. Differentiation of human embryonic stem cells into hepatocytes in 2D and 3D culture systems in vitro. Int J Dev Biol (2006) 50:645–52.

502. **d'Aldebert E, Quaranta M, Sébert M, Bonnet D, Kirzin S, Portier G**, et al. Characterization of Human Colon Organoids From Inflammatory Bowel Disease Patients. Front Cell Dev Biol (2020) 8:363.

8. References

503. **Sarvestani SK, Signs S, Hu B, Yeu Y, Feng H, Ni Y**, et al. Induced organoids derived from patients with ulcerative colitis recapitulate colitic reactivity. Nat Commun (2021) 12:262.

504. **Ojo BA, VanDussen KL, Rosen MJ**. The Promise of Patient-Derived Colon Organoids to Model Ulcerative Colitis. Inflamm Bowel Dis (2022) 28:299–308.

505. **van de Wetering M, Francies HE, Francis JM, Bounova G, Iorio F, Pronk A**, et al. Prospective derivation of a living organoid biobank of colorectal cancer patients. Cell (2015) 161:933–45.

506. **Michels BE, Mosa MH, Streibl BI, Zhan T, Menche C, Abou-El-Ardat K**, et al. Pooled In Vitro and In Vivo CRISPR-Cas9 Screening Identifies Tumor Suppressors in Human Colon Organoids. Cell Stem Cell (2020) 26:782-792.e7.

507. **Li X-L, Sluijter M, Doorduijn EM, Kale SP, McFerrin H, Liu Y-Y**, et al. Limited density of an antigen presented by RMA-S cells requires B7-1/CD28 signaling to enhance T-cell immunity at the effector phase. PLoS One (2014) 9:e108192.

508. **Ewart L, Apostolou A, Briggs SA, Carman CV, Chaff JT, Heng AR**, et al. Performance assessment and economic analysis of a human Liver-Chip for predictive toxicology. Commun Med (Lond) (2022) 2:154.

509. **Kasendra M, Tovaglieri A, Sontheimer-Phelps A, Jalili-Firoozinezhad S, Bein A, Chalkiadaki A**, et al. Development of a primary human Small Intestine-on-a-Chip using biopsy-derived organoids. Sci Rep (2018) 8:2871.

510. **Park J-W, Park W-J, Futerman AH**. Ceramide synthases as potential targets for therapeutic intervention in human diseases. Biochim Biophys Acta (2014) 1841:671–81.

511. **Marasas WF**. Discovery and occurrence of the fumonisins: a historical perspective. Environ Health Perspect (2001) 109 Suppl 2:239–43.

512. **Wang E, Norred WP, Bacon CW, Riley RT, Merrill AH**. Inhibition of sphingolipid biosynthesis by fumonisins. Implications for diseases associated with Fusarium moniliforme. Journal of Biological Chemistry (1991) 266:14486–90.

513. **Cao C, Xian R, Lin F, Li X, Li X, Qiang F**, et al. Fumonisin B1 induces hepatotoxicity in mice through the activation of oxidative stress, apoptosis and fibrosis. Chemosphere (2022) 296:133910.

514. **Szabó A, Szabó-Fodor J, Kachlek M, Mézes M, Balogh K, Glávits R**, et al. Dose and Exposure Time-Dependent Renal and Hepatic Effects of Intraperitoneally Administered Fumonisin B$_1$ in Rats. Toxins (Basel) (2018) 10.

515. **Chen J, Wen J, Tang Y, Shi J, Mu G, Yan R**, et al. Research Progress on Fumonisin B1 Contamination and Toxicity: A Review. Molecules (2021) 26.

516. **Delgado A, Casas J, Llebaria A, Abad JL, Fabrias G**. Inhibitors of sphingolipid metabolism enzymes. Biochim Biophys Acta (2006) 1758:1957–77.

517. **Brinkmann V, Davis MD, Heise CE, Albert R, Cottens S, Hof R**, et al. The immune modulator FTY720 targets sphingosine 1-phosphate receptors. Journal of Biological Chemistry (2002) 277:21453–7.

518. **Lahiri S, Park H, Laviad EL, Lu X, Bittman R, Futerman AH**. Ceramide synthesis is modulated by the sphingosine analog FTY720 via a mixture of uncompetitive and noncompetitive inhibition in an Acyl-CoA chain length-dependent manner. Journal of Biological Chemistry (2009) 284:16090–8.

172

519. **Zwara A, Wertheim-Tysarowska K, Mika A**. Alterations of Ultra Long-Chain Fatty Acids in Hereditary Skin Diseases-Review Article. Front Med (Lausanne) (2021) 8:730855.

520. **Eckl K-M, Tidhar R, Thiele H, Oji V, Hausser I, Brodesser S**, et al. Impaired epidermal ceramide synthesis causes autosomal recessive congenital ichthyosis and reveals the importance of ceramide acyl chain length. J Invest Dermatol (2013) 133:2202–11.

521. **Hu B, Zhong L, Weng Y, Peng L, Huang Y, Zhao Y**, et al. Therapeutic siRNA: state of the art. Signal Transduct Target Ther (2020) 5:101.

522. **Gangopadhyay S, Gore KR**. Advances in siRNA therapeutics and synergistic effect on siRNA activity using emerging dual ribose modifications. RNA Biol (2022) 19:452–67.

523. **Foster DJ, Brown CR, Shaikh S, Trapp C, Schlegel MK, Qian K**, et al. Advanced siRNA Designs Further Improve In Vivo Performance of GalNAc-siRNA Conjugates. Mol Ther (2018) 26:708–17.

524. **Chernikov IV, Ponomareva UA, Chernolovskaya EL**. Structural Modifications of siRNA Improve Its Performance In Vivo. Int J Mol Sci (2023) 24.

525. **Shiohama Y, Fujita R, Sonokawa M, Hisano M, Kotake Y, Krstic-Demonacos M**, et al. Elimination of Off-Target Effect by Chemical Modification of 5'-End of siRNA. Nucleic Acid Ther (2022) 32:438–47.

526. **Scaggiante B, Dapas B, Farra R, Grassi M, Pozzato G, Giansante C**, et al. Improving siRNA bio-distribution and minimizing side effects. Curr Drug Metab (2011) 12:11–23.

527. **Osborn MF, Khvorova A**. Improving siRNA Delivery In Vivo Through Lipid Conjugation. Nucleic Acid Ther (2018) 28:128–36.

528. **Mainini F, Eccles MR**. Lipid and Polymer-Based Nanoparticle siRNA Delivery Systems for Cancer Therapy. Molecules (2020) 25.

529. **Kulkarni JA, Witzigmann D, Chen S, Cullis PR, van der Meel R**. Lipid Nanoparticle Technology for Clinical Translation of siRNA Therapeutics. Acc Chem Res (2019) 52:2435–44.

530. **Padda IS, Mahtani AU, Parmar M.** StatPearls: Small Interfering RNA (siRNA) Based Therapy. Treasure Island (FL) (2023).
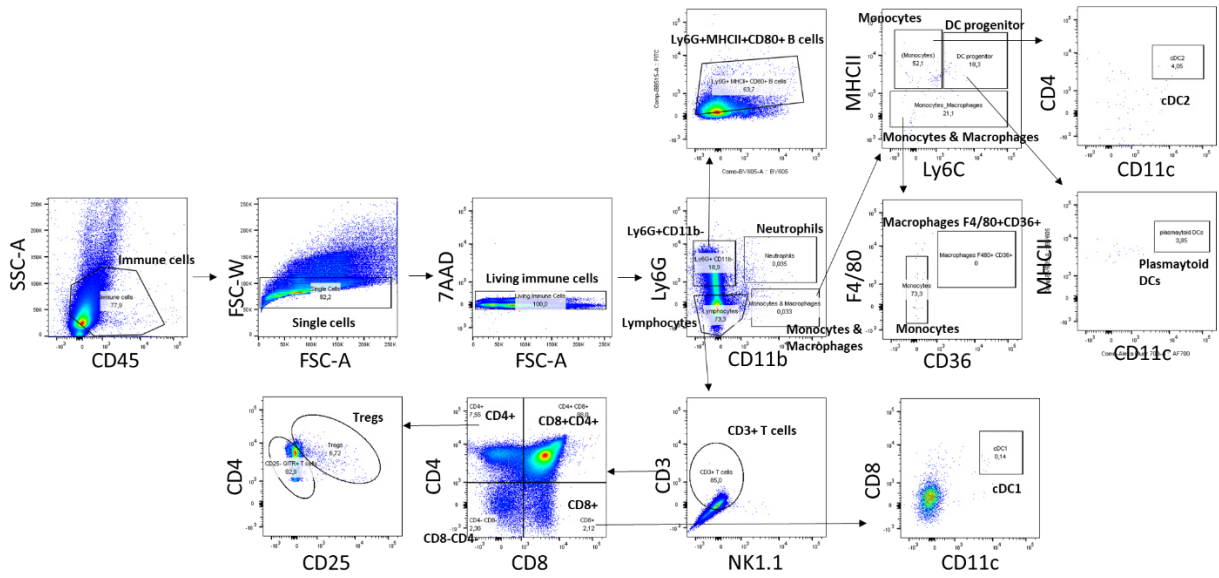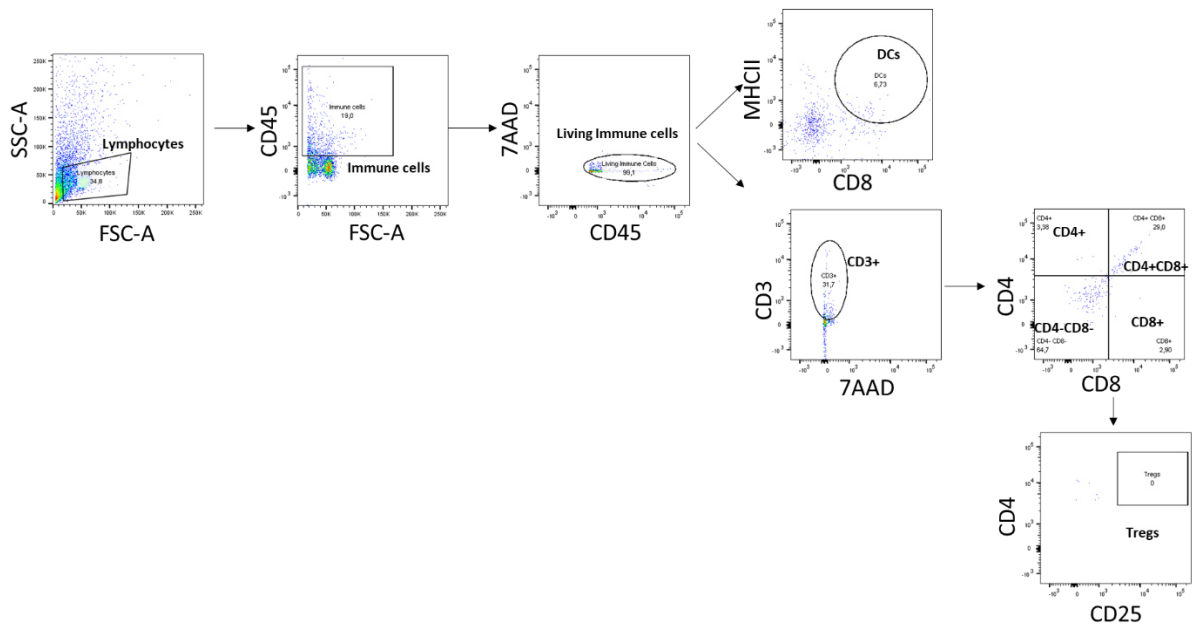
9. Supplements
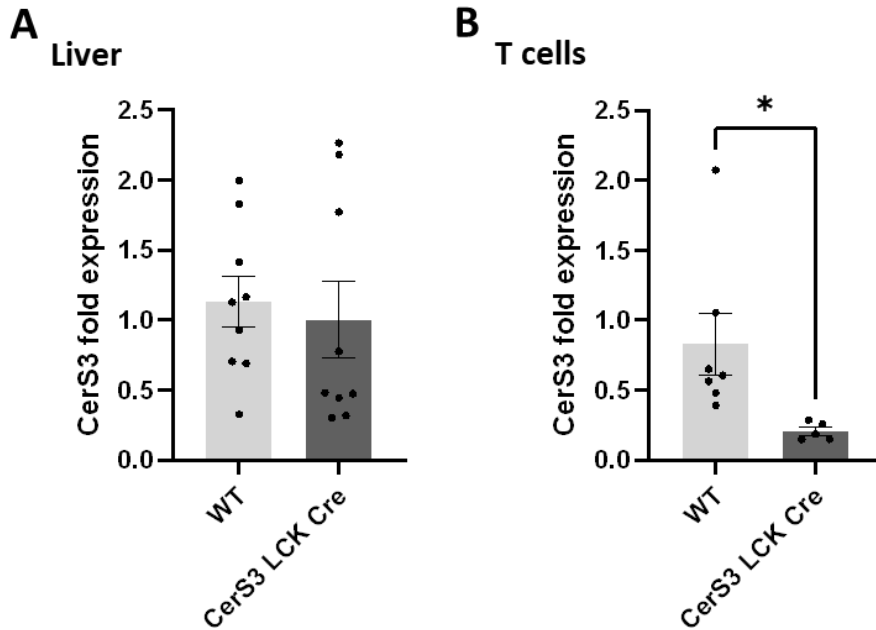
Supplementary Figure 1: CerS3 expression in liver tissue and T cells isolated from WT and CerS3 LCK Cre mice. RNA was isolated from liver tissue or T cells from WT and CerS3 LCK Cre mice. MRNA expression of CerS3 was assessed and normalized to PPIA levels. **A)** Liver CerS3 mRNA levels of WT mice compared to CerS3 LCK Cre mice. **B)** T cell CerS3 mRNA levels of WT mice compared to CerS3 LCK Cre mice. Data are mean ± SEM. Statistical analysis was performed with a one-way ANOVA with a Dunnett's multiple comparison test (* $p < 0.05$) Group sizes: n=3 measured in triplicates
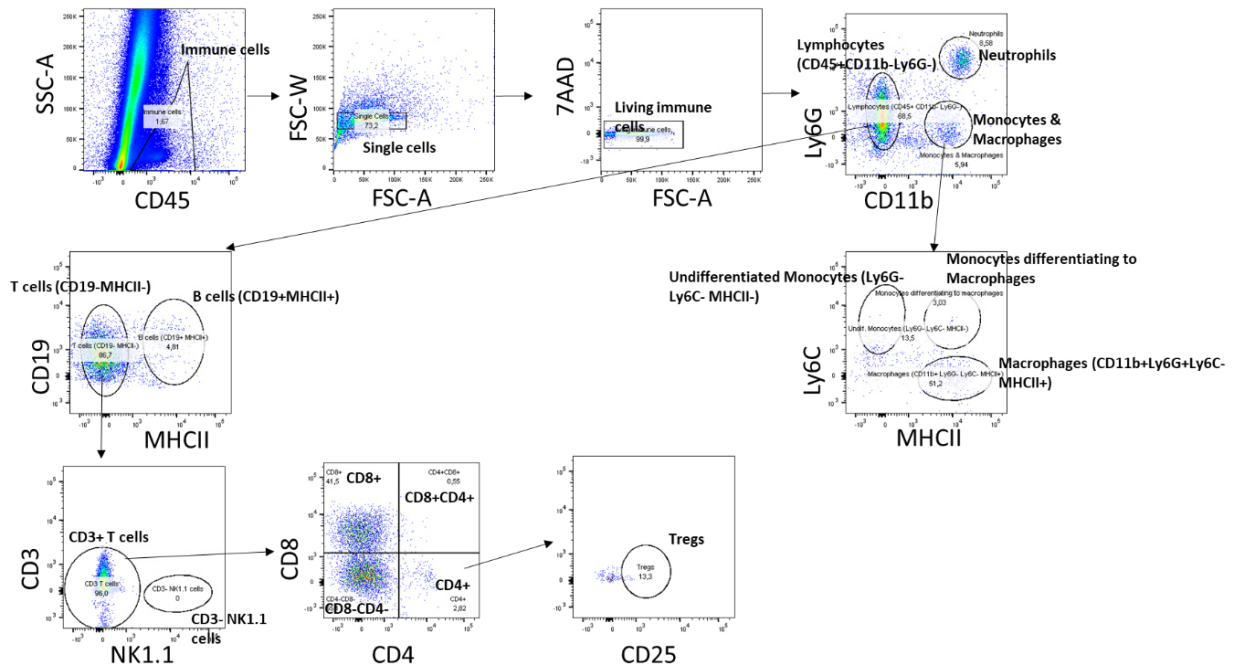
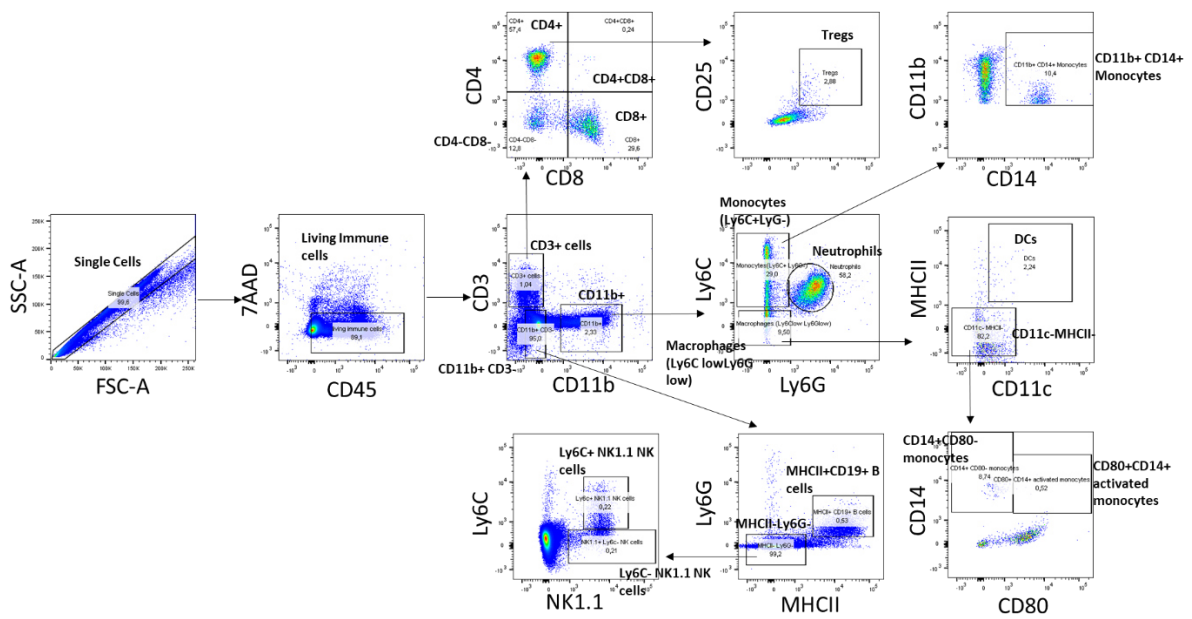**Supplementary Figure 2: Gating Strategy for IEL and LP.**

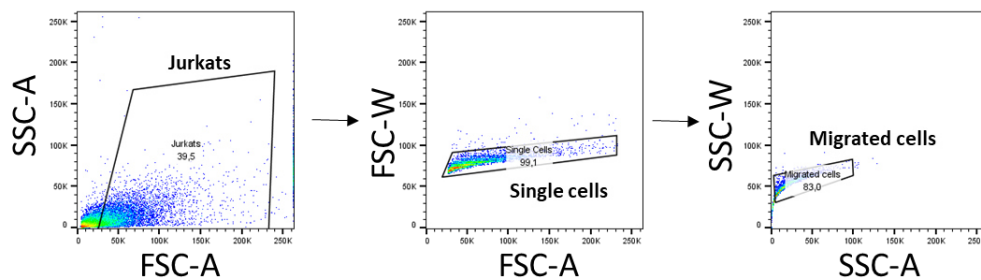**Supplementary Figure 3: Gating Strategy for spleen and thymus.**

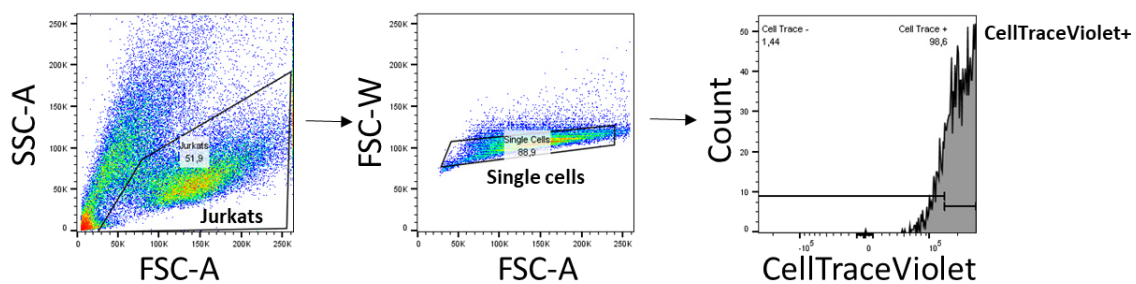
Supplementary Figure 4: Gating Strategy for lymph nodes.

Supplementary Figure 5: Gating strategy for blood.

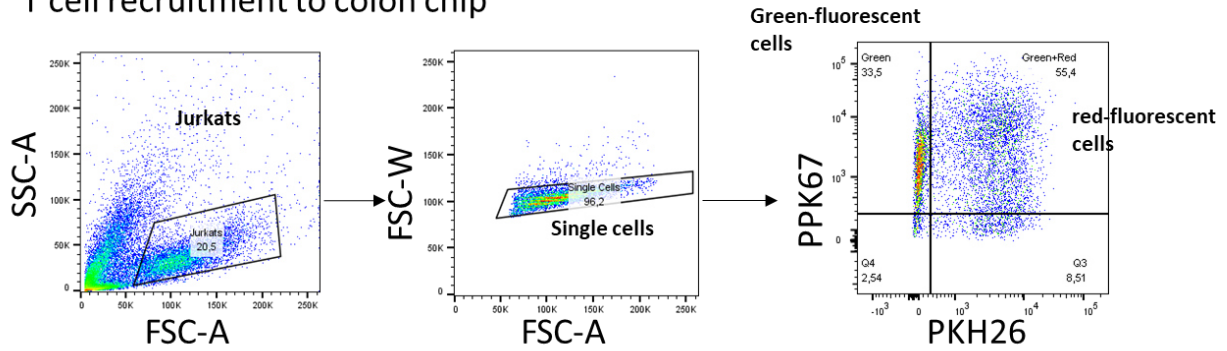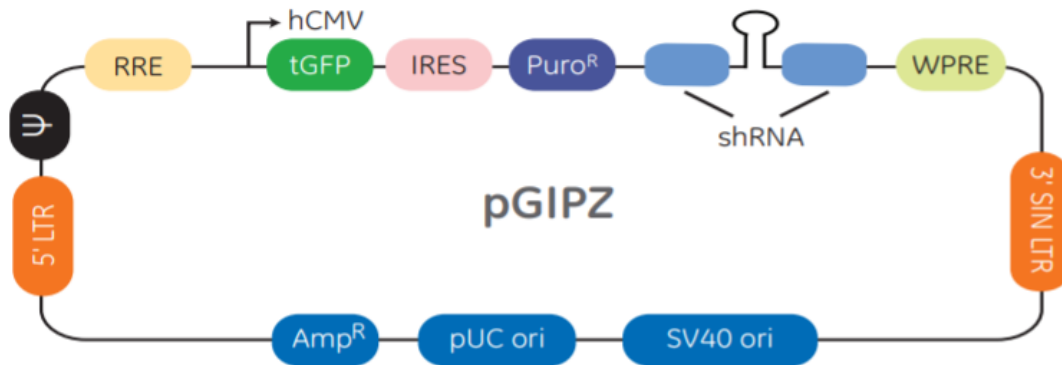**Supplementary Figure 6: Gating strategy for migration and proliferation assay.**

Supplementary Figure 7: Gating strategy for T cell recruitment to colon chip.

Supplementary Figure 8: Schematic sketch of pGIPZ vector. All shRNA vectors were conducted similarly, only the shRNA encoding part was designed for either shNC, shCerS1 or shCerS3. Picture from horizondiscovery.com **hCMV:** Human cytomegalovirus promoter, enhances transgene expression; **tGFP:** TurboGFP reporter; **PuroR:** Puromycin resistance; **AmpR:** Ampicillin resistance; **IRES:** Internal ribosomal entry sites enables expression of TurboGFP and puromycin resistance genes in one transcript; **LTR:** long terminal repeat; **Ψ:** Psi packaging sequence enables packaging of viral genome via lentiviral packaging systems; **RRE:** Rev response element enhances virus titer through enhancement of packaging efficiency; **WPRE:** Woodchuck hepatitis posttranscriptional regulatory element upregulates transgene expression in target cell
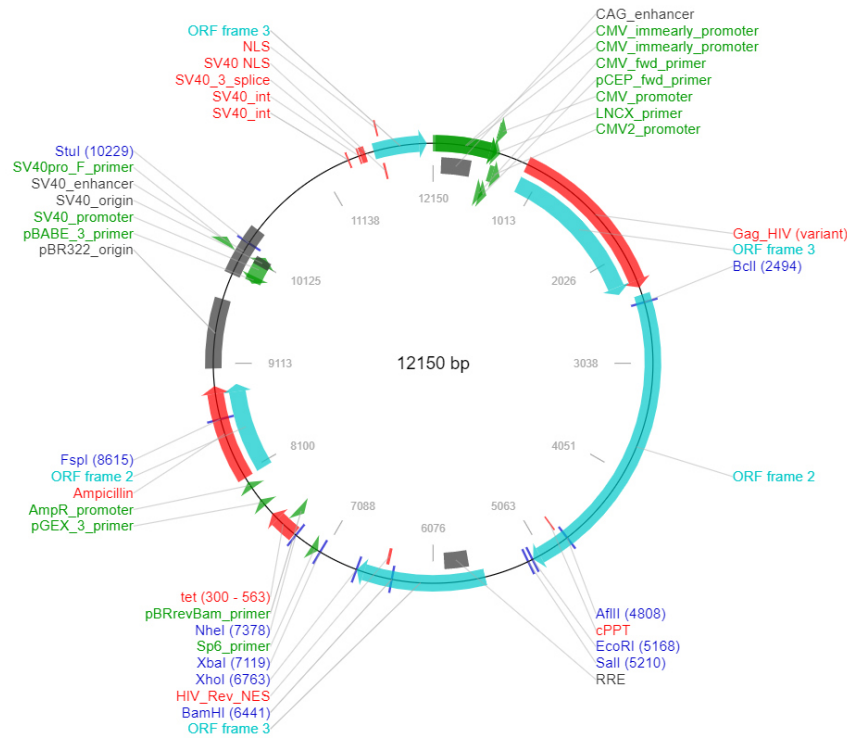
Supplementary Figure 9: Plasmid map of gag/pol vector. Sketch of plasmid map with Open Reading Frame (ORF), SV40 promotor, Ampicillin resistance and cutting sites of restriction enzymes. Originally this plasmid was kindly gifted to us by AG Fulda (former group in the Institute for experimental tumor research). Figure was obtained from addgene.com
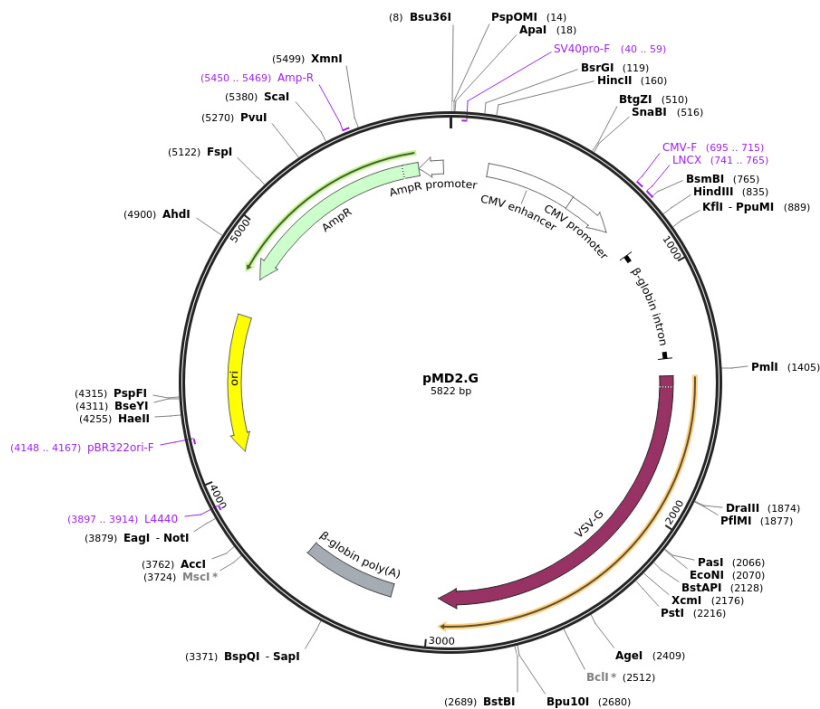
Supplementary Figure 10: Plasmid map of env-vector. Schematic depiction of the plasmid that encodes important genes for lentiviral packaging. Originally this plasmid was kindly gifted to us by AG Fulda (former group in the Institute for experimental tumor research). Figure was obtained from addgene.com
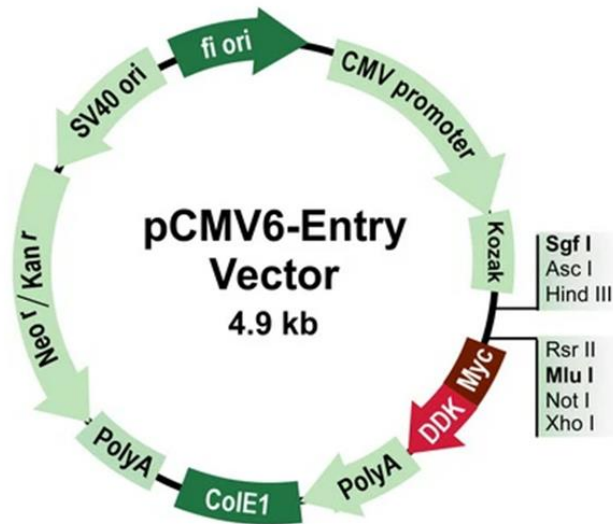
Supplementary Figure 11: Control vector for overexpression. Plasmid map of NCmyc vector used as control for overexpression of CerS1 and CerS3. Depiction of Neomycin and Kanamycin resistance, as well as Myc/DDK-tag and CMV promotor. Picture obtained from origene.com
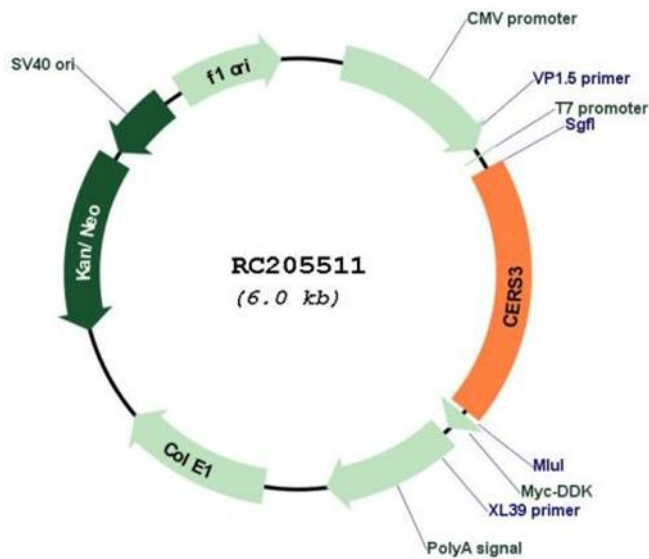
Supplementary Figure 12: LASS3 (CERS3) Human Tagged ORF Clone plasmid map Schematic plasmid map of CerS3myc overexpression plasmid with all important features of Neomycin and Kanamycin resistance, as well as CerS3 tagged with Myc/DDK-tag and CMV promotor. Plasmid map obtained from origene.com

10. Abbreviations

%	percent
$[Ca^{2+}]_i$	Intracellular Calcium
°C	Degree Celsius
µg	microgram
µM	micromolar
3D	Three-dimensional
3-KR	3-Ketosphinganine reductase
7 AAD	7-Aminoactinomycin D
aCDase	Acid Ceramidase
Akt	Protein Kinase B
ANOVA	Analysis of Variances
AOM	Azoxymethane
AP1	Activating protein 1
APC	Antigen presenting cell
aSMase	Acid shphingomyelinase
BCL10	B-cell chronic lymphocytic leukemia/lymphoma 10
bFGF	Basic fibroblast growth factor
bp	Base pair
bpm	Beats per minute
BSA	Bovine Serum Albumin
C1P	Ceramide 1 Phosphate
$CaCl_2$	Calcium chloride
CARD11	Caspase recruitment domain family, member 11
CBA	Cytometric Bead Array
CBM	CARD11-BCL10-MALT1
CCR	C-C Chemokine receptor
CD	Cluster of Differentiation
Cer	Ceramide
CerS	Ceramidesynthase
CERT	Ceramide transfer protein
cm	centimeter
COP	Coat protein complex
CRC	Colorectal cancer
CSK	C-terminal sarcoma-cellular (src) Kinase
CXCR	C-X-C motif chemokine receptor
d	Day(s)
DAG	Diacylgylcerol
DC	Dendritic cell

DCCV	Deutsche Morbus Crohn/Colitis ulcerosa Vereinigung
DMSO	Dimethyl sulfoxide
DNA	Deoxyribonucleic acid
DPBS	Dulbecco's Phosphate-Buffered Saline
DSMZ	German Collection of Microorganisms and Cell Cultures GmbH
DSS	Dextran Sodium Sulfate
DTT	Dithiothreitol
E	Extension
e.g.	Example given
EAA	Essential Amino Acids
ECBM	Endothelial cell basal medium
ECM	Extracellular matrix
EDTA	Ethylenediaminetetraacetic acid
EGF	Endothelial growth factor
EGTA	Ethylene glycol-bis(β-aminoethyl ether)-N,N,N′,N′-tetraacetic acid
EMA	European Medicine Agency
ER	Endoplasmic Reticulum
ERK	Extracellular signal-regulated kinases
ESR	Erythrocyte sedimentation rate
FA	Fatty CoA-acyl chains
FACS	Fluorescence-activated single cell sorting
Fas	Fas Cell Surface Death Receptor
FBS	Fetal Bovine Serum
FDA	Food and Drug Administration
Fisher's LSD	Fisher's least significant difference
FoxP3	Forkhead box protein 3
g	gram
GalCer	Galactosylceramide
GATA	GATA box binding protein
GEF	Guanine nucleotide exchange factor
GFP	Green fluorescent protein
GlcCer	Glycosylceramide
GM-CSF	Granulocyte-macrophage colony-stimulating factor
Golgi	Golgi Apparatus
GPI	Glycosylphosphatidylinositol
GPR15L	G protein-coupled receptor 15 ligand
GSK3	Glycogen synthase kinase 3
GTP	Guanine nucleotide
GvHD	Graft vs. host Disease

10. Abbreviations

GV-SOLAS	Gesellschaft für Versuchstierkunde-Society of labarotary animal science
h	Hour(s)
H_2O	Water
H_2O_2	Hydrogen peroxide
H_3PO_4	Phosphoric acid
HBSS	Hank's balanced salt solution
HEPES	4-(2-hydroxyethyl)-1-piperazineethanesulfonic acid
HIMEC	Human intestinal microvascular endothelial cell
HRP	Horseradishperoxidase
HUVEC	Human umbilical vein endothelial cell
IBD	Inflammatory Bowel Disease
ICD	International Statistical Classification of Diseases and Related Health problems
IEL	Intra-epithelial lymphocyte
Ig	Immunoglobulin
IKKγ	Inhibitor of nuclear factor kappa B kinase subunit gamma
IL	Interleukin
ILC	Innate lymphoid cell
IP10	Interferon gamma induced protein 10
IP_3	Inositol triphosphate
ITAM	Immunoreceptor tyrosine-based activation motif
JAK	Janus kinase
JNK	c-Jun terminal kinase
KCl	Potassium chloride
KH_2PO_4	Potassiumdihydrogenphosphate
$KHCO_3$	Potassiumhydrogencarbonate
KO	Knockout
l	liter
Lass	Longevity assurance genes
LAT	Linker activator of T cells
LB	Lennox Broth
LCK	Lymphocyte-specific protein tyrosine kinase
LC-MS/MS	Liquid chromatography coupled with tandem mass spectrometry
LITAF	Lipopolysaccharide induced TNF factor
LP	Lamina Propria
LPS	Lipopolysaccharide
M	molar
MALT1	Mucosa-associated lymphoid tissue lymphoma translocation gene 1
MAPK	Mitogen-activated protein kinase

MAPKK	Mitogen-activated protein kinase kinase
MAPKKK	Mitogen-activated protein kinase kinase kinase
MCP-1	Monocyte chemoattractant protein 1
MEC	Mucosae associated epithelia chemokine
$MgCl_2$	Magnesium chloride
min	Minute(s)
MIP-3 α	Macrophage inflammatory protein-3 alpha
ml	milliliter
mM	millimolar
mRNA	Messenger RNA
mTOR	Mammalian target of rapamycin
myc	v-myc avian myelocytomatosis viral oncogene homolog
Na_2CO_3	Sodiumcarbonate
Na_2HPO_4	Di-sodiumhydrogenphosphate
$NaHCO_3$	Sodiumhydrogencarbonate
NC	Negative control
NEAA	Non-essential amino acids
NFAT	Nuclear factor of activated T-cells
NFκB	Nuclear Factor kappa B
NH_4Cl	Ammonium chloride
NIK	NFκB inducing Kinase
NK	Natural Killer
nM	nanomolar
nm	nanometer
NO	Nitrogen oxide
NP40	9-Octylphenolethoxylate
NSM	Neutral Sphingomyelinase
p	p-value (probability value)
P/S	Penicillin-Streptomycin
PCR	Polymerase chain reaction
PDMS	Polydimethylsiloxane
pg	picogram
PIP_2	Phosphatidylinositol 4,5-Biphosphate
PIP_3	Phosphatidylinositol (3,4,5)-trisphosphate
PKC	Protein kinase C
PKCγ	Phospho Kinase C γ
PKCθ	Phospho Kinase C θ
PLCγ	Phospho Lipase C
PME	Progressive myoclonic epilepsy

10. Abbreviations

PMSF	Phenylmethylsulfonylfluoride
PP2A	Protein Phosphatase 2
PPARγ	Peroxisome proliferator-activated receptor γ
PPIA	Cylcophilin A gene
qRT-PCR	Quantative Realtime PCR
R3-IGF-1	Long R3 insulin like growth factor
Raf1	Rapidly accelerated fibrosarcoma 1
RAG	Recombination activating gene
RAS	Rapidly accelerated sarcoma
RASGPR1	RAS- guanyl nucleotide-releasing protei
RNA	Ribonucleic acid
RORγ	RAR-related orphan receptor gamma
RPL13A	Ribosomal Protein L13a
rpm	Revolutions per minutes
RPMI	Roswell Park Memorial Institute Medium
s	seconds
S	Severity
S1P	Sphingosine-1-phosphate
SCID	Severe combined immunodeficency
SDF-1α	stromal cell-derived factor
SDS	Sodium dodecyl sulfate
SDS-PAGE	Sodium dodecyl sulfate polyacrylamide gel electrophoresis
SET Protein	Protein Phosphatase 2 inhibitor
shRNA	Short-hairpin RNA
siRNA	Small-interfering RNA
SLE	Systemic lupus erythematosus
SMS1	Sphingomyelin Synthase 1
Sph	Sphingolipid
SphK	S1P-Kinase
SPT	Serine palmitoyltransferase
STAT	Signal transducer and activator of transcription
TACE	TNFα converting enzyme
Tbet	T-box expressed in T cells
TCA	Trichloroacetic acid
TCR	T cell receptor
TECK	Thymus-expressed chemokine
TGF	Tumor-growth factor
TH	T helper cell
TLR	Toll-like receptor

TM	Transmembrane
TMB	Tetramethylbenzidine
TNF	Tumor-necrosis factor
Treg	Regulatory T cell
Trm	Tissue-resident memory T cell
U	Units
UC	Ulcerative colitis
UDP	Uridine diphosphate
UGCG	UDP-glucose glycosyltransferase
V	Volt
v/v	Volume percent
VDJ	Variable, Diversity, joining
VEGF	Vascular endothelial growth factor
w/v	Mass/volume
WB	Western Blot
Wnt	Wingless/Integrated
WT	Wild type
Zap70	Zeta-chain-associated protein kinase 70